

CRANFIELD UNIVERSITY

SCHOOL OF APPLIED SCIENCES
Welding Engineering

PhD THESIS

Academic year: 2010-11

Patrick Van Rymenant

MECHANICAL CHARACTERISATION AND MODELLING
OF RESISTANCE WELDING

Supervisor David Yapp

July 2011

Abstract

Resistance welding is used very extensively in industry for a wide range of applications. Knowledge and measurement of the dynamic characteristics of resistance welding equipment is important in the design of the equipment and in optimization of welding procedures using finite element software. This is especially true for projection welding where accurate measurements of effective lumped mass and damping of the welding head as well as its maximal acceleration and velocity are required for accurate modelling.

This thesis describes a new concept where a mechanical model of the welding head is used together with the imposition of a mechanical load step function with simultaneous measurement of resulting head motion to calculate effective lumped mass and damping factor. Two test systems were devised to implement the step function. In the “free fracture test”, a metal or ceramic bar is loaded to its breaking point and resulting welding head velocity is measured. This data allows accurate calculation of machine parameters. The second test uses the explosion of a small metallic element to impose a step function, when the welding current causes the metallic element to explode. The final version of this test “the exploding button test” uses a small cylindrical element fabricated from welding filler wire, with the advantage that both button geometry and material can be controlled. The exploding button test has proved to be very effective, can easily be used for in-situ measurements and avoids the vibrations associated with the free fracture test. These test were applied to evaluate a range of resistance welding machines.

Finally, an innovative projection geometry was developed to significantly increase projection weld quality and this design has now been used extensively in industry.

The techniques developed in this thesis have been shown to be practical and effective and have enabled much better understanding of machine kinematics. The measurements provide essential data for modelling of projection welding and in guiding the development of resistance welding machines and procedures.

Acknowledgements

I wish to express my gratitude to the following people for their contribution,

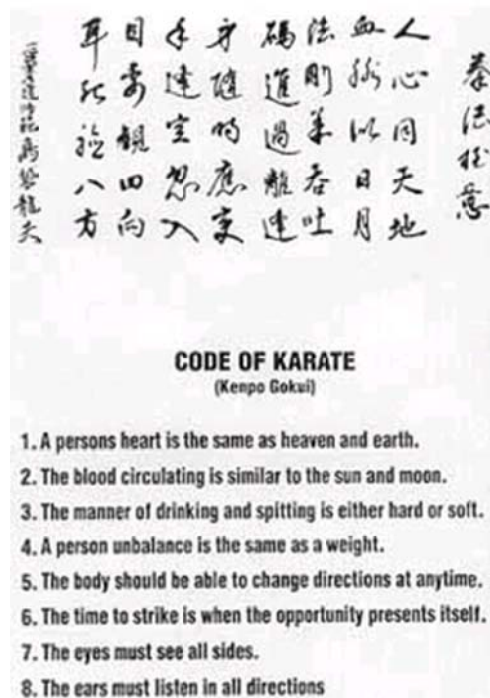
My supervisor, David Yapp;

My colleagues welding engineers working in my research group in welding, for their appreciated support during all work for industry that we conducted over the past 20 years.

Special thanks to Marijn Casteels, for guiding the construction of our new Welding Technology Centre (currently being built) over the past year. It will be our new workplace for the coming twenty years and the result is stunning;

Also special thanks to Wim Vandenberk from Philips Turnhout for his help on high speed camera recording on micro resistance welding equipment;

My karate sensei for patiently teaching me the meaning of ‘Gokui’ and for giving me the awareness and the drive to start and finish this PhD study;



“Gokui”

Japanese meaning the strive to understand more and improve!

And finally and most important, my wife Diane and my children Nele, Dries and Ward for their patience and calm during the past 6 years. Sorry for the time missed...

I now understand why some people quote Charles Dickens in their thesis:

“It was the best of times, it was the worst of times”

To my aunt Rachel (sister Germa, age 87)

Dank u wel tante celleke, uw enthousiasme in de technische installaties van het klooster en de school in Essen werkten aanstekelijk en wekten in mij van kindsbeen af de interesse in wetenschap en technologie. Ik waardeer het bijzonder dat je ook nu nog op uw gezegende leeftijd interesse blijft tonen in mijn werk. Op naar de leeftijd van 100!

Translation:

Thank you aunty celleke for your enthusiasm in the technical installations of the convent and the school where you lived and worked during my childhood days. For sure it infected me as a child with interest and fascination in science and technology. I truly appreciate it enormously that up to date, with your blessed age, you keep showing high interest in my work. Let's go for the age of 100!

List of contents

Abstract	<i>i</i>
Acknowledgements	<i>ii</i>
List of contents	<i>iv</i>
List of figures	<i>viii</i>
List of tables	<i>xiii</i>
Nomenclature	<i>xiv</i>
Abbreviations	<i>xv</i>
1 Introduction	1
1.1 Origin of resistance welding	8
1.2 Overview of resistance welding processes	10
1.2.1 Spot welding.....	10
1.2.2 Seam welding	11
1.2.3 Projection welding	13
1.2.4 Resistance butt welding	15
1.2.5 Flash butt welding.....	15
1.3 Resistance welding machine set up	16
1.3.1 Machine frame.....	16
1.3.2 Electrode force actuator	18
2 Literature review	29
2.1 Mechanical behaviour	29
2.1.1 Dynamical mechanical characteristics	32
2.1.2 Theoretical modelling	33
2.1.3 Simulation on laboratory machines	37
2.1.4 Effect analysis based on ‘real’ welding tests.....	40
2.1.5 Modelling techniques for resistance welding processes.....	45
2.1.6 FEA based on ‘In-Situ’ characterisation tests.....	53
2.2 Projection geometries	55
2.2.1 Artificial standardised projections	55
2.2.2 Artificial other projections	55
2.2.3 Natural projections and artificially altered projections	58
3 Aims and Objectives	61
4 Equipment used	63
4.1 Resistance welding machines	63
4.1.1 AWL multi purpose spot/projection welder.....	63
4.1.2 PECO roll membrane spot/projection welder (pneumatic)	64
4.1.3 ARO multi purpose spot/projection welder (pneumatic)	65
4.1.4 ARO multi purpose spot/projection welder (servo electric)	66
4.1.5 Mc Gregor μ -resistance welding head	67

4.2	Measuring Equipment	68
4.2.1	LMI Laser Twin displacement Sensor (LTS)	68
4.2.2	Solartron Linear Variable Differential Transducer (LVDT).....	70
4.2.3	Polytec CLV 1000 laser vibrometer	76
4.2.4	PEM UK ROGOFLEX RGF 150, 300 and 300S Current Transducers.....	78
4.2.5	Miyachi MM-601A Load Cell	81
4.2.6	Dewetron 2010 – Portable industrial data-acquisition system.....	83
4.3	Measuring procedures	85
4.3.1	Voltage – Current [U-I] – characteristics of a Resistance Welding Power Source.....	85
5	Experimental Procedure	87
5.1	Machine Mechanical Model	89
5.1.1	Model of the moving welding head	89
5.1.2	Model of the fixed welding head	91
5.1.3	Difference between Step or Impulse response	92
5.2	Data Processing Procedure	93
5.2.1	Starting from welding head displacement measurements	93
5.2.2	Starting from welding head velocity measurements	95
5.3	Evaluation of step function imposing tests	96
5.3.1	Free Fracture Test	96
5.3.2	Explosion Test	102
5.4	High speed camera evaluation	108
5.5	Stick – Slip Test	110
5.5.1	Test setup for stick-slip test	110
5.5.2	Test procedure stick-slip measurements	111
5.5.3	Processing of results.....	111
5.6	Stick-slip test with application of lateral force	111
5.6.1	Test setup.....	111
5.6.2	Test procedure	112
5.6.3	Processing of results.....	112
5.7	Test methodology on different machines tested	113
5.7.1	AWL machine	113
5.7.2	PECO roll membrane machine	117
5.7.3	ARO multi-purpose spot/projection welder (pneumatic)	118
5.7.4	Mc Gregor μ -resistance welding head	119
6	Results	120
6.1	Processing of Kinematical measurements	120
6.2	AWL machine	123
6.2.1	Free fracture tests.....	123
6.2.2	Explosion Test	128
6.2.3	Comparison of fracture and explosion test.....	136
6.2.4	General motion of welding head.....	137
6.2.5	Influence of current on machine behavior.....	140
6.2.6	Fracture tests with application of current.....	144
6.2.7	Fracture tests with lateral force.....	146
6.2.8	Stick – Slip test	149
6.2.9	High speed camera evaluation	150
6.3	PECO roll membrane machine	164
6.4	ARO multi-purpose spot/projection welder (pneumatic)	165

6.4.1	Fracture and explosion tests	165
6.4.2	High speed camera evaluation	167
6.5	Mc Gregor μ-resistance welding head	170
6.5.1	Explosion tests.....	170
6.5.2	High speed camera evaluation	171
6.6	ARO Servo electric	180
6.7	Overview of results per machine tested	180
7	<i>Discussion</i>	<i>181</i>
7.1	Step function imposing tests and machine evaluations	181
7.1.1	Fracture test	181
7.1.2	Explosion test	183
7.2	Measurements on AWL machine.....	184
7.2.1	Fracture and explosion tests	184
7.2.2	Influence of current on machine behaviour.....	184
7.2.3	Fracture tests with application of lateral force	186
7.2.4	Stick – slip test.....	186
7.2.5	High speed camera evaluation	187
7.3	Measurements on PECO roll membrane machine.....	187
7.4	Measurements on ARO pneumatic multi-purpose machine.....	187
7.4.1	Fracture and explosion tests	187
7.4.2	High speed camera evaluations	188
7.5	Mc Gregor μ-resistance welding head	188
7.5.1	Explosion tests.....	188
7.5.2	High speed camera evaluations	188
7.6	ARO servo electric.....	189
8	<i>Application of testing methodology to projection welded parts</i>	<i>190</i>
8.1	Innovative welding cycle.....	190
8.2	Innovative projection geometry	192
9	<i>Conclusions</i>	<i>196</i>
10	<i>Recommendations for further work.....</i>	<i>198</i>
	<i>References</i>	<i>199</i>
	<i>Appendix A - Physical properties materials used</i>	<i>206</i>
	<i>Appendix B - Theoretical Model</i>	<i>207</i>
	<i>Appendix C - Test procedure Free Fracture test</i>	<i>215</i>
	<i>Appendix D - Processing procedure Fracture/Explosion test.....</i>	<i>225</i>
	<i>Appendix E - Design procedure Spring Follow Up system.</i>	<i>228</i>
	E1 Based on Belleville washers (not intended for conducting current).....	228
	E2 Based on Copper leaf springs (intended for conducting current)	232
	<i>Appendix F - Procedure and manual for processing the Voltage – Current U-I- Characteristics of a Resistance Welding Power Source.</i>	<i>235</i>

List of figures

Figure 1-1	Principal types of resistance welds.....	1
Figure 1-2	Principle of resistance spot welding.....	2
Figure 1-3	General welding cycle of a resistance weld.....	4
Figure 1-4	Resistances in circuit and resulting temperature distribution.....	5
Figure 1-5	Drawings of US 347140 by Elihu Thomson.....	8
Figure 1-6	Overview of welding processes according to BS EN 14610 - 2004.....	10
Figure 1-7	'Direct' spot welding (ISO 669).....	11
Figure 1-8	'Indirect' spot welding (ISO 669).....	11
Figure 1-9	Lap seam welding (ISO 669).....	12
Figure 1-10	Mash seam welding (ISO 669).....	12
Figure 1-11	Seam welding with strip (ISO 669).....	12
Figure 1-12	Foil butt-seam welding (ISO 669).....	13
Figure 1-13	Direct projection welding (ISO 669).....	13
Figure 1-14	Indirect projection welding before and after welding (ISO 669).....	14
Figure 1-15	Resistance butt welding (ISO 669).....	15
Figure 1-16	Flash butt welding before and after welding (ISO 669).....	15
Figure 1-17	Different elements in resistance welding machines.....	16
Figure 1-18	Pedestal pneumatically driven C-type spot welder.....	17
Figure 1-19	PW Portable C-type spot welding gun.....	17
Figure 1-20	PW Portable Y-type spotwelding gun.....	18
Figure 1-21	LEAS portal type roller seam welding machine on radiator production line.....	18
Figure 1-22	Handheld Tecna direct spotwelding gun.....	19
Figure 1-23	Tecna motor body repair unit.....	19
Figure 1-24	Fixed stroke air cylinder.....	20
Figure 1-25	Adjustable stroke air cylinder.....	20
Figure 1-26	Tandem air cylinder.....	20
Figure 1-27	Hydraulical oil cylinder.....	21
Figure 1-28	Pressotechnic power package operation sequence.....	22
Figure 1-29	Diaphragm air cylinder.....	22
Figure 1-30	Single and double acting diaphragm cylinder.....	23
Figure 1-31	Implementation of ARO Servo Guns inside Europe in 2009.....	25
Figure 1-32	Implementation of ARO Servo Guns outside of Europe in 2009.....	25
Figure 1-33	ARO Servo electric actuator motor.....	26
Figure 1-34	Water cooled motor (upper) and air cooled motor (lower).....	27
Figure 1-35	Belleville spring follow-up system.....	28
Figure 2-1	Contact fault in spot and seam welding equipment (ISO 669).....	30
Figure 2-2	Contact fault in projection welding equipment (ISO 669).....	30
Figure 2-3	Contact fault in butt welding equipment (ISO 669).....	31
Figure 2-4	Measurement accessory for spot welding equipment (ISO 669).....	31
Figure 2-5	Measurement accessory for spot- and projection welding equipment (ISO 669).....	31
Figure 2-6	Schematic dynamic behaviour of spot welding equipment [1].....	32
Figure 2-7	Single-mass vibration system [19], [20].....	34
Figure 2-8	Ball melting model [23].....	36
Figure 2-9	Four types of spot welding machine setups [28].....	38
Figure 2-10	Sketch of Simulating device [31].....	40
Figure 2-11	Changing of stiffness of lower electrode arm [34].....	41

Figure 2-12 Device for adding adjustable friction [35].....	41
Figure 2-13 Changing welding head moving mass [34]	42
Figure 2-14 Schematic representation of secondary current path [37]	43
Figure 2-15 Sketch diagram of characteristic parameters extracted [39].....	44
Figure 2-16 Element configuration and governing equation used in Gould’s model [42]	46
Figure 2-17 Contacting surfaces with microasperities and surface waviness [60]	48
Figure 2-18 Comparison of contact resistance variation as a function of pressure at room temperature [60].....	49
Figure 2-19 Contact resistance-temperature-pressure diagram according to [60]	49
Figure 2-20 Schematic setup of material tests on Gleeble [70]	51
Figure 2-21 Coupling scheme of models with contact [71].....	52
Figure 2-22 Sandwich upsetting aluminium–brass–aluminium in different contact situations [72]	52
Figure 2-23 Sandwich upsetting brass–aluminium–brass in different contact situations [72]	52
Figure 2-24 Representing model used by Chen [76].....	53
Figure 2-25 Punch, Die and projection geometry according to Harris & Riley [13].....	56
Figure 2-26 Electromagnetic stirring in weld nugget [80].....	57
Figure 2-27 Advised setup for cross tube projection welding [82].....	58
Figure 3-1 Thesis objectives flowchart graph	62
Figure 4-1 LTS sensor.....	68
Figure 4-2 Principle of operation	69
Figure 4-3 LVDT sensor	70
Figure 4-4 Operation principle LVDT	70
Figure 4-5 Coil coupling in LVDT	71
Figure 4-6 Left Positioning of ferrite core in LVDT	72
Figure 4-7 Right positioning of ferrite core in LVDT	72
Figure 4-8 Influence of welding current on LVDT displacement signal	73
Figure 4-9 Head of LVDT sensor	74
Figure 4-10 Plastic ball joint connected to upper end of LVDT	74
Figure 4-11 Comparison of LTS and LVDT displacement signals	75
Figure 4-12 Polytec compact laser vibrometer	76
Figure 4-13 PEM UK Rogoflex current transducer	78
Figure 4-14 Integrator added to output of Rogowski coil.....	79
Figure 4-15 Miyachi MM-601A load cell.....	81
Figure 4-16 Strain gage attached to object.....	81
Figure 4-17 Dewetron 2010 portable industrial data-acquisition system	83
Figure 4-18 Schematic view of variable resistance.....	85
Figure 4-19 Photograph of variable resistance.....	86
Figure 5-1 Flowchart experimental procedure	88
Figure 5-2 Mass – damper – system (moving welding head)	89
Figure 5-3 Mass-damper system with reaction force	90
Figure 5-4 Mass – spring – damper system (stationary welding head).....	91
Figure 5-5 Deformation of pin before fracture.....	93
Figure 5-6 Operation principle of fracture test, A, B and C.....	96
Figure 5-7 A, B and C Laboratory Fracture test rig on different machines	96
Figure 5-8 Closed design of Fracture test	97
Figure 5-9 High speed camera images from fracture test (sequential images A to F).....	98
Figure 5-10 Continuation of high speed camera images from fracture test (sequential images G to L)	99
Figure 5-11 Fracture test with current bypass	100

Figure 5-12	Fracture test with application of lateral force.....	101
Figure 5-13	Operation principle of explosion test, A, B and C	102
Figure 5-14	Mechanical test procedure	103
Figure 5-15	Bearing ball positioned on intermediate layer.....	104
Figure 5-16	Indentation in intermediate layer.....	104
Figure 5-17	Bearing ball positioned in between electrodes with two intermediate layers	105
Figure 5-18	Different supporting elements for explosion test	106
Figure 5-19	Clamping device for production of support elements for explosion tests	107
Figure 5-20	Clamping device mounted on Wire eroding EDM.....	108
Figure 5-21	Explosion test setup with counter LED lighting.....	109
Figure 5-22	Test setup for stick-slip measurements.....	110
Figure 5-23	Test procedure for stick-slip measurements	111
Figure 5-24	Application of lateral force on welding head	112
Figure 5-25	AWL moving welding head coupling system (spring and compression limiter).....	113
Figure 5-26	Moving welding head schematic block diagram (left) + corresponding components (right)	114
Figure 6-1	Screenshot of measured signals in a fracture test.....	120
Figure 6-2	Screenshot of zoom at point of fracture	121
Figure 6-3	Velocity and pressure signal from fracture in Flexpro.....	121
Figure 6-4	Velocity signal, calculated acceleration and displacement signals in Flexpro... ..	122
Figure 6-5	AWL welding head velocity signals as response to fracture tests.....	123
Figure 6-6	AWL fracture test velocity signals group A (~0,75kN actuator force).....	123
Figure 6-7	AWL fracture test velocity signals group B (~1,4kN actuator force)	124
Figure 6-8	AWL fracture test velocity signals group C (~3kN actuator force)	124
Figure 6-9	AWL fracture test velocity signals group D (~5kN actuator force).....	124
Figure 6-10	Fracture test results AWL equipped WITH spring.....	126
Figure 6-11	Fracture test results AWL NO spring	126
Figure 6-12	AWL welding head velocity signals as response to exploding button tests.....	128
Figure 6-13	AWL welding head velocity signals as response to exploding ball tests	128
Figure 6-14	Exploding button test results AWL equipped WITH spring	130
Figure 6-15	Exploding ball test results AWL equipped WITH spring	130
Figure 6-16	Comparison AWL velocity response to free fracture and exploding button test.....	131
Figure 6-17	Comparison AWL displacement response to free fracture and exploding button test	131
Figure 6-18	AWL velocity response to exploding button test WITH spring mounted.....	132
Figure 6-19	AWL velocity response to exploding button test NO spring mounted	132
Figure 6-20	Velocity and current signal, NO spring, 510N	133
Figure 6-21	Velocity and current signal, NO spring, 660N	133
Figure 6-22	Velocity and current signal, NO spring, 891N	134
Figure 6-23	Velocity and current signal, NO spring, 1155N	134
Figure 6-24	Exploding button test results AWL equipped with and without spring	135
Figure 6-25	Velocity response on fracture and explosion tests	136
Figure 6-26	Lateral (horizontal) displacement of moving welding head assembly, manual actuation	137
Figure 6-27	Lateral (horizontal) displacement of moving welding head assembly, fracture test at 2677N	138
Figure 6-28	Lateral (horizontal) motion of upper part of welding cylinder, fracture test at 2930N	138
Figure 6-29	Downward (vertical) motion of upper part of welding cylinder, fracture test at 4888N	139

Figure 6-30 Slopes in AWL velocity response to explosion test at 891N, NO connecting spring.....	140
Figure 6-31 AWL velocity response to explosion test at 891N, NO connecting spring.....	140
Figure 6-32 AWL velocity response to explosion test at 1406N, NO connecting spring.....	141
Figure 6-33 AWL velocity response to explosion test at 1705N, NO connecting spring.....	141
Figure 6-34 AWL velocity response to explosion test at 694N, WITH connecting spring ...	142
Figure 6-35 AWL velocity response to explosion test at 1564N, WITH connecting spring .	142
Figure 6-36 AWL velocity response to explosion test at 1864N, WITH connecting spring .	143
Figure 6-37 Reduction in actuator force caused by the welding current following explosion tests	143
Figure 6-38 Displacement responses fracture tests 900N with and without application of current	144
Figure 6-39 Displacement response fracture test 898N including current signal	144
Figure 6-40 Measuring displacement responses with and without current flowing	145
Figure 6-41 Displacement responses fracture test 2507N with and without lateral force on welding head	146
Figure 6-42 Displacement responses fracture test 3333N with and without lateral force on welding head	147
Figure 6-43 Displacement responses fracture test 5000N spring/NO spring in actuator assembly and without lateral force on welding head	147
Figure 6-44 Results stick-slip measurements on AWL multi purpose spot/projection welder	149
Figure 6-45 Photo of material splashing away during exploding button test on AWL	150
Figure 6-46 Exploding ball test AWL (part 1)	151
Figure 6-47 Exploding ball test AWL (part 2)	152
Figure 6-48 Exploding ball test AWL (part 3)	153
Figure 6-49 Exploding ball test AWL (part 4)	154
Figure 6-50 Current and velocity signal from exploding ball test on AWL	155
Figure 6-51 Current and velocity signal from exploding ball test on AWL (zoom).....	155
Figure 6-52 Cross-section through intermediate layers after explosion test (ball bearing) ...	156
Figure 6-53 Exploding button test AWL (part 1).....	157
Figure 6-54 Exploding button test AWL (part 2).....	158
Figure 6-55 Exploding button test AWL (part 3).....	159
Figure 6-56 Exploding button test AWL (part 4).....	160
Figure 6-57 Exploding button test AWL (part 5).....	161
Figure 6-58 Current and velocity signal from exploding button test on AWL	162
Figure 6-59 Current and velocity signal from exploding button test on AWL (zoom)	162
Figure 6-60 Cross-section through intermediate layers after explosion test (button)	163
Figure 6-61 Fracture test results on PECO roll membrane machine.....	164
Figure 6-62 Processed results fracture and explosion tests on ARO pneumatic.....	165
Figure 6-63 Evaluation of 5mm x 1mm diameter AISI 304 filler wire as exploding element	166
Figure 6-64 Setup for high speed video recording on ARO pneumatic.....	167
Figure 6-65 Positioning of wire and button without intermediate layers.....	167
Figure 6-66 Exploding button test ARO pneumatic, no intermediate layers (part 1)	168
Figure 6-67 Exploding button test ARO pneumatic, no intermediate layers (part 2)	169
Figure 6-68 Processed results explosion tests on Mc Gregor μ -welding head	170
Figure 6-69 High speed video recording setup for exploding button test on Mc Gregor machine.....	171
Figure 6-70 Exploding button test on Mc Gregor (part 1)	172

Figure 6-71 Exploding button test on Mc Gregor (part 2)	173
Figure 6-72 Exploding button test on Mc Gregor (part 3)	174
Figure 6-73 Exploding button test on Mc Gregor (part 4)	175
Figure 6-74 Exploding button test on Mc Gregor (part 5)	176
Figure 6-75 Exploding button test on Mc Gregor (part 6)	177
Figure 6-76 Current, velocity and displacement signal from exploding button test on Mc Gregor	178
Figure 6-77 Current, velocity and displacement signal from exploding button test on Mc Gregor (zoom).....	178
Figure 6-78 Fronius Deltaspot process tape with 0.8mm x 1.2mm diameter button	178
Figure 6-79 Button and intermediate layers positioned between electrodes on Mc Gregor ..	179
Figure 7-1 AWL piston seal	185
Figure 8-1 Temperature time curve of a node in the HAZ calculated with Sorpas®	190
Figure 8-2 Example of machine parameter setting and resulting current flow	191
Figure 8-3 Hardness measurements, weld with good (left) and useless (right) machine parameter settings	191
Figure 8-4 Prototype μ -surf scan (left) and series production projection (right).....	192
Figure 8-5 Dimensions of test pieces	193
Figure 8-6 Projection design without groove	193
Figure 8-7 Projection design with groove	194
Figure 8-8 Cross-sectional geometry after welding	194
Figure 8-9 Clamping device for mechanical testing	194
Figure 8-10 New projection design in casted stainless steel handles for cookware	195

List of tables

Table 1-1	ARO welding technologies production data 2009	24
Table 2-1	Proposed set up of machine parameters for best machine behaviour [19]	35
Table 2-2	Influences on dynamic mechanical machine properties [26].....	37
Table 2-3	Dimensions according to Harris & Riley [13].....	56
Table 4-1	Specifications LMI LTS displacement sensor	69
Table 4-2	Specifications LVDT	72
Table 4-3	Specifications Polytec CLV 1000 laser vibrometer.....	77
Table 4-4	Specifications PEM UK Rogowski current coils.....	79
Table 4-5	Specifications Miyachi MM601A load cell.....	82
Table 4-6	Specifications Dewetron 2010 data-acquisition	84
Table 5-1	Test setup for free fracture tests on AWL machine	115
Table 5-2	Test setup for explosion tests on AWL machine	116
Table 5-3	Test setup for fracture tests with application of current	116
Table 5-4	Test setup for fracture tests with application of lateral force	117
Table 5-5	Test setup for friction measurements on AWL machine	117
Table 5-6	Test setup for free fracture tests on PECO roll membrane machine	118
Table 5-7	Test setup for free fracture and explosion tests on ARO pneumatic	119
Table 5-8	Test setup for exploding button tests on Mc Gregor μ -resistance welding head.	119
Table 6-1	Results fracture tests on AWL multi-purpose spot/projection welder.....	125
Table 6-2	Results exploding ball & button tests on AWL multi-purpose spot/projection welder	129
Table 6-3	Results exploding button tests on AWL machine with and without spring mounted.....	135
Table 6-4	Δ acceleration explosion test 891N, no spring.....	140
Table 6-5	Δ acceleration explosion test 1406N, no spring.....	141
Table 6-6	Δ acceleration explosion test 1705N, no spring.....	141
Table 6-7	Δ acceleration explosion test 694N, with spring.....	142
Table 6-8	Δ acceleration explosion test 1564N, with spring.....	142
Table 6-9	Δ acceleration explosion test 1864N, with spring.....	143
Table 6-10	Results stick-slip measurements on AWL	149
Table 6-11	Results fracture tests on PECO roll membrane	164
Table 6-12	Results fracture- and exploding wire tests on ARO pneumatic	165
Table 6-13	Results explosion tests on Mc Gregor μ -resistance welding head	170
Table 6-14	Overview of machine data on all machines tested.....	180
Table A-1	206

Nomenclature

a	Acceleration	mm/s ²
a_1	Acceleration while current is flowing	mm/s ²
a_2	Acceleration while current is interrupted	mm/s ²
b	Damping factor	kg/s
c	Stiffness factor	N/m
D	Diameter	mm
D_i	Internal diameter	mm
D_u	External diameter	mm
e	Throat gap	mm
E_a	Impact energy	J
F	Force	N
F_{fracture}	Force at fracture or explosion	N
F_{max}	Electrode force	N
F_r	Reaction force	N
G	Earth acceleration	9,81m/s ²
H	Height	mm
h	Recess height	mm
I	Current	kA
I_{20}	Short circuit secondary current	kA
I_{2cc}	Max. Secondary current in short circuit	kA
I_w	Welding Current	kA
k	Spring constant	N/m
l	Throat depth	mm
m	Mass	kg
P_1	Admission pressure	bar
Q	Generated heat	J
R	Ohmic resistance	μohm
S_{50}	Nominal power at 50% duty cycle	kVA
S_{max}	Maximum welding Power	kVA
S_n	Nominal power	kVA
t	Time	s
U_{1N}	Supply voltage	V
U_{20}	Secondary no load alternate voltage	V
U_a	Auxiliary voltage	V
v	Velocity	m/s
x	Distance	m
ζ	Damping ratio	
μ	Magnetic permeability	H/m
σ	Material fracture stress	N/mm ²
ρ	Density	kg/m ³
ω	Natural frequency	Hz
ω_0	Undamped natural frequency	Hz
ω_d	Damped natural frequency	Hz

Abbreviations

AWL	Aarding Weerstand Lastechniek (machine constructor)
AWS	American Welding Society
COTS	Commercial Off The Shelf
DSP	Digital Signal Processor
DVS	Deutsches Verband für die Schweisstechnik
EDM	Electrical Discharge Machining
EWS	Electro Slag Welding
FEA	Finite element analysis
FEM	Finite Element Modelling
H&R	Harris and Riley
HID	High Intensity Discharge
HIP	Hot Isostatic Pressing
HSLA	High Strength Low Alloy
IIW	International Institute of Welding
IPC	Industrial Portable Computer
LB	Laser Beam
LTS	Laser Twin displacement Sensor
LVDT	Linear Variable Differential Transducer
MAG	Metal Active Gas
MBR	Motor Body Repair
MFDC	Medium Frequency Direct Current
MIG	Metal Inert Gas
MMA	Manual Metal Arc
PSD	Position Sensitive Detector
RMS	Root Mean Square
RSW	Resistance Spot Weld
RWMA	Resistance Welding Manufacturers Association
SAW	Submerged Arc Welding
SORPAS	Simulation of Resistance Projection And Spot Welding
TIG	Tungsten Inert Gas
TWI	The Welding Institute

1 Introduction

Resistance welding covers a wide range of specific processes, mainly used for highly automated or even fully mechanised welding applications, the majority in mass production. All these processes, except one (ESW, electroslag welding), need a mechanical clamping and pressurising system to compress the workpiece areas intended to be welded prior to welding. Thus, these welding applications are categorised as resistance pressure welding processes. (see Figure 1-1)

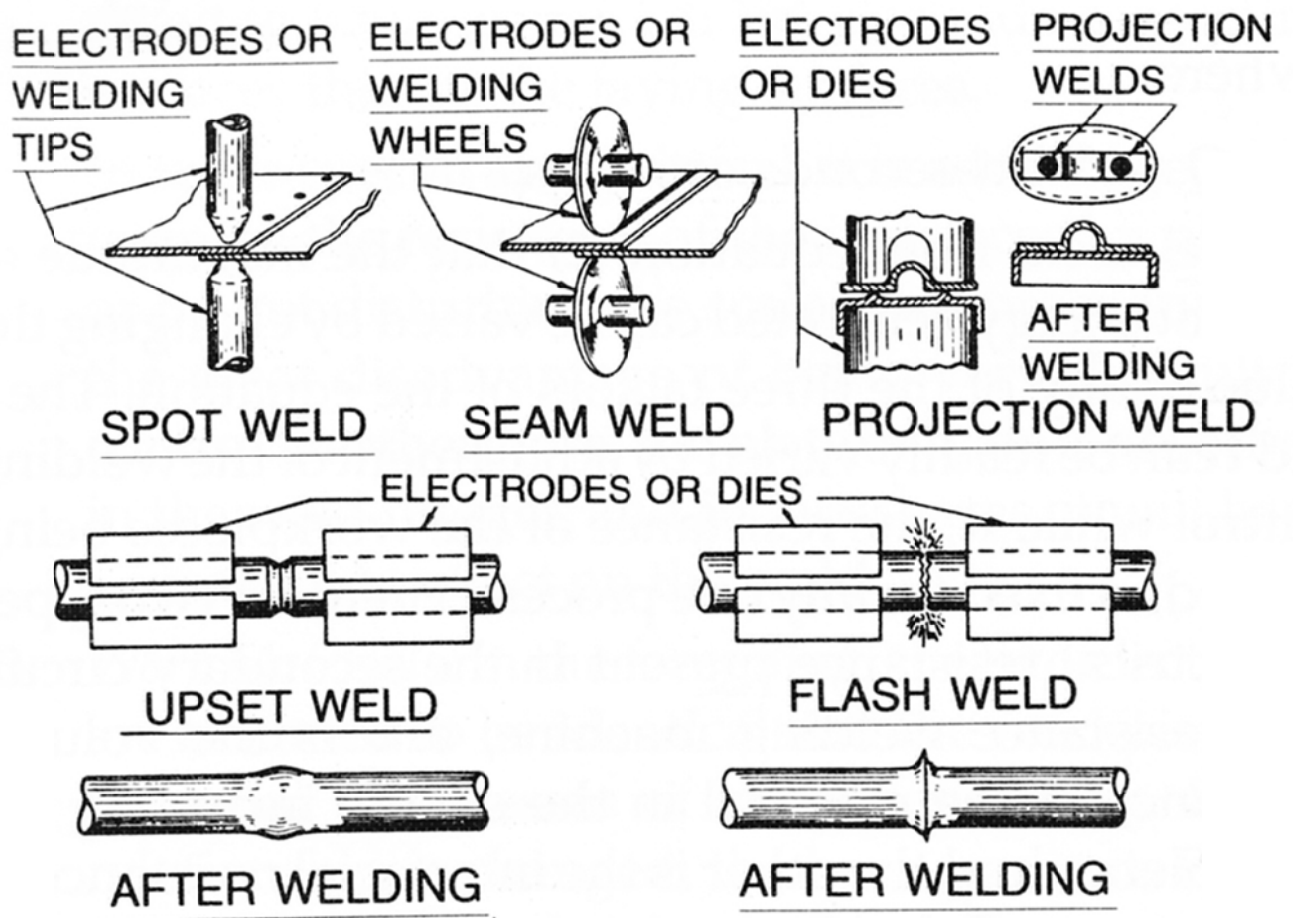
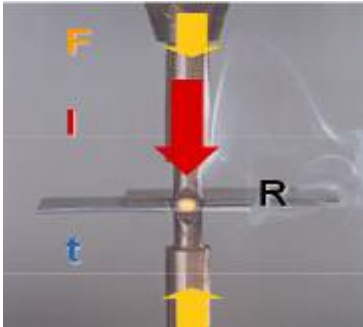


Figure 1-1 Principal types of resistance welds
(RWMA Resistance Welding Manual 4th edition)

In Resistance Spot Welding, passage of a relatively high welding current I [kA] throughout a locally compressed workpiece area (by means of an electrode force F [daN]) during a properly defined period of time t [cyc, ms] heats this area due to resistive heating following Joule's law (Figure 1-2),

$$Q(t) = \int_0^T R(t) \cdot i^2(t) \cdot dt$$



with:

- Q = the heat generated [J];
- R = the ohmic resistance [μohm];
- i = the welding current [A];
- t = time [s];
- T = total weld time [s];

Figure 1-2 Principle of resistance spot welding

As the momentary value of both welding current and resistance changes continuously throughout the duration of the welding time, the integral over the welding time needs to be calculated to get a correct value of the heat generated in the welding area.

Only a fraction of the generated heat serves to create a molten weld nugget in between the workpieces that solidifies during cooling down under maintained pressure by the electrodes on the workpieces. The rest of the heat generated disappears into the electrodes and their cooling system, the workpieces and the surrounding atmosphere.

The three most commonly known processes, also covering the majority of applications, are spot-, seam- and projection-welding. These three processes and their variants are extremely suited and popular to serve as a means of jointing in assembly of overlapping, mainly plate-like structures.

Since energy necessary for making a good weld (Energy $\sim R \cdot I^2 \cdot t$) theoretically can be generated within an infinite range of combinations of welding current and welding time (Energy $\sim R \cdot I^2 \cdot t = R \cdot (I/2)^2 \cdot 4t = R \cdot (I/3)^2 \cdot 9t, \dots$) at a chosen specific force level, setting up welding parameters seems difficult and is mainly based on practical experience. Of course the reasoning above is incorrect, since energy losses will lead to a lower current level where no melting will occur and overheating will lead to an upper current level leading to splash welds.

Values for Welding Force [daN], Welding Current [kA] and Welding Time [cyc, ms] are available in database format, and these values are commonly used to make a base setting to start from. Fine tuning within the parameter range (weldability lobe) can be done in order to optimise towards a specific application according to EN ISO 14327-2004 (Resistance welding – Procedures for determining the weldability lobe for resistance spot, projection and seam welding). Such a weldability lobe covers a range of combinations of welding current and welding time at a specific welding force level that lead to welds with sufficient dimensions, with a lower boundary indicating “stick” welds, and then an area of increasingly growing weld size towards the maximal possible weld size, followed by the upper boundary leading to splash welds. A so called stick weld is a weld that didn't receive enough energy during its resistance welding cycle, resulting in the workpieces 'sticking' together without a molten weld nugget being formed. As a result, the workpieces can be separated again with the application of minimal force on the joint. A splash weld receives excessive energy during its weld pulse, leading to overheating of the molten weld nugget causing the molten metal to

partly vaporise leading to molten metal from the weld nugget to ‘splash’ away with an explosive character. The selection of all auxiliary settings that need to be made are also advised in standards [1], [2] and in publications by user groups (eg. RWMA Resistance Welding Manufacturers Association, Deutsches Verband für die Schweisstechnik, etc.).

Resistance welding is popular due to its interesting advantages:

- High energy efficiency (heat generated at the exact location of the joint);
- High productivity;
- Short cycle times;
- Forgiving (Flexible) accommodating poor mechanical fit up of workpieces to join (compressing force);
- Possibility of imposing a thermal cycle on the workpieces in one single clamping operation (heat treatment and welding in one combined cycle);

Nevertheless, in general, even amongst engineering staff in a production environment using the process on a daily basis for assembly, resistance welding has the image of being rather old fashioned and there has been a trend to replace resistance welding by alternative welding processes that currently boom in popularity (eg. Laser Welding, Arc Welding, Hybrid processes, etc.).

Laser based processes have been introduced in the automotive assembly industry where in several production plants of different constructors, spot welding was massively replaced with laser welding, laser brazing and laser hybrid welding applications [3].

However, after about a decade of practical production experience in automotive body in white assembly, many constructors have (partially) returned to the resistance welding processes because of their specific benefits as stated above, and because of their relatively trouble-free operation and low operational costs in an aggressive production environment.

Another major advantage of the resistance welding processes over any other welding process is the feature that heat necessary for weld formation is generated at the exact location where the joint needs to appear (i.e. in between the workpieces to be joined). This offers the possibility to highly reduce the time to complete a weld resulting in cycle times being competitive over other welding processes. Depending on the sheet thickness, welding times are in the order of a few to a few hundred milliseconds, including clamping and releasing of the workpiece.

Another advantage is the absence of a molten weld pool penetrating from one side through a workpiece, resulting in less aesthetical damage to the workpiece surfaces.

The necessity for a pressurizing or a clamping device in Resistance Pressure welding is obvious and integrated in the physical machine setup of all resistance pressure welding processes.

In addition, modern high strength steels are very sensitive in respect to the thermal cycle they experience during welding. Alternative welding processes, certainly the high energy processes like laser welding, due to their very localised heating, induce a high cooling rate in the weld area. The latter increases the risk of unacceptable mechanical properties of the as-welded assembly [4]. Of all welding processes, it is only resistance welding that offers the possibility to easily influence the thermal cycle forced on to the weld area [5]. Moreover, it is the only process where pre- and post-weld heat treatment can be made in a continuous process cycle and in one single clamping operation, without releasing the workpieces and with the very equipment (electrodes, power source and control system) that is also used to produce the weld.

It is obvious that clamping under a controllable force is a major feature of all resistance pressure welding processes and mechanical behaviour of these force-delivering devices for compressing the workpieces with the welding electrodes is important as they primarily need to fulfil the following demands:

- Fast closure of the electrodes without impact on the workpiece surface;
- Fast follow-up behaviour at workpiece collapse during welding;

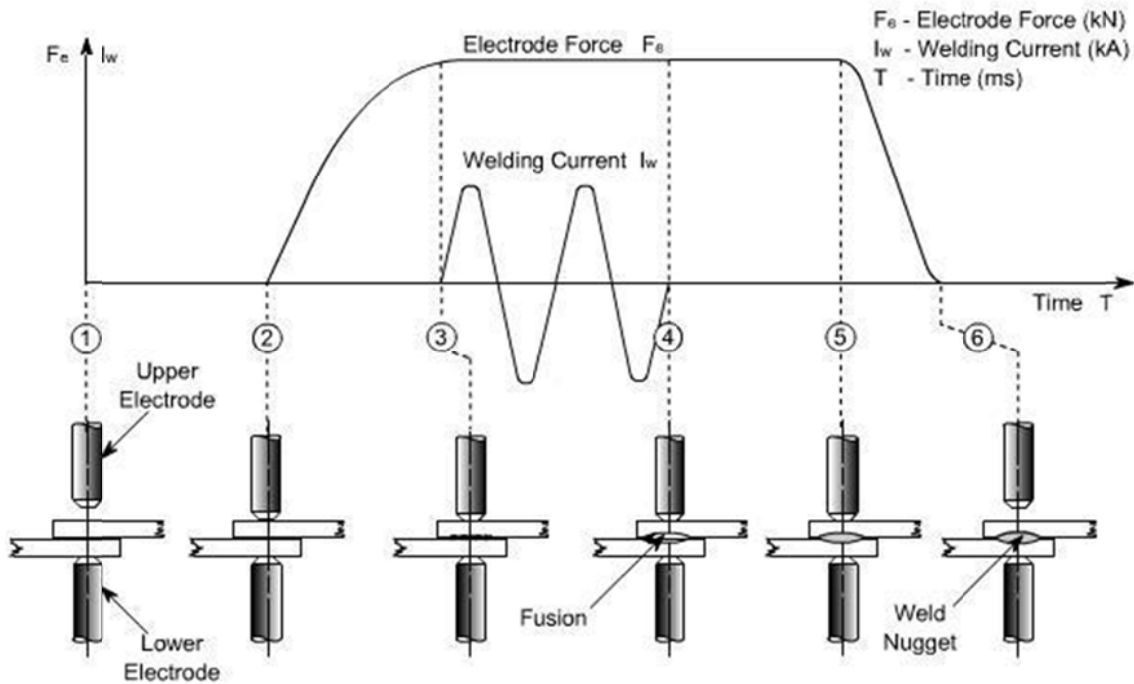


Figure 1-3 General welding cycle of a resistance weld

As can be seen in Figure 1-3, a weld cycle can be divided into a number of stages:

- pre-squeeze stage (1 to 2);
- squeeze stage (2 to 3);
- weld stage (3 to 4);
- hold stage (4 to 5);
- and release stage (5 to 6);

In the pre-squeeze stage, the moving electrode closes towards the workpieces, resulting in contact between the electrodes and the workpieces. The velocity of the electrodes at this very point of impact is very important considering that too high impact energy will result in excessive electrode wear [6]. In the squeeze stage, the electrodes are forced on the workpiece surfaces by means of the force actuating system and this offers the possibility to deform the workpieces to ensure sound contact between them. The latter is a very important feature of resistance welding over other processes. In the weld stage, while force remains on the workpieces, current will be flowing through the electrodes and the workpieces, heating up every part in the secondary weld circuit proportional to the effective resistance present at each point. As can be observed in Figure 1-4, there are generally seven resistances, close to the area where the molten weld nugget is due to be formed, that need to be considered as highly influencing on heat generation and heat transfer in this area.

The resistances presented with a blue symbol represent bulk material resistances, those with a red symbol represent contact resistances.

- R_1 and R_2 : electrode material;
- R_3 and R_4 : contact resistance electrode-workpiece interface;
- R_5 and R_6 : workpiece material;
- R_7 : contact resistance workpiece-workpiece interface;

These resistances of course will change over time, since temperatures will change due to the heat generated in the materials. Normally, at the start of each weld, contact resistance between the workpieces to be welded will be the highest in the circuit, followed by the contact resistances between electrodes and workpiece surfaces. Temperature profile between the electrodes will follow this initial resistance profile and will change to a more uniform profile near the end of the weld time. (see Figure 1-4)

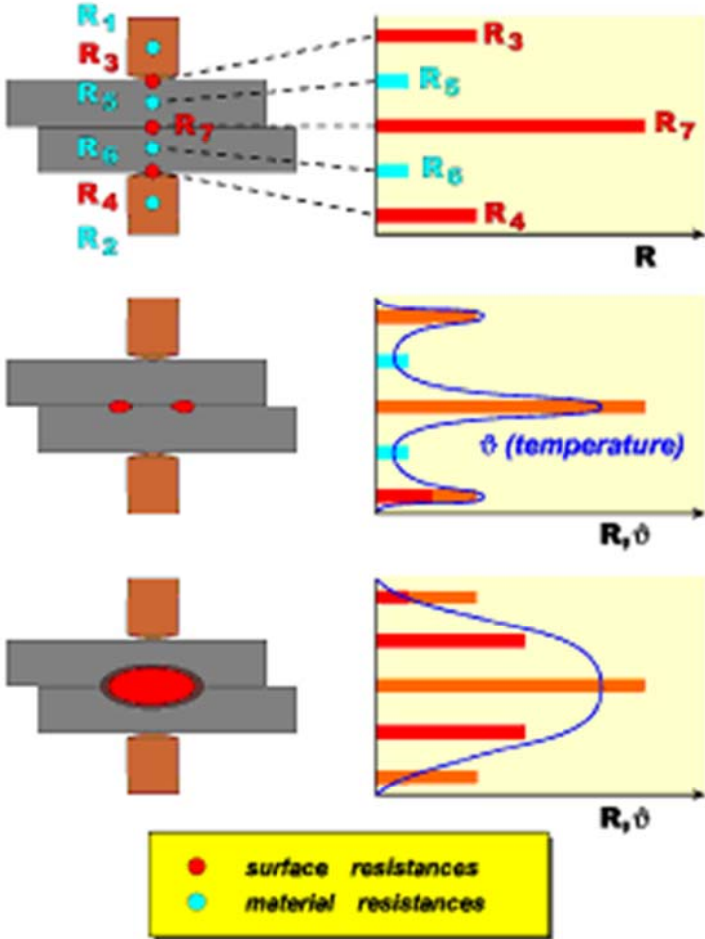


Figure 1-4 Resistances in circuit and resulting temperature distribution
 (Image from IIW MSc in Welding Engineering course material)

In the hold stage, the current is cut off and the produced weld is allowed to solidify and cool down under maintained pressurizing force. This enables the cooler material surrounding the weld nugget to follow the shrinkage of the weld nugget by deforming the surrounding (cooler and less deformable) material. In this way, welds without shrink holes or cracks can be produced. After sufficient holding time, the electrodes release the workpiece and the cycle is complete. It is obvious that in spot- and seam welding, only small deformations are needed to ensure this follow-up of the weld nugget and in practice the mechanical behaviour of the welding head during the closing and follow-up stage in the weld cycle is adequate. There is actually the indenting effect of the welding electrodes into the workpiece surface due to the expanding welding nugget that even forces the welding force to rise rather than to drop.

On the other hand, in projection welding, mechanical behaviour of the pressurising system becomes of outmost importance. In critical applications such as:

- battery cells

- radiator fins, connecting nipples and attachments
- thin-walled (hydroformed) tubes (increasingly important in automotive assembly)
- tubes and/or wires in a cross welding setup
- foils with extreme low thicknesses that need to be welded to massive workpieces, etc.,

only low forces can be applied on the workpieces, and each of these is easy deformable, even at low pressurizing force levels.

The different force actuating systems available for resistance welding machines on the market each have their specific advantages and disadvantages. They all behave slightly differently during the closing and follow-up stage of the welding head. Depending on the physical design of a machines' welding head, a portion of the actuating force is sacrificed for the welding heads' follow-up movement to try and maintain contact during the deformation of the workpiece. In practice this will result in a lower effective welding force.

It is apparent that obtaining knowledge of the mechanical behaviour of the welding head of a specific welding machine is of utmost importance to assess the potential welding situation or to define an optimized workpiece geometry for a specific application.

On the other hand, as a valuable alternative for the "experience and knowledge base" way of dealing with a welding problem, Finite Element Analysis (FEA) modelling can offer great opportunities to understand and solve difficult resistance welding problems, especially in the development of complex projection welding assemblies. However, in order to make correct numerical simulations that mimic reality as closely as possible, accurate data on machine and material behaviour is essential. The more realistic the input data, the more potential the FEA model gains to generate a correct output. The most critical input data is as follows:

- Workpiece and electrode geometry can be defined into the model, together with all relevant electrical and material mechanical properties as a function of temperature.
- Electrical machine specific settings also need to be entered into the program and thus need to be measured and defined.
- Machine specific mechanical parameters:
 - the total lumped mass of machine components
 - moving electrode assembly
 - moving electrode mounting plate
 - the machines' moving mass in its linear bearing
 - the moving mass in the force actuator
 - a portion of the mass of the moving fixed current leads attached to the electrode mounting plate;
 - maximum acceleration attainable by the moving electrode at a specific actuator mechanical force level
 - maximum velocity reached by the moving electrode after a specific displaced distance at a preset actuator mechanical force level.

Generating this essential data, in order to enable to correctly input it in an FEA model demands the development and construction of accurate test equipment and procedures that can be used in-situ in a running production environment. The use of such test equipment and procedures will provide a major advance in optimising resistance welding setups in a wide range of difficult applications and it could enlarge the applicable working range of resistance welding as a jointing technology towards more difficult, complex and new applications. This test equipment and procedures would have to be capable to generate and reproduce unambiguous data as accurate as possible and should be applicable in an easy and non disturbing way in every working production environment on whatever resistance welding process in use.

The latter issue is important, since it necessitates bringing measuring and assessment equipment out of the laboratory scale into a working industrial production environment.

In summary, knowledge of machine kinematics is essential to accurate modelling of projection welds involving low actuator forces. The machine kinematics can then be used as a direct input to Finite Element Modelling programmes and to influence machine design.

This project has a series of major objectives, all associated with collecting accurate machine specific data for resistance welding machines. This includes:

- Development of measuring techniques capable of being used in situ in a production environment;
- Development of a universal, solid state electrical loading system and a test procedure for resistance welding machine electrical measurements, capable of being used in situ;
- Development of a mechanical test and a test procedure for resistance welding machine mechanical measurements, capable of being used in situ;
- Investigation of the effects that specific machine components have on the machines' mechanical behaviour;
- Investigation of the effects of programmed welding force on the resulting mechanical behaviour on different actuator systems;
- Investigation of the effect of welding current on the machines' mechanical behaviour;

As a higher general goal, increasing awareness with development and production engineers regarding the capabilities resistance welding can offer, namely a fast and reliable technique for joining complex assemblies in state-of-the-art materials, is a major objective to reach with the aid of increased understanding of a specific practical machine configuration and its resulting mechanical behaviour.

1.1 Origin of resistance welding

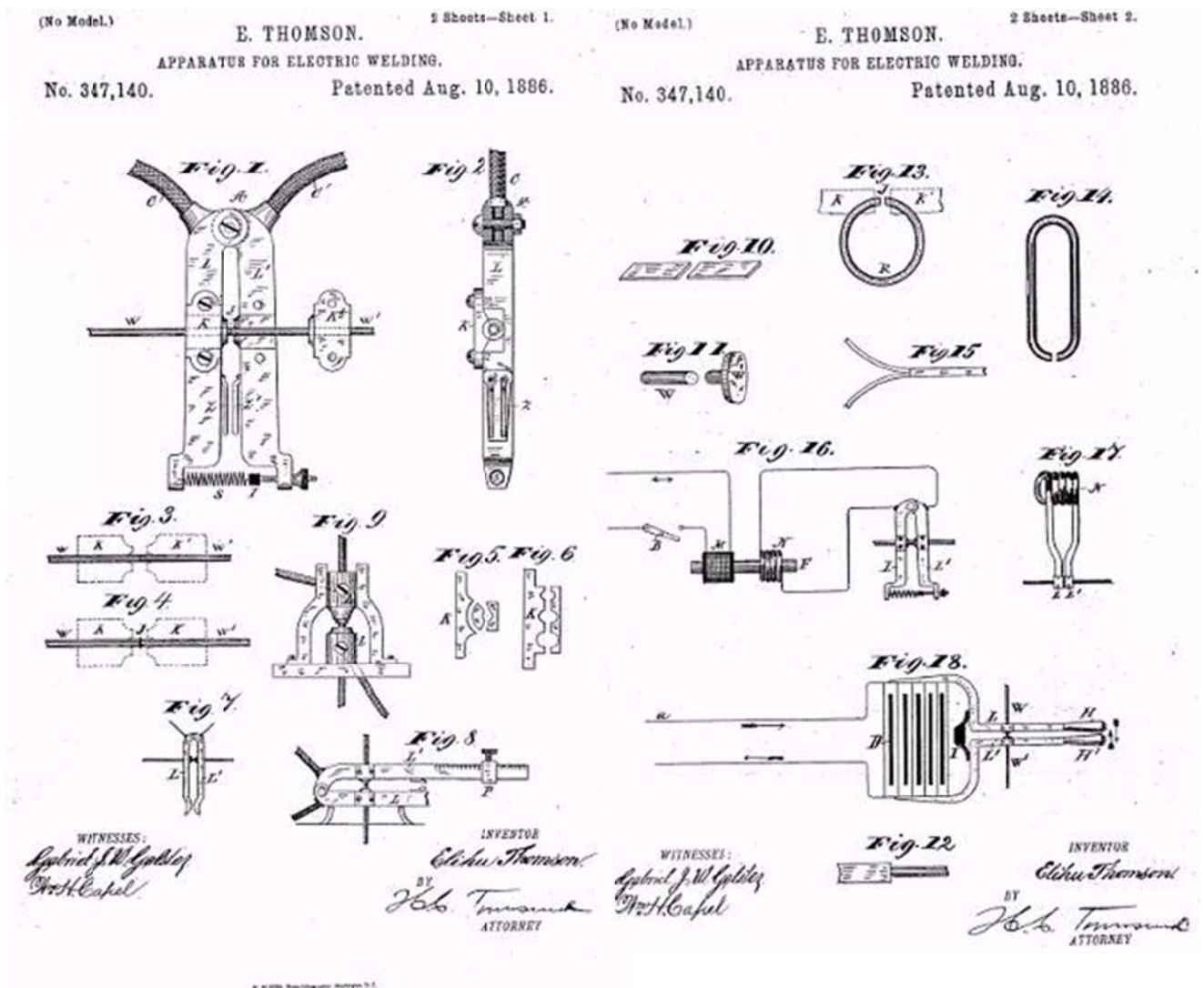


Figure 1-5 Drawings of US 347140 by Elihu Thomson

Resistance welding seems so obvious, especially with hindsight. However, it would be good to give the credit for inventing the use of electricity flowing through metallic materials thus leading to heating of all resistances built up in the circuit to Elihu Thomson (1853-1937).

He was born in Manchester on March 29, 1853 of a Scotch father, Daniel and an English mother, Mary Rhodes and the family emigrated (due to scarcity of work in England in that era) to America in 1858, settling in Philadelphia.

Elihu Thomson applied his genius largely toward harnessing electricity for the work and comfort of man. In 1879, Thomson invented and patented a three coil arc dynamo (US 219157), the first three phase generator, which was the basis of solving the problem of generating adequate current to supply applications with high demands for energy. This generator is now on display in the Smithsonian Institution and commonly known as the 'bakery machine' because of its use for lighting a large bakery in Philadelphia. It was that machine upon which the later Thomson-Houston Electric Company (founded in 1882) was based. Thomson originated dozens of patents in arc lighting systems. The Thomson-Houston Electric Company merged in 1892 with the Edison General Electric Company. This merger

allowed Professor Thomson to give undivided attention to research and technical development thus demonstrating the value of industrial research.

Some of his inventions are well known also in arc welding, like constant current transformers including a magnetic leakage shunt (1889) and a movable secondary (1894). His most important invention in relation to this thesis is his 'process of electric welding' (1886) (US 347140) whereby the welded surfaces were fused and united by the heat developed on account of the resistance in the contact between them. Professor Thomson describes the genesis of this invention as follows:

"While preparing a lecture on Electricity (one of a course of five) at the Franklin Institute at Philadelphia, early in 1877, I had the temerity to pass the discharge of a Leyden battery through the fine wire secondary of a Ruhmkorff induction coil, while the primary coil of quite coarse wire had its terminals resting together in contact. As the Ruhmkorff was my own, one I had made, I could take the risk of breaking down the insulation. On the passage of the condenser spark of about 35 mm. length, a bright flash appeared at the ends of the heavy primary in contact, and I afterward found them firmly welded together. This suggested to me the possibility of electric welding, and later, about 1885, as soon as opportunity afforded, I built the first electric welder, using a transformer to step down to a very short and heavy secondary between the terminals of which, by suitable clamps, the pieces to be welded were held in juxtaposition or contact. The first trials of this apparatus were highly successful, and welds were made not only between pieces (bars) of the same metal, but many different metals were so united."

Figure 1-5 Drawings of US 347140 by Elihu Thomson gives an impression of one of the earliest patents (US 347140) relating to resistance welding belonging to Professor Thomson.

The drawings, description and claims of this patent shows us a very basic form of upset welding of bar, plate and/or tube, equipped with features as force, current, voltage and time setting.

Deeper reading of dozens of welding related of his patents show the evolution in application oriented thinking by Professor Thomson, describing features to enable production of endless band saw blades, valve stems, chain links, etc...

Clearly, resistance welding processes such as spotwelding, projection welding, seam welding, butt or upset welding, flash butt welding and high frequency welding originate out of the inventions of Professor Thomson.

1.2 Overview of resistance welding processes

BS EN 14610 - 2004 “Welding and allied processes – Definitions of metal welding processes”, actually based on the earlier German standard DIN 1910, divides the metal welding processes into two main groups, namely fusion and pressure welding processes.

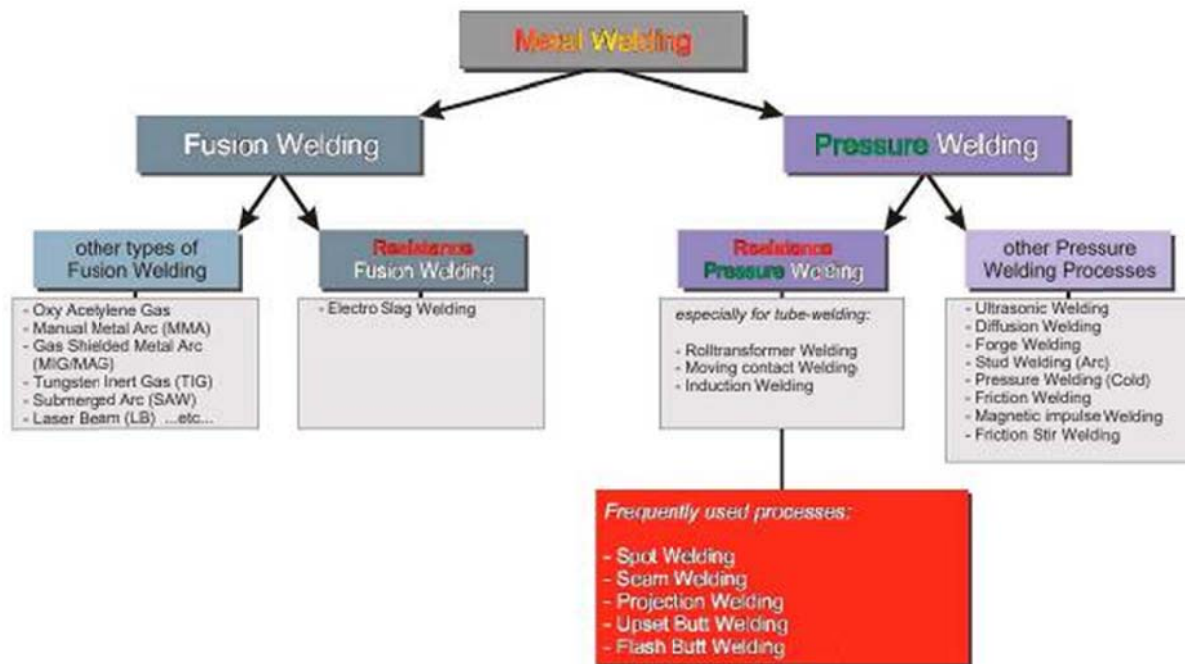


Figure 1-6 Overview of welding processes according to BS EN 14610 - 2004
(Image from IIW MSc in Welding Engineering course material)

However, the processes aimed at in the context of this thesis are all found in the group of the pressure welding processes (Figure 1-6), comprising the following processes:

Spot welding, seam welding, projection welding, upset butt welding and flash butt welding.

In the following section, the major resistance welding processes are briefly discussed as they are categorised in BS EN 14610.

1.2.1 Spot welding

Spot welding is used in two basic setups, namely ‘direct’ (Figure 1-7), where electrodes are positioned on both sides of the overlap to be welded and ‘indirect’ (Figure 1-8), leaving both electrodes on one side of the overlap to be welded.

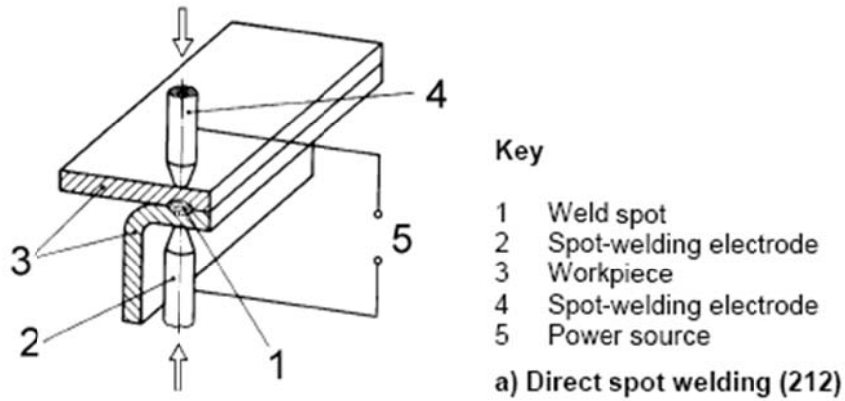


Figure 1-7 'Direct' spot welding (ISO 669)

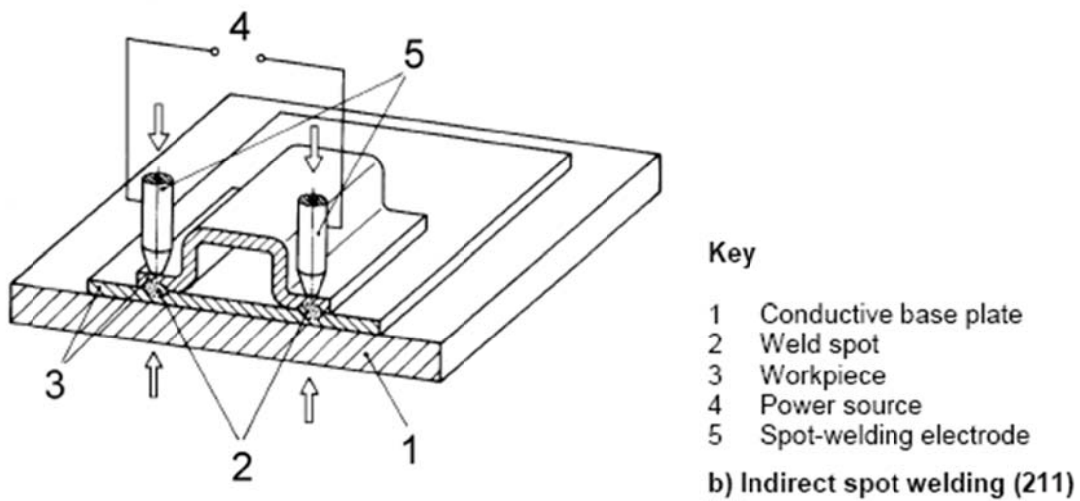


Figure 1-8 'Indirect' spot welding (ISO 669)

The 'direct' variant of the process is the most commonly used and known, offering the optimal conditions to achieve stability in the welding result. The welding current through the weld spot to be made suffers from shunting to weld spots already present in the assembly. If possible, a welding application should be designed to be welded in this set up. In its 'indirect' version, the process is also used, often to avoid indentations and thermal marking on one side of the work piece assembly. The 'indirect' variant is nowadays gaining importance due to the increasing use of prefabricated hydroformed beams to be used in automotive assembly.

1.2.2 Seam welding

Seam welding (Figure 1-9) also finds its applications in different set-ups: lap seam welding, mash seam welding, seam welding with strip and foil-butt seam welding

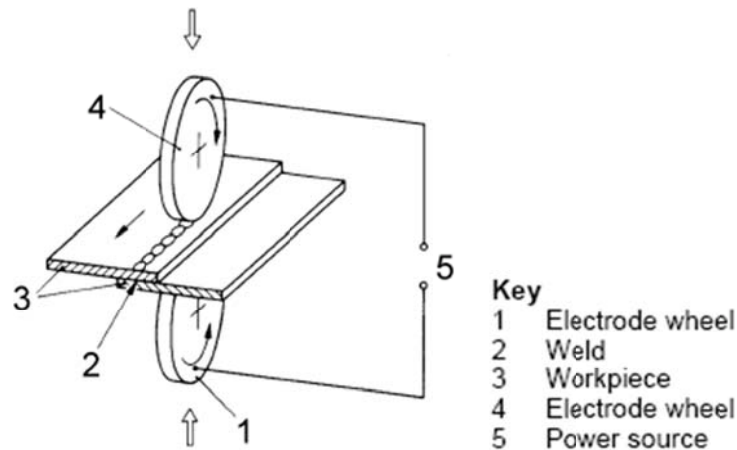


Figure 1-9 Lap seam welding (ISO 669)

As its name suggests, lap seam welding is the version of the process where plates to be welded are effectively overlapping, offering a sufficient area for the welding process to be executed. This version of the process is also the most commonly known in numerous applications.

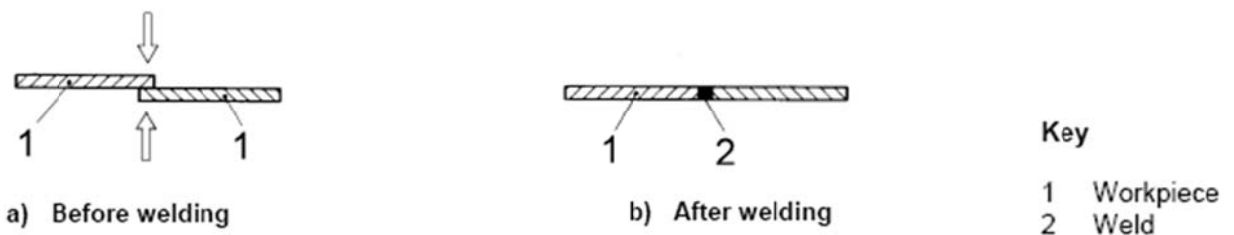


Figure 1-10 Mash seam welding (ISO 669)

Mash seam welding (Figure 1-10) is widely used in assembly of fluid receivers (drums, fuel tanks, etc...)

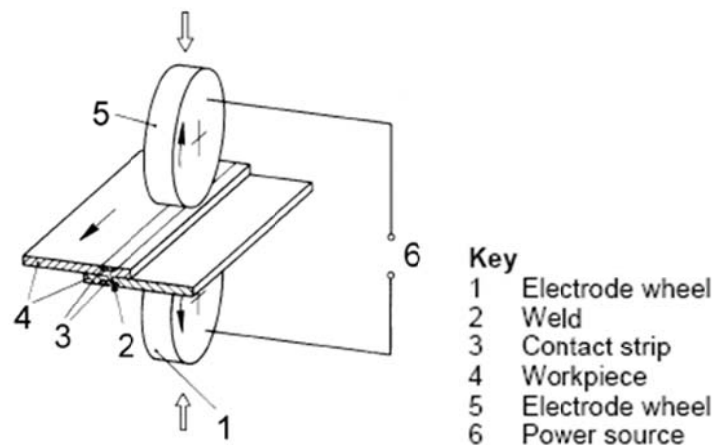


Figure 1-11 Seam welding with strip (ISO 669)

Seam welding with strip (Figure 1-11) is a process variant that is mainly used for increasing electrode wheel life in mass production, especially on coated steels. However, there are applications where the use of the strip is intended to modify the heat balance between the electrode wheels and the workpieces to be welded.

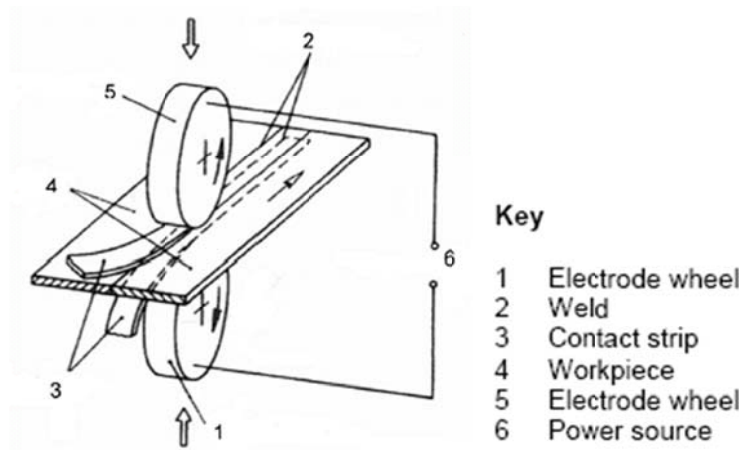


Figure 1-12 Foil butt-seam welding (ISO 669)

The foil-butt seam welding process (Figure 1-12) is also known as ‘conductive heat seam welding’.

1.2.3 Projection welding

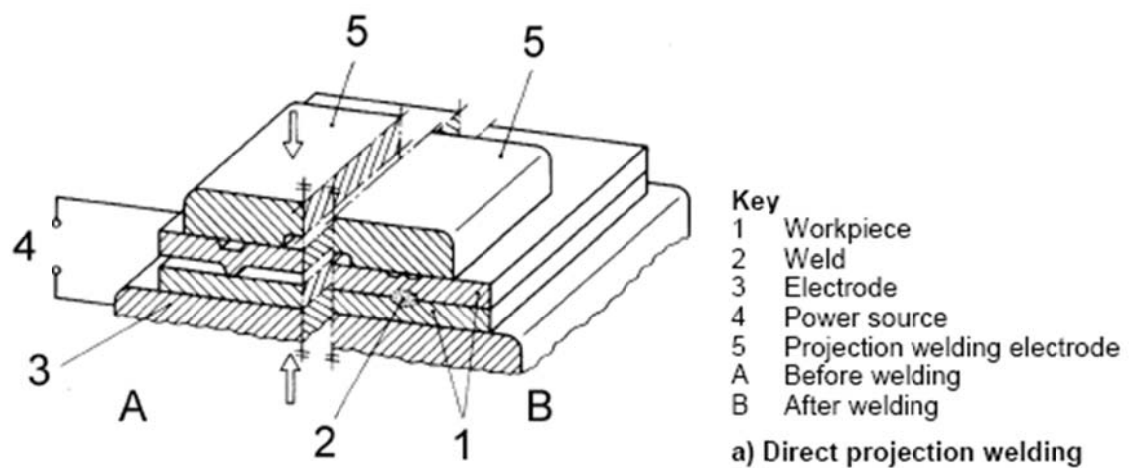


Figure 1-13 Direct projection welding (ISO 669)

Projection welding can as spot welding also be executed in a direct (Figure 1-13) or indirect set up (Figure 1-14).

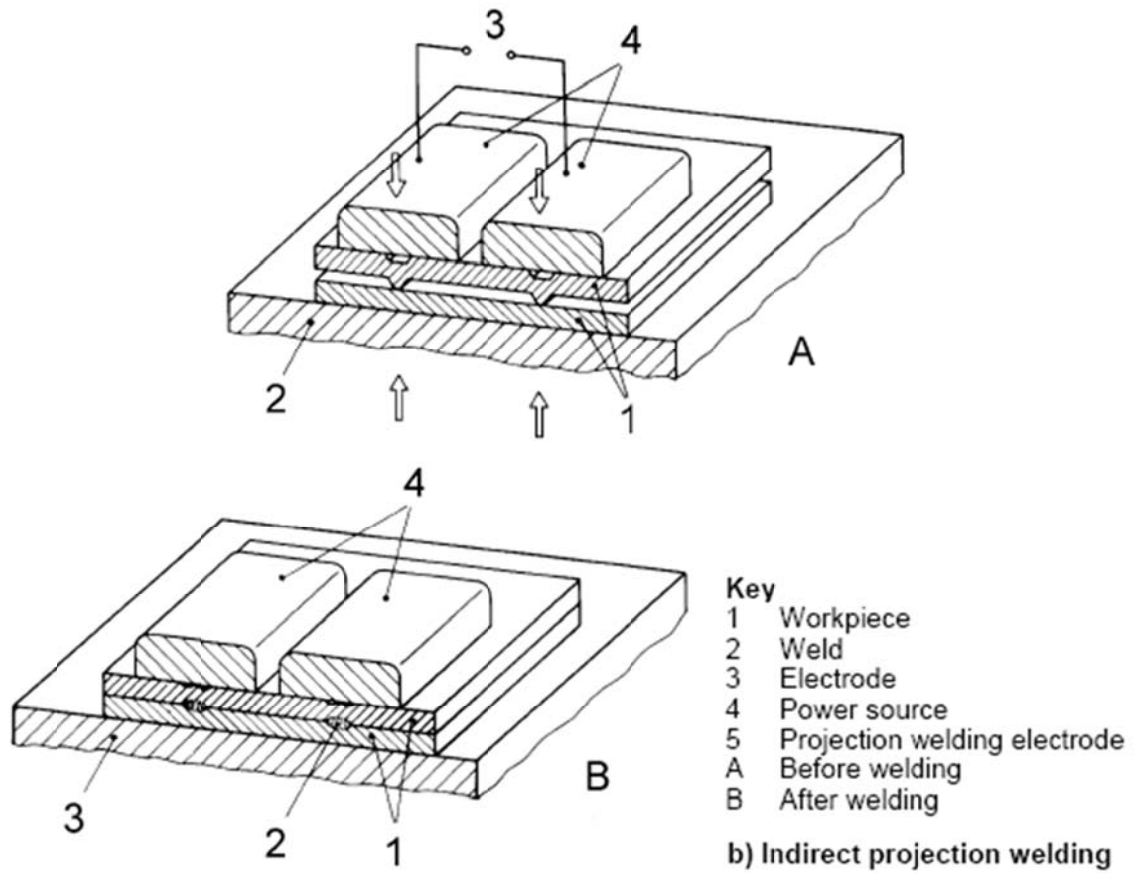


Figure 1-14 Indirect projection welding before and after welding (ISO 669)

Comparable to indirect spot welding, projection welding can also be executed in this set up. Major advantages and disadvantages of the indirect set up remain.

1.2.4 Resistance butt welding

The earlier patents of Elihu Thomson actually describe this welding set up.

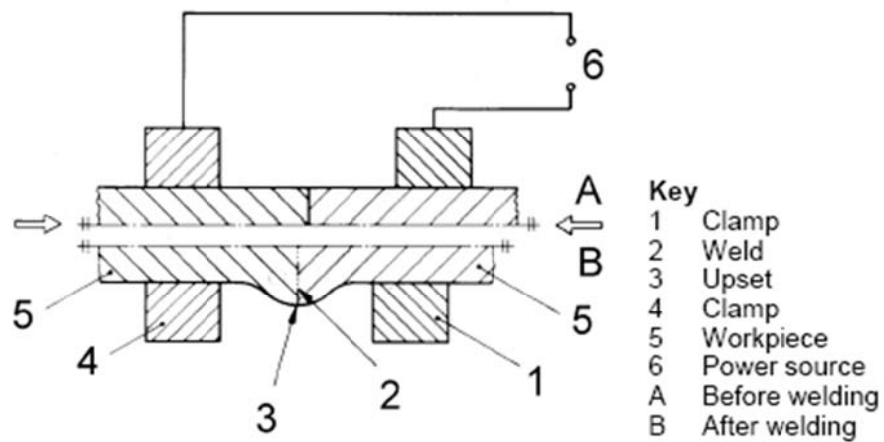


Figure 1-15 Resistance butt welding (ISO 669)

1.2.5 Flash butt welding

Derived from resistance butt welding, this process allows for welding without the need for a powerful electrical mains connection and also the disadvantage of having to securely prepare facing surfaces to be welded is overcome in this process.

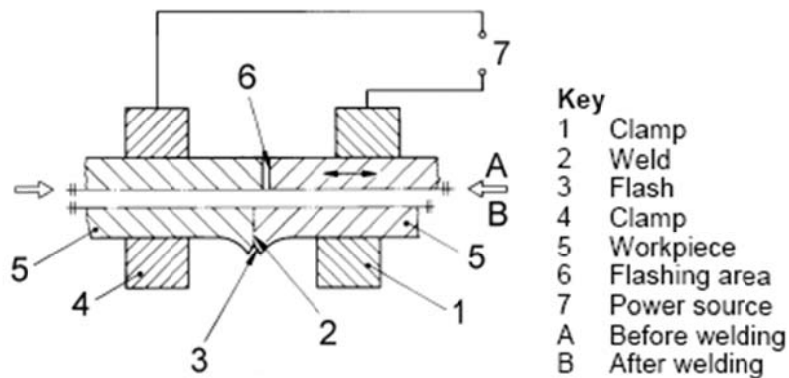


Figure 1-16 Flash butt welding before and after welding (ISO 669)

1.3 Resistance welding machine set up

There are a number of common elements (see Figure 1-17) in every resistance welding machine set up:

- machine frame, the core on which the other elements can be mounted;
- an electrode force actuating device (pneumatic, hydraulic or electro-mechanic) enabling application of a mechanical welding force on the workpieces to be welded;
- a power source enabling current flow in a well defined profile throughout the workpieces;
- a highly conductive electrical circuit to lead welding current to the welding electrodes and through the workpieces to be welded;
- and a control system capable of setting and controlling current, force and time for welding.

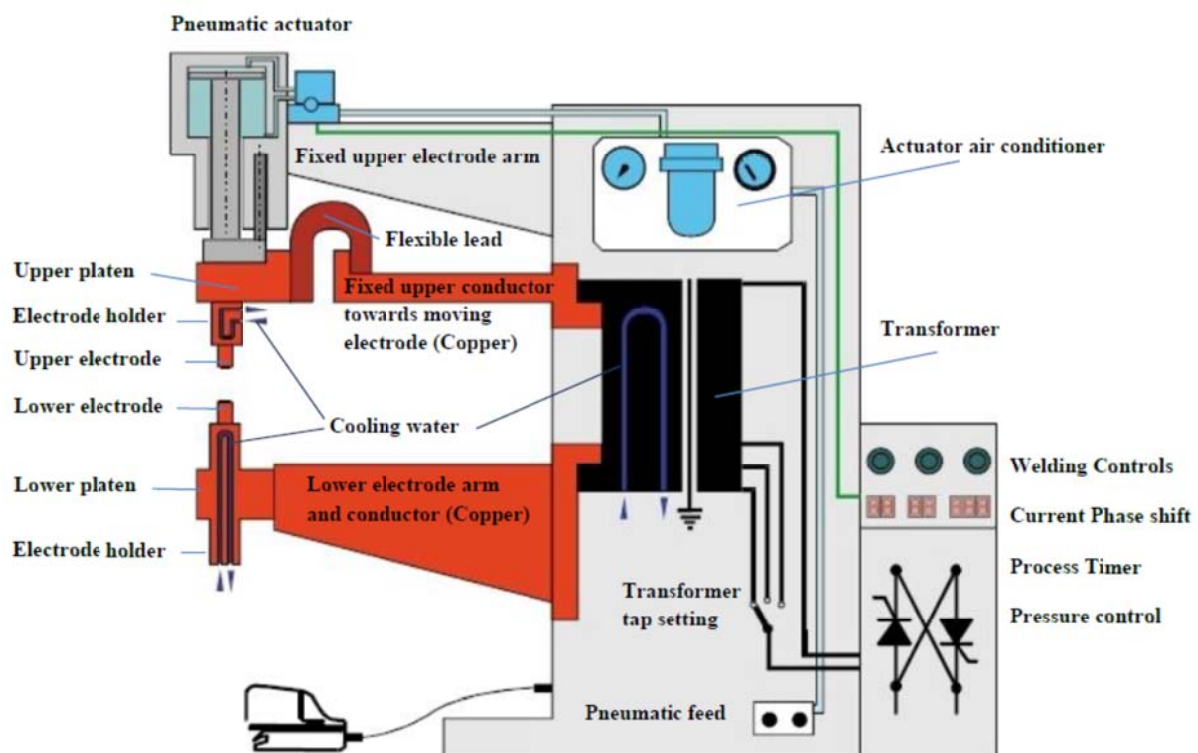


Figure 1-17 Different elements in resistance welding machines
(Image from IIW MSc in Welding Engineering course material)

1.3.1 Machine frame

The machine frame primarily serves to enable workpieces to be mechanically compressed before, during and after welding while maintaining geometrical stability. This means, especially in projection welding, that the frame has to be very rigid to ensure the electrode mounting platen remains parallel, even under maximum electrode force. Only in this way can prevention of changes in geometry of the contacting members to be welded be assured. A non-parallel electrode platen will result in non-uniform electrode forces and proportional differences in welding currents over the contact zone. The latter is extremely critical in simultaneous multiple projection welding. Two types of frames are capable of ensuring parallel electrode platens under load: the C-type and the portal type. Both these setups have

the upper electrode platen directly mounted on the force actuator (welding cylinder), resulting in a rectilinear movement of the upper electrode. However, flexibility in the arms of e.g. a portable (manual or robotic) spot welding gun can have the advantage of superior follow-up behaviour during welding collapse. The disadvantage in this case is the reduced geometrical accuracy of the welding machine. In the case of the rigid constructions, follow-up during weld collapse needs to be ensured by means of the pressurising system itself or by additional follow-up improving devices. Frames can be simple, as in stationary pedestal versions (see Figure 1-17 and Figure 1-18) where they are most often made of a welded plate assembly, or combined with the current conducting elements of the machine, as in portable and/or robot welding guns for spot welding (see Figure 1-19 and Figure 1-20) where the machine's frame core is most often a cast aluminium alloy fixture. Other frames can be rather complex like in multi spot welding where the frame is often of a portal type to support multiple welding guns at once or as in linear seam welding machines (see Figure 1-21) where there are often large welding displacements over the workpiece surface that need to be ensured.



Figure 1-18 Pedestal pneumatically driven C-type spot welder
(photo courtesy of PW)



Figure 1-19 PW Portable C-type spot welding gun
(photo courtesy of DAF trucks)



Figure 1-20 PW Portable Y-type spotwelding gun
(photo courtesy of DAF trucks)



Figure 1-21 LEAS portal type roller seam welding machine on radiator production line
(photo courtesy of Quinn Radiators)

1.3.2 Electrode force actuator

A typical resistance welding cycle always combines a mechanical force program and an electrical current program. Both of them have to be correctly set within the welding window [7] and have to be well synchronised to one another, otherwise a sound weld will not be obtained. Being a pressure welding process, an electrode force actuator is an essential part of a resistance welding system, with major influence on cycle times in automated welding, quality of the weld and electrode wear and lifetime. Hence it is not at all surprising that great care should be taken in the choice, set up and use of the actuator. There is a possibility to deliver the necessary electrode force by manpower (with leverage), pneumatically, hydraulically, combined pneumatic-hydraulic, servo electrically or electro-mechanically.

1.3.2.1 Manual actuation

The systems operated by manpower are mainly the earlier pedestal machines that often also don't have electrical synchronisation with the mains supply. Force is applied manually through a leverage against a spring. It is very difficult to find optimal parameter settings to achieve welds of repeatable quality with these machines. The other manpowered systems currently available are the handheld spotwelding systems (see Figure 1-22) for 'in-situ' welding, eg. to make welds of roof-lining or repair welding, often in car body repair shops.

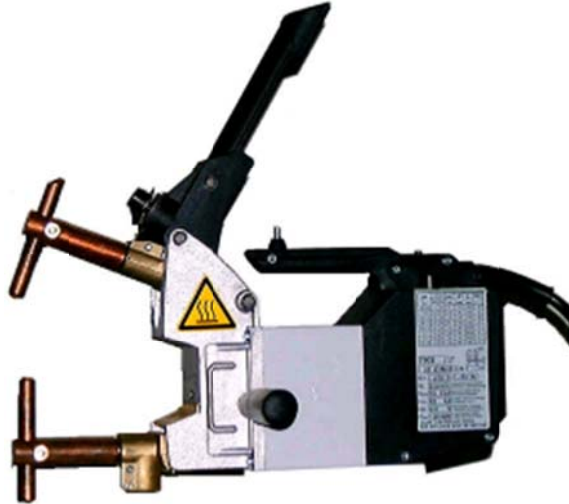


Figure 1-22 Handheld Tecna direct spotwelding gun

They are synchronised to the mains and the two electrode versions allow for current flow after reaching sufficient electrode force.

The other manpowered systems are the so-called manual spotters (see Figure 1-23), mainly used in car repair bodyshops, although these are also used to weld side panels on touring cars and buses.

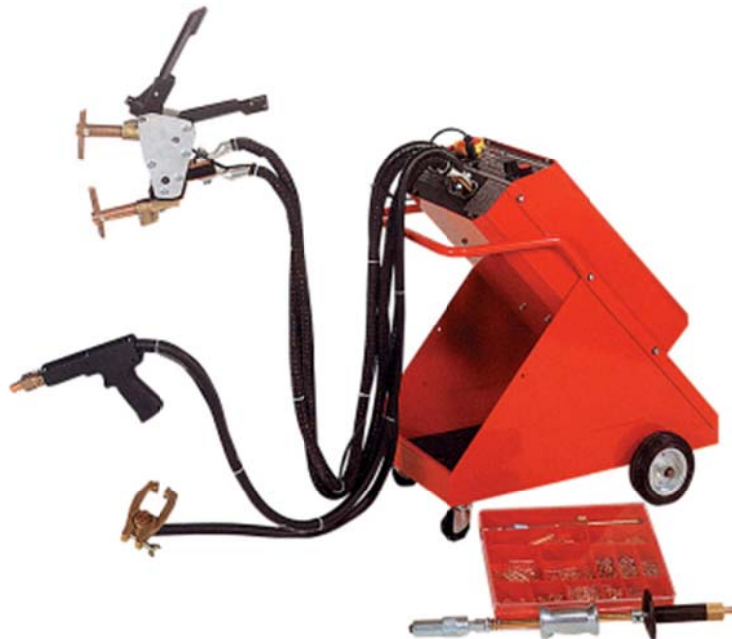


Figure 1-23 Tecna motor body repair unit

1.3.2.2 Pneumatic and hydraulic actuators

Most widely spread and used in industrial applications are pneumatic actuators. (see Figure 1-24, Figure 1-25, Figure 1-26 and Figure 1-27) They are available in different variants. Fixed (Figure 1-24) and adjustable stroke air cylinders (Figure 1-25) are the most common. Tandem cylinders for the multi-purpose resistance welding machines and roll-membrane or diaphragm cylinders never found wide application, although they do have the advantage of very low friction in the piston.

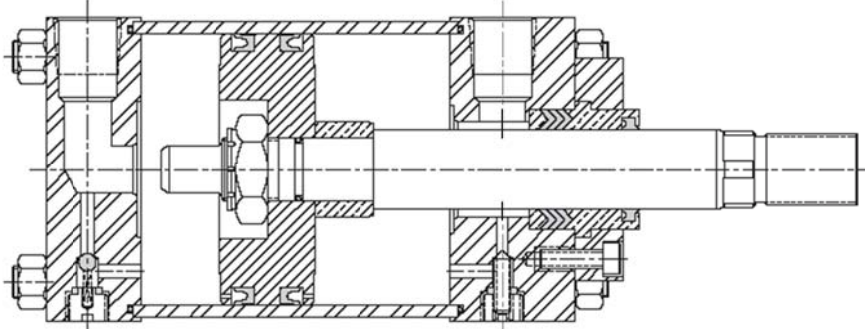


Figure 1-24 Fixed stroke air cylinder

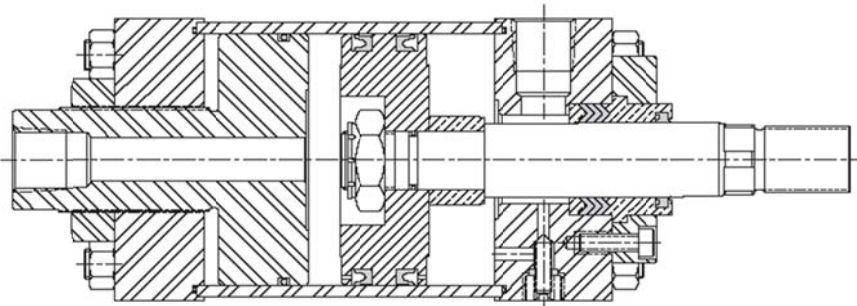


Figure 1-25 Adjustable stroke air cylinder

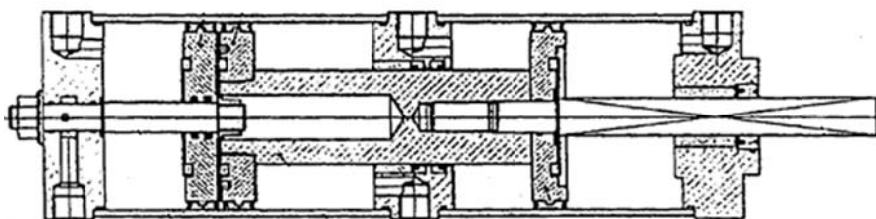


Figure 1-26 Tandem air cylinder

The tandem air cylinder type (Figure 1-26) offers more possibilities to cope with the disadvantages of using compressed air as a medium to apply force to the workpieces to be welded.

Hydraulic oil cylinders are used most of the time to enable very short cycle times in highly mechanised welding. Figure 1-27 shows a hydraulic oil cylinder pressurising a welding head on a mechanised welding station to weld windscreen wipers. Notice the orange spring beneath

the oil cylinder and between the cylinder and the welding head. Follow-up is thus assured by the spring instead of the cylinder. Moreover, in the majority of the hydraulically actuated resistance welding applications, the piston is moved to its extreme outward position, in this way compressing a spring equipped with a divided setting nut enabling exact compressing force setting, that transfers the actuating force to the electrode and workpiece.

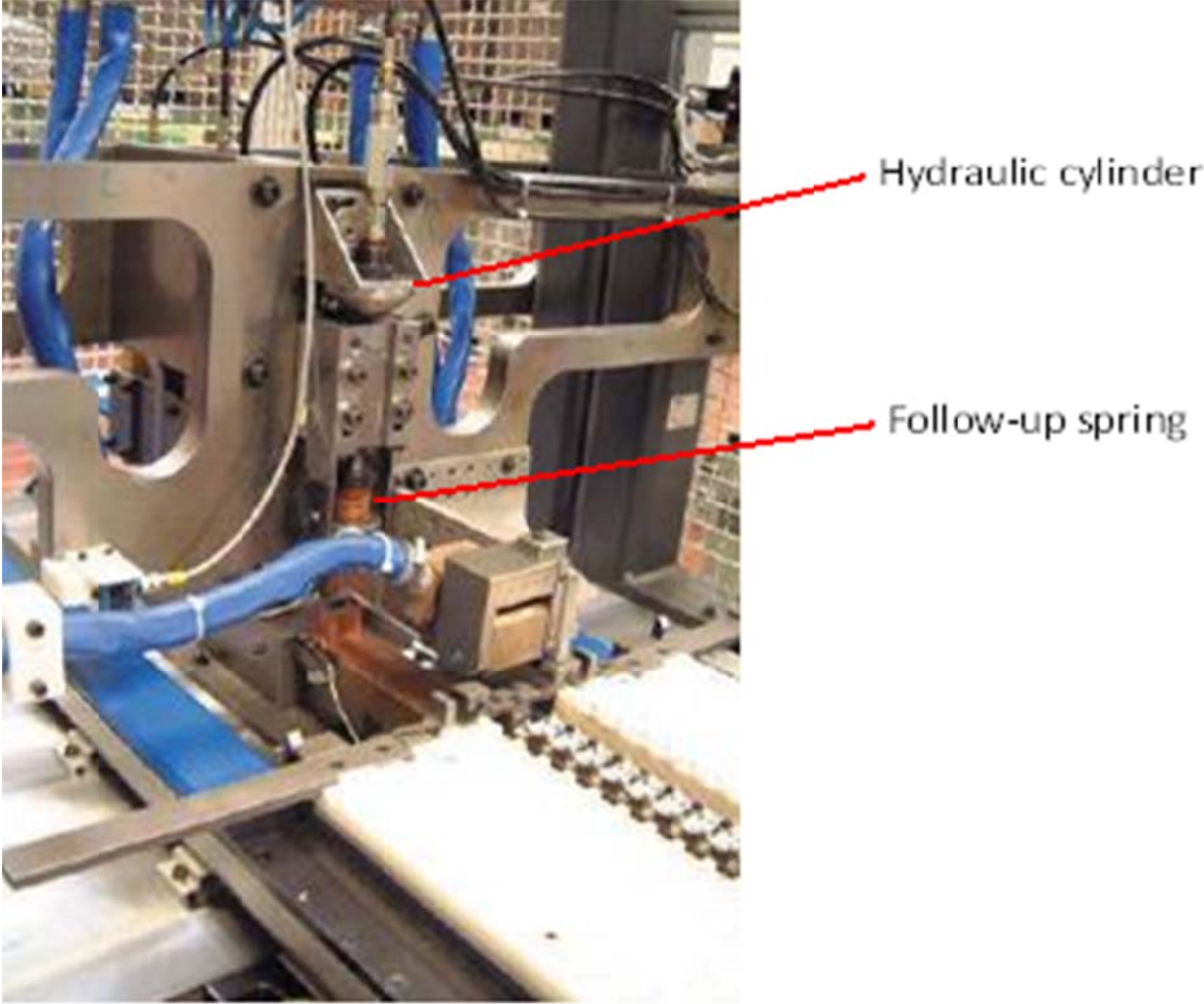


Figure 1-27 Hydraulic oil cylinder
(photo courtesy of Bosch)

A serious step forward in application possibilities is the combined hydro-pneumatic cylinder, for instance the ‘Power Package welding cylinder’ by Pressotechnik (see Figure 1-28). This offers the advantage of less air consumption and controlled set-down of the electrodes on the workpiece surface (leading to far less electrode wear and noise) due to their much lower moving mass and also a superior follow-up behaviour.

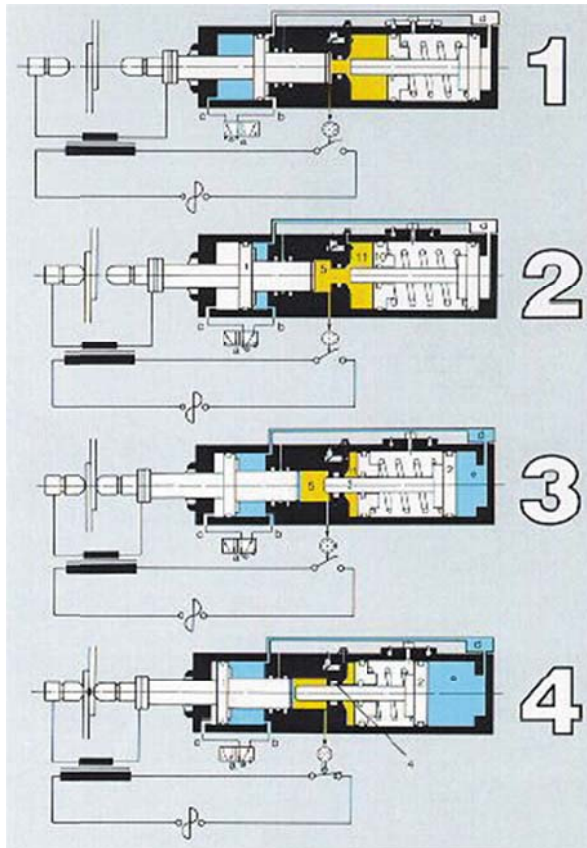


Figure 1-28 Pressotechnic power package operation sequence

Also worth while mentioning is the so called friction free roll-membrane or diaphragm air cylinder shown schematically in Figure 1-29 and Figure 1-30.

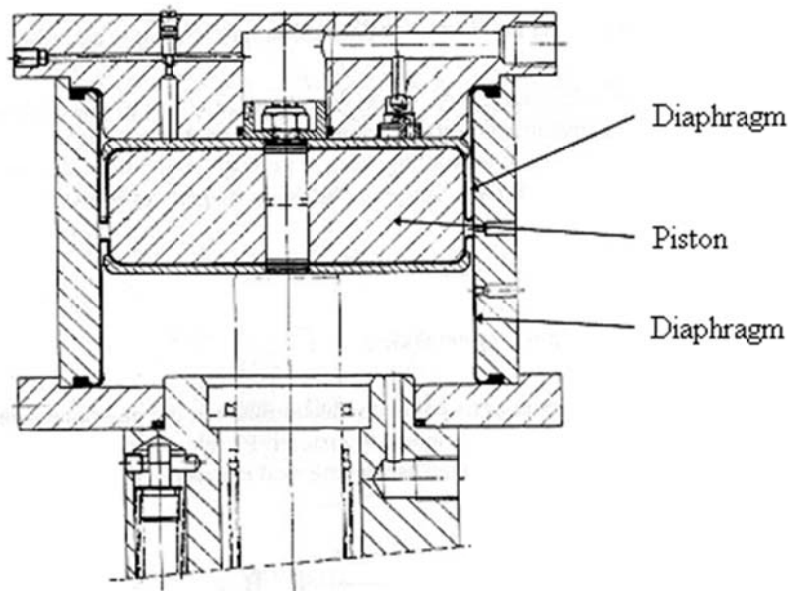


Figure 1-29 Diaphragm air cylinder

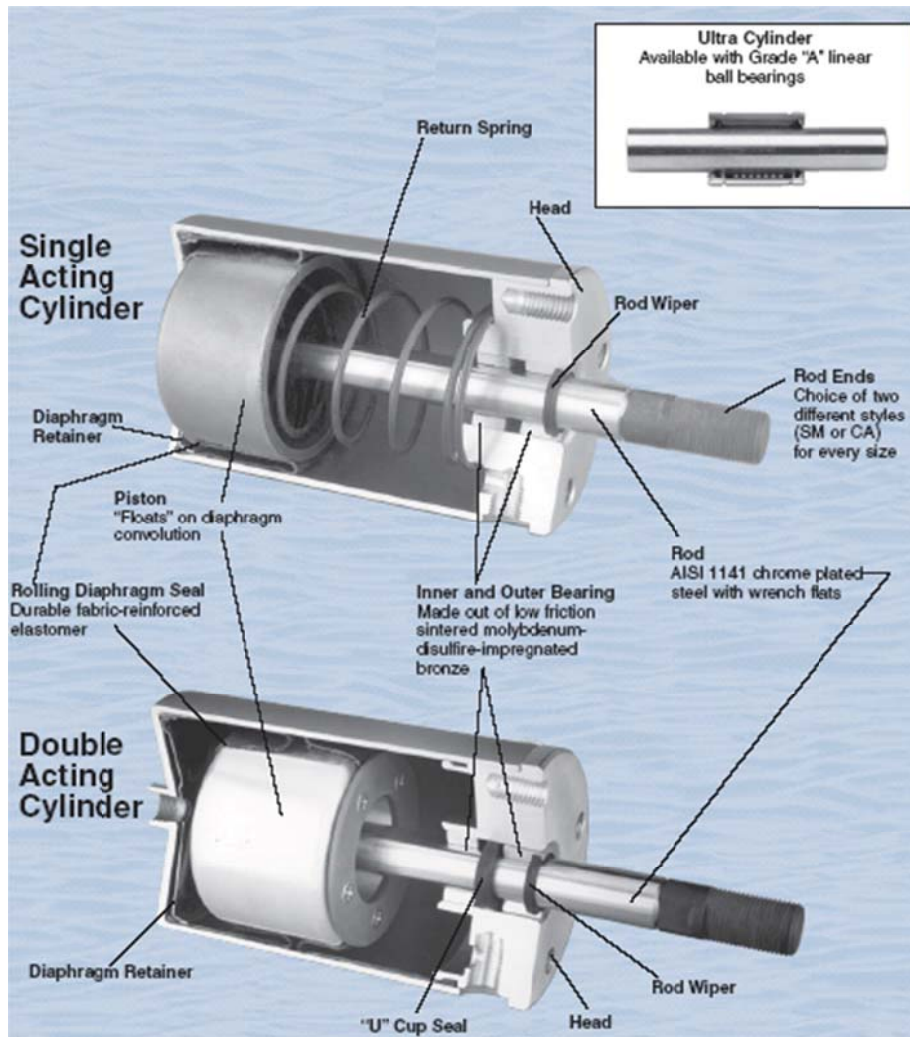


Figure 1-30 Single and double acting diaphragm cylinder

1.3.2.3 Electrical actuators

Before discussing the electrical actuators, it is perhaps useful to give realistic data for the year 2009 on the worldwide sales from the ARO welding technologies group.

Products	Quantities		
Guns (w/o MBR)	3191	63% Robot 37% Manual	61% Servo 39% Pneumatic
Machines	128		
Transformers	3268		
Servomotors	1343		
Controllers	1225		
MBR Motor Body Repair	521		

Table 1-1 ARO welding technologies production data 2009
(ARO group Key Figures February 2010)

There is of course the influence of the industry. ARO supplies to mainly automotive assembly, explaining the high amount of robotic welding applications in comparison with manual. There is a trend to change from pneumatic actuated machines to servo-electric actuated ones, but this is highly dependent on the company philosophy at each constructor (see Figure 1-31 and Figure 1-32).

These ratios will be slightly different for machines installed by other constructors. However, ARO being one of the major players on the market in this field, the ratios are likely to be of the same order.

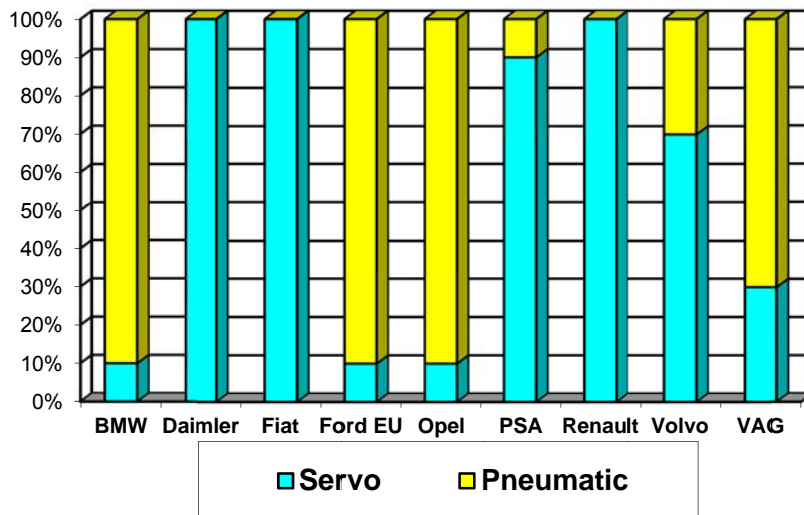


Figure 1-31 Implementation of ARO Servo Guns inside Europe in 2009
(data courtesy of ARO welding technologies)

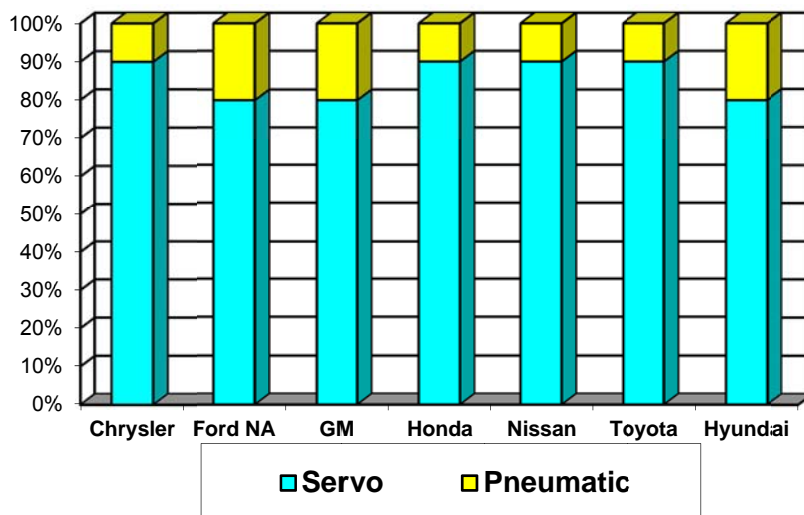


Figure 1-32 Implementation of ARO Servo Guns outside of Europe in 2009
(data courtesy of ARO welding technologies)

It is apparent that servo actuators are becoming more popular, depending on the specific company policy. Some automotive constructors have switched completely to servo actuators, and most are using them, although a few don't use them. They have the advantage that, in combination with a suitable control unit, they enable very flexible force programs in the welding schedules, and their benefits in resistance spot welding of aluminium alloys cannot be denied. On the other hand, the need for a compressed air supply network throughout a factory may incur increased costs.

More and more automotive assembly plants are designed nowadays as cells on standard container platform bases, only with electrical connections and offering enormous flexibility when redesigning and/or moving the factory to another location.

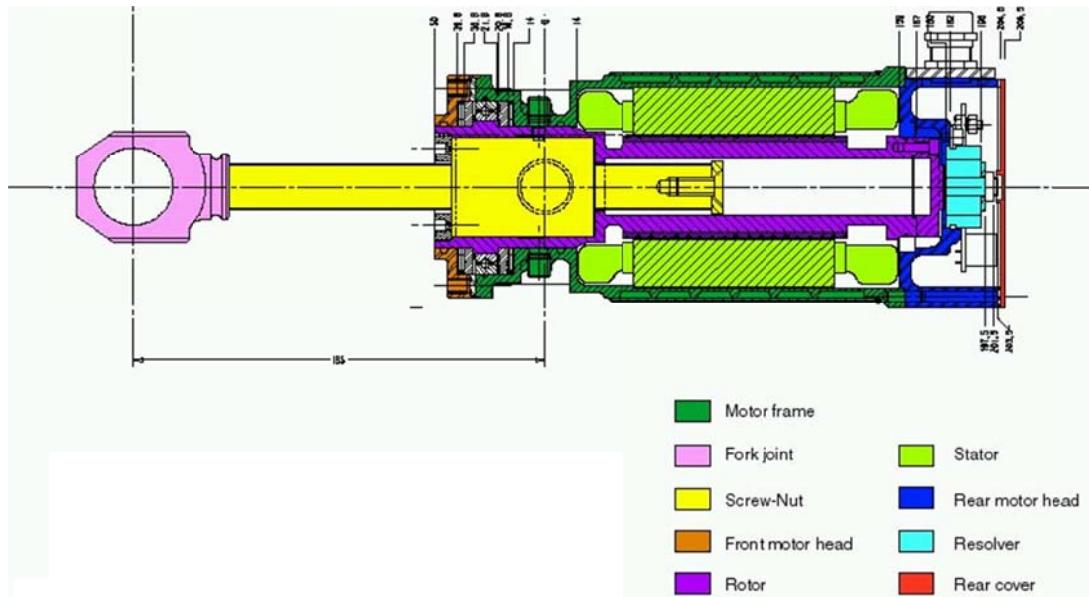


Figure 1-33 ARO Servo electric actuator motor
 (image courtesy of ARO welding technologies)

As can be seen in Figure 1-33, the servo motor rotor (purple) equipped with permanent magnets is connected to the nut (yellow) that drives the ball screw (yellow) actuating the welding head movement. Positioning feedback for the servo can be established by means of a resolver (cyan) or an encoder on the rear head of the motor. These actuators are available in water cooled and air cooled versions as can be seen in Figure 1-34.



Figure 1-34 Water cooled motor (upper) and air cooled motor (lower)
 (photo courtesy of ARO welding technologies)

There is indeed an undeniable advantage in using electrical Servo Motor technology for pressure welding applications in comparison with pneumatic systems:

- Freely programmable strokes and weld forces;
- Force build-up up to five times faster in comparison with a pneumatic cylinder;
- Significantly shorter cycle times;
- Jolt-free placing of electrodes, thus:
 - less electrode wear;
 - no hammering effect during workpiece striking;
 - significantly less noise production;
- Avoidance of sheet deformation;
- Possibility for synchronised movement of welding gun and robot;
- Possibility to monitor sheet pairing and thickness;
- Possibility of monitoring dressing of electrodes;

It however needs to be mentioned that EVERY electrical Servo Motor driven resistance welding head is equipped with a spring follow-up system between the ball screw driven by the motor and the welding head it is intended to actuate. (see Figure 1-35)

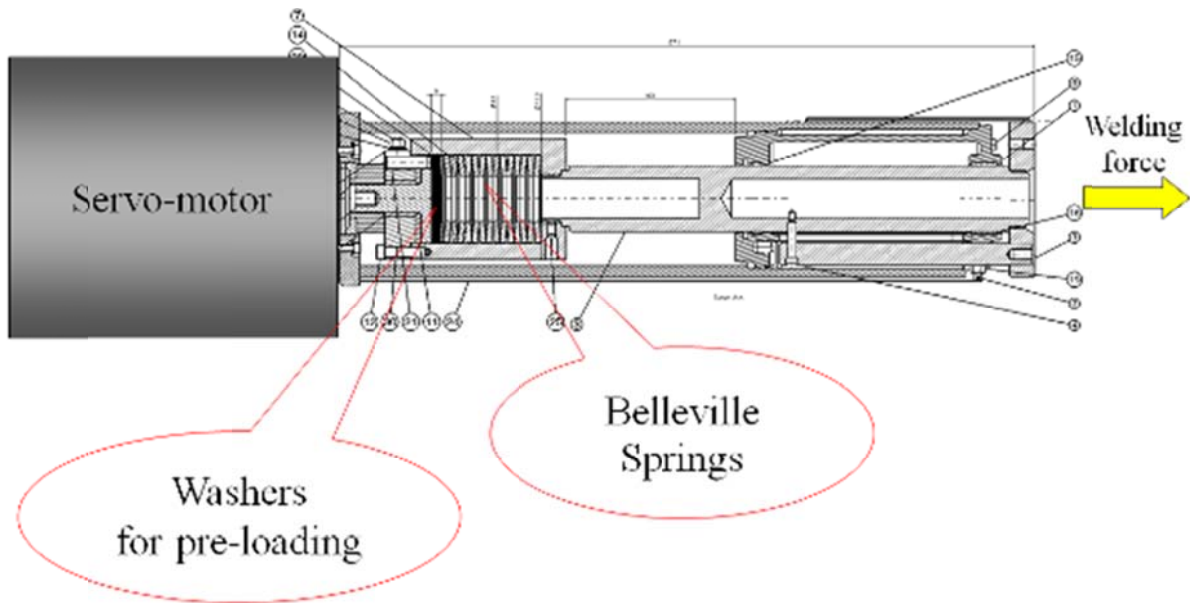


Figure 1-35 Belleville spring follow-up system

Purpose of this system is specifically to protect the motor against damage from impacts of the welding head on a workpiece or on the fixed welding head. Let us keep in mind that this protective construction alters the welding heads' behaviour dramatically. It is only the lumped mass below the springs that needs to be accelerated during workpiece collapse.

It is however nearly unknown to the machine users that this system is present inside the welding head and thus nobody comes with the demand to alter this system in function of one or another more difficult application.

2 Literature review

Research oriented towards resistance welding applications has been documented since the 1940's, with most of the publications before 1980 mainly dealing with geometrical issues related with spot and projection welding or describing possible applications [8], [9], [10], [11], [12], [13], [14], [15].

Steve Westgate gives a good overview on the evolution in resistance welding and related technology [16], [17].

Since all resistance welding processes are based on Joule heating, two major subsystems can be found in every machine built to apply these processes in practice, electrical and mechanical. The electrical part of resistance welding machines mainly serves to transfer electrical energy to the very spot where heat is required to realise a weld and is not focussed on in the frame of this work.

However, the physical coupling of these power sources secondary output with the welding electrodes in contact with the workpieces to be welded is a very prominent part of the mechanical system of a resistance welding machine. It adds mass to the moving welding head and thus additionally influences its mechanical behaviour. The mechanical subsystem of a machine, combined out of a multitude of possible components of different type and make, will lead to very specific behaviour and will have significant influence on the machine performance, its possible field of application, the set of optimal parameters to be used on it, and also electrode wear and quality level of the welds resulting from it. This thesis specifically deals with assessment of mechanical behaviour of all types of resistance welding machines, spot- and projection- but also seam- and butt welding machines.

2.1 Mechanical behaviour

In the past decades, several researchers have made significant efforts to understand the effects of all factors in the different physical combinations that exist in different machine constructions on the mechanical behaviour of the welding machine in operation.

This work can be categorised into static and dynamic properties, both specified in the ISO 669 standard 'Resistance welding – Resistance welding equipment – Mechanical and electrical requirements' [1], but dealt with to a largely different degree of detail.

Static mechanical behaviour

In ISO 669 [1], contact faults resulting from eccentricity and deflection of electrodes or electrode platens and the setup and procedure to measure them are described for spot, seam, projection and butt welding.

Eccentricity or horizontal shift of the electrodes (g) and deviation of electrodes (α), (Figure 2-1), correspond to two aspects of the figure at two successive loads as represented by the following formulae:

$$g = b - a \quad (\text{expressed in mm})$$

and: $\alpha = \alpha_1 - \alpha_2$ (expressed in radians)

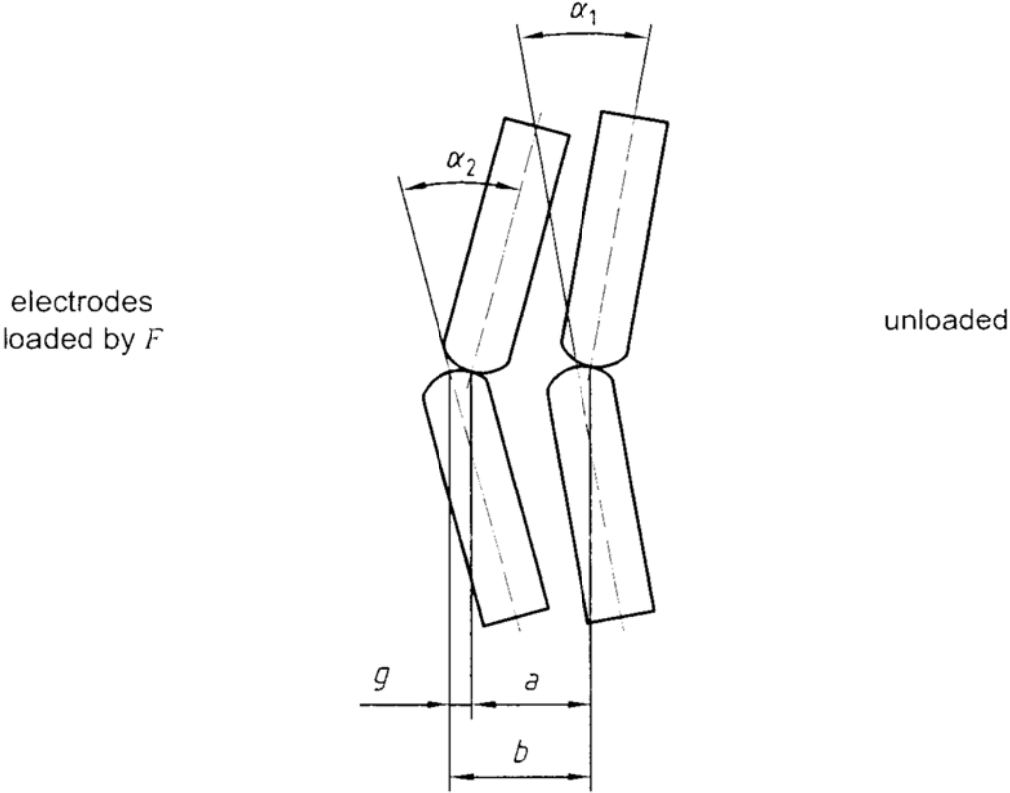


Figure 2-1 Contact fault in spot and seam welding equipment (ISO 669)

For projection welding equipment (Figure 2-2): $\alpha \approx \tan \alpha = (b_1 - b_2) / b_3$

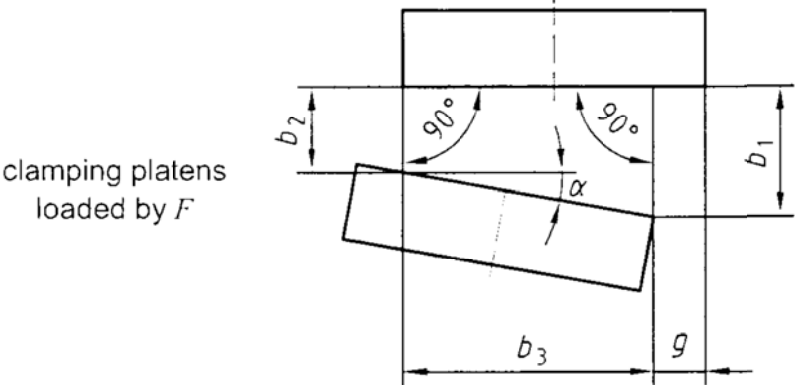


Figure 2-2 Contact fault in projection welding equipment (ISO 669)

For butt welding equipment (Figure 2-3): $\alpha \approx \tan \alpha = \frac{b}{k}$

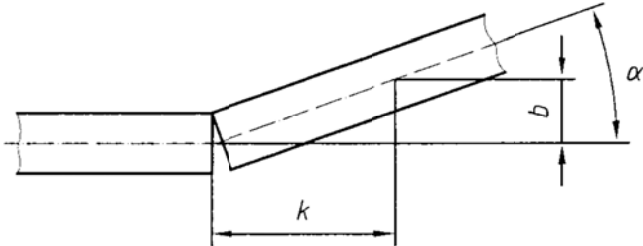


Figure 2-3 Contact fault in butt welding equipment (ISO 669)

Figure 2-4 illustrates a uniform apparatus useable according to procedures described in ISO 669 for measurement on spot welding equipment.

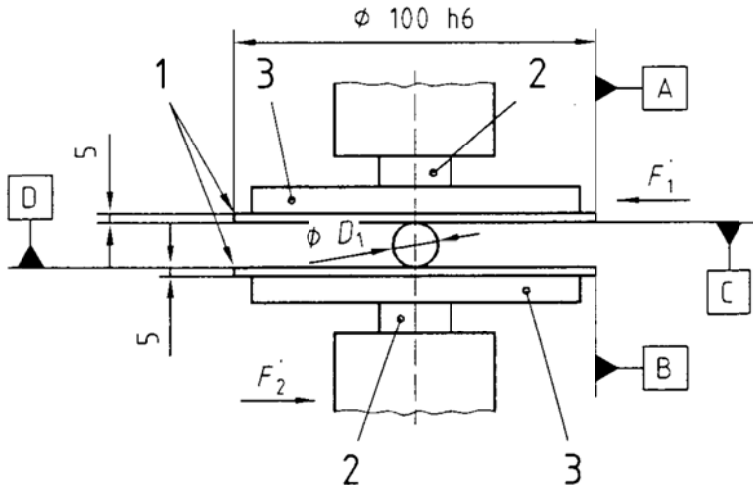


Figure 2-4 Measurement accessory for spot welding equipment (ISO 669)

Figure 2-5 illustrates a comparable apparatus according to procedures described in ISO 669 for measurement on projection welding equipment.

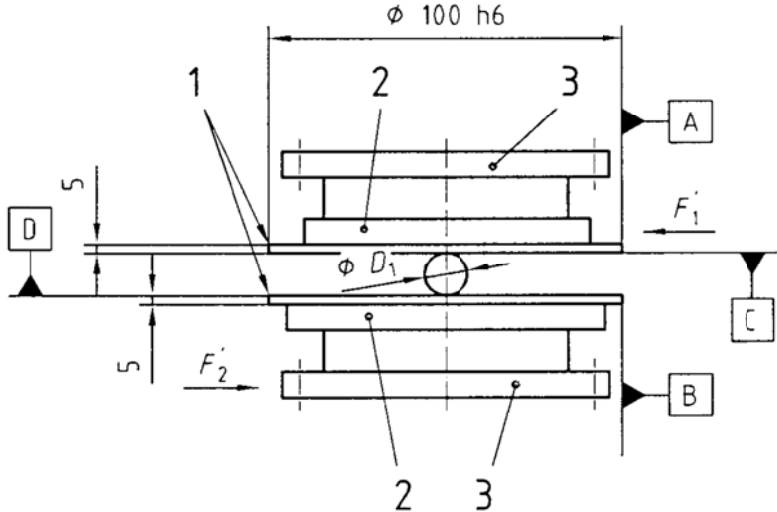


Figure 2-5 Measurement accessory for spot- and projection welding equipment (ISO 669)

Dynamic mechanical behaviour

In order to create a common basis for discussion in the international engineering community, the new technical terms and the experimental method for measuring these characteristics are given in ISO 669, annex A.

2.1.1 Dynamical mechanical characteristics

(according to ISO 669 annex A)

These characteristics define the manner in which spot, projection or seam welding equipment oscillates when electrode contact and follow-up occurs with the component to be welded. (see Figure 2-6)

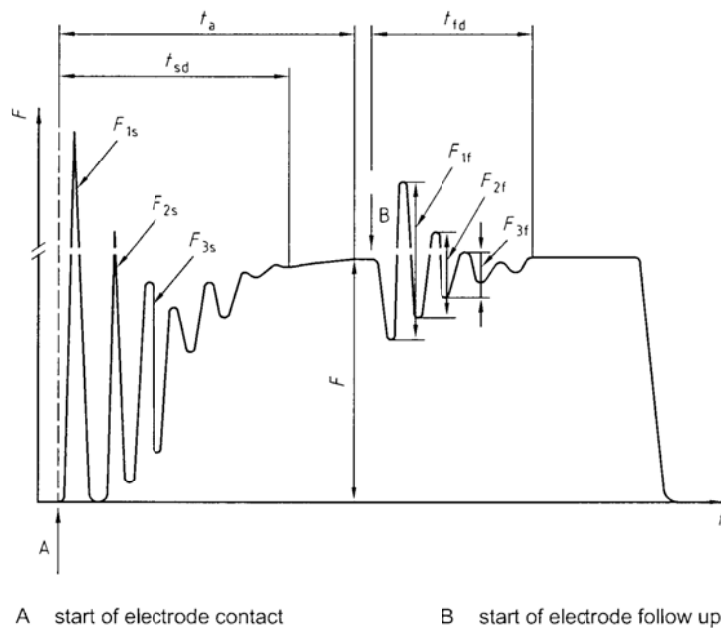


Figure 2-6 Schematic dynamic behaviour of spot welding equipment [1]

As can be observed in the figure, electrode contact is represented by point A and electrode force ascent starts at that point up to the static electrode force F . After contact of the moving electrodes, force oscillations may occur that can be measured by means of a force transducer. Also electrode bounce may occur after electrode impact. Follow-up of the welding equipment, starting at point B in Figure 2-6 occurs during expanding and contracting of the material while heating and cooling, due to indentation of the electrodes into the components or when projection collapse occurs. During this follow-up stage, force oscillations may also occur. In the same Annex 3 of ISO 669, some characteristic quantities are defined:

- Impact velocity (v_a) = velocity of moving electrode or platen immediately prior to contacting.
- Impact energy (E_a) = the kinetic energy of the moving mass of the lumped mass of the moving welding head (welding head, electrode holder, electrode and a portion of the flexible conductors) just before electrode contact.

$$E_a = \frac{m(v_a)^2}{2}$$

- Coefficients of force (K_F , K_{FS} and K_{Ff})

$$K_F = \frac{F_1 + F_2 + F_3}{3F}$$

* With K_F and forces F_1 , F_2 and F_3 written with index s to indicate contact and index f to indicate follow-up.

* Forces F_1 , F_2 and F_3 are the first three complete oscillations upon electrode contact or follow-up.

- Force rise time (t_a) = the time span from initial contact of the electrodes up to the point when nominal static electrode force has been reached (see Figure 2-6)
- Decay time (t_{sd} , t_{fd}) = the force oscillations resulting from the electrode contact or follow-up process.
- Follow-up behavior is determined by means of a simulation test, where a circular projection in accordance with BS EN 28167 : 1992, [18], stamped into a steel sheet is rapidly melted away by using a sufficiently high current impulse ($T = 1$ cycle) above the splash limit. The follow-up of the electrode is determined by measuring the height of the projection weld after application of the electrode force. Evaluation of the force amplitudes is carried out in accordance to the above.

Consideration:

The ISO 669, in its last revision dating 2001, up to date with the status of still being current, describes very interesting straightforward measurements to be made on whatever resistance welding machine, establishing important geometrical data on machine stability. And the latter is important, since it will be an indication for undesired movement between the electrodes, leading to increased electrode wear and possible loss of technical and esthetic quality of the resulting welds. Concerning the dynamic mechanical characteristics of a resistance welding machine however, it offers a mutual base platform of approach and understanding to serve as start for further scientific research.

Publications dealing with the sequential evolution in the state of the art in dynamic mechanical behavior of resistance welding machines can be categorized in four major categories, depending on how the issue of dynamic behaviour is approached, namely:

- Theoretical modelling
- Simulation of conditions on laboratory machines
- Effect analysis based on ‘real’ welding test
- FEA based on ‘In-Situ’ characterisation tests

2.1.2 Theoretical modelling

Römer, Press and Krause [19], [20], were the first to mathematically model the different main influencing machine parameters on a resistance welding machine before, during and after welding takes place.

They used a single-mass vibratory unit as substitute of a resistance spot welding machine with a C-frame while assuming a rigid frame of the machine. (see Figure 2-7)

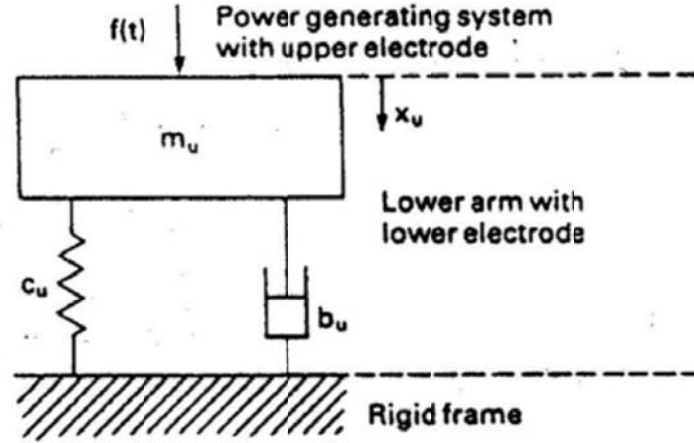


Figure 2-7 Single-mass vibration system [19], [20]

They used the sudden contact between the touching electrodes as a shock function $f(t)$.

$$f(t) = \frac{I}{m} \delta(t)$$

With m the moving mass of the upper moving welding head, I the shock intensity and $\delta(t)$ the Dirac delta function, i.e.

$$\delta(t) = \begin{cases} 0 & \text{for } t \neq 0 \\ 1 & \text{for } t = 0 \end{cases}$$

As a result the differential equation for describing the response of the lower welding head and arm following the shock excitation is:

$$m_u \ddot{x}_u + b_u \dot{x}_u + c_u x_u = f(t)$$

With as solution:

$$x_u = \frac{I}{m_o \omega} e^{-D_u t} \cdot \sin \omega t \quad \text{and with } D_u = \frac{b_u}{2 m_u} \quad (2.1)$$

Where m_u , b_u and c_u represent the mass, damping and stiffness of the lower welding head and arm.

During the welding- and hold stage of the welding cycle, as soon as heating due to the welding current flowing takes place, materials will soften or if possible by their geometry, they will collapse. This induces the electrodes to move towards each other in the direction of the electrode force acting on the workpiece. The upper electrode accelerates downwards due to the welding force F_o and its movement is described by the following equation:

$$m_o \ddot{x}_o + b_o \dot{x}_o = F_o \quad (2.2)$$

With as solution:

$$x_o(t) = \frac{F_o}{4 m_o D_o^2} [2D_o t - (1 - e^{-2D_o t})] \quad \text{with } D_o = \frac{b_o}{2m_o} \quad (2.3)$$

Where m_o and b_o represent the mass and damping factor of the upper welding head and arm.

So during collapse, the machines' welding heads move towards each other. The upper electrode with significant damping effects due to its velocity building up, the lower electrode, only displaying structural damping in a decaying vibrating way.

Bearing these phenomena in mind, Römer and his co-workers concluded that for optimal behaviour both before and during/after welding, contradictory demands have to be made to the mechanical system. (see Table 2-1)

Approach and contacting		Electrode follow-up	
Lower electrode	Upper electrode	Lower electrode	Upper electrode
Mass m_l low	Mass m_u low	Mass m_l low	Mass m_u low
Damping ζ_l low	Damping ζ_u high	Damping ζ_l high	Damping ζ_u high
Stiffness c_l low	Contact velocity v_a constant	Stiffness c_l high	

Table 2-1 Proposed set up of machine parameters for best machine behaviour [19]

Römer also mentions the suggested use of a spring follow-up system between the upper electrode and the force actuating system to improve mechanical behaviour.

In 1994, **Gould et al.** [21] focussed on the theoretical analysis of weld head motion, again revealing the complexity of the subject, and only solvable by using simplifying assumptions, each representing different stages in the process. He was the first to model motion of the welding head as an energy balance per unit of time.

$$m \frac{dx}{dt} \frac{d^2x}{dt^2} + m(x+X_0) \frac{d^3x}{dt^3} + F_r \frac{dx}{dt} = P_1 \dot{V} \quad (2.4)$$

Where the term on the right is the energy delivered to the system per unit of time, the term on the far left expresses the work done per unit of time of the force at any specific instance against the lumped mass of the welding head. The term in the middle represents the work done per unit of time due to the rate of change of the force against the lumped mass of the welding head and the final term on the left represents the work done due to friction

The latter is an extremely realistic way of presenting the weld head motion. Gould considered four stages in movement before contact on a pneumatic actuated welding head, including:

- Stage 1, Pre-motion (due to friction): where the applied force acting on the piston is insufficient to exceed the friction forces; (building up of pressure)
- Stage 2, Small head velocities: at initiating movement, the developing pressure in the actuator cylinder is attempting to accelerate the welding head;
- Stage 3, Quasi stable pressure motion or Low jerk (d^3x/dt^3) motion; meaning change in welding head acceleration is relatively small due to only very small changes in pressure in the actuator cylinder;
- Stage 4, Constant velocity head motion: where actual motion is only caused by the rate of air flow in the actuator cylinder.

This work is very important in general understanding of cylinder movement in a very wide range of applications.

Limited verification trials were done by Gould on two welding machines.

Feng [22] developed two analytical models in 1997 that describe electrode displacement during the squeeze stage of pneumatic actuated spot welding machines. The first model, called weld head model describes electrode movement during the approaching stage, prior to contact, the second model, named dynamic response model, describes electrode movement after contact (bouncing characteristics) but before the welding current is applied.

Feng assumes that no separation would occur on impact.

In using these models, velocity of approach prior to contact, impact force, bouncing frequency, pressure build-up and force stabilising time can be estimated. Feng validated his models by experimental tests.

As a matter of fact, Feng's models and the conclusions he makes are very similar to those made by Gould [21].

In his later work in 1999 [23], **Gould** extended his earlier work in this field in describing a follow-up process based on his so-called ball model. (see Figure 2-8)

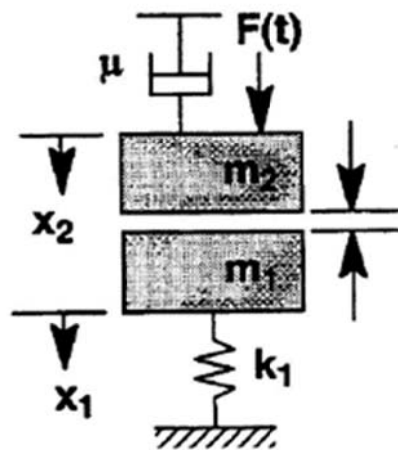


Figure 2-8 Ball melting model [23]

It is assumed that two resistance welding electrodes are separated by a small metal ball. The ball is used to provide reaction loads to the applied welding force, and is of a height that is representative of a welding projection or a potential indentation (as if actual materials were being welded). In this ball test, the ball is vaporised when the current is initiated. Follow-up behaviour can then be monitored directly through the subsequent motion of the electrodes.

Gould assumed two possible conditions in the follow-up of a machine equipped with an air-operated welding head, one where a constant electrode force is applied, the other in a closed air system.

The former system implies that pressure remains constant in the welding cylinder during workpiece collapse, an assumption that is extremely realistic towards welding applications both in spot and projection welding. Only those projection applications where large displacements are due to be made during collapse, such as cross-welding of tubular components or projections with extreme heights, will not comply to this suggested behaviour.

In the latter system Gould assumes no air flow into the welding cylinder.

The analytical expressions of both these cases enable squeeze and follow-up characteristics of a machine to be related to machine design.

Although Gould's theoretical approach is a true milestone in regard of understanding and predicting machine behaviour during two important stages of the welding process, namely squeeze and follow-up, Gould did not report procedures and methods which would enable determination of machine kinematics .

In 1980, **Rivett and Westgate** [24] define electrode follow-up as follows:

“Head follow-up is a measure of the ability of a welding machine to respond so as to maintain electrode force under conditions of rapid electrode movement, as when weld splash occurs.”

They developed a procedure which could be used to characterise the follow-up capabilities of the welding machine used. To simulate splash welding, a 1.6mm steel ball bearing was placed between two sheets of Nimonic alloy between the electrode tips. Force, current and welding time were set, so that the ball bearing exploded within a single cycle. Each time, head displacement and current were recorded and to gain an indication of the machine characteristics, the time taken for the head to travel a predetermined distance (in their examinations 0.4mm) from the onset of current was measured.

Williams [25] describes in his report EUR 15712EN: “*Factors influencing weldability and electrode life when welding coated steels in multi-welders and robotic cells*“, how measurement of head follow-up characteristics were made using the same exploding ball test as mentioned by Gould and Rivett. Williams clearly refers to the technique as previously adopted at TWI:

“A 1.6mm diameter ball bearing was placed between two sheets of 1.7mm stainless steel and the electrode force was applied. A current was passed through the ball causing it to explode and be expelled from between the stainless steel sheets. The time taken for the moving head to respond to the resulting loss of force and to follow up a given distance was recorded.”

On questioning Steve Westgate on the origin and the use of the exploding ball test, it appears that the test was only used for measuring maximum velocities reached by the moving welding head at different distances travelled. These data obtained from different machines subsequently could be used to compare machine capabilities. Equally it appears that Williams used the same test to compare reaction times of a moving welding head to a complete loss in support for the moving welding head.

2.1.3 Simulation on laboratory machines

Krause and Lehmkuhl [26, 27] stated that dynamic machine properties are due to specific machine construction and summarised influencing machine specific parameters (Table 2-2).

Pressurising Piston	Pressure delivery system	Stiffness
Friction in bearings	Air or hydraulic oil	Machine frame upper and lower
Friction in seals	Magnetic valve switching	Force delivery system
Friction in piston seals	Valve Cross section	
Friction in current leads	Flow rate pressure regulator	
Elasticity of piston seals	Positioning of elements	
Properties of cylinder	Choke effect in lines	
Follow up systems	Accumulators	
Piston movement		

Table 2-2 Influences on dynamic mechanical machine properties [26]

The basic purpose of this work was to internationally define and standardise mechanical machine properties to lead to optimised mechanical machine behaviour. They stated that a resistance welding machine is a vibrating system with masses, spring constants and damping effects. Forces that apply during electrode contacting and electrode follow up lead to deformations of several machine components. Their proposed approach basically refers to

DVS 2913 (1978) “Guidelines for testing single phase spot, projection and roller seam welding equipment”, later adapted in DIN ISO 669 (1981) “Kenngrößen für Widerstandsschweisseinrichtungen” or “Rating of Resistance Welding Equipment”.

Most likely, the parameters that Krause proposed to measure in order to enable machine comparison and better understanding back in 1984, were made starting from DIN ISO 669 (1981) considering that schematical images in his publication are exact copies of the standard. Given the fact that this standard is still current for the moment in nearly unchanged condition in ISO 669:2000; BS 3065:2001, one could conclude that it offers a strong platform to evaluate machines. See 2.1.1.

In 1988, **Satoh et al.** [28] designed and built a spot welding machine with the ability to alter its mechanical construction to result in four different setups: (see Figure 2-9)

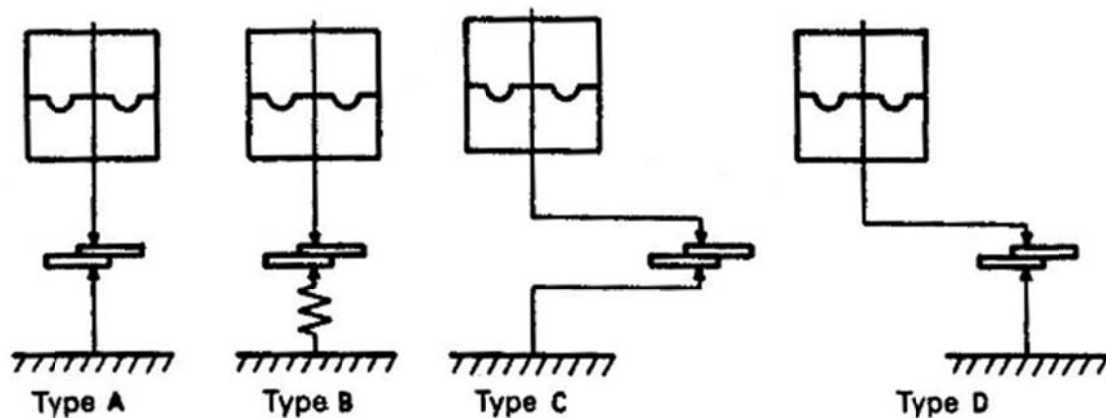


Figure 2-9 Four types of spot welding machine setups [28]

- Type A: Force exerting upper electrode axis in line with very rigid lower electrode arm;
- Type B: As type A but with a low rigidity lower electrode arm (by adding a spring in the lower electrode);
- Type C: Force exerting upper electrode axis not in line with the electrode axis and both upper and lower arm of the same (lower) rigidity;
- Type D: As type C but with upper and lower arm of different rigidity;

For these four setups, influence of moving mass and friction on resulting spot weld quality (weld nugget diameter) and electrode wear were examined while welding on mild steel sheet.

Main conclusions were the following:

- Mass of moving upper electrode has little effect on nugget diameter in all cases except A, whereas friction also has a considerable influence in case A;
- When rigidity is low (B, C and D), friction has little effect;
- In types C and D, nugget shape becomes an ellipse under many conditions;
- Impact energy on electrode contact is important towards electrode life and related to moving mass, friction and stiffness of electrode arms;
- With low rigidity electrode arms, neither moving mass nor friction influenced electrode life

Lehmkuhl et al [29] also described methods to obtain and handle process parameter data during resistance spot welding. Improvements in computer capabilities are emphasised. Monitoring of current, voltage, dynamic resistance, electrode force, pressure, electrode acceleration and electrode travel and uses of the data for process analysis and real time control are described. Types of sensor systems are listed and factors affecting choice of a sensor are presented. They also described the measuring equipment and techniques to enable evaluation.

Hahn et al [30] developed an experimental spot welding gun to use on a robot with the following features:

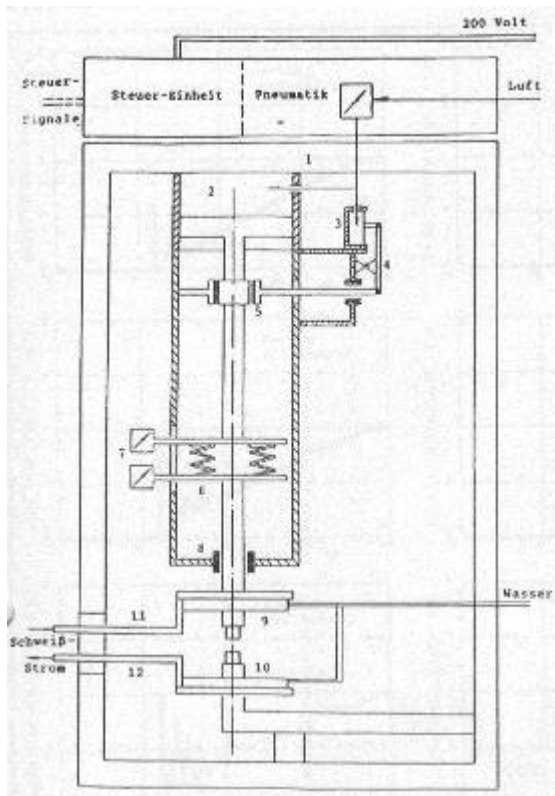
- Altering moving mass of the electrode arms by adding extra mass;
- Altering stiffness by adding an additional spring unit;
- Altering friction by replacing welding cylinders;
- Choice between pneumatic and hydraulic actuators;

Deep-draw quality steel sheet was used for practical tests where weld quality was evaluated by examining the weld nugget dimensions in metallographic sections and by measuring weld tensile shear strength.

Main conclusions were the following:

- Static mechanical properties as well as dynamic touching behaviour are sensitive to moving mass and stiffness of the electrode arms;
- Hydraulic actuator, due to their lower mass and higher damping show a low peak force and fast decay both in touching and follow-up behaviour;
- Follow-up of a robotic spot welding gun is mainly governed by bending of the electrode arms. As a result, stiffness and moving mass have low influence on quality of the welded joints just below the splash limit, but they do affect the scatter in strength value. A reduction in scatter of the latter is found with lower moving mass and less stiffness.

Dorn and Xu [31] developed and built a simulation device (see Figure 2-10) to study the influence of properties like moving mass, stiffness and friction of the moving welding head that could easily be changed on the simulating device. They built simulating facilities on a resistance welding machine that enabled them to define the influences of different properties on dynamical machine behaviour, especially during approach and electrode contact and during follow-up when welding.



Key

- 1. Frame
- 2. Pneumatic cylinder (force)
- 3. Pneumatic cylinder (friction)
- 4. Leverage
- 5. Friction shoes
- 6. Follow-up system
- 7. Additional mass
- 8. Electrode bearing
- 9. Upper electrode holder
- 10. Lower electrode holder
- 11. Upper platen
- 12. Lower platen

Figure 2-10 Sketch of Simulating device [31]

They concluded the following:

- Machine parameters could be changed independent for systematic testing;
- Conditions could be accurately set;
- Reduced stiffness of the machines frame improves contacting and follow-up behaviour of the electrodes but it also increases bouncing effects;
- Low friction improves follow-up, but makes contacting worse;
- Moving mass could not show a clear influence on follow-up in the tested area, in contacting a low mass is better to avoid bouncing.

In their further work [32] they refined their simulation tests with different friction material used in the pneumatic cylinder seals and piston seals to reveal the very complex interactions of mechanical influencing variables on the dynamic behaviour of a resistance welding machine.

Touching behaviour cannot be improved simultaneously with follow-up behaviour by one single combination of mass, friction and stiffness.

Dorn also point outs the benefit of an additional spring follow-up system between electrode and force actuator.

2.1.4 Effect analysis based on ‘real’ welding tests

Dorn et al. [33] simulated spot welding equipment to assess the effects on electrical resistance of variations in lower arm stiffness, friction, mass moved during the electrode movement and electrode travel. Static behaviour (contact resistance) was assessed according to DIN ISO 669 by measurement of the contact error as a result of bending and eccentricity at

10, 50 and 100% of the nominal electrode force. Dynamic behaviour (dynamic resistance) was described by use of the electrode force curve and the follow-up. They could identify a close relationship between the contact resistance and dynamic resistance and the static and dynamic behaviour, determined by the mechanical characteristics of the welding equipment.

Tang et al. [34], [35] studied mechanical characteristics of resistance spot welding machines, such as stiffness, friction, and moving mass and their complex influences on the resistance welding process and weld quality. They actually built facilities on a laboratory pedestal welder to enable the changing of mechanical characteristics like stiffness, friction and moving mass, comparable to the earlier work conducted by Dorn et al [33]. Stiffness of the lower electrode arm could be lowered by adding springs, as shown in Figure 2-11 below or it could be raised by adding a supporting leg from the floor to the lower arm of the machine.

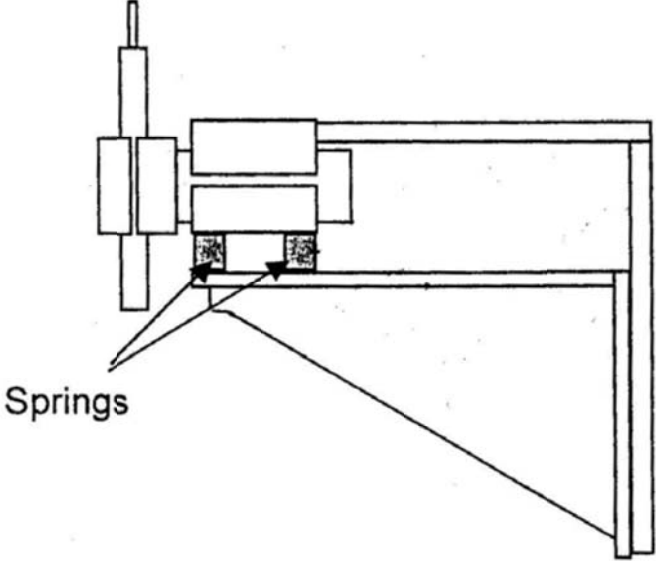


Figure 2-11 Changing of stiffness of lower electrode arm [34]

An additional device adding adjustable friction to the upper moving electrode was mounted to vary the friction force. (see Figure 2-12)

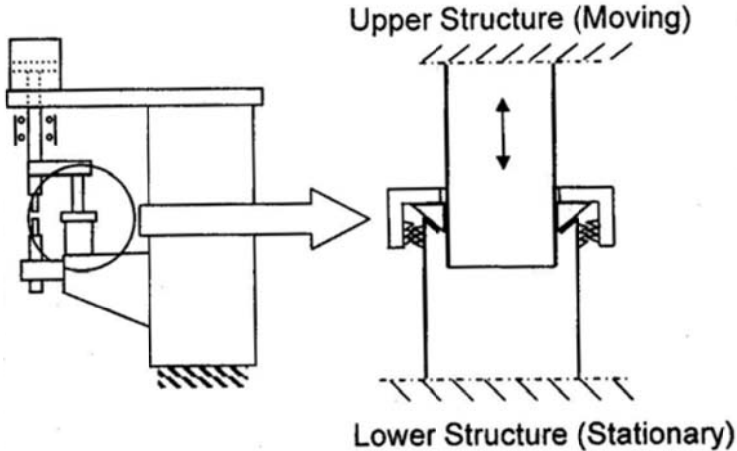


Figure 2-12 Device for adding adjustable friction [35]

Welding head moving mass could be varied by mounting additional weight to the moving electrode. (see Figure 2-13)

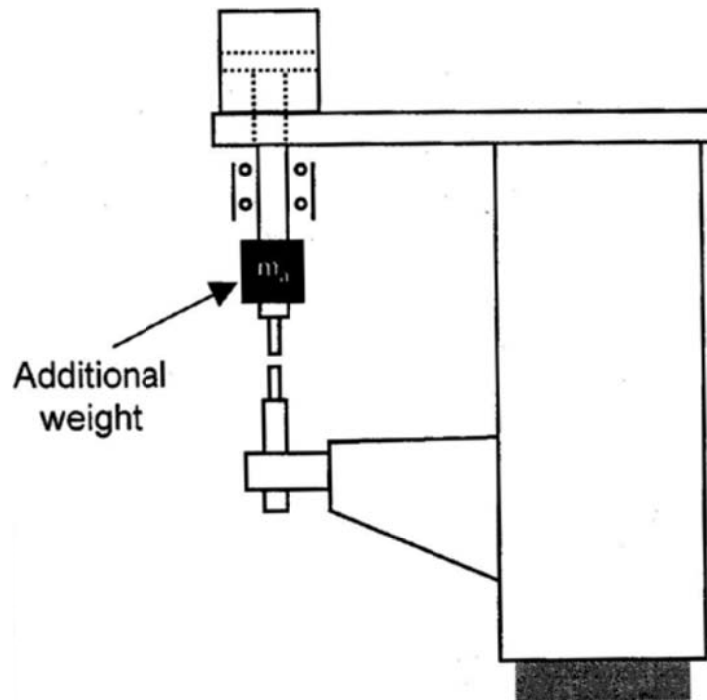


Figure 2-13 Changing welding head moving mass [34]

In their work, those influences were systematically investigated through experiments. The mechanisms of the influences are explored by analysing process signatures, such as welding force and electrode displacement, and other process characteristics, such as electrode alignment. A better understanding of the influences is achieved through this analysis. This study shows machine stiffness and friction affect welding processes and weld quality. The latter influences are identified through metallographic examination.

High stiffness reduces electrode misalignment, raises the expulsion limit and increases the forging effect, resulting in the recommendation of high stiffness in this study. Machine friction should be reduced when possible due to its negative effect on weld quality. It also confirms that moving mass does not significantly affect the process and quality of resistance spot welding. Materials tested on were steels and aluminium base alloys. Interesting to notice is their use of FEA software to assess the influence of changed machine setup on electrode arm deflection, electrode misalignment and contact pressure distribution.

Williams et al. [6], [7] concluded from their practical welding tests that the type and design of the welding machine also significantly determines the electrode life, with important parameters being (i) the mechanical characteristics of the electrode head assembly defined in terms of the force-time relationship developed on applying the welding force (frictional effects and machine rigidity are important in this context) and (ii) secondary transformer configuration, e.g. series, push-pull, indirect and parallel welding.

Williams [25] also noticed cyclic variations in electrode force, when welding under short circuit conditions with AC current. Tests using DC current showed a steady state condition of electrode force, free of any superimposed cyclic pattern. Williams attributes this variation in load to the electromagnetic attraction induced between the upper and the lower electrode arms.

The mutual force F per unit length between two infinite wires ‘ a ’ metres apart in a medium of permeability ‘ μ ’ is:

$$F = \frac{\mu I_1 I_2 L}{2\pi a} \text{ [Nm}^{-1} \text{]}$$

and with the definition of an Ampère generating a force of $2 \times 10^{-7} \text{ Nm}^{-1}$ in two parallel wires one meter apart, the latter leads to the permeability of free space being defined as:

$$\mu_0 = 4\pi \cdot 10^{-7} \text{ [Hm}^{-1} \text{]}$$

and with

$$I_1 = I_2 = I$$

this gives

$$F = \frac{\mu I^2 L}{2\pi a} \text{ [Nm}^{-1} \text{]} \quad (2.4)$$

Williams used this to estimate the values for these Lorentz forces for one of the machines tested in this research project [25], resulting in force values on the upper and lower arm for a machine with a throat depth of 1000mm with applied currents of 8kA and 10kA of 36.1N and 56.3N respectively and with a throat depth of 580mm with similar current levels of 20.9N and 32.7N respectively.

In 1997, **Fujimoto et al.** [36] investigated the relation between dynamic properties of a resistance welding machines loading system and weldability. They drew attention to the large electromagnetic forces generated between electrodes in high current density spot welding, confirming conclusions made in this field by Williams [25]. These forces induce welding force fluctuations that adversely affect weldability. The latter fluctuations in force vary depending on the force actuating systems stiffness, friction and follow-up behavior.

Wu [37] also investigated these Lorentz forces generated between conductors in the electrode arms due to the welding current passing. In the left part of Figure 2-14 below, Wu gives a schematic overview of the secondary current path in a resistance welding machine, with 1 the transformer, 2 the lower electrode arm, 3 the flexible lead towards the upper electrode arm, 4 the upper electrode arm, 5 the upper electrode holder fixture, 6 the upper electrode holder, 7 the upper electrode and 8 the workpieces.

In the right part of the same figure, Wu draws a simplified theoretical current path, indicating

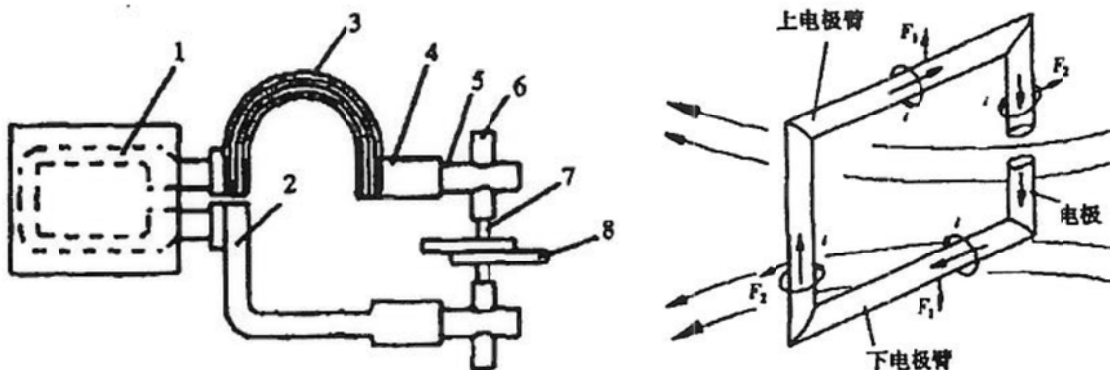


Figure 2-14 Schematic representation of secondary current path [37]

the current, magnetic field and resulting force directions in, around and on the elements of the current path.

Dupuy [38] discusses the effects of specifically inertia and damping and also identified stick-slip effects in friction by using the hysteresis in the application of increasing and decreasing pressure. He partially tested this on five different pneumatically activated machines. He also proposes that the operational stiffness and friction of the electrode actuating system influences the current range over which nuggets of acceptable size can be formed. Welding tests were performed with 1 mm thickness HSLA 360 steel in accordance with ISO 18278-2.

Zhang and co-workers [39] used dynamic resistance and electrode displacement signals and by extracting a large set of characteristic parameters (see Figure 2-15) out of these recorded displacement signals correlated them to tensile-shear strength of spotwelds.

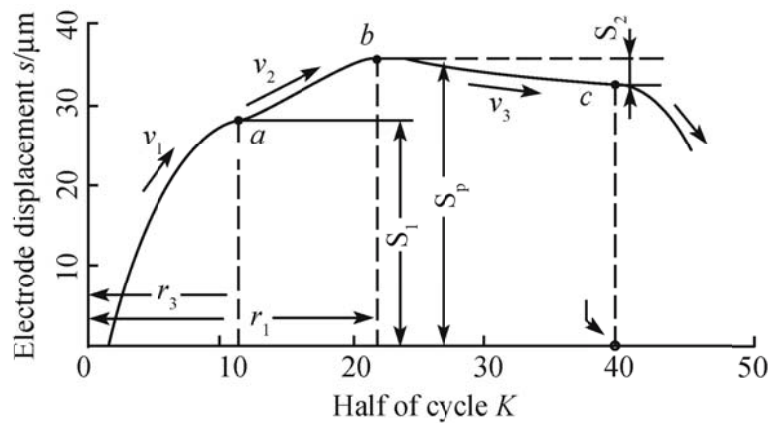


Figure 2-15 Sketch diagram of characteristic parameters extracted [39]

Their main conclusions are that electrode displacement signals containing the characteristic parameters could be used as measurement factors to monitor joint quality. The monitoring models need further study if this technique is to be applied to practical fieldwork.

Wang et al. [40] analysed the mechanism of fluctuation of electrode displacement by collecting primary welding current and electrode displacement during welding and extracted the incremental pulse expansion out of the electrode displacement. They named the latter the ‘displacement fluctuation peak’. From metallurgical experiments, the relationship of this displacement fluctuation peak with weld nugget growth during RSW was analysed. Their conclusion is that displacement fluctuation characteristics can be used to evaluate weld quality.

2.1.5 Modelling techniques for resistance welding processes

The most important issue for an end user of resistance welding equipment is basically the availability of a spot weld qualification procedure to ensure, that for a given material combination, a weld nugget of adequate size without defects can be achieved. The traditional operation mode has been to estimate nugget sizes from various destructive tests like peel or chisel testing. More recently, ultrasonic testing or dynamic resistivity profiles have been used for the same purpose.

Simulation of resistance spot welding through analytical modeling has drawn the attention of many researchers in the past decades. The early mathematical models were however unable to deliver realistic analysis of the process due to their complexity. Involving interaction between mechanical, electrical, thermal, surface and metallurgical phenomena. Most of the attempts made to simulate the process by theoretical models were limited to heat transfer problems and surface phenomena and all neglected the thermo mechanical interactions.

According to **Nied** [41], early models (pre-1980) were only devoted to determining temperature distributions during the weld cycle. In all publications before Niede's, the thermomechanical coupling was completely neglected. One assumed the contact area between the electrode and the workpiece as equal to the diameter of the flat on the end of the electrode. Bearing in mind that the contact area is established during the squeeze cycle and dependent on the electrode load used, an initial assumption of the contact diameter can be a source of large error, especially if spherical end electrodes are used in the process. Nied reports use of nonlinear thermomechanical coupling and contact behaviour using a commercial ANSYS code was used to provide more realistic simulation of the welding process but points to the necessity of correct temperature dependent material properties.

A one-dimensional heat transfer model describing the spot welding process was studied by **Gould** [42] in 1987 in comparison with weld nugget development as a function of three variables: welding current, welding time and sheet thickness. Nugget development was studied using optical microscopy techniques. The thermal model was formulated to include effects of: melting, temperature dependent thermal and electrical properties of the steel used in the tests, heat transfer in the liquid and contact resistances. Gould compared the model results with the microstructural observations and used the latter to understand the influence of various factors on nugget development. This initial and rather simple thermal model is actually an energy balance for each element in the stack of plate like elements in the configuration (see Figure 2-16 A and B).

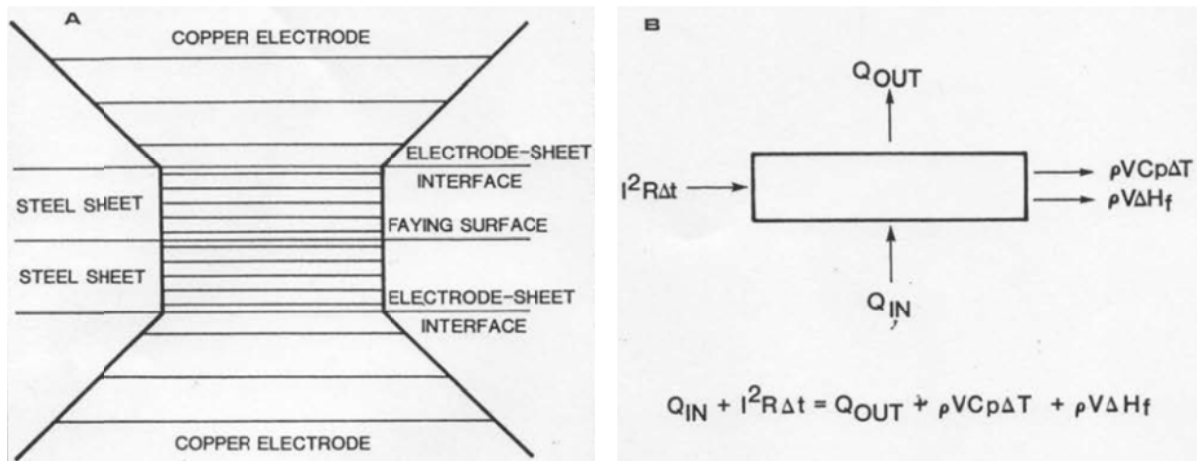


Figure 2-16 Element configuration and governing equation used in Gould's model [42]

Energy is introduced to the element in two ways: by internal (Joule) heating and by conduction. This in turn is balanced by accommodating the heat internally (by increasing the element temperature or by melting) and by heat loss through conduction. Heat flow in his model is one-dimensional, meaning that heat is assumed to be generated within the weld and conducted out through the copper electrodes. Also symmetry is assumed to allow for only half the weld configuration to be calculated. Boundary conditions are very simplified in respect of initial temperatures (that of the cooling water), no heat transfer across the faying surfaces and with respect to the heat of melting, the steel was assumed to behave as pure iron.

It is clear that many assumptions had to be made due to lack of available data. For instance the relationship between the faying surface resistance and temperature is assumed to be linear. Results are basic and were used to calculate cooling rates in the weld.

Han et al. [43] further developed the heat transfer model above resulting in 1989 in the capability to predict temperature as a function of time for any location in the workpiece. More developed numerical modeling of resistance welding processes requires us to view them as electrical-thermal-mechanical processes. Many researchers have made huge efforts in the past two decades to lift finite element simulation of resistance spot welding to a level trustworthy to justify its use in practical welding.

In 1992, **Tsai et al.** [44] used ANSYS finite element code to model and simulate resistance spot welding, revealing the state of stress attained during the squeeze cycle and showing a stress concentration at the periphery of electrode/workpiece interface and the workpiece faying surface. A ring-like weld nugget was initiated at a distance from the electrode center and expanded in- and outwards during the weld cycle.

Browne et al. [45], [46] published their experiences of developing coupled finite element modeling software capable of incorporating the electrical, thermal and mechanical aspects of the resistance welding process on Alcan aluminium products in 1995, revealing the effect that the applied force and resulting mechanical deformation has on nugget formation is due to the determination of the contact area and current density at the faying surface. Contact resistance is a key factor, as is shunting effect of previously formed welds. Also the effect of domed electrodes was studied.

Li [47] from Battelle Memorial Institute in 1997 pointed out one of the major weak spots in every numerical simulation solution available on the market, namely the complete absence of realistic physical material data characterizing contact properties between metals stacked up in a resistance welding application ready to be welded. Moreover, these data need to be readily available in the complete temperature field crossed during a resistance welding cycle. Li states that measured static contact resistance values are mostly attributed to the film effects and thus are dependent on the surface condition, the current level used in the measurements, temperature and applied force.

Film resistance breaks down very early in the welding process, typically in a fraction of the first quarter cycle. So the measured static resistance prior to film breakdown does not represent the contact resistance in the rest of the welding process. It is believed that measuring dynamic resistance offers values more representative to the resistive heating during an actual welding process. However, there are so many factors that would affect the dynamic resistance values, including electrode geometry, welding current, sheet thickness, electrode force, etc. and their effects are extremely difficult to be quantified starting from a purely theoretical approach.

Li proposed a contact resistance model derived from the characteristics of voltage and resistance of electric contacts and validated his theoretical model with experimental measurements on spot welding of 0.8mm bare steel. Li used ANSYS commercial finite element code with however a lot of simplifications to cope with data being unavailable such as the assumption of electrode force remaining constant during squeeze, weld and hold cycles or the use of thermal, electrical and mechanical properties of both copper electrode material and carbon steel from materials handbooks. Although all these parameters are treated as nonlinear, temperature dependent properties, they remain static measured values. Li's results however are a major step forward in understanding the effects of welding parameters on nugget formation.

Wenqi Zhang and **Niels Bay** [48], [49], [50], [51], [52] from the Department of Mechanical Engineering at DTU in Copenhagen, continuously developed SORPAS (Simulation of Resistance Projection And Spot welding) software during the past decade. One of the major reasons why this software, specifically dedicated only to resistance welding is gradually improving and gaining more and more users worldwide, is the very close interaction of the DTU research department, SWANTEC, a spin-off company from DTU commercializing the software and the numerous companies with their specific applications in the field. When an application causes difficulties to be simulated, all efforts are made to find the cause and to supply a solution, the latter in turn often resulting in another optimization of the software. There is also a large user group, exchanging experiences at the bi-annual seminars on the advances in resistance welding or over the [innoweld.net](http://www.innoweld.net) network. Several publications based on user experiences result from the latter. [53], [54], [55], [56], [57], [58]

Dupuy et al. [59] used commercial finite element code SYSWELD+ to perform electrical-thermal simulations. Their approach lead them to define three types of input parameters, the appropriate mesh geometry, contact boundary conditions and material properties. Using a two dimensional axis-symmetric mesh, only flat tip electrodes were used since the model did not include a mechanical simulation necessary to reproduce the evolution of contact size during welding associated with rounded tips.

Current waveforms used are derived from real measured signals, but also purely imagined current waveforms were used. Radiative and convective heat transfer coefficients at the boundaries were chosen from literature, as well as the materials electrical and thermal

properties, which are considered as functions of temperature. Electrical and thermal contact properties were assigned to extremely thin layers of contact elements at each interface.

Since Dupuy aimed to apply the model for welding on coated steels, adaptation of the model by introducing additional elements with intrinsic properties of the coating as well as changes at each interface were used.

Practical problems occurring in his approach are the use of domed electrodes in his experiments where the model can only deal with flat tip electrodes. The modeled results are disappointing in respect of quantitative resulting values, but they were useful in understanding the necessity of a mechanically coupled model and of correct data input of materials and contact properties as a function of temperature and pressure.

According to **Feng** and his co-workers [60], [61], there are strong interactions (coupling) among the electrical, thermal and mechanical aspects of the process that pose significant difficulties in numerically modeling the resistance spot welding process. Materials ready to be resistance spot welded show electrical properties as their bulk resistance and contact resistance that strongly depend on temperature and contact pressure. Feng et al. also state that changes in the temperature field in the workpieces and the electrodes due to Joule heating will result in changes in the Joule heat generation rate that in turn will influence the evolution of the temperature field. Feng et al [60] used Abaqus, a commercial general-purpose finite element code that they enhanced with a number of user subroutines and modules. Since electrical contact resistance has a very dominant effect on the formation of the weld nugget, they proposed a model to describe the variation of contact resistance as functions of temperature, pressure and material yield strength. This dependence of contact resistance on the contact pressure and temperature is incorporated in the incrementally coupled finite element model.

Contact resistance consists of the constriction resistance and the surface contaminants (or film) resistance. When two metal surfaces, each with certain roughness are brought into contact, the real contact area of the mutually deformed asperities is much smaller than the apparent contact area as long as the normal pressure is below the yield stress of the softer material. (see Figure 2-17)

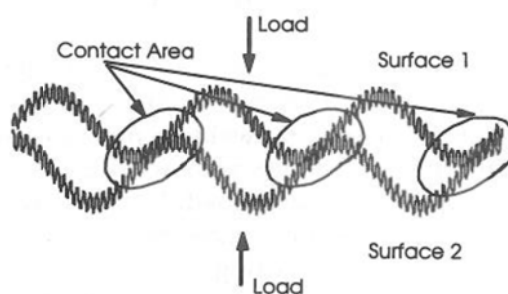


Figure 2-17 Contacting surfaces with microasperities and surface waviness [60]

When a current runs through the interface, then the current flow lines bundle together passing through the separated conducting spots of real contact. This constriction of the electric current by the contact spots reduces the volume of metal used for electrical conduction locally at the interface and leads to the rise of the resistance value.

The film resistance on the other hand is due to less-conductive surface films such as oxides, oil, water vapor and other surface contaminants. This film resistance is not taken into account by Feng [60]. Contact resistance becomes an explicit function of temperature, pressure and bulk resistivity for a given contact interface.

Feng et al. measured the electrode to workpiece and that at the faying surface under iso-pressure conditions and at ambient temperature. (see Figure 2-18)

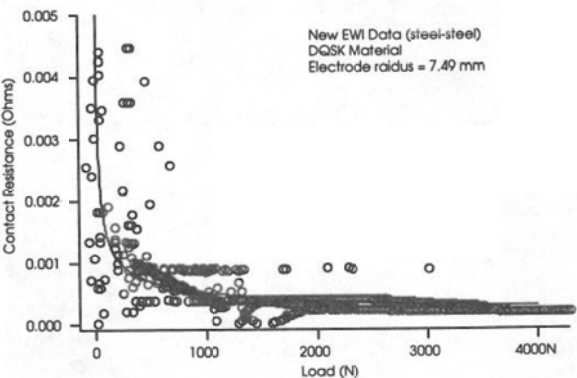


Figure 2-18 Comparison of contact resistance variation as a function of pressure at room temperature [60]

They calculated an estimation of the contact resistance variations at the faying interface of the DQSK steel with 6.33mm electrode face diameter used in one of their simulations. (see Figure 2-19)

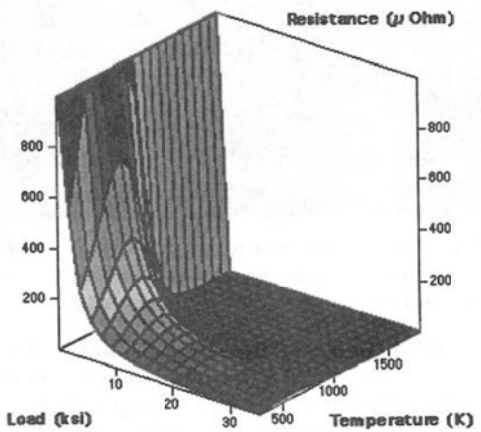


Figure 2-19 Contact resistance-temperature-pressure diagram according to [60]

Their analysis revealed significant pressure and contact area variations during welding, necessitating the use of three-way coupled electrical-thermal-mechanical modeling in order to accurately capture heat generation, thermal history and deformation history during a resistance spot weld.

Sudnik et al. [62] in 1999 focussed on implementation of electrical parameter setting into the SPOTSIM FEM software to enable more accurate input of machine electrical settings. Active resistances of the welding circuit as well as conduction angle of the welding current are taken into account. Spotsim was developed for Resistance spot welding as the name suggests. The model is based on the equations of electric potential and thermal productivity. It reproduces plastic deformation of the metal and takes into account electrode geometry. Machine dynamics are not accounted for. Quite a large error margin remains between the size of the calculated molten welding nugget and the values measured in metallographic examination.

In 2000 and 2001, **Sun** [63], [64], [65] published the results of several studies using Abaqus commercial code where she also dealt with simulation of resistance projection welds. The latter revealing a new problem not accounted for in any of the former investigations, namely changes in pressure distribution due to changes in the collapsing stage of the welds.

In their publication in 2002, **Vichniakov, Herold and Greitmann** [66] disseminated the results of their study on projection welding showing large displacements during the follow-up stage in the welding cycle using Ansys commercial code. They concluded that FEM can also in this range of workpieces be used for determination of welding range diagrams.

Later, in 2002, **Robin et al.** [67], in a joint venture coordinated by PSA Peugeot-Citroen and with Usinor research centre involved for material characterization also focused on the contact interactions during spot welding leading to better prediction of reality in the case of using rounded electrode tips in spot welding simulations. They also used Sysweld software with a model with coupling between electrical, thermal, metallurgical and mechanical fields and concluded that contact element formulation is important to generate more realistic results. There however still remains the difficulty to obtain practical data ready to be introduced as material related properties into the models input.

In their publication in 2003, **Chang and Zhou** [68] studied electrode force as important process parameter when using DC current on a small scale resistance spot welding application. Variations of contact radii, current density distribution and temperature profile at the sheet-sheet and electrode-sheet interfaces, the threshold weld times and the maximum diameters of the weld nuggets under different electrode forces were investigated, resulting in the following conclusions:

- contact radius at both interfaces decreases during the welding process.
- Increasing electrode force increases the contact radius at both interfaces.
- The minimal contact radius at the electrode-sheet interface is larger than that at the sheet-sheet interface.
- Welding current density distributes evenly initially, to later increase with decreasing of the contact area at both interfaces and finally concentrates at the molten nugget region.
- Increasing force decreases the current density because of the increased contact area. Temperature at the central part of the workpieces is the highest at both interfaces.
- Molten nugget initiates at the sheet-sheet interface center.
- Temperature increases more quickly under a lower electrode force because of the decreased contact area and increased current density.
- Shorter threshold weld time or lower threshold welding current is needed for nugget initiation when the electrode force is decreased. However, decreasing electrode force also increases the cooling rate at the nugget center.

Thomas Dupuy [69] published a comprehensive review on the state of the art in numerical simulation of resistance welding processes in 2004. He sums up the potential benefits but also points at the Achilles heel, potentially present in all publications above, namely the absence of effective procedures to generate correct physical data on the materials used and their contact properties under loading and at different temperature levels.

Song, Zhang and Bay [70] were the first in 2005 to publish procedures to generate 'real' physical material data using a Gleeble machine. (see Figure 2-20)

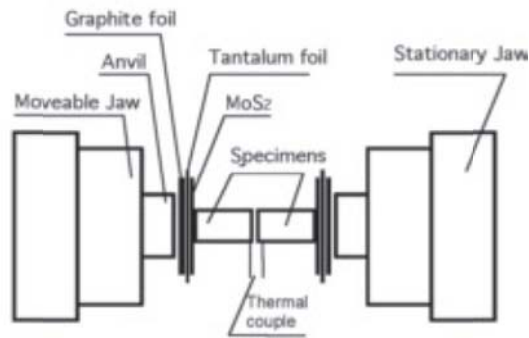


Figure 2-20 Schematic setup of material tests on Gleeble [70]

A Gleeble system is actually a dynamic testing machine that can simulate a wide variety of thermal/mechanical and metallurgical situations. Samples can be heated and mechanically loaded following a preset program, while in the mean time, parameters of interest are measured and recorded for later analysis. A major benefit in the use of a Gleeble machine is that it heats the specimens by resistance heating, exactly as in resistance welding. In this way, contact resistance during a process similar to resistance welding can be studied.

Materials tested by Song including low carbon steel (AISI 1018), stainless steel (AISI 304) and aluminium (AA1050) are widely applied in industry. Test specimen (cylinders 7,5 x 6mm) were machined to a uniform surface roughness, rinsed with compressed air and stored indoor for approximately 2 months. No subsequent cleaning, rinsing or degreasing was carried out prior to the experiments to ensure surface conditions similar to those in industrial use.

During each experiment, the following parameters were measured: force, deformation of specimens, interface temperature, heating current and voltage drop over the interface

In 2006, **Song et al.** [71], [72], working in the same department at DTU in Copenhagen made a major step forward in finite element based numerical modeling for resistance welding as a tool for development and optimization of complex joints by introducing a more appropriate model of the contact between the workpieces. A contact model is developed for simulation of resistance spot as well as projection welding that deals with the mechanical, thermal and electrical contact problem. Mechanical contact including frictionless as well as sticking and sliding friction contact. Thermal and electrical contact are modeled by introducing an artificial contact layer. Song makes the distinction between frictionless contact, constraining contact only to the normal direction of the contact element, sticking contact, in most resistance welding situations like spot welding, where tangential sliding at the interface is minimal and frictional sliding contact allowing sliding by angular oriented elements as in projection welding. Song succeeded in coupling the three models (see Figure 2-21), enabling more realistic simulations of resistance projection welded complex joints and welding of dissimilar materials.

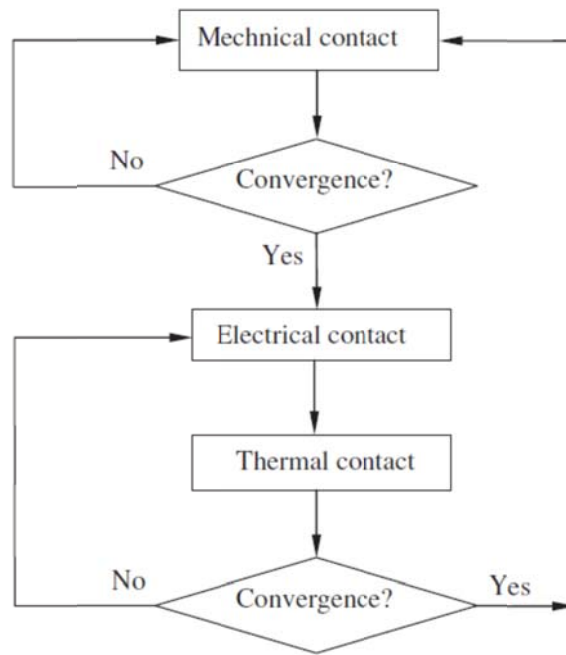


Figure 2-21 Coupling scheme of models with contact [71]

In his experimental validation of the former publication [72], Song compares the results of practical tests with simulation deformation results made with Sorpas of compressed sandwiches of different materials and with the three contact situations. (see Figure 2-22 and Figure 2-23)

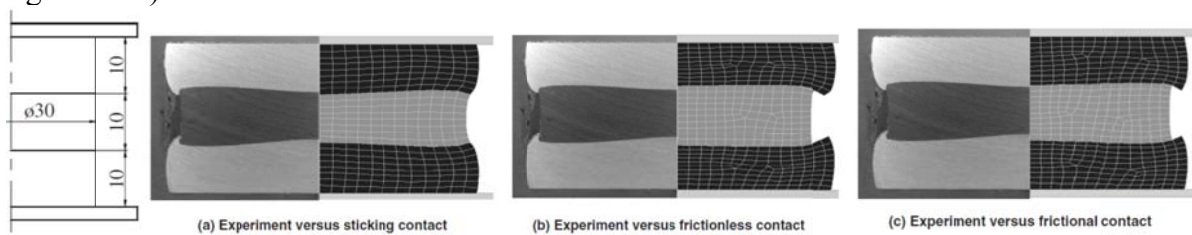


Figure 2-22 Sandwich upsetting aluminium–brass–aluminium in different contact situations [72]

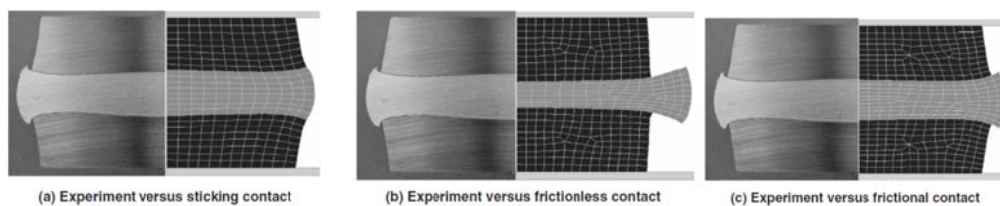


Figure 2-23 Sandwich upsetting brass–aluminium–brass in different contact situations [72]

Satisfactory accuracy between reality and simulation is reached. The frictional conditions resemble those in resistance spot welding. A similar experiment was carried out on projection welding of flat disc – solid ring projection and validated the contact model.

Material data are offered in a large database in the commercial software SORPAS (simulation of resistance projection and spotwelding), commercialized by the Danish Swantec company.

2.1.6 FEA based on 'In-Situ' characterisation tests

A key development in determination of machine kinematics was the development of a new concept by this author.

This involved imposition of a step function on the welding head and measurement of subsequent head response. These measurements could then be used in a model of machine behaviour to calculate welding head effective lumped mass and welding head damping.

In 2002, the author presented a paper [73] at the 2nd International Seminar on the Advances in Resistance Welding in Aachen where this new concept of measuring representative mechanical machine parameters such as lumped moving mass of the moving welding head, damping coefficient, maximum velocity after a distance travelled and maximal acceleration was described.

The author later realised that the step function could be imposed on the welding head by using a supporting pin fracturing away underneath the upper electrode. This test was named the free fracture test, and was developed following an original suggestion by Niels Bay [74] who used this test method to measure maximal welding head velocities attained after a certain distance travelled on different machines.

The upper welding head is represented as a force actuated mass-damper system, similar to Gould's [23] concept. The lower welding head should be represented as a mass-spring-damper system, but with very low structural damping. This concept was developed in the attempt to find a solution to one of the weakest spots in the FEA software, namely the lack of data on specific machine behaviour. Experience in production welding applications reinforced the need to generate data in-situ to allow the input of specific machine data into the FEA software.

Wu et al. [75] later developed a spring supported fracture test at the Technical University of Denmark where a more weld-mimicking or resembling movement is offered at the pressurising system by inserting a spring support underneath the fracture tests upper anvil. This followed a period where Wu worked in the author's laboratory during a period of secondment in 2002 and acquired detailed information on the free fracture test.

Chen et al [76] use measured displacement and force signals of small scale resistance welding machines to input in a Simulink model and calculate stiffness and damping coefficients of the model (see Figure 2-24)

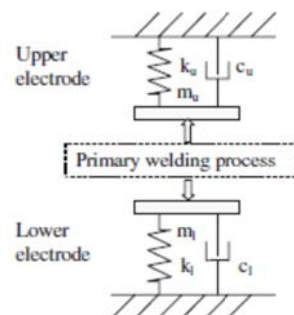


Figure 2-24 Representing model used by Chen [76]

Chen needs to dismantle the machine's head with its appendages and weigh all components to get a notion of the representing lumped mass of the moving welding head. Apart from this, his approach also necessitates a force measurement integrated in the lower electrode assembly. This approach is very interesting, and copes with reality as validated by his experiments with test welds without expulsions, and with small and with large expulsions. However, in the current setup, it cannot be used out of the laboratory application because of the invasive character of the test setup.

2.2 Projection geometries

Over the years working on this thesis, the importance of workpiece geometry, especially in projection welding has proven to be of outmost importance. Although not the core of my thesis, I did examine the influences of different projection geometries on their weldability and on behaviour in specific applications.

In general, projections can be divided into artificial and natural types. Artificial when any machining needs to be performed in order to change workpiece geometry to obtain a projection. This can be embossing in plate like structures, cutting, bending or even additive casting for more massive workpieces. Some of the artificial projections are standardised, the majority of them are not.

On the other hand there are natural projections, created by simply bringing two workpieces to be joined into contact. These applications include concrete steel reinforcement nets, cross wire grid in shopping baskets and trolleys, or cross welding of steel tubing. There are interesting applications where artificial changes on natural projections can dramatically change weldability as well as joint properties.

2.2.1 Artificial standardised projections

Standard embossed projections, mainly for thin steel plate are proposed in BS EN 28167:1992 [18].

It is important to mention that only round projections are dealt with in this standard.

Longitudinal and annular ring projections are described in DIN 8519:1996 based upon DIN 8519:1978 [77].

These cover the majority of applications in thin steel plate welds, that need to be able to withstand torsional loads and or provide leak tightness.

2.2.2 Artificial other projections

In projection welding, there is a tremendous design freedom for creating projection shapes and geometries.

Nevertheless, different organisations, like IIW, AWS, RWMA tend to propose geometries towards their members. However, it is clear that there is some ambiguity concerning the optimum designs.

Hess and Childs [8], [9] published a pioneering paper on projection welding in 1949. Hess and Childs limited their investigations to coined embossed projections with a spherical shape. The latter because those researchers assumed that this type of geometry offered the best possibilities for symmetrical current distribution and uniform projection collapse. Using a strain gage based device attached to the electrodes and coupled to an oscillograph, they measured and recorded electrode displacement during projection collapse.

Their conclusion were mainly the following:

- that projection height/diameter ratio highly influenced weld strength levels over a greater range of welding conditions,
- that the projection diameter was not very critical within a wide range of values,
- that multiple projection welds did not result in shear or normal tension strengths proportional to single welds,

- that fusion only started after projection collapse was practically complete (and occurring in the first 15% of the weld time,
- that to avoid merging of multiple projections, they should be spaced at least 2.5 times the diameter of the fused zone.

Nippes et al. [10], [11] built further on Hess and Childs' work. Projection welding of steel with low thicknesses, steel in heavy gages and projection welding of steel with dissimilar thicknesses was investigated.

It is interesting to note the use of spring loaded electrodes to provide the low welding pressures required for the low thickness steels and still give sufficiently rapid follow-up during projection collapse.

Harris and Riley [13] proposed projection geometries, both for thin and heavy gage materials, also covering unequal thicknesses and especially introducing the use of recessed projections (see Figure 2-25 and Table 2-3) to enable complete setdown of the plates after welding and covering a variety of equipment to assist in its selection.

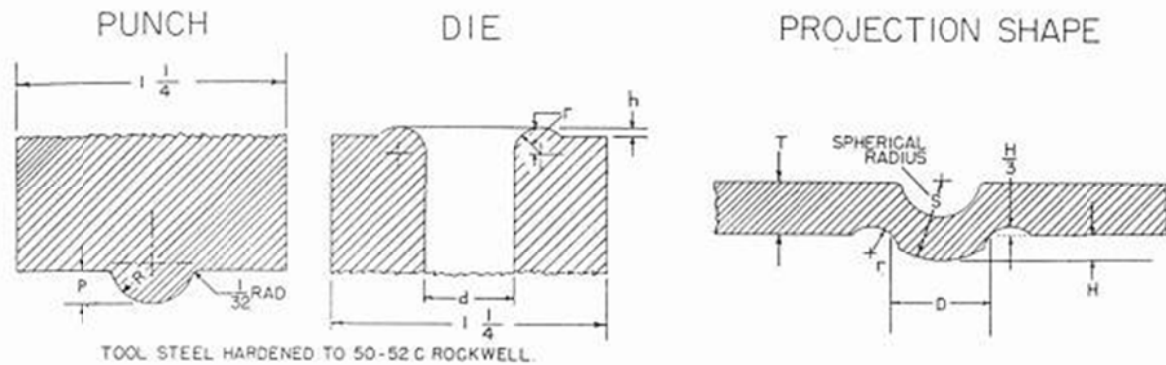


Figure 2-25 Punch, Die and projection geometry according to Harris & Riley [13]

Plate	Projection			Punch		Die		
Thickness	Height	Diam.	Radius	Radius	Height	Diam.	Recess radius	Recess height
T (mm)	H (mm)	D (mm)	S (mm)	R (mm)	P (mm)	d (mm)	r = S/3	h = H/3
3,12	1,47	6,86	4,98	2,39	1,91	5,61	1,65	0,48
3,43	1,57	7,62	5,46	2,77	2,06	6,35	1,83	0,51
3,89	1,63	8,38	5,97	3,18	2,16	6,86	1,98	0,53
4,17	1,73	9,14	6,30	3,58	2,31	7,54	2,11	0,58
4,55	2,03	9,91	6,96	3,96	2,64	8,33	2,31	0,69
4,95	2,13	10,41	7,26	3,96	2,82	8,59	2,41	0,71
5,33	2,29	11,18	7,75	4,75	3,05	9,09	2,57	0,76
5,72	2,54	11,94	8,26	4,75	3,35	9,35	2,74	0,84
6,22	2,84	13,46	9,27	4,75	3,71	10,31	3,07	0,94

Table 2-3 Dimensions according to Harris & Riley [13]

Cunningham et al. [78], [79], [80] used high speed photography to study the formation of a projection weld (with the use of sectioned projections without expelling metal during the weld). They studied weld collapse, the effect of projection height, projection geometry, nugget formation, heat generation and heat flow as well as weld quality.

One of their major conclusions was that variation of projection height from the earlier recommended values by 50% seldom results in changes of strength greater than about 6%, although consistency in weld production was modified to a greater degree. These researchers also observed a phenomenon called electromagnetic stirring of molten metal in the nugget (see Figure 2-26)

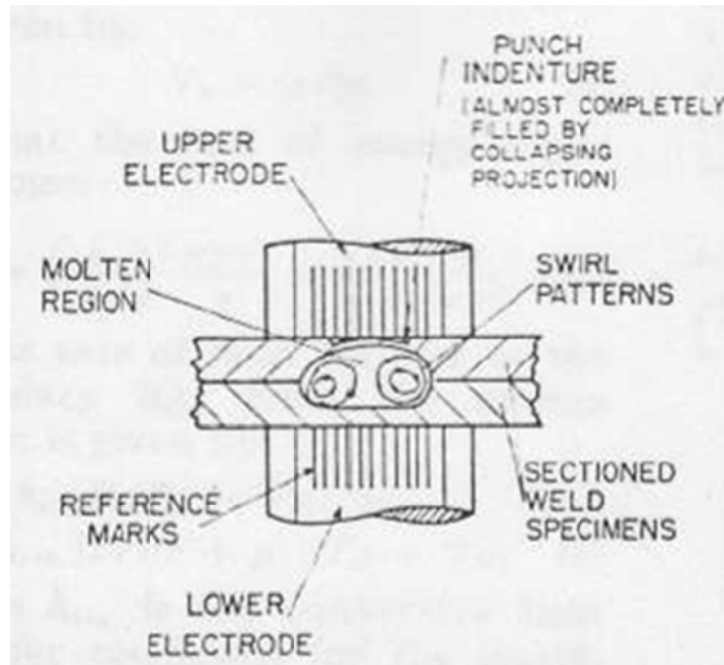


Figure 2-26 Electromagnetic stirring in weld nugget [80]

Adams et al. [81] investigated the AWS, IIW and H&R projection geometries, standard in that era and concluded the following:

- in comparable welding conditions, AWS and H&R projections made stronger welds
- IIW projections consistently were the first to expel liquid metal
- in comparable welding conditions, strength and nugget areas of AWS and H&R were practically identical
- IIW projections generate heat in a single centre point source where AWS and H&R projections generate heat in an annular ring
- manufacture of H&R projections is more complex since the die does not limit projection height
- different weld settings are needed for each projection geometry to produce optimum weld strength

Sun [65] investigated the same three projection geometries as discussed above with different projection heights by using an incrementally coupled, thermal-electrical-mechanical finite element modeling procedure. The predicted heating patterns were then compared with weld cross sections.

She concluded that her predicted results on nugget formation and projection collapse compared reasonably well with the available experimental data. Apart from the confirmation of earlier work, it also demonstrates that FEA can be used as a powerful tool to study the detailed physics of a highly dynamic coupled process such as projection welding. Results can

provide some quantitative understanding and guidelines about projection design and weld parameter selection.

She states that with this tool, it is possible to develop improved procedures for determining weld conditions, requiring only a nominal amount of experimental work as a means of verification

Another important conclusion regarding projection geometry is the following:

- in extremely high projections, the rate of localized heat generation is faster than the rate of projection collapse and as a result, weld collaring and expulsion will occur during the early welding cycles.
- On the other hand, when low projection heights are used, premature collapse of the projection will reduce current density and delay nugget formation.

Resulting, dynamic balance between projection collapse and heat generation must be maintained to achieve an optimized projection welding process.

2.2.3 Natural projections and artificially altered projections

ARO, [14], [82] based on their experience with customers and their application published a code of good conduct for resistance projection welding of tubular components.

They are the first to publish the technique of indenting tubular components (see Figure 2-27), formerly a practice to bend tubes, with the intention to create multiple contact points on the overlap between workpieces. The latter giving a huge advantage over single contact overlapping joints in respect of transferring torsional loads into multiple shear loads. Joint properties under static and dynamic loading are lifted to a higher level as a result.

RESISTANCE WELDING OF WELD STEEL TUBES
EXAMPLES

TYPE OF ASSEMBLY	WELDED ASSEMBLY	CROSS-SECTION OF WELD	ELECTRODE SHAPES	PREPARATION OF TUBES	WELD SEQUENCE	*
Cross welding of tubes				None	Simple	A Page 11
Cross tube welding with SOS collapse				None	Complex	B Page 12
Cross welding of tubes with SOS collapse using pre-shaped tubing				Pre-shaping of both tubes	Simple	C Page 13
Cross welding of tubes without overlap				None	Simple	D Page 13
Back-to-back welding of bent tubes				None	Simple	E Page 13
T welding of tubes with one flattened end				Flatten end of one tube and form dimples		F Page 13

* SEE FOLLOWING PAGES FOR ADDITIONAL DETAILS

Figure 2-27 Advised setup for cross tube projection welding [82]

Conclusion of literature review:

Mechanical properties of resistance welding applications are specified in the ISO 669 standard 'Resistance welding – Resistance welding equipment – Mechanical and electrical requirements' [1]. The latter standard dealing in detail with the static machine properties and supplying test procedures to enable their measurement.

Static machine properties are important in both spot- and projection welding, since they are responsible for contact errors in electrodes due to eccentricity and deflection of electrode arms and electrodes.

In respect of dynamic machine properties, the standard emphasises pre-weld machine behaviour during the approach and contacting stage of the weld cycle and it mentions the importance of follow-up behaviour during workpiece collapse, the latter specifically in projection welding, where it is possible that acceleration of the electrode during projection collapse absorbs a (too large) part of the electrode force, thus leading to oscillations in the welding force or worse, even complete loss of contact between the electrodes and the workpiece, immediately leading to expulsion of molten metal, the latter resulting in poor weld quality.

These working conditions are only possible when actuator force levels have to be set low by necessity, for instance when workpieces cannot support high mechanical loads as in welding thin sheet metal, aluminium alloys, projection welding high melting to low melting materials or welding of thin-walled tubular components.

One can conclude that in order to ensure proper weld quality, fast follow-up behaviour of the electrode is an essential feature to maintain contact between electrodes and workpieces. The latter being a very important feature in respect of the dynamic mechanical characteristics of resistance (projection) welding machines.

Lumped moving mass, friction and stiffness of the moving welding head, including the force actuator are characterizing factors that will define mechanical machine characteristics. Researchers have built simulation devices or specially re-designed production machines to enable experimental evaluation of these characterizing factors by varying them. Contradictory demands result, depending on properties one wishes to improve or depending on specific machine design. Where moving mass has no significant influence on weld quality as such, it has a large influence in follow-up in projection welding.

Römer et al. [19], [20], supply us with the mathematical models that through qualitative analysis lead to a guideline for improved machine design.

Feng et al. [22], modelled the touching behaviour in air-operated machines, where

Gould et al. [23] provide the mathematical models both for the touching as for the follow-up behaviour, offering a true milestone in approach.

Many researchers have supplied us with improved understanding of the influence of machine mechanical properties on weld quality and with recommendations to enable improvement of these machine properties. However, most of these investigations do not lead to modeling procedures that can be used in practice, they all stay limited to more qualitative analysis based on rather invasive measurements.

In respect of the Finite Element Analysis software dedicated towards resistance welding, research can be divided in two categories, the general purpose commercial software codes on the market on the one hand, used by many researchers to input resistance welding applications, and mainly limited to spot welding, apart from a few.

On the other hand, in spite of so much effort, to enable realistic simulation, especially towards projection welding applications, availability of correct material and process data are a necessity. Generation of these data was surely lifted to a higher and realistic level by the Department of Mechanical Engineering at DTU in Copenhagen, resulting in SORPAS FEM software, dedicated ONLY to resistance welding applications. However, there remain two Achilles heels, namely the effective contact properties of materials available on the market or even of different batches of the same material and mechanical machine properties, influencing machine dynamics.

Furthermore, three references, Williams [25], Fujimoto et al. [36] and Wu et al. [37] deal with electromagnetic forces induced by the welding current and acting on the welding arms, while one reference, Dupuy [38] emphasizes on friction and stick-slip effects during welding head movement.

Finally, since projection welding is especially vulnerable for poor fitness for purpose in respect of a machines' mechanical properties, this less optimal design can be overcome by using smarter projection design.

3 Aims and Objectives

Widening the application field of resistance welding is a challenge in this era where many other high energetic welding processes experience a massively increasing popularity. Resistance welding however has systematically evolved during its ages of existence and application. It's a state of the art joining technology ready to conquer new application fields, mainly for automated and/or mass production. Finite element analysis (FEA) techniques incorporating very complete databases covering accurate data of workpiece and electrode geometries, materials used and parameter sets programmed into the welding machine are available and they surely increase common general knowledge and in depth specialized know how amongst welding engineers and assist them in their choice and their practical design of joining solutions in existing and future applications. Nevertheless, it needs to be mentioned that sufficient correct data is available in the databases of FEA software for most of the spot and seam welding applications, thus generating correct output and leading to satisfying results in numerous applications. However, especially in projection welding of complex geometries or in those application that incorporate exotic material combinations and/or thin walled tubular geometries and in all applications where larger displacements are due to be made by the welding head during workpiece collapse in the deformation stage of the welding cycle, there is an absence of available data on the mechanical characteristics of the welding machine to be used. It is a fact that there are thousands of combinations of specific resistance welding machine assemblies of so many different constructors on the market. Indeed, it needs to be mentioned that many machines are custom built around a specific application with components from different constructors.

At the start of this work, only limited data characterising resistance welding machine behaviour was available that merited to be inputted as mechanical data into FEA software or that could be used to assess a welding situation in practice.

The objectives of this work therefore can be summarised as follows:

- a. Development of mobile measuring techniques capable of collecting all necessary mechanical and electrical data from a resistance welding machine In Situ in a working production environment without interfering in the production process.
- b. Development and evaluation of In Situ mechanical tests and test procedures capable of imposing a sudden step in the pressurizing force between the welding electrodes, inducing the welding head to make a displacement at its maximum dynamic possibilities.
- c. Development of a measuring and processing procedure to record this sudden displacement in time and delivering machine specific mechanical data ready to be used in assessment of specific machine potential and/or in Finite Element Analysis as a restricting boundary condition.
- d. Development of a machine mechanical model and corresponding analysis method for generating machine specific parameters.
- e. Study of the mechanical test procedure results on machines with different actuator systems.
- f. Study of the influencing variables on machine model results.
- g. Development of a correct machine evaluation procedure.
- h. Evaluation of influence of welding current on machine mechanical behaviour.
- i. Study on the interaction between projection design and machine behaviour and resulting weld quality.

Figure 3-1 shows the thesis objectives flowchart graph

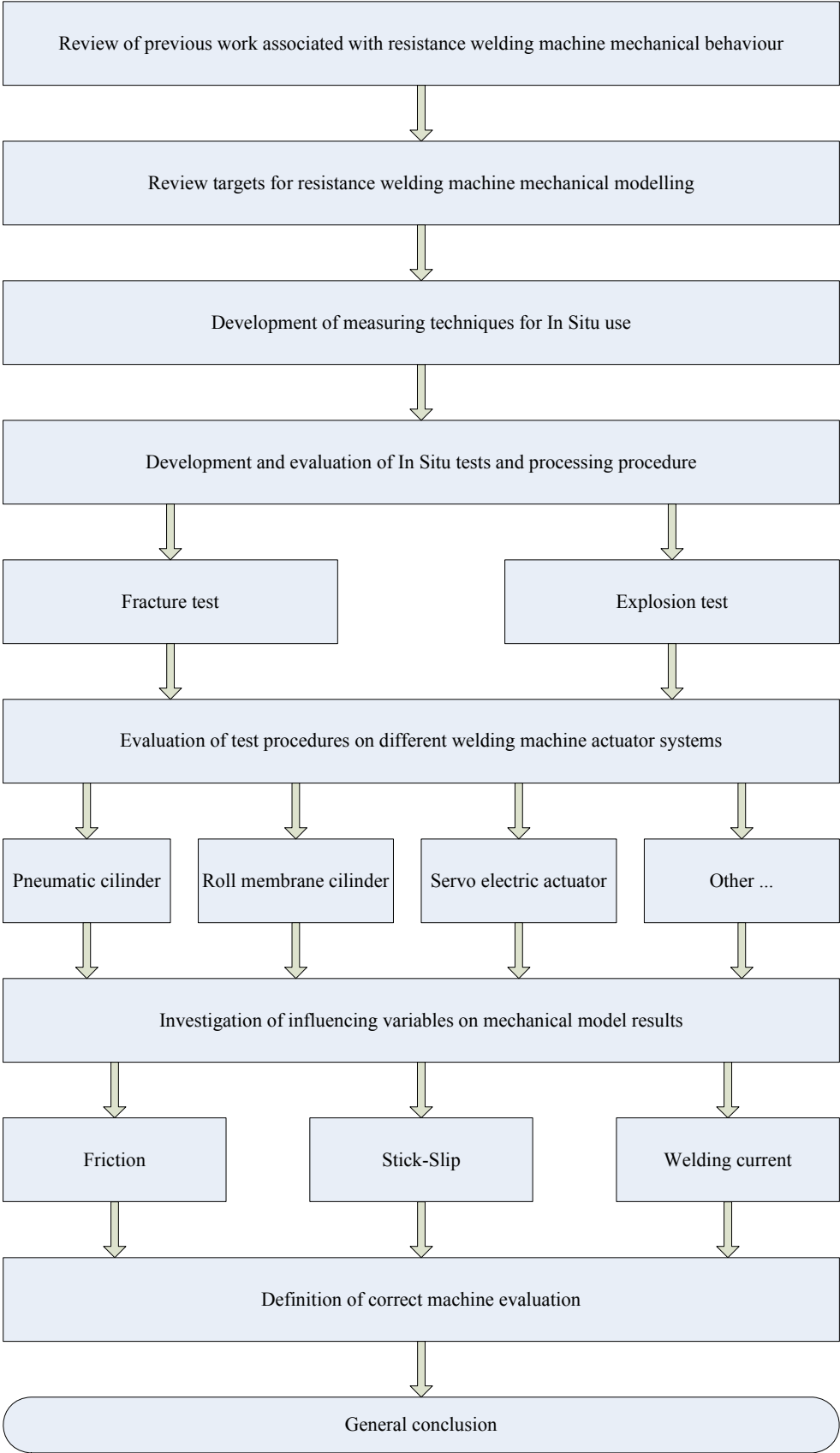



Figure 3-1 Thesis objectives flowchart graph

4 Equipment used

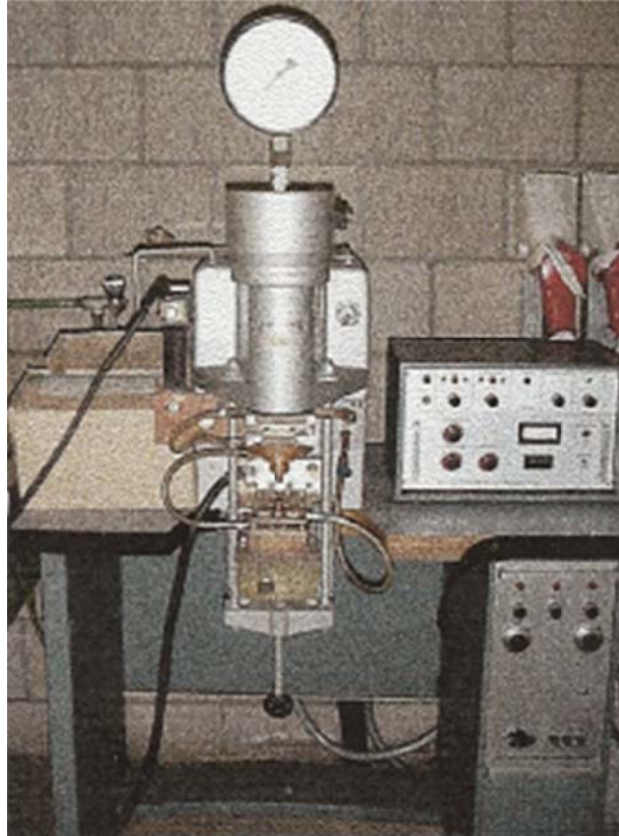
4.1 Resistance welding machines

4.1.1 AWL multi purpose spot/projection welder

Location: Lessius Mechelen, Campus De Nayer, Laboratory of alternative welding processes			
Type description: AWL wp 63 rl range 2 63 kVA/50% 380 Volt/50Hz			
Control unit: SER Mega			
			
Electrical Properties			
Type of welding current	AC		
Mains voltage	380 V		
Mains frequency	50 Hz		
Nominal power at 50% duty cycle, S_{50}	63 kVA		
Maximum welding power, S_{max}	810 kVA		
Transformer tap settings	1		
Secondary no load alternate voltage U_{20}	7.1 V		
Short circuit secondary current I_{cc}	25 kA (350mm)		
Mechanical Properties			
Force system	pneumatic	spring load follow-up syst.	
Electrode force	min. -	max. 6 kN at 8,1 bar	
Cylinder diameter	100 mm		
Throat gap, e and depth, l	120mm to 380 mm	$l = 320$ mm	
Mass of movable parts	4,58kg + 4,52kg	Electrode assembly + slide	
	3,02kg	Piston rod + spring assembly	
	3,88kg	Flexible lead	

4.1.2 PECO roll membrane spot/projection welder (pneumatic)

Location: Lessius Mechelen, Campus De Nayer, Laboratory of alternative welding processes
Type description: PECO-Messer Griessheim roll membrane 50Hz AC 25kVA
Control unit: Peco



Electrical Properties

Type of welding current	AC			
Supply Voltage U_{1N}	500 V			
Auxiliary Voltage U_a	240V			
Mains frequency	50 Hz			
Power at 100% duty cycle, S_p				
S_{50}				
Maximum welding power, S_{max}				
Secondary open circuit voltage U_{20} in 1 step				
Max. secondary in short circuit I_{2cc}				

Mechanical Properties

Force system	Pneumatic	
Electrode force, F_{max}	740 daN	
Admission pressure P_1	6 bar	
Throat gap, e and depth, l	200 mm to 320 mm	$l = 185$ mm
Mass of movable parts	4,402 kg	Electrode assembly
	3,384 kg	Piston rod
	2,299 kg	Flexible lead

4.1.3 ARO multi purpose spot/projection welder (pneumatic)

Location: Lessius Mechelen, Campus De Nayer, Laboratory of alternative welding processes

Type description: ARO 72500 PA 91 DC 2 x 90 kVA/50% 500 Volt/1000Hz

Control unit: ARO



Electrical Properties

Type of welding current	DC			
Supply Voltage U_{IN}	500 V			
Auxiliary Voltage U_a	240V			
Mains frequency	50 Hz	Inverter:	1000 Hz	MFDC
Power at 100% duty cycle, S_p	2 x 63 kVA			
Power at 50% duty cycle, S_{50}	2 x 90 kVA			
Maximum welding power, S_{max}	240 kVA			
Secondary open circuit voltage U_{20} in 1 step	10 V			
Max. secondary in short circuit I_{2cc}	30 kA			

Mechanical Properties

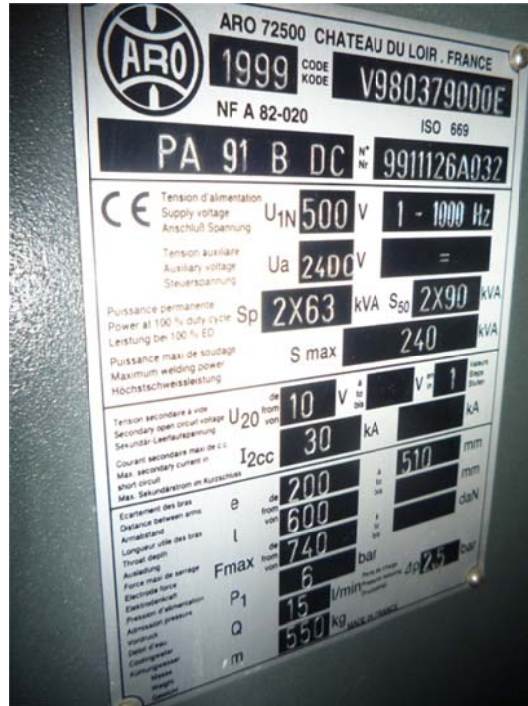
Force system	Pneumatic	
Electrode force, F_{max}	740 daN	
Admission pressure P_1	6 bar	
Throat gap, e and depth, l	200 mm to 510 mm	$l = 600$ mm
Mass of movable parts	8,47 kg	Electrode assembly
	12,34 kg	Piston rod + seals
	0,363 kg	Flexible lead

4.1.4 ARO multi purpose spot/projection welder (servo electric)

Location: Lessius Mechelen, Campus De Nayer, Laboratory of alternative welding processes

Type description: ARO 72500 PA 91 DC 2 x 90 kVA/50% 500 Volt/1000Hz

Control unit: ARO



Electrical Properties

Type of welding current	DC			
Supply Voltage U_{1N}	500 V			
Auxiliary Voltage U_a	240V			
Mains frequency	50 Hz	Inverter:	1000 Hz	MFDC
Power at 100% duty cycle, S_p	2 x 63 kVA			
Power at 50% duty cycle, S_{50}	2 x 90 kVA			
Maximum welding power, S_{max}	240 kVA			
Secondary open circuit voltage U_{20} in 1 step	10 V			
Max. secondary in short circuit I_{2cc}	30 kA			

Mechanical Properties

Force system	Servo electric	
Electrode force, F_{max}	740 daN	
Throat gap, e and depth, l	200 mm to 510 mm	$l = 600$ mm
Mass of movable parts	8,47 kg	Electrode assembly

4.1.5 Mc Gregor μ -resistance welding head

Location: Philips Turnhout, welding laboratory, company mechanization group
Type description: Mc Gregor standard opposed welding head module (pneumatic)
Control unit: None, intended for integration in mechanization
Welding power source: Unitek Myiachi Dual Pulse 250 Capacitor discharge



Electrical Properties

Input Power				
Input voltage	230V	50/60Hz		
Max input current	5A			
Output Power				
Output voltage	6.7V			
Max output current	6700A			

Mechanical Properties

Force Range:	2 – 70 N	
Stroke:	Not Applicable	
Dimensions:	25 x 50 x 179 mm	
Compression:	10 mm	
Mass of moving welding head components	0,136 kg	Electrodes included
		Flexible lead included

4.2 Measuring Equipment

With the restriction of not being invasive in a running production environment, there are only 3 parameters that can be measured during welding: welding current, voltage, and displacement and/or velocity of the welding head, (the latter dependent on the sensor choice). Force measurements would require mounting of auxiliary pancake or weld through load cells and thus the necessary dismantling of parts of the electrode setup. Following this restriction, for this thesis, the following equipment was used:

- a set of current measuring Rogowski-coils;
- solid state crocodile measuring clamps to measure the voltage;
- a laser triangulation sensor, an LVDT or a Laser Vibrometer to measure displacement or velocity of the moving welding head. The choice between the last three measuring systems can quickly be narrowed by the non-invasive restriction above to only a Laser Vibrometer as remaining technology.

During a fracture and/or explosion test, displacement and/or velocity of the moving welding head is measured. If necessary, the welding force as set can be measured with a portable loadcell.

Each of these sensors has its own operating principle, accuracy and measuring range. As a result of this, the sensor is chosen towards a specific application. These sensors of course are used in combination in order to make a qualitative assessment of the different measurement systems.

Each measuring instrument used for measuring the welding parameters as well as the parameters during fracture and explosion tests is discussed below. Moreover, their advantages and disadvantages are discussed based on their use within this work and in industrial evaluations by the author.

4.2.1 LMI Laser Twin displacement Sensor (LTS)

(Figure 4-1)

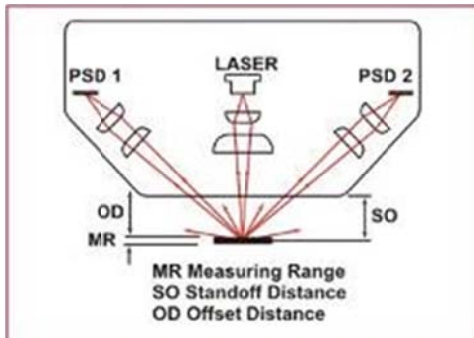


Figure 4-1 LTS sensor

4.2.1.1 Principle of operation

(Figure 4-2 and Table 4-1)

When the laser beam emitting from the LTS displacement sensor hits a moving object, light is reflected in all directions. Part of the reflected light is focussed by means of optical lenses and



hits a position sensitive detector (PSD) as a light spot. The PSD is a special photo diode with 2 current exits. The ratio of these exits depends on the position where light hits the detector. When the object measured makes a displacement relative to the LTS, the angle of the light reflected changes, making the incoming light spot either to move more to the right or more to the left on the detector thus changing the ratio of the current exits. This ratio is transferred into a distance value.

Figure 4-2 Principle of operation

In order to obtain higher reliability and a better measuring accuracy, the LTS is equipped with 2 PSD's.

4.2.1.2 Specifications

Measuring distance	15 mm
Measuring range	12mm
Accuracy	$\pm 10\mu\text{m}$
Resolution	$0,8\mu\text{m}$
Measuring frequency	100kHz
Temperature range	0-50°C
Humidity	Max 90%
Output signals:	
Distance (X)	-7,5 / +4,5 Vdc
Intensity (I)	0...5 Vdc
Enable (E)	-0,7 Vdc within range +4,7 Vdc sensor out of range
Load (X,I,E)	$R > 10\text{k}\Omega$
Sensitivity	1mV/ μm
Weight	750 (± 50) gram
Supply voltage	$\pm 15\text{Vdc} \pm 1\%$
Power consumption	Max. 5W
Laser	30mW (780nm)

Table 4-1 Specifications LMI LTS displacement sensor

Measuring distance 10,5mm (+4,5mm) X= +4,5Vdc
 Measuring distance 22,5mm (-7,5mm) X= -7,5Vdc

When the sensor is out of measuring range, X output becomes +13Vdc.

4.2.1.3 Practical Experience

4.2.1.3.1 Advantages

- High measuring accuracy ($\pm 10\mu\text{m}$)
- The laser beam is insensitive to electromagnetic fields as produced by the resistance welding machines. Additionally, the aluminium housing of the sensor assures a good shielding of the electronic components and is not influenced by the electromagnetic fields.
- The high internal measuring speed (100kHz) results in an accurate measuring signal.

4.2.1.3.2 Disadvantages

- Small measuring range (12mm). This demands rather an invasive application in the machines' working area. Especially in use on projection welding machines where the displacement during the upsetting stage of welding can be rather high.
- The sensor needs to be positioned at about $\pm 15\text{mm}$ away from the moving object. In a multitude of welding machines, the sensor cannot be used due to lack of space. This demands for the use of auxiliary elements to be constructed and attached to get the welding head in the field of view of the sensor.

4.2.2 Solartron Linear Variable Differential Transducer (LVDT)

(Figure 4-3)



Figure 4-3 LVDT sensor

4.2.2.1 Principle of operation

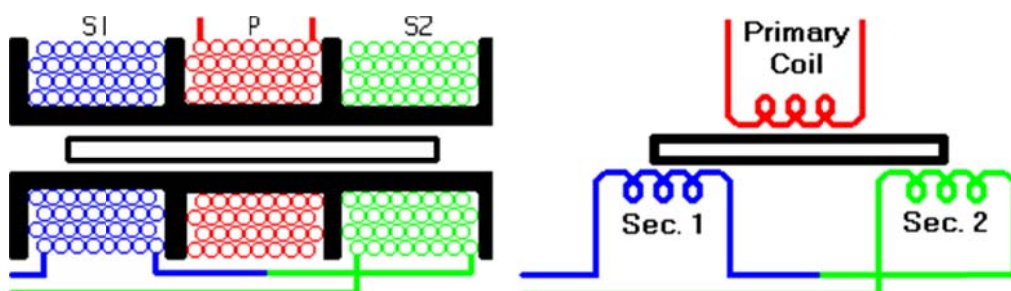


Figure 4-4 Operation principle LVDT

An LVDT is built out of a tube wound with 3 coils. (see Figure 4-4) Towards the mid primary coil, a sinusoidal voltage between 0,5V to 5V with a frequency of 1 to 30 kHz is fed. The other two secondary coils are wound so that the voltage generated in both coils is equal when the ferrite core is in the central position. The secondary coils are also coupled in opposite direction (phase shift of 180 degrees) which leads to the resulting voltage in the central position to become zero. The latter is illustrated in Figure 4-5 below.

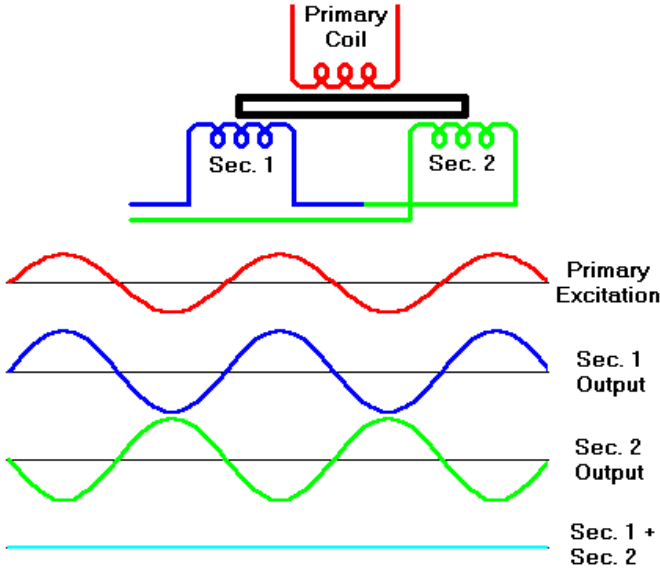


Figure 4-5 Coil coupling in LVDT

The ferrite core is connected to the environment by means of a rod. When this rod is moved out of its central position, the core is positioned more in the one secondary coil in comparison with the other. The difference in voltage leads to an output voltage different from zero. The amplitude of the output voltage covers information on the translation the rod made, as where the phase shift (0° or 180°) compared to the input signal gives an indication on the direction in which the rod moved. Figure 4-6 below shows how the ferrite core is positioned more in the first secondary coil and less in the second one. In that first secondary coil there will be more voltage generated than in the second one. Through the winding direction of the coils, the resulting voltage has the same phase as the primary voltage telling us in what direction the rod moved. The amplitude of the voltage indicates over which distance the rod moved in that specific direction.

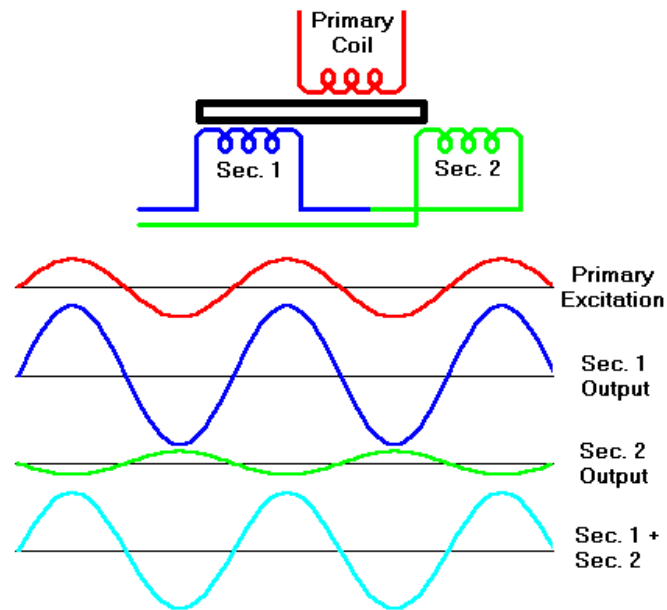


Figure 4-6 Left Positioning of ferrite core in LVDT

If the core translates more in the second secondary coil (see Figure 4-7), that will result in more voltage generated there in comparison with the first secondary coil. The phase of the resulting output voltage will then be opposite to the primary voltage.

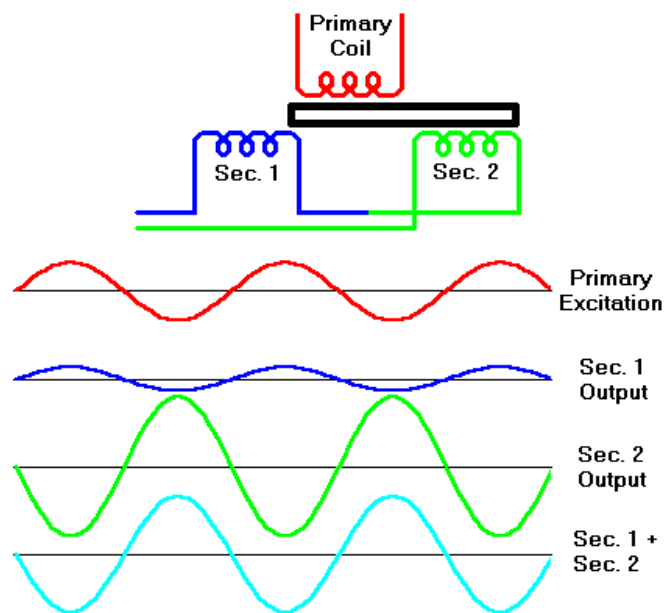


Figure 4-7 Right positioning of ferrite core in LVDT

4.2.2.2 Specifications

Transducer type	Bs110
Mesuring range	28 mm
Sensitivity	28,05 mV/V/mm
Non linearity	0.07%

Table 4-2 Specifications LVDT

4.2.2.3 Practical Experience

4.2.2.3.1 Advantages

- Compact sensor taking very little space.
- The LVDT offers the possibility to measure on welding guns. Indeed, a welding gun has no fixed reference in space. This is why one of its arms needs to be used as a reference. In this case, the LVDT is connected to both arms of the welding gun.
- The relatively large measuring range enables for measuring all applications of projection welding.

4.2.2.3.2 Disadvantages

- The LVDT operates inductively and even with its physically good shielding still remains very sensitive to the emanating electromagnetic fields of resistance welding machines. This disturbs the effective displacement signal during welding. A low pass filter with a cutoff frequency lower than 50hz is required. For use in fracture tests without current it serves well. Figure 4-8 shows how the sensor reacts in the electromagnetic field of a welding machine. This measurement was made without the sensor even being attached physically to the machine.

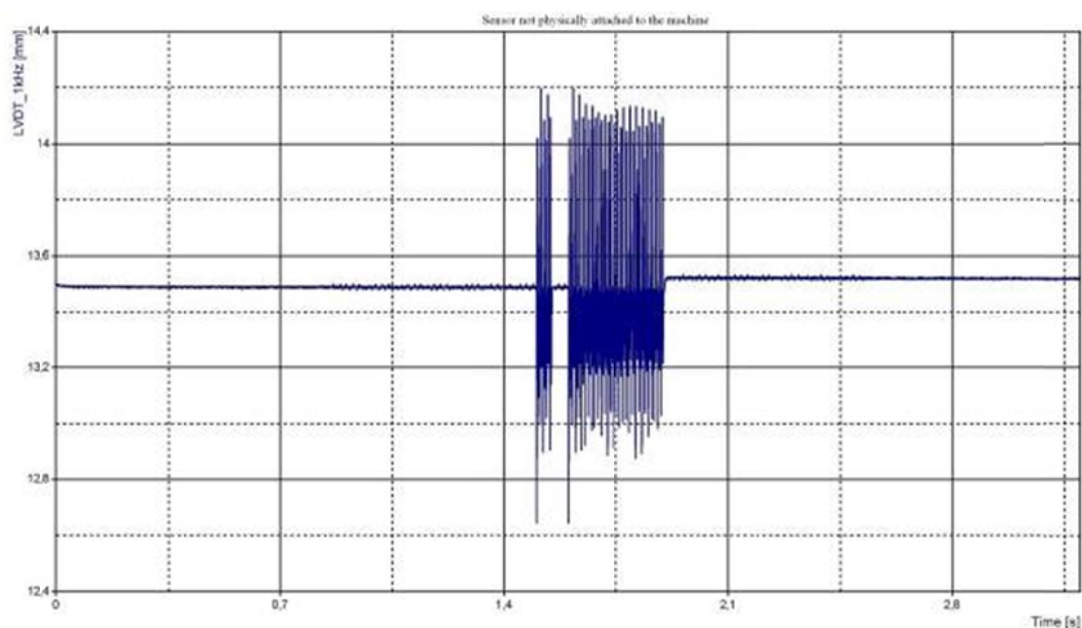


Figure 4-8 Influence of welding current on LVDT displacement signal

- It is also of utmost importance that the LVDT is attached very firmly to the machine.
- During positioning, some precautions are necessary. Since the LVDT is mostly attached on both sides of the machine, it is very easy to damage the sensor when the welding head makes a displacement that is too large. In standard delivery form, the LVDT is equipped with a ball bearing head. (see Figure 4-9)



Figure 4-9 Head of LVDT sensor

By means of a spring loading system, the ball bearing head is maintained in contact with the surface of the object to be measured. Experience revealed that the standard spring was too flexible to follow the sudden accelerations of the welding heads and hence a fixed mechanical connection was used. The upper end of the LVDT that is threaded is connected by means of a plastic ball joint to the welding head (see Figure 4-10). This immediately has the advantage that the LVDT is electrically insulated from the welding machine to ensure no shunting currents flow through the LVDT. The disadvantage of this is the increased risk for damage.



Figure 4-10 Plastic ball joint connected to upper end of LVDT

4.2.2.4 Comparison with LTS

To define to what extent the displacement signals of both LVDT and LTS matched, both sensors were mounted simultaneously on a laboratory test machine. Both sensors were fed the same reference followed by a known displacement of the welding head. The output signals of

both sensors were compared to this and to each other. In a first measurement it was observed that the LTS displacement signal perfectly matched the real displacement. The displacement measured by the LVDT was larger than the real distance travelled. Hence the LTS was used as a reference and the LVDT was recalibrated so that both signals matched as can be seen in Figure 4-11 below.

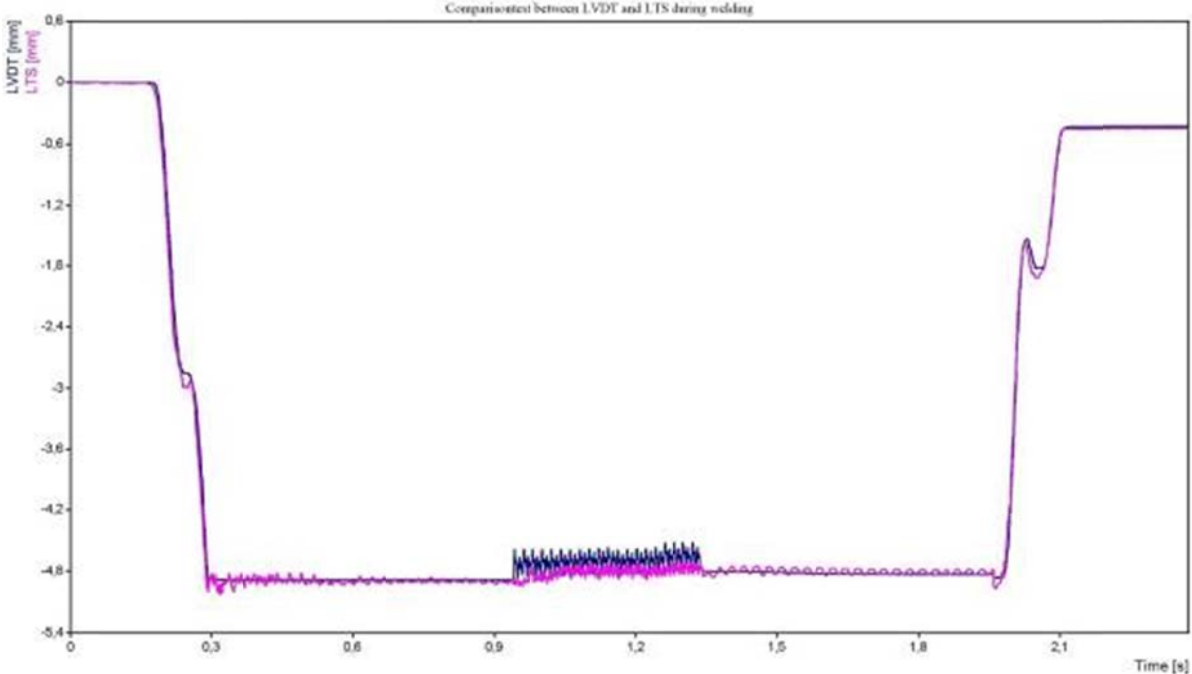


Figure 4-11 Comparison of LTS and LVDT displacement signals

4.2.3 Polytec CLV 1000 laser vibrometer

(Figure 4-12)



Figure 4-12 Polytec compact laser vibrometer

4.2.3.1 Principle of operation

The measuring principle of a laser vibrometer is based on the Doppler effect. Whenever a monochromatic beam of laserlight is reflected on a moving object, it suffers a frequency shift proportional to the velocity of the moving object. This is known as the Doppler effect. If the object moves towards the light source, the reflected beam will show an increase in frequency. If the object moves away from the light source, the frequency of the reflected light will decrease. If the object vibrates, the frequency of the reflected light will be modulated with the so-called Doppler frequency. This Doppler frequency is proportional to the speed of the object. That is why measuring the Doppler frequency provides a direct measurement of the velocity of the moving object.

4.2.3.2 Specifications

The laser vibrometer consists of a unit housing a HeNe laser module, an input module, a decoder module and an output module. The laser beam generated by the laser module is transferred through an optical fibre with a length of 3 meter to a sensor head. This sensor head

houses a number of optical lenses to enable focusing the laser beam manually, independent of the distance between the sensor head and the object to monitor.

The input module amplifies the signal returned by the sensor head. The intensity of the received laser beam is displayed in an led bar on both the input module and the sensor head. The more leds that highlight, the better the signal reception.

The decoder module transfers the modulated laser beam into an analog velocity signal. The input of the decoder is digitized first, followed by processing the signal in a DSP to a digital velocity signal that is converted by a D/A converter in an analog signal again. On this module, the velocity range can be set in several stages by means of a switch.

The output module generates a voltage signal proportional to the velocity of the moving object. This signal is immediately available for data acquisition. The signal is also amplified and filtered a last time. This filter can be set by means of a switch to a number of settings. The high pass filter is especially interesting in an industrial environment where disturbing low frequent noise is present. The low pass filter can be used to limit the bandwidth of the velocity signal.

CLV-700 Sensor Head	
Laser type	HeNe, <1mW
Laser security class	II
Protection rating	IP64
Operating temperature	+0°C...+45°C
Working distance	0,11m tot >10m
Weight	0,5kg
Dimensions	202mm × 48mm × 38.8mm

CLV-1000 General specifications	
Supply	100...240VAC
Consumption	Max.80VA
Operating temperature	+5°C...+40°C
Weight	Ca. 6kg depending on installed modules
Dimensions	450mm × 355mm × 134mm
Calibration interval	Every 2 year

Built in modules	
Input module CLV-M200	Maximum velocity 1250mm/s
Decoder module CLV-M030	Velocity ranges available in 3 levels 5 mm/s/V, 25mm/s/V, 125mm/s/V Resolution 2µm/s
Output module CLV-M002	Low pass filters : 5/20/100kHz/off High pass filters : 100Hz/off

Table 4-3 Specifications Polytec CLV 1000 laser vibrometer

4.2.3.3 Practical experience

4.2.3.3.1 Advantages

- The laser beam is totally insensitive for electromagnetic fields. Vibrations detected during welding are effectively coming from the welding machine and not related to noise.
- The sensor head is a very light and compact unit that can be positioned far away from the welding head by means of a stand. The laser beam can easily be focussed on every surface.
- Maximum measuring range of 1,25m/s is highly sufficient for all resistance welding applications.
- High resolution of 2 μ m/s.

4.2.3.3.2 Disadvantages

- The whole of the equipment is rather large, what makes transport a little heavier.
- For a few applications where accessibility to the machine is limited, the optical fibre of 3 meter is sometimes on the short side. This mostly can be solve by positioning the complete unit on top of a machines' housing.
- The laser demands a sufficient time to heat up. During this heating stage, the signal shows an offset drift that needs to be accounted for. Especially when integrating the signal. Also on changing the velocity range, the signal tends to drift for a few minutes.

4.2.4 PEM UK ROGOFLEX RGF 150, 300 and 300S Current Transducers

(Figure 4-13)



Figure 4-13 PEM UK Rogoflex current transducer

4.2.4.1 Principle of operation

Rogowski coils are used to measure alternating current. They ‘sense’ the magnetic field around a current bearing conductor without having to be in contact with it.

Rogowski coils operate according to a simple principle. When a coil (with N windings), uniformly wound around a non magnetic core with a constant cross section ($A\text{m}^2$) is placed around a current bearing conductor, the alternating magnetic field around the conductor induces a voltage in this coil. In this case, the induced voltage is proportional to the frequency of the current. The faster the current changes, the more voltage will be induced in the coil. This is shown in the equation below.

$$E = \mu_0 \cdot N \cdot A \cdot \frac{dI}{dt} = H \cdot \frac{dI}{dt}$$

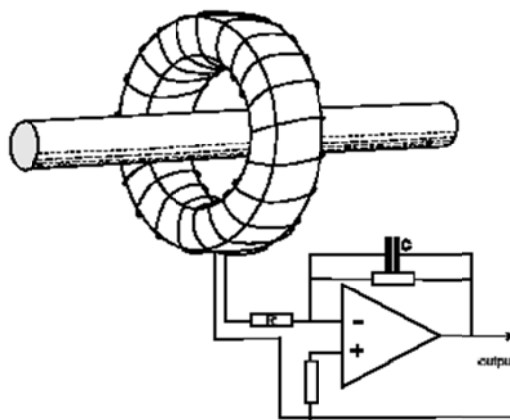


Figure 4-14 Integrator added to output of Rogowski coil

To display the current as an analog voltage signal, an integrator is added to the output of the coil (Figure 4-14).

4.2.4.2 Specifications

Three different Rogowski coils, an RGF 150, RGF 300 and an RGF 300S were used. The difference between the first two is only the measuring range. They were chosen to cover a measuring range of 0 to 60 kA. The RGF 300S has the same measuring range as the RGF 300, but was specifically made to measure pulsed DC-currents enabling us to measure on a DC or a MFDC welding machine.

Type	Sensitivity (mV/A)		Peak current (KA)		Peak dI/dt (kA/ μ s)		Max DC offset (mV) @55°C		Max Noise (A pk-pk)	Droop Typ (%/ms)
	$\times 5$	$\times 1$	$\times 5$	$\times 1$	$\times 5$	$\times 1$	$\times 5$	$\times 1$		
RGF 150	1,0	0,2	6,0	30,0	6	6	1,5	0,5	3,0	0,55
RGF 300	0,5	0,1	12,0	60,0	6	6	1,5	0,5	6,0	0,45
RGF 300s	0,5	0,1	12,0	60,0	6	6	1,5	0,5	6,0	0,45

Table 4-4 Specifications PEM UK Rogowski current coils

4.2.4.3 Practical experience

4.2.4.3.1 Advantages

- The coils are very simple in use and can be positioned in a fast and easy way around any conductor. For resistance welding machines there is no problem whatsoever since the secondary conductors are well accessible.
- The wide current range enables to measure both on micro resistance welding machines as well as on 60 kA machines.

4.2.4.3.2 Disadvantages

- A welding machine delivering a constant DC-current for a long time (eg. a DC seam welder) can not be measured straight forward.
- Changing the measuring range or switching the unit off and on results in a sudden change in the integrator. A slowly disappearing transient results. It takes several seconds for the output signal to stabilize.

4.2.5 Miyachi MM-601A Load Cell

(Figure 4-15)



Figure 4-15 Miyachi MM-601A load cell

4.2.5.1 Principle of operation

A load cell is classified as a force transducer. It converts a force to an electrical signal. Load cells are often based on strain gages. When force is exerted on a strain gage, its internal resistance changes. The gages are made of ultra thin heat treated metallic foil chemically bonded with a thin dielectric layer.



Figure 4-16 Strain gage attached to object

The gages are attached to an object that will suffer deformation according to the applied load by means of custom made adhesives (see Figure 4-16). The precise positioning of the gage, the way it is positioned and the materials used all have their effect on the quality of the load cell.

When the surface to which the strain gages are connected deform due to compression or traction resulting from the load to be measured, their resistance changes proportional to the load supplied. If several strain gages are used in a load cell, then they are connected in a Wheatstone bridge.

When a voltage is supplied to this bridge, the output voltage will change proportional to the applied force on the cell. This output voltage can be measured after amplification.

4.2.5.2 Specifications

Range	20-950kg
Accuracy	-3% full scale
Speed	4 times/s
Max. impulse force allowed	150% full scale
Display functions	Decimal point and unit: automatic
	Overload: "OVER" on display + alarm
	Charge request : flashing "BATTERY" signal
Auto Power-off	Automatic after 7 min, without new input
Holding input	Stores the last measured value on screen when an external signal triggers this input
Analog input	6,7mV/kg (after calibration)
Power	Ni-Cd batterij 1,2Vx4 (4,8V), use for 5 hr Lader MA 510 included
Dimensions	170mm × 75mm × 30mm
Weight	480 g batteries included

Table 4-5 Specifications Miyachi MM601A load cell

4.2.5.3 Practical experience

4.2.5.3.1 Advantages

- Compact and easy to use.
- Measuring range sufficient for most resistance welding machines.
- Due to the analog output it is possible to monitor the force in real time during a fracture test or an explosion test.

4.2.5.3.2 Disadvantages

- Only limited for the applications operating with lower forces (<1000 daN).
- One needs to ensure that NO welding current can pass through the sensor head. It would damage the sensor permanently. So it can not be used to measure force during welding.

4.2.6 Dewetron 2010 – Portable industrial data-acquisition system



Figure 4-17 Dewetron 2010 portable industrial data-acquisition system

4.2.6.1 General

The DEWE – 2010 is one of the most popular IPC (Industrial Portable Computer) the Dewetron company sells in its range of Data-acquisition products. It has a good balance between inner space and external dimensions. It is a very robust all metal system with the size and shape of a small microwave oven.

It is equipped with a very bright 15” TFT screen. During transport, the complete front is covered with a closure made of impact resistant resin in which the keyboard is integrated.

When looking in the system, we immediately notice the presence of “COTS” (Commercial Off The Shelf) hardware and software, although it is a selection of the ‘better’ material on the market. The mother board contains 3 to 4 PCI- slots and one AGP- slot with a video card attached. One RS232 serial port, one parallel port, a USB port and an Ethernet card are installed for communication. A 1 GHz Pentium III processor with 512Mb RAM make the core of the system, together with a hard disk.

In one of the available PCI- slots, a second mother board is connected, a DAP 4400a/446. This card is the basis of the integrated measuring system and is specifically optimized for data-acquisition. This mother board is equipped with its own i486DX4 processor with a clock frequency of 96MHz, 16Mb RAM memory and an “onboard” control system, DAPL 2000. In this way, the main processor is freed from the complete measuring activity.

The DAP card has 4 onboard A/D converters each with a sample frequency of 800kHz. When combining these 4 input channels, a total sample frequency of 3,2 MHz is possible. To each A/D converter maximum 16 analog inputs can be connected. The DEWE-2010 has a rack on its rear side where 16 optional measuring input modules can be inserted. All measuring input

modules of the rack are connected to one of the four A/D converters. The remaining A/D converters allow the system to be expanded with 3 external racks of 16 analog inputs each. Currently, 15 analogue modules are mounted:

- 6 voltage modules;
- 4 thermocouple modules;
- 5 auxiliary (charge, power supply,...)

4.2.6.2 Specifications

DEWE-2010-IPC portable industrial PC	
Main system	
Display	12.1" TFT with 800 x 600 pixel
Processor	1 GHz Intel® Pentium III
RAM	256 MB
Hard disk	40 GB
Floppy Disk drive	3.5" / 1.44 MB
CD-ROM drive	24x, internal
Interfaces	2x RS-232, 1x LPT, 2x USB, 10/100BaseT Ethernet (RJ45), PS/2 keyboard and trackball
Operating system	WINDOWS® 2000 Professional
System specifications	
Operating temperature	-10 to +50 °C (enhanced temperature range on request)
Storage temperature	-20 to +70 °C
Humidity	10 to 80 % non condensing, 5 bis 95 % rel. humidity
Vibration	MIL-STD 810F 514.5, procedure I
Shock	MIL-STD 810F 516.5, procedure I
Power supply	115 / 230 VAC
Dimension (W x D x H)	410 x 230 x 290 mm (16.1 x 9 x 11.4 in.)
Weight	typ. 9.5 kg (21 lb.)
Options	
WIN-XP	Upgrade to WINDOWS® XP Professional operating system
RAM-256-512	Upgrade to 512 MB RAM
HDD-2010-80	Upgrade to 80 GB harddisk
CD-WRITER	Upgrade to internal CD writer, 24/10/24x, incl. software
DVD-CD-WRITER	Upgrade to internal combo drive, 8x DVD, 16/10/24x CD writer, incl. software
ZIP-250	Upgrade to internal 250 MB ZIP drive
DEWE-BAY-5.25-xx	5.25" drive bay for IDE or SCSI devices (streaming, ...)
DEWE-2010-AC-DC-UPS	AC/DC power supply (115 / 230 VAC and 10 to 32 VDC) with internal UPS battery
DISP-1024-15	Upgrade to 15" TFT display, 1024 x 768
DEWE-2010-TOUCH-15	15" touch-screen for internal display
MOB-DISP-6	Additional external 6.5" display 640 x 480, 300 cd/m ² , 3 m VGA cable, windshield mounting adapter
MOB-DISP-12	Additional external 12" display 800 x 600, 350 cd/m ² , 3 m VGA cable, windshield mounting adapter
MOB-DISP-12-TOUCH	Touch-screen for MOB-DISP-12
SPLASH-KEYBOARD	Splash-proof keyboard
DEWE-2010-BP-20	DEWE-2010 back panel with 20 BNC connectors, grouped and labeled, wired to separately ordered A/D card

Table 4-6 Specifications Dewetron 2010 data-acquisition

4.2.6.3 Practical experience

4.2.6.3.1 Advantages

- Very advanced data-acquisition system upgradable in the future.
- Dewesoft is a very user friendly measuring software. Also support from the Benelux dealer as well as from the Austrian main company is very sound. Reporting software bugs and propositions to enhance the software are always accounted for.
- Extremely good shielding against electrical and electromagnetic fields.
- Superb screen in difficult ambient light.
- Very high flexibility in choice of different measuring modules. Some of them can be adapted to the needs of the application.

4.2.6.3.2 Disadvantages

- Cooling fan is rather noisy. The latter is off course of no importance during measuring in an industrial environment, but when processing data at the office it is rather annoying.

4.3 Measuring procedures

4.3.1 Voltage – Current [U-I] – characteristics of a Resistance Welding Power Source

Since power sources for resistance welding machines are in a completely different range of available power in comparison with arc welding power sources, loading with a continuously variable load is not possible as it is with arc welding power sources. This forces us to measure a discrete amount of effective working points to define the U-I-characteristic.

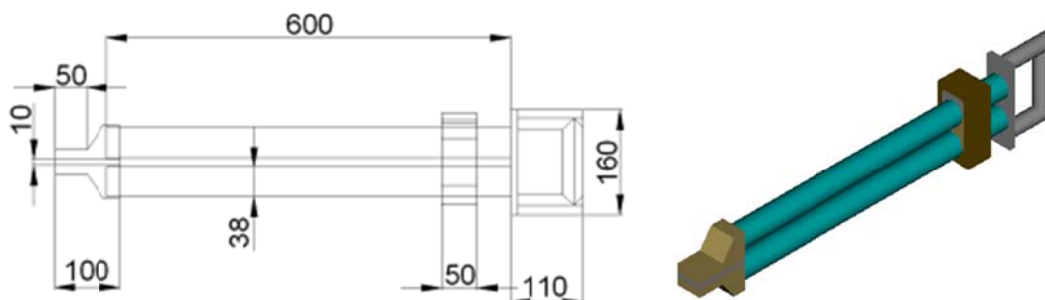


Figure 4-18 Schematic view of variable resistance

To allow us the ease of different loads to be set in a discrete manner, a variable resistance was designed as shown in Figure 4-18 and Figure 4-19.

The resistance consists of 2 Hastelloy 276C bars and with the aid of flat copper endpieces it can be introduced between the electrodes of the machine on test. A sliding intermediate

connection in copper can be moved to vary the load resistance. The use of a precision torque wrench to tighten the bolt is necessary to ensure a constant and minimal contact resistance between the intermediate connection and the Hastelloy bars.

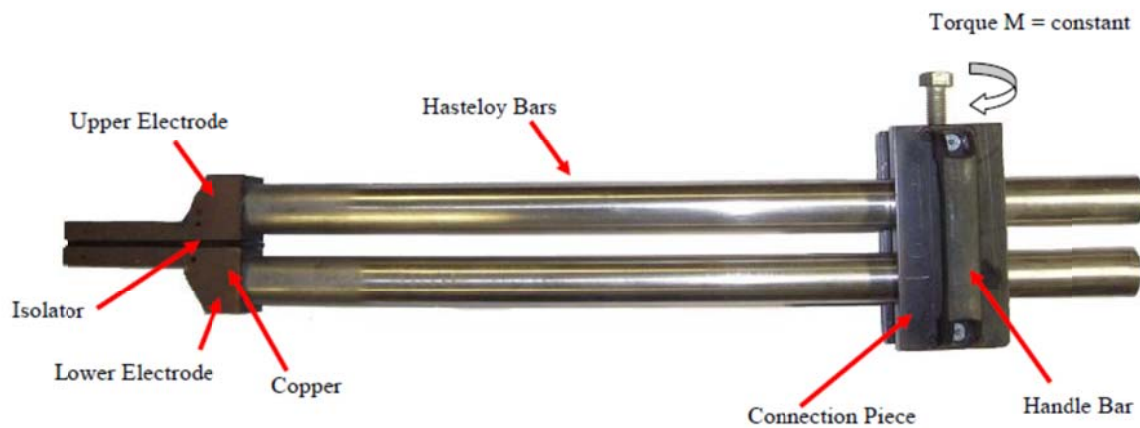


Figure 4-19 Photograph of variable resistance

This design has a number of advantages:

- It is compact and portable
- Resistive load can be set accurately from a few $\mu\Omega$ to a few $m\Omega$
- Inductive effects are minimal
- Resistance is NOT temperature dependant
- Heat generated during high loading can be dissipated without heating of the resistance.

Several points of the U-I-characteristic are measured in a discrete way and can be exported to Flexpro processing software in a single or in multiple files, depending on the measuring procedure. To enable fully automatic processing, the number of discrete points per U-I-characteristic (per load setting) is limited to 10.

The intention of the procedure is to find out how the U-I-characteristics behave at different current settings. Also for this purpose, the number of U-I-characteristics that can be calculated simultaneously was limited to a maximum of 10. The latter meaning in practice that in a measurement, current can be altered in steps of 10% from 10% to 99% power setting.

Measuring procedure and subsequent data processing are presented in Appendix F

5 Experimental Procedure

From my literature survey, it is obvious that there are 2 major models describing mechanical behaviour of resistance welding machines developed in the past. The first by Römer, Press and Krause [19], [20], the second model by Gould [23]. The first model uses machine response to an impulse function, the latter is generated by having the electrodes (welding heads) of the machine collide. The Gould model theoretically describes machine response to a step function, imposed on the machine welding heads by means of support between them disappearing by evaporating it. This is referred to as the 'Ball Model'. This model is only available as an internal research report by Gould through EWI. No practical information is given on the development of the model or on the practical design and/or execution of the step function imposing test. Other UK based researchers, Steve Westgate at TWI [24] or N.T. Williams [25] from British Steel mention the exploding ball test as a means to compare welding head velocities following support between welding heads breaking away at a predefined actuator force with the aim of comparing different actuator systems on different resistance welding machines. As already mentioned in the aims and objectives of this thesis, choice of a model describing mechanical behaviour of a resistance welding machines' welding head, specifically during its follow-up after workpiece collapse, is primary. Furthermore, it is important to transfer this model into a realistic test procedure and practical test set-up, enabling to test not only in laboratory conditions, but most of all in-situ in a working production environment.

The experimental procedure is first of all focussed on the evaluation of a practical test procedure and on the evaluation of two practical test set-ups, namely the Free Fracture Test, where support between the welding heads of the machine under study is suddenly taken away by breaking a brittle supporting pin on the one hand and the Explosion Test, where support between the welding heads of the machine under study is suddenly taken away by evaporating the supporting conductive element.

Furthermore, the experimental procedure must reveal the influence of the basic difference between both test set-ups, the Free Fracture Test being executed without any current flowing in the machines' secondary circuit whereas the Explosion Test will have large currents flowing through the machines' secondary circuit.

The literature survey also revealed the influence of welding current on the mechanical behaviour of a welding machine, noticed by Williams [25], Fujimoto [36] and Wu [37].

Study of this influence on machine behaviour and thus on the results delivered by the two practical test set-ups is accounted for in the experimental procedure.

To determine the cause of the influence of current flowing through the machine on its mechanical behaviour is also examined in the experimental procedure by exerting a lateral force on the moving welding head of a machine under study.

Finally, the literature review revealed the opinion of researchers like Thomas Dupuy [38] at Arcelor-Mittal that welding head friction and 'stick-slip' effects in the moving welding heads' force actuator and its slide would dramatically influence a machine's moving welding head follow up behaviour. The latter is also studied in the experimental procedure.

In general, the evaluation of the mechanical behaviour of a resistance welding machine is organised as described schematically in the flowchart in Figure 5-1 below.

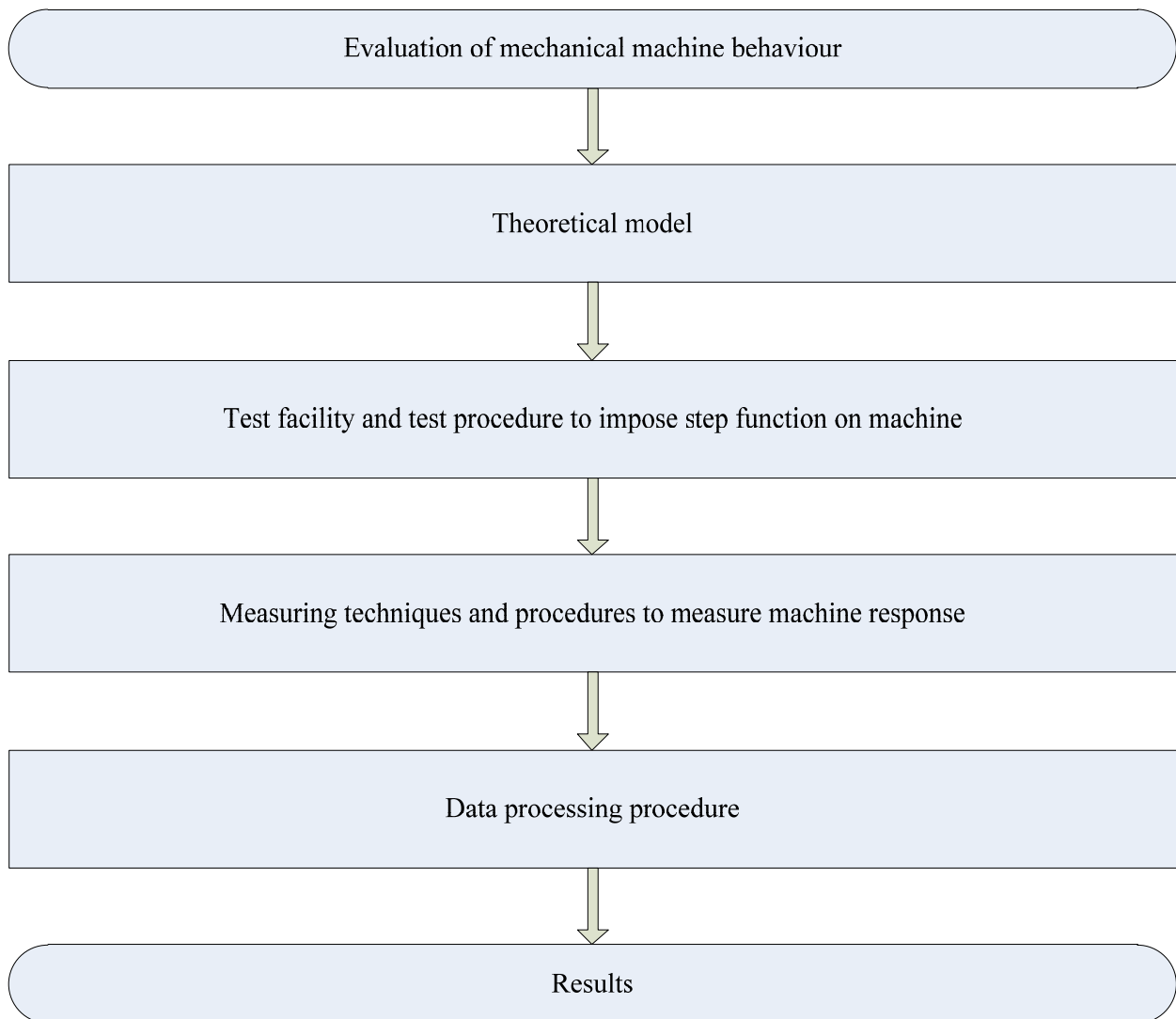


Figure 5-1 Flowchart experimental procedure

All the steps in the flowchart must be made in order to obtain useable results. Regardless of the objective, such as:

- a pure determination of machine specific parameters of a machine one intends to use on an application to enable correct input in for instance Finite Element Analysis software,
- very practical evaluation of a working machine on a welding application
- the evaluation of all influencing boundary conditions as discussed above,

5.1 Machine Mechanical Model

5.1.1 Model of the moving welding head

Mass – damper – system

In this model, the moving welding head with its actuator is represented as a mass – damper – system. (Figure 5-2) This system is actuated with a force F_a , exerted by the moving welding heads actuator.

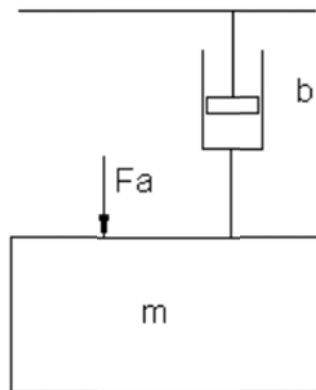


Figure 5-2 Mass – damper – system (moving welding head)

The following machine parameters are taken into account:

- Mass (m): inertia forces of the moving welding head.
- Damping coefficient (b): damping effect of slides and bearings through viscous friction and stick-slip.

Force is imposed to the mass by means of compressed air acting on the actuator piston and transferring it through the piston rod towards the electrode assembly. Movement of the mass is slowed down through the presence of damping forces. The total damping factor of the driven part is one of the machine specific parameters to define.

During the welding process, pressure will build up in the actuator pneumatic piston leading to the squeezing of the workpieces to be welded. Resulting to the latter, the workpiece will exert a reaction force opposed against the mass of the welding head. (see Figure 5-3 Mass-damper system with reaction force)

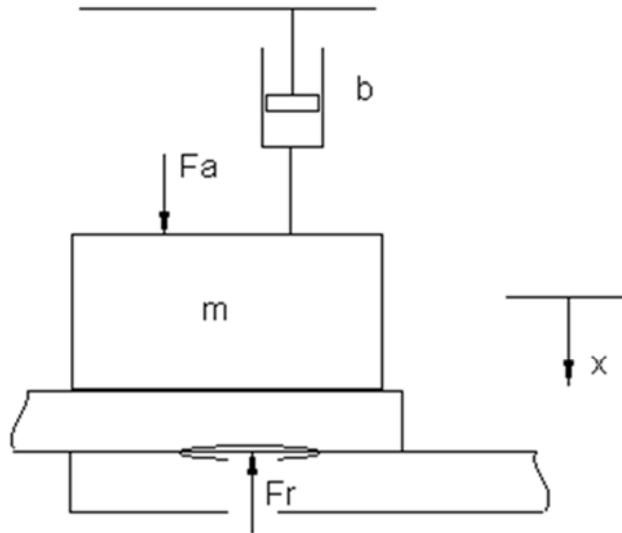


Figure 5-3 Mass-damper system with reaction force

The force balance can be written as follows:

$$F_a - F_r = m \cdot a + b \cdot v$$

$$F_a - F_r = m \cdot \frac{d^2x}{dt^2} + b \cdot \frac{dx}{dt}$$

Where v is velocity of the moving welding head, x is the displacement and t is time. The reaction force F_r is of metallurgical nature and will change as the welding cycle evolves in time. At the moment that metallic material becomes plastically deformable due to heating whilst welding, reaction force will drop and welding head movement will result. The extreme condition is reached when material in between the electrodes disappears (for instance when excessive splash takes place due to overheating). The latter can be simulated by a fracture of a brittle pin during a fracture test. At that moment, $F_r = 0$ and the governing differential equation then becomes:

$$F_a = m \cdot \frac{d^2x}{dt^2} + b \cdot \frac{dx}{dt}$$

After solving this differential equation, the following basic formula results:

$$\rightarrow x(t) = \frac{F_a(t) \cdot m}{b^2} \cdot \left(e^{-\frac{b}{m}t} + \frac{b}{m} \cdot t - 1 \right)$$

5.1.2 Model of the fixed welding head

Mass – damper – spring – system

In this model, the fixed welding head is represented by a mass – damper – spring – system. (see Figure 5-4) Through the workpieces ready to be welded, this system is equally loaded with the same moving welding head actuator load F_a .

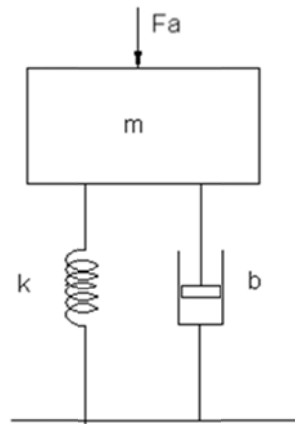


Figure 5-4 Mass – spring – damper system (stationary welding head)

The following machine parameters are taken into account:

- Mass (m): inertia forces of the stationary welding head.
- Damping factor (b): damping effect of material of stationary welding head. (the latter will be very low since it is only structural damping in the material of the lower welding head)
- Spring constant (k): generating a reaction force by means of elastic deformation of stationary welding head and bending of fixed part of machine frame.

In case of further development of this system, a transfer function results that allows for calculation of lower welding head displacement as a function of time. Following an impulse response, one can continue working straightforward with the force.

- *Step function response*

$$X = \frac{F}{s(ms^2 + bs + k)}$$

- *Impulse response*

$$X(ms^2 + bs + k) = F$$

Both are the Laplace transformations of displacement and force respectively.

5.1.3 Difference between Step or Impulse response

Prior to discussing the fracture test further in detail, it is interesting to consider the difference between the welding machines' physical response following an imposed impulse in force (comparable to an impact) or following an imposed step in force (a sudden change in the force level).

Impulse response (Dirac function)

In practice, the situation of a collision between the moving electrode (moving welding head) and the stationary electrode (fixed welding head) can be interpreted as an impulse imposed on the stationary electrode (fixed welding head) by means of the moving electrode (moving welding head). The impulse response of the mechanical system subsequently can be recorded with a force measurement in time. Starting from the measured response combined with the theoretical response, the typical machine parameters involved can be calculated.

This specific method uses the recorded force signal as a function of time of the according mass – damper – spring - system.

Although discussed in detail by several researchers [19], [20], the usefulness of this approach is limited because of the difficulty in reproducing a correct impulse in practice and because of the difficulty to make force measurements on a machine in a working production environment. These considerations resulted in the focus on tests and procedures useable in-situ in a working production environment for this thesis.

Step response

With a step response, the Free Fracture or Explosion test is used to impose the best possible approximation of a step function on both electrodes (welding heads).

The moving electrode is described as a mass – damper – system. Elastic spring action isn't taken into account since this influence is neglectable [19], [20] (as is also showing from the practical tests). The stationary electrode is described as a mass – damper – spring - system.

The step response uses the velocity of the moving welding head as a function of time. The latter can accurately be measured in practice in a working production environment.

From the welding machines' response to this sudden change in mechanical load (step function) the machine specific parameters subsequently will be calculated.

Further theoretical development can be found in Appendix B.

5.2 Data Processing Procedure

In Section 5.1 a formula is derived that links theory and a practical procedure to follow on the work floor. This formula can be further rearranged to include only variables capable for measurement in practice during a fracture or an explosion test (welding head displacement or welding head velocity).

$$\text{Basic formula} \quad \rightarrow \quad x(t) = \frac{F_a(t) \cdot m}{b^2} \cdot \left(e^{-\frac{b}{m}t} + \frac{b}{m} \cdot t - 1 \right)$$

Development of equations

5.2.1 Starting from welding head displacement measurements

Values for displacement of the moving electrode will be measured directly using an LVDT, or an optical triangulating laser sensor, or they can be calculated from the true measured welding head velocity measured with a laser vibrometer. This measured signal can be compared with the theoretically calculated values of the displacement on the same moments in time.

Theoretical displacement is calculated as follows:

$$\rightarrow \quad x_{th}(t) = -\frac{F_{fracture} \cdot m}{b^2} \cdot \left(e^{-\frac{b}{m} \cdot (t+t_0)} + \frac{b}{m} \cdot (t+t_0) - 1 \right) \quad (5.1)$$

The time of the true measurement is added with an imaginary time t_0 . This represents the time difference between the time where initial velocity is zero and the time where fracture takes place. Indeed, this value is important when using the free fracture test as a procedure to impose a step function on the welding heads. Loading the fracture pin with the welding force initiates elastic and plastic deformation of the pin (see Figure 5-5) with a specific welding head velocity $v(t_0) = v_0$ that is NOT equal to zero. The presence of this initial velocity is taken into account by introducing t_0 in the formula.

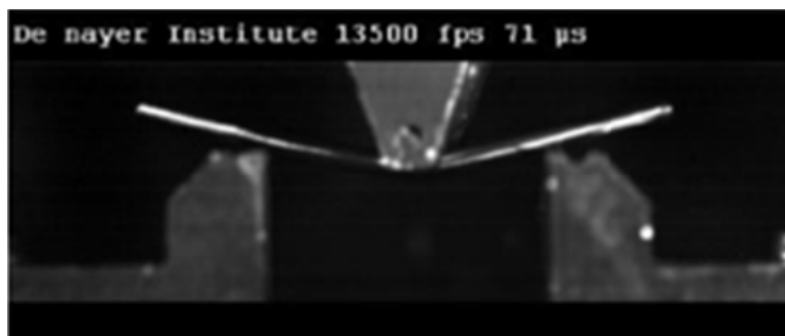


Figure 5-5 Deformation of pin before fracture

Because t_0 is added with the time t , displacement will differ from zero (normally speaking, displacement = 0 at time $t = 0$ without t_0). If we subsequently want to compare the measured signal, starting from a rest position with the calculated values, then it is necessary to introduce a shifted displacement. In this case, theoretical start value of displacement ($t + t_0 = t_0; t = 0$) is subtracted from the theoretical displacements.

Imaginary time

As mentioned above, velocity prior to fracture must be taken into account when processing measured data. Time t_0 can be found in the formula for displacement:

$$\rightarrow x_{th}(t) = \frac{F_{fracture} \cdot m}{b^2} \cdot \left(e^{-\frac{b}{m} \cdot t} + \frac{b}{m} \cdot (t-1) \right)$$

$$\leftrightarrow x_{th}(t) = \frac{F_{fracture} \cdot m}{b^2} \cdot e^{-\frac{b}{m} \cdot t} + \frac{F_{fracture}}{b} \cdot t - \frac{F_{fracture} \cdot m}{b^2}$$

$$\frac{dx}{dt} \Rightarrow v_{th}(t) = -\frac{F_{fracture}}{b} \cdot e^{-\frac{b}{m} \cdot t} + \frac{F_{fracture}}{b}$$

$$\leftrightarrow v_{th}(t) = -\frac{F_{fracture}}{b} \cdot \left(e^{-\frac{b}{m} \cdot t} - 1 \right)$$

When t is replaced with t_0 :

$$\leftrightarrow v_{th}(t_0) = -\frac{F_{fracture}}{b} \cdot \left(e^{-\frac{b}{m} \cdot t_0} - 1 \right) \quad \text{with: } v(t_0) = v_0$$

$$\leftrightarrow -\frac{v_0 \cdot b}{F_{fracture}} + 1 = e^{-\frac{b}{m} \cdot t_0}$$

$$\leftrightarrow \ln\left(-\frac{v_0 \cdot b}{F_{fracture}} + 1\right) = -\frac{b \cdot t_0}{m}$$

$$\leftrightarrow t_0 = -\frac{m}{b} \cdot \ln\left(-\frac{v_0 \cdot b}{F_{fracture}} + 1\right)$$

(4.2)

5.2.2 Starting from welding head velocity measurements

Velocity can be calculated from the displacement formula:

$$\frac{dx}{dt} \Rightarrow v_{th}(t) = -\frac{F_{fracture}}{b} \cdot e^{-\frac{b}{m}t} + \frac{F_{fracture}}{b}$$

$$\Leftrightarrow v_{th}(t) = -\frac{F_{fracture}}{b} \cdot \left(e^{-\frac{b}{m}t} - 1 \right)$$

And if we want to compare the true welding head velocity signal with the theoretical values, the initial welding head velocity must be taken into account:

$$\rightarrow v_{th}(t) = -\frac{F_{fracture}}{b} \cdot \left[e^{-\frac{b}{m}(t+t_0)} - 1 \right]$$

t_0 is then entered:

$$\Leftrightarrow v_{th}(t) = -\frac{F_{fracture}}{b} \cdot \left[e^{-\frac{b}{m} \left(t - \frac{m}{b} \ln \left(-\frac{v_0 \cdot b}{F_{fracture}} + 1 \right) \right)} - 1 \right]$$

$$\Leftrightarrow v_{th}(t) = -\frac{F_{fracture}}{b} \cdot \left[e^{-\frac{b}{m}t} \cdot e^{-\frac{b}{m} \left(\frac{m}{b} \ln \left(-\frac{v_0 \cdot b}{F_{fracture}} + 1 \right) \right)} - 1 \right]$$

$$\Leftrightarrow v_{th}(t) = -\frac{F_{fracture}}{b} \cdot \left[e^{-\frac{b}{m}t} \cdot \left(\frac{v_0 \cdot b}{F_{fracture}} + 1 \right) - 1 \right]$$

$$\Leftrightarrow v_{th}(t) = v_0 e^{-\frac{b}{m}t} - \frac{F_{fracture}}{b} \cdot e^{-\frac{b}{m}t} + \frac{F_{fracture}}{b}$$

$$\rightarrow v_{th}(t) = -\left[\left(-\frac{F_{fracture}}{b} \cdot \left(e^{-\frac{b}{m}t} - 1 \right) \right) - \left(v_0 e^{-\frac{b}{m}t} \right) \right]$$

(5.3)

This is the theoretical formula describing the welding head velocity as a function of time at a specific actuator force ($F_{fracture}$ in the case of a fracture test), with welding head mass and welding head damping factor as variables. It can be inputted in a spreadsheet program to calculate a curve that fits the measured true welding head velocity signal as closely as possible, using the least squares method.

Instructions for use of this procedure in an MS Excel calculation sheet can be found in appendix D.

5.3 Evaluation of step function imposing tests

5.3.1 Free Fracture Test

Following the theoretical approach described in 5.2, a mechanical support device was designed and tested. A range of fracture pins is used, designed to fracture in a brittle manner at pre-set actuator loads. In this way, the loaded welding head suddenly (step function) loses the reaction force exerted by the fixed welding head on it and thus is left 'free' to move towards the fixed welding head that is positioned a predefined distance away from the moving welding head. (See Figure 5-6 below)

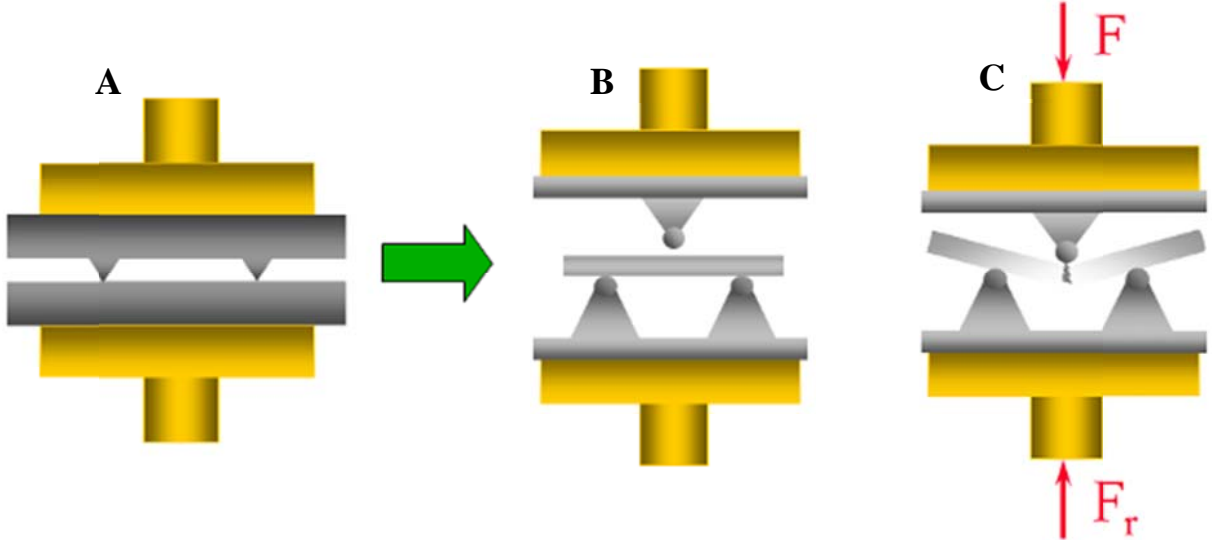


Figure 5-6 Operation principle of fracture test, A, B and C

Instead of the workpiece (in the case of Figure 5-6 A above schematically proposed as a projection welding workpiece) transferring the actuator force of the moving welding head to the stationary welding head, the latter is realized by a brittle steel pin Figure 5-6 B (Parallel dowel pins according to BS EN ISO 8734: 1998) that, depending on the pin diameter used in the test and the distance between the lower support, breaks away in Figure 5-6 C at a predefined actuator force.



Figure 5-7 A, B and C Laboratory Fracture test rig on different machines

This first open laboratory test rig looks as shown in Figure 5-7, **B** above and was quickly modified to a closed design (see Figure 5-8 below) in order to prevent the remains of the broken pins damaging equipment or causing injuries to personnel. This is very important when measuring in an industrial environment where employees may be working in the vicinity of a machine. However, the open test (Figure 5-7, **B**) is still used for high speed camera evaluations (see Figure 5-9 and Figure 5-10) and for measurements on specific applications where it is difficult to implement the closed version of the test, as in Figure 5-7, **A** on a seam welder and Figure 5-7, **C** on a spotwelding C-gun (right).



Figure 5-8 Closed design of Fracture test

The essential new concept developed in this thesis is to use this test not only to measure maximum accelerations and velocity values of a welding head under a specific actuator load, but specifically to use it to impose a step function in support on a loaded welding head and subsequently calculate specific machine parameters (mass m , damping factor b) out of the recorded response signal measured on the machines welding head to characterize machine mechanical behavior during its operation.

The test was named the 'Free Fracture Test', since the test intends to shift the support between full support and zero support, thus allowing 'free' movement of the welding head.

In order to obtain machine specific data, the Free Fracture Test offers the capability to measure the maximum potential a moving welding head has under a specific actuator load to accelerate and to reach a certain velocity after a predefined displacement.

It is a simple and minor-invasive test, that requires only small mechanical changes on the welding head in order to be mountable on the machine. Additionally, it offers the possibility to assess the machine potential during a 'Free' movement after fracture, thus enabling us to assess the drop in force that will occur during real welding when measuring welding head velocity during real welding. This is very important to assess the risk of expulsions during welding.

The full description of the test procedure and boundary conditions attainable with the test can be found in Appendix C.

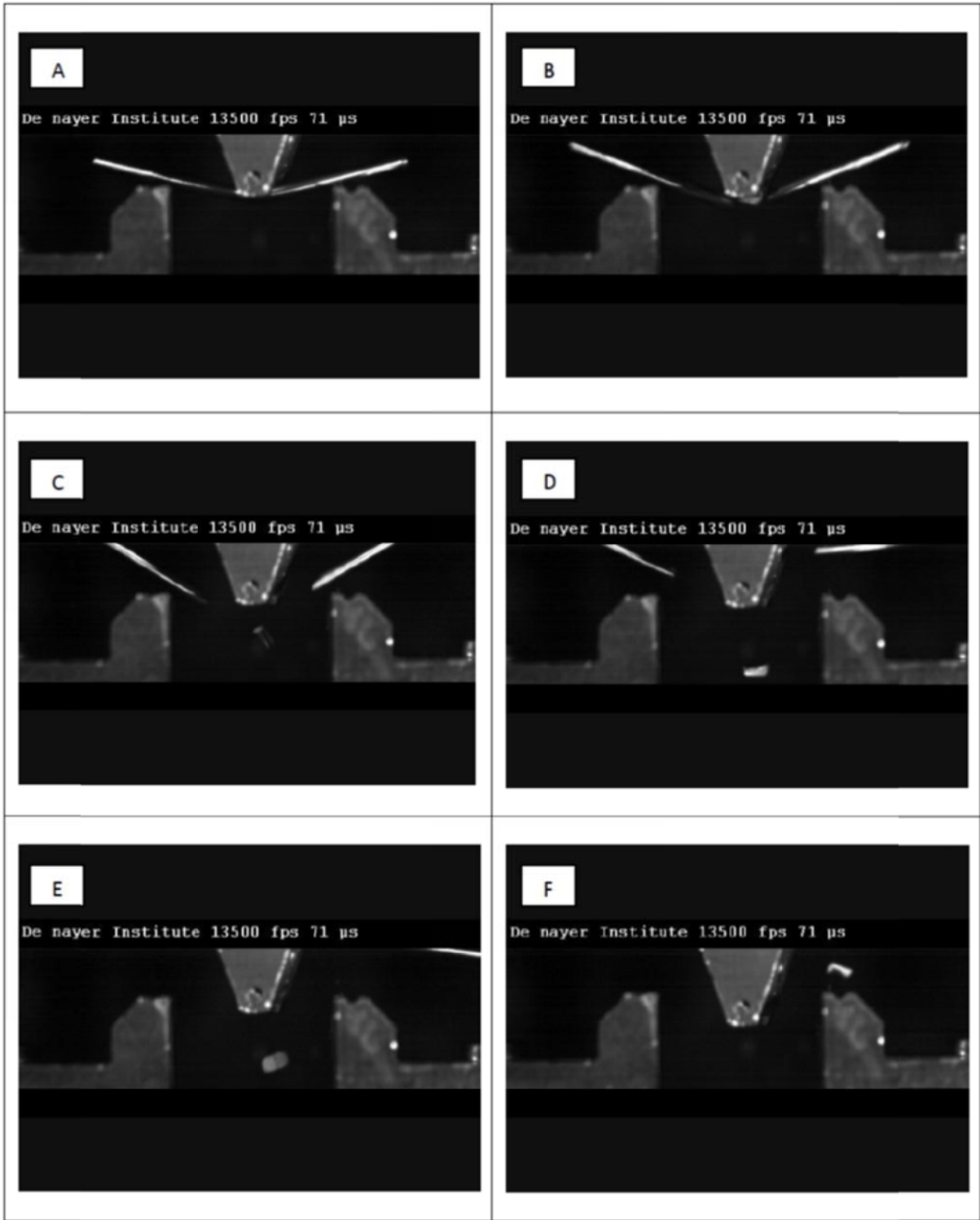


Figure 5-9 High speed camera images from fracture test (sequential images A to F)

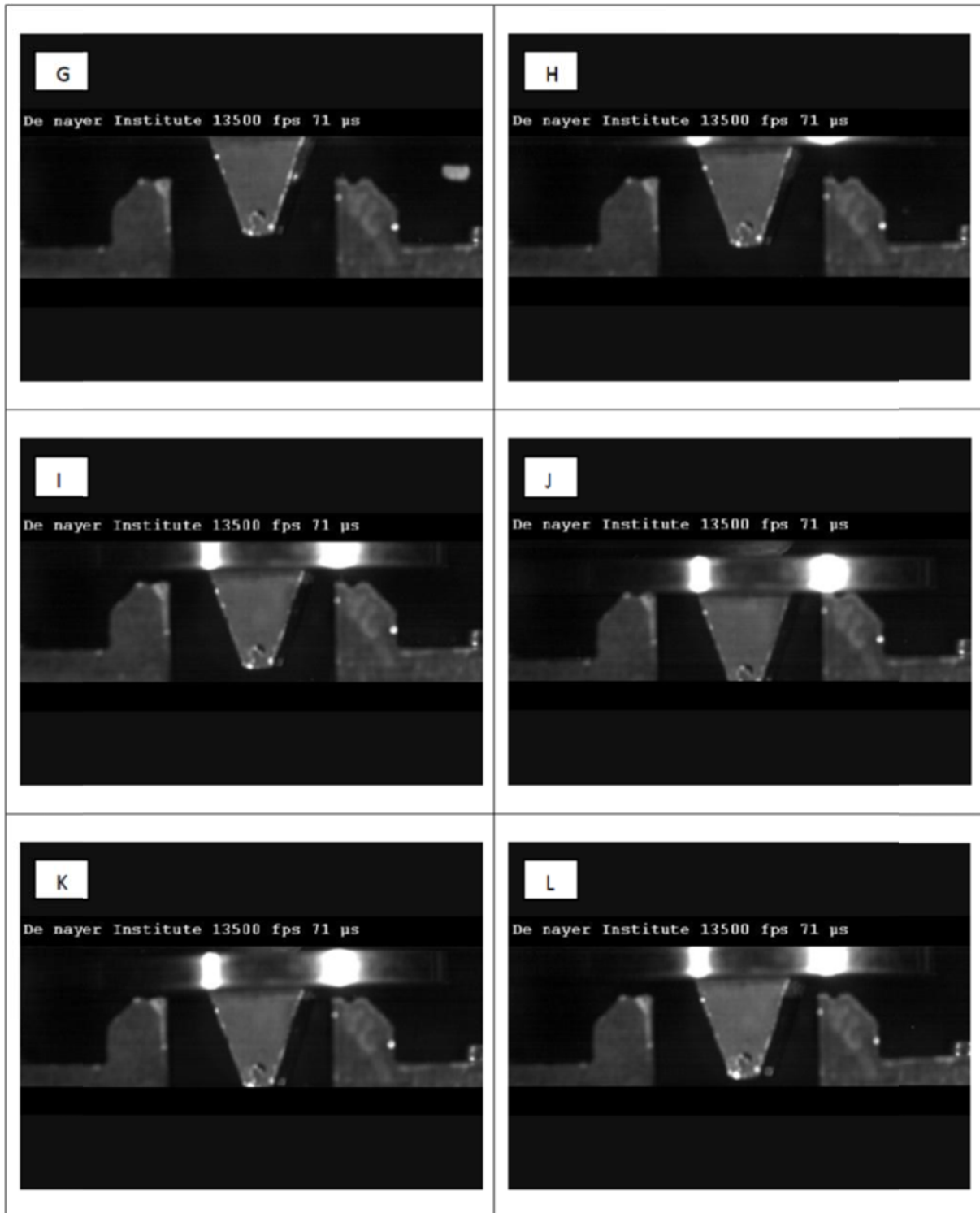


Figure 5-10 Continuation of high speed camera images from fracture test (sequential images G to L)

Note that a further version of the test, the “Supported Fracture Test” [75] where support after fracture is taken over by a spring mimicking plastic deformation behaviour of a normal, non-splashing resistance weld, was developed by Wu, a PhD student seconded in 2002 to work under my supervision. This work is not reported in this thesis.

5.3.1.1 Without Welding Current

Under normal conditions, the Free Fracture test is executed without welding current flowing during the test. I refer to this as the 'Dry Free Fracture Test', since no 'juice' (welding current) is flowing during a normal test.

5.3.1.2 With Welding Current

For the examination of the influence that welding current has upon the mechanical behaviour of a resistance welding machine, a laboratory setup was made to investigate the latter. (see Figure 5-11 below)

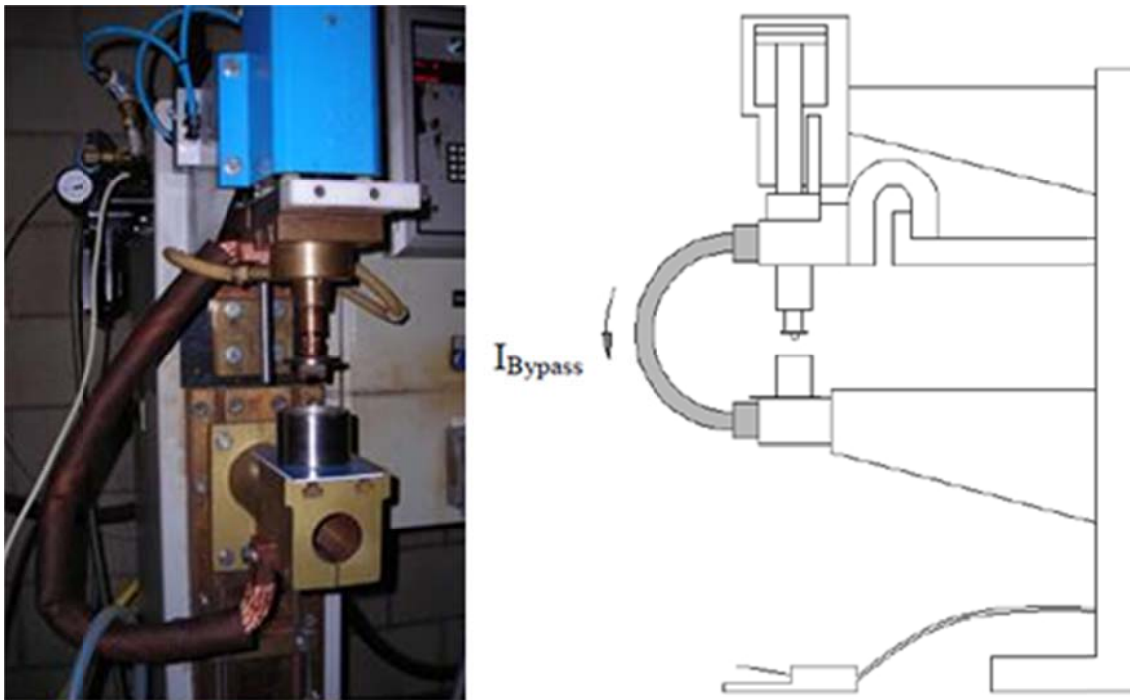


Figure 5-11 Fracture test with current bypass

In this test setup, a current bypass shunting the normal current path is attached to the electrode mounting platens of the welding heads, enabling current to flow while an insulator is placed between the lower encapsulating body of the Free Fracture Test. Fracture tests with and without welding current are made on exactly the same machine setup with the current bypass mounted in both cases.

5.3.1.3 With application of lateral force on welding head

To enable examination of the influence of welding current in generating a lateral acting force on the moving welding head, a laboratory setup was made to investigate the latter. (Figure 5-12)

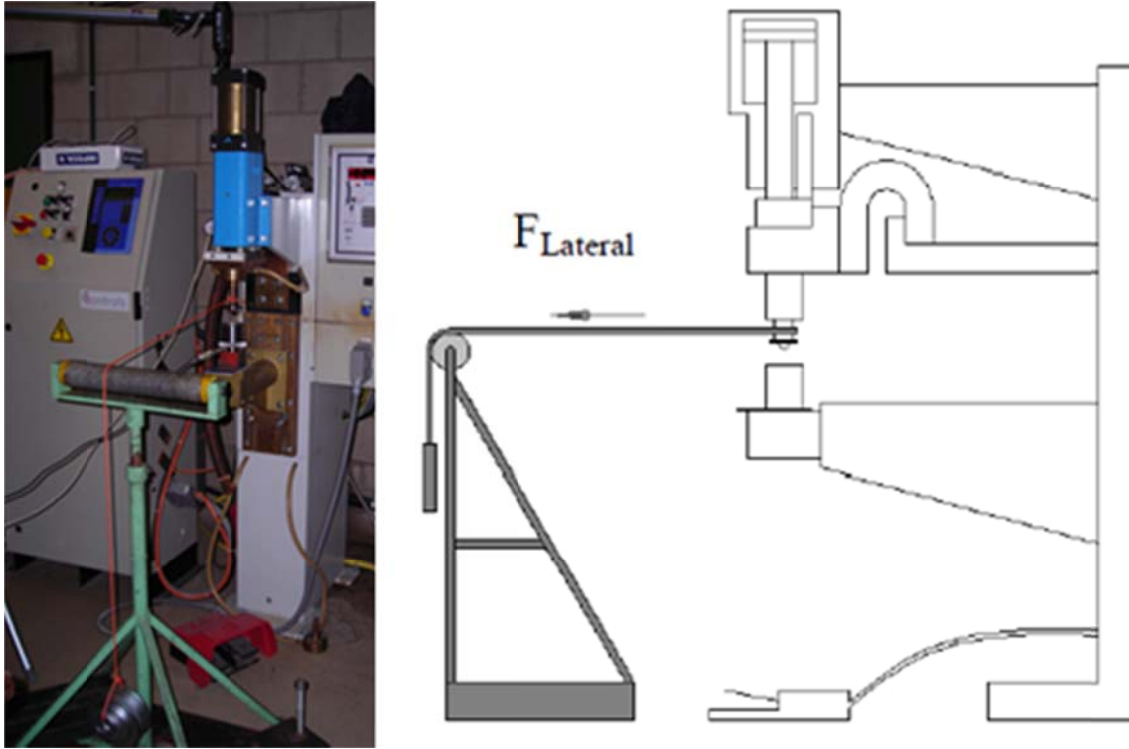


Figure 5-12 Fracture test with application of lateral force

5.3.1.4 Fracture test with different breaking elements

As an alternative for brittle hardened steel dowel pins to serve as breaking elements in the fracture test, application of a notch in the pins and alternative materials have been studied to evaluate their possible use as breaking elements to make machine assessments at lower welding head actuator loads (breaking forces). See Appendix C.

5.3.2 Explosion Test

The Free Fracture test has a number of limitations: it is still remaining rather invasive in a production environment, it is always applied without welding current, it has relatively large dimensions, and it imposes a step function that leads to extremely large displacements that only occur extremely rare in practice. Hence use of the Exploding Ball Test previously used by other authors [23], [24], [25] for comparison of follow-up behaviour of different machines was considered. This test imposes a step function on the welding head of a machine, regardless of the fact that it is located in a laboratory or in a working production environment.

However, the test was now developed to obtain machine specific data following the theoretical model described earlier in the context of this thesis. The processing procedure is identical to the one used with the Free Fracture test.

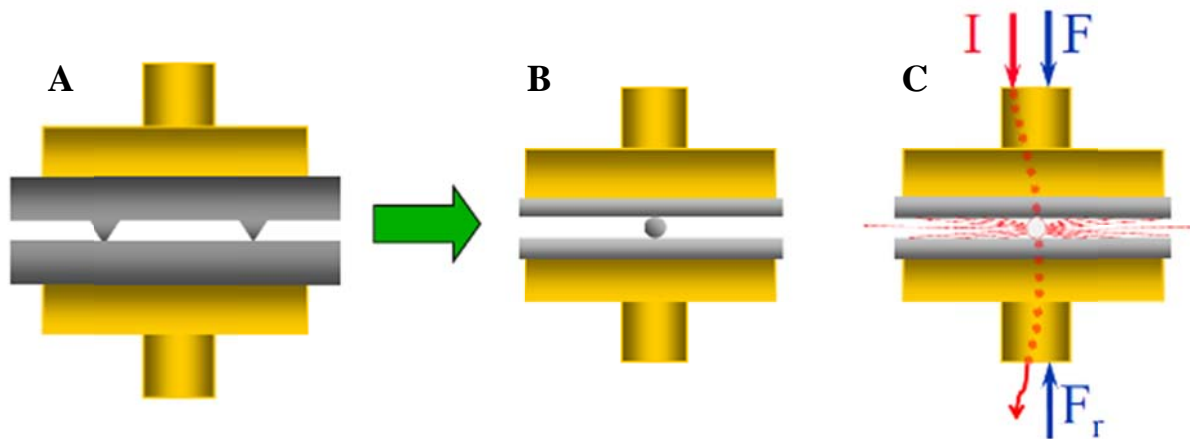


Figure 5-13 Operation principle of explosion test, A, B and C

As can be seen in Figure 5-13, **A** above, where the projection welding workpiece is represented, transferring the actuator force of the moving welding head to the stationary welding head, in Figure 5-13, **B**, the latter force transfer is realized by a metallic element (a ball bearing or a piece of metallic wire) that in Figure 5-13, **C** also conducts the welding current and that evaporates (explodes) from between the electrodes at a predefined actuator force.

The test may be conducted with the conductive element (ball bearing or piece of metallic wire) positioned directly in between the copper electrodes or positioned in between the electrodes by means of 2 intermediate conductive layers (as is shown in Figure 5-13, **B** and **C**) resulting in higher contact resistances and a higher bulk resistance. This will increase heat generation and results in the heating process and the explosion penetrating into the intermediate layers and importantly, protecting the copper welding electrodes against damage. In this way, the test becomes totally Non-Invasive, since not a single element of the welding heads needs to be dismantled and there will be no damage to the electrodes. Additionally, the test can be conducted with exploding metallic elements mounted in between the electrodes that mimic the height of the projections used in the real welding application under study, thus leading to displacements that are very close to those occurring in real welding.

The complete procedure to acquire machine relevant mechanical data of a machine under study can be found in the flowchart as presented in Figure 5-14.

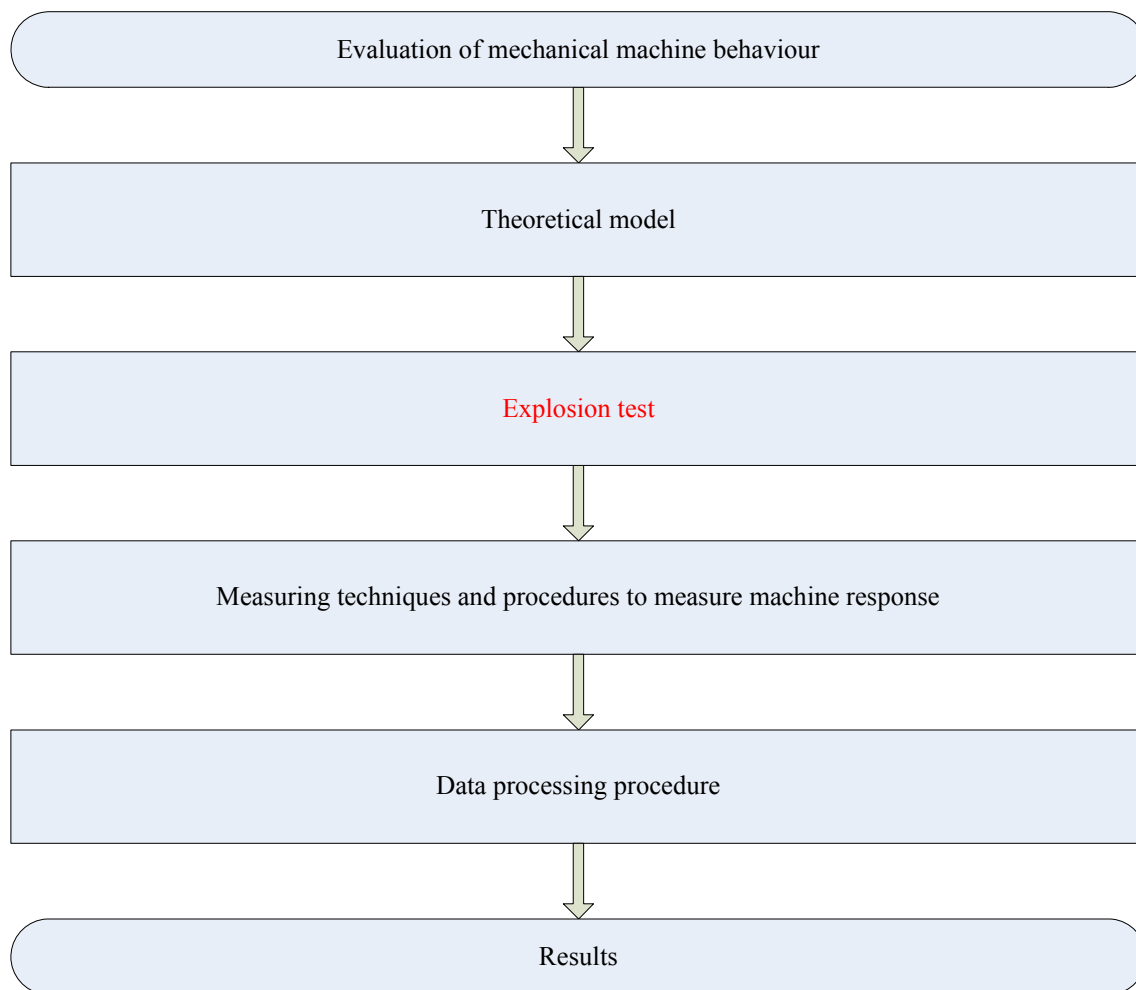


Figure 5-14 Mechanical test procedure

5.3.2.1 Ball Bearing

The explosion test conducted with a ball bearing element follows brief descriptions in literature [23], [24], [25].

In the explosion test, the supporting element transferring the mechanical load from the moving welding head to the fixed welding head is assured by a bearing ball according to BS ISO 3290:2001 Roller bearings – Balls – Dimensions and tolerances and BS ISO 3290-1:2008 Roller Bearings – Balls – part 1, Steel Balls.

The steel ball is placed directly in between the welding electrodes of a machine under study or is placed in between the electrodes by means of two intermediate conductive layers. The latter intermediate layers are preferably plates in a high resistive alloy and with a thickness in the order of the ball diameter and length and width that allow for ease of application. It is convenient to position the sandwich layer – ball – layer between the electrodes as they close under the welding force by safely holding the sandwich between the thumb and index finger of one hand. In the tests conducted within the scope of this thesis, the test piece dimensions were as follows:

Bearing Ball dimension: 1,5mm diameter

Intermediate layer: AISI 304; 1,5mm thickness; 10mm x 25mm

In Figure 5-15 below is a photograph of a bearing ball positioned on an intermediate layer.

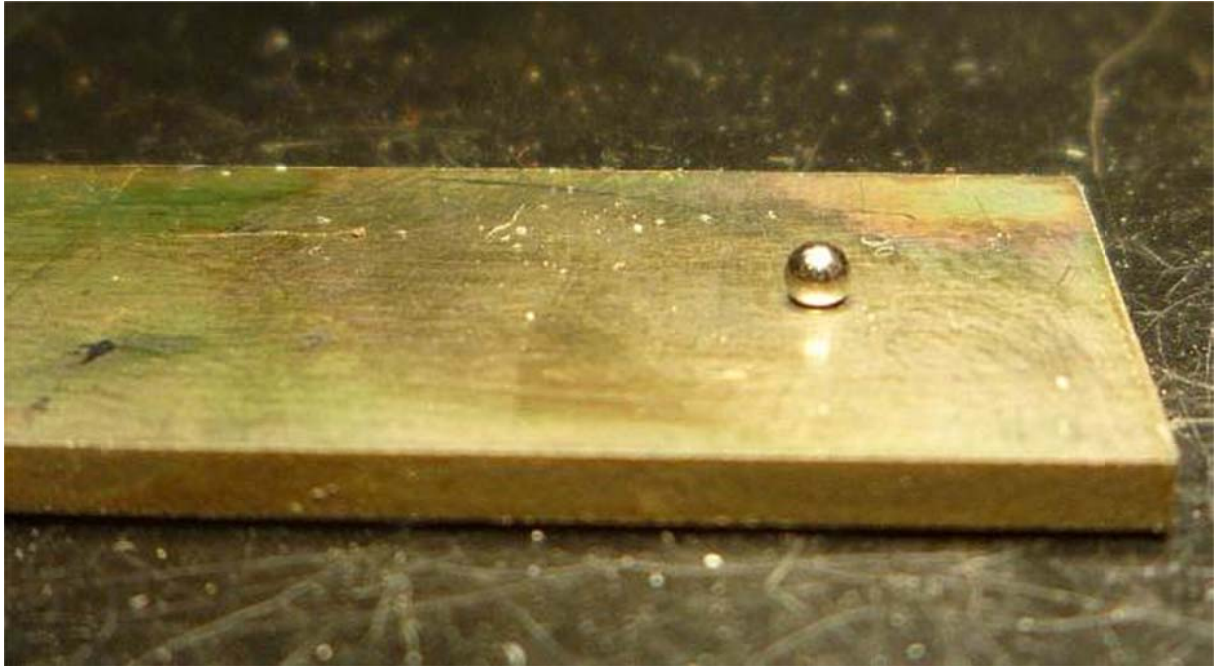


Figure 5-15 Bearing ball positioned on intermediate layer

A problem that occurs in using a bearing ball as element to explode is that the ball does not remain immobilized on a flat surface.

This can be overcome by indenting the intermediate layer with a center punch as can be seen in Figure 5-16. Indentations should however be made identical to ensure comparable contact resistances.

Bearing balls of small dimensions are also extremely expensive and hard to find.

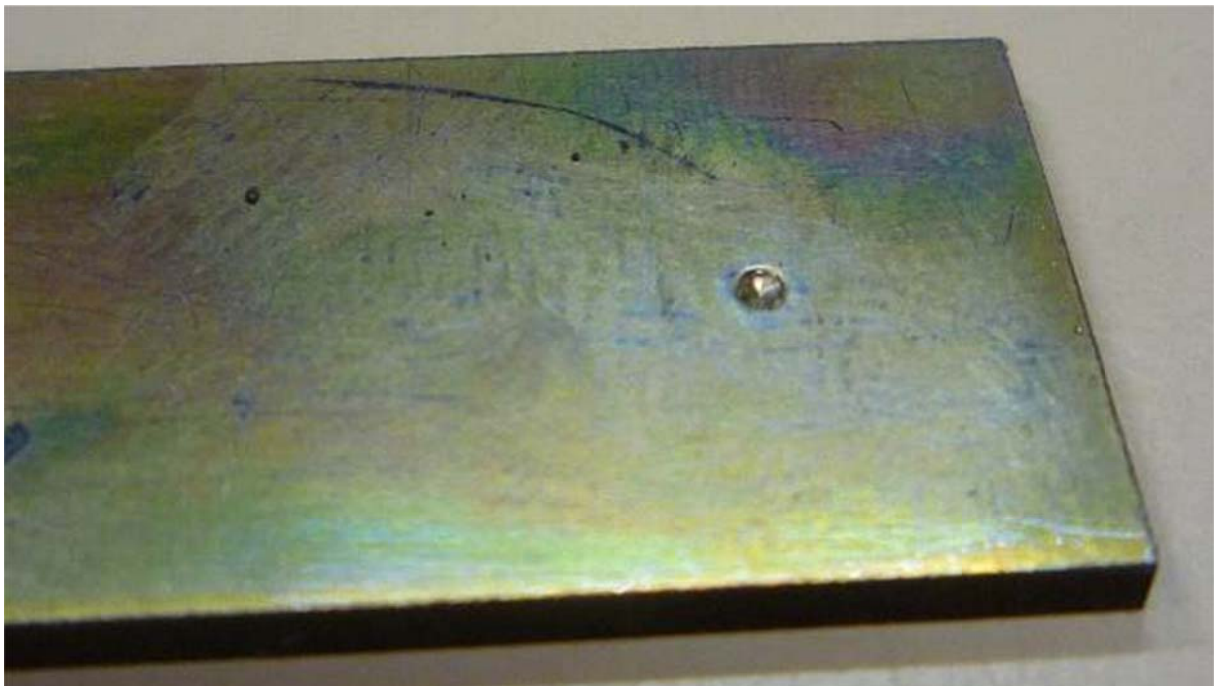


Figure 5-16 Indentation in intermediate layer

The complete sandwich: intermediate upper layer – bearing ball – intermediate lower layer positioned in between the welding electrodes of a machine under study can be seen in Figure 5-17.

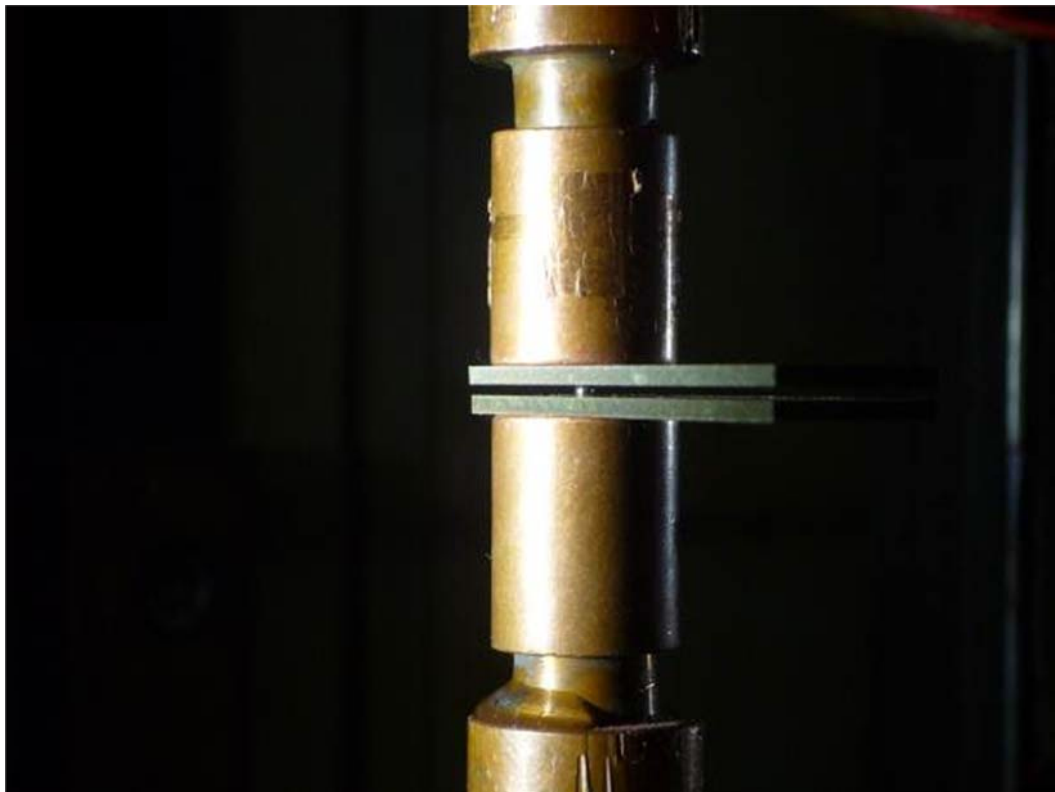


Figure 5-17 Bearing ball positioned in between electrodes with two intermediate layers

5.3.2.2 Wire Piece and Button

To overcome the practical problems with the ball bearing elements, their general availability, their availability in different small dimensions, difficult positioning on an electrode or an intermediate layer, their high price and most of all to enable flexibility in materials choice, two new options were developed, the use of wire (exploding wire test) and the use of buttons, small cylinders cut from wire (exploding button test). Welding filler wire was used since it is available in different diameters and alloys. Small cylindrical buttons, with a length smaller than the diameter, can also be machined from welding wire. .

The wire piece (a small length of welding wire) has, like the ball bearing elements, the tendency to roll off the electrode or the intermediate layer, and the separation of the electrodes is limited to dimensions according to the available welding filler wire diameters.

However, the use of a button machined from wire has the following advantages:

- Available alloys with high resistivity;
- Easy to machine into the preferred thickness;
- Easy to collect when a magnetic alloy is chosen;
- Easy to position;
- Easy to mimic real projection heights;
- Reproducible resistance boundary conditions;
- Cheap.

Clearly, the exploding button test is superior on all issues over any other elements to serve as exploding supporting element.

All three elements capable to serve as supporting element to explode can be seen in Figure 5-18.

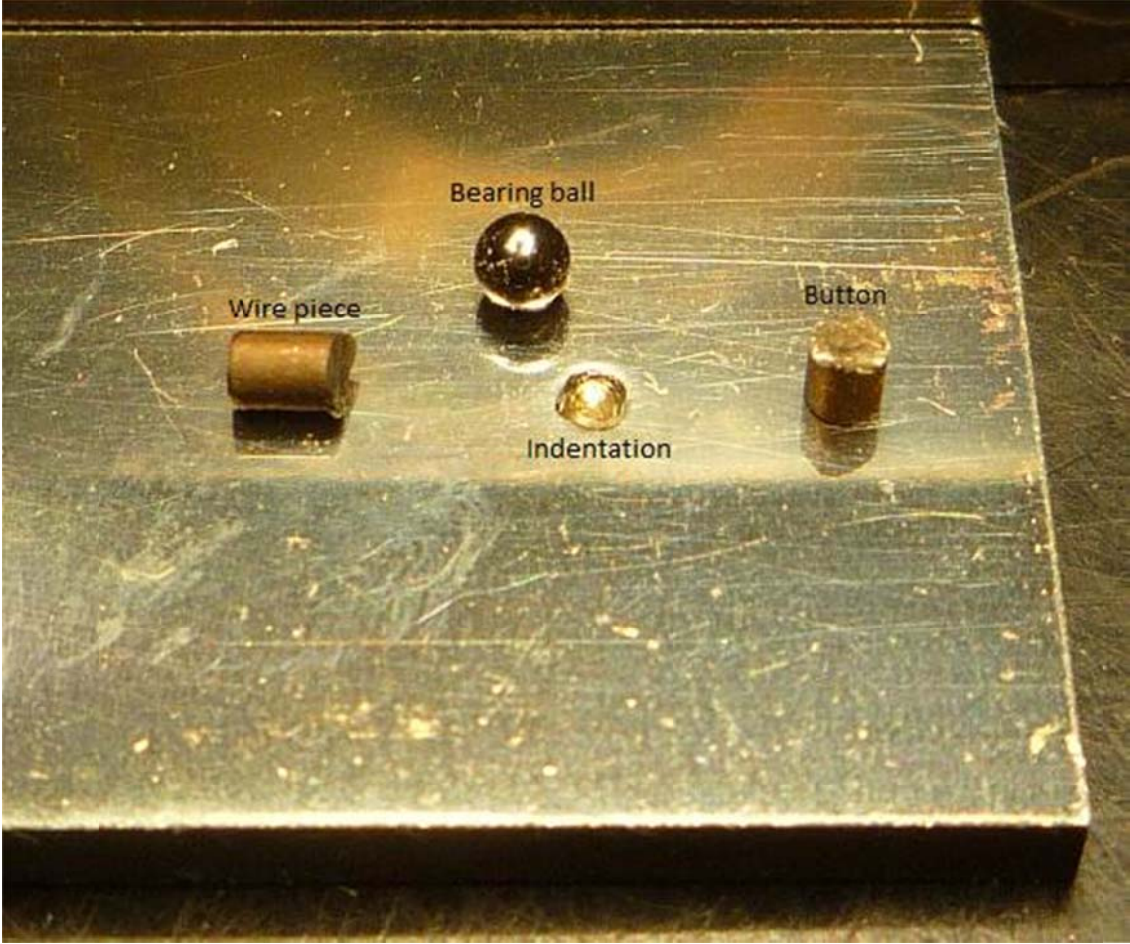


Figure 5-18 Different supporting elements for explosion test

5.3.2.3 Production of Test Pieces

Producing test pieces out of welding filler wires was in practice best made by means of Electric Discharge Machining (EDM) through wire erosion.

The choice of this very accurate production technique leads to the need to provide a means of clamping the welding filler wire to be cut. This was achieved by developing a magnetic clamping device. The same magnet holding the wire ready to be cut also serves to collect and retain the small button after it is cut from the wire.

This clamping device (see Figure 5-19) houses a strong Neodymium button magnet capable of immobilizing the welding filler wire during the wire cutting process. The magnet also collects the button or wire piece as it is cut and thus prevents the very small elements being flushed away by means of the very strong flow of dielectric fluid around the eroding wire. The latter is a very important issue since otherwise all of the eroded small pieces will disappear into the dielectric fluid conditioning system. It also necessitates the use of welding filler wires that have magnetic properties.

Practical tests revealed that 17% Chromium wires offer the best combination of high resistivity and magnetic properties.

Additionally, the wire guide provides guidance for the most common welding filler wire diameters available on the market (0.8mm, 1.0mm, 1.2mm, 1.6mm,...).

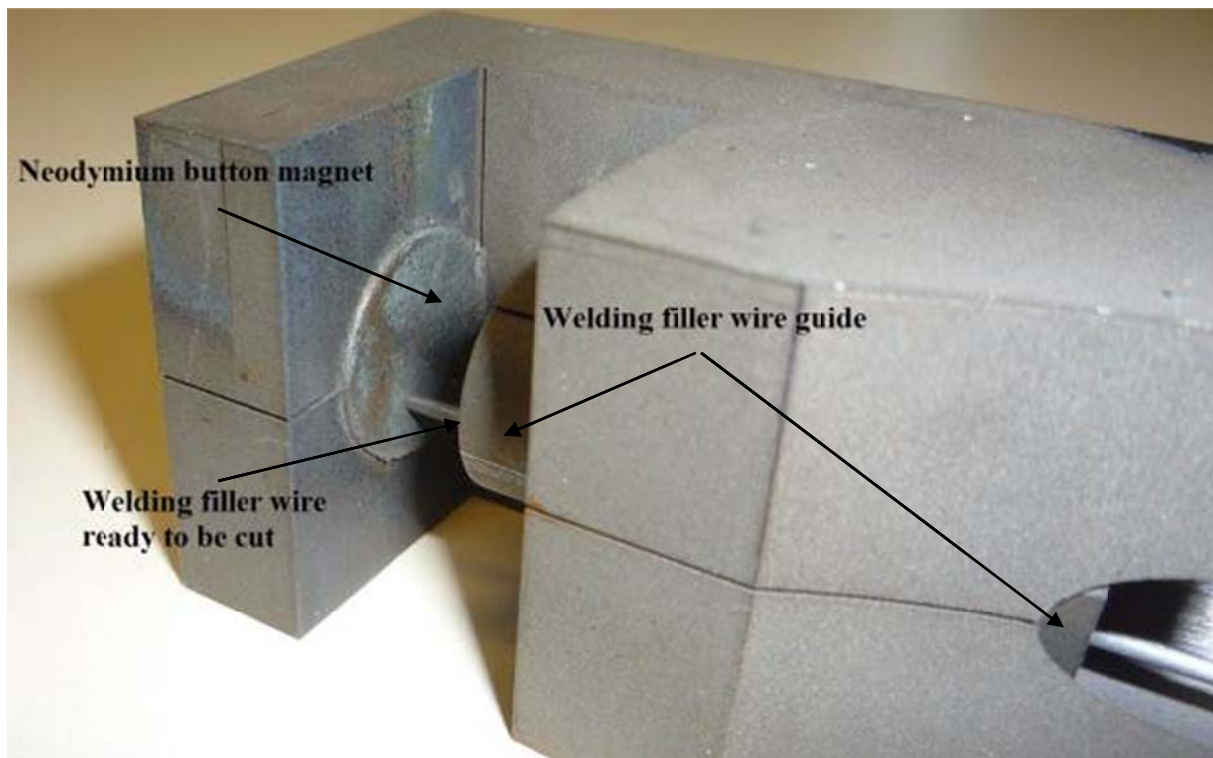


Figure 5-19 Clamping device for production of support elements for explosion tests

The clamping device mounted on an Agie EDM wire eroder can be seen in Figure 5-20 below.



Figure 5-20 Clamping device mounted on Wire eroding EDM

5.4 High speed camera evaluation

To assist evaluation of the different test procedures, high speed video images were recorded. These are important to assess the bending of the fracture pins prior to fracture and to evaluate the heating, melting and vaporising of the conductive exploding elements. For capturing images of the fracture test, the camera (IDT Motionpro Y4L) was positioned at 0.5 – 0.7m distance from the fracture test and after several trials the best setting was established and is as follows: shutter speed or exposure time $71\mu\text{s}$, frame delay $1\mu\text{s}$, resolution of the image 512×220 pixels, sampling rate 13500fps.

The lens used was a Nikon 60mm macro objective.

For capturing images of the explosion test, the same camera (IDT Motionpro Y4L) was fitted with an Infinity K2/S long distance microscope objective with a supplementary zoom module allowing view in between the intermediate layers encapsulating the element to explode and was positioned at 0.6 – 0.8m distance from the welding electrodes. Stroboscopic LED counter lighting was used to enable vision in the dark stages (just before and just after the explosion) and to avoid overexposure during the effective explosion. See Figure 5-21 where LED stroboscopic lighting is positioned on the left side and video camera on the right side.

When making high speed video images, the machine used to perform the tests was equipped with a safety glass shielding encapsulating three out of four directions starting from the fracture / explosion place, thus protecting personnel and equipment against injury and damage.

It needs to be mentioned that fracture tests in the open design test rig and explosion tests

performed without the use of additional intermediate layers both produce a real risk of injury and damage whereas the explosion test conducted with the use of additional intermediate layers hardly lead to expulsions leaving the encapsulating layers. So in practical application, when no video recordings are made, these tests can be conducted without any risk and without shielding.

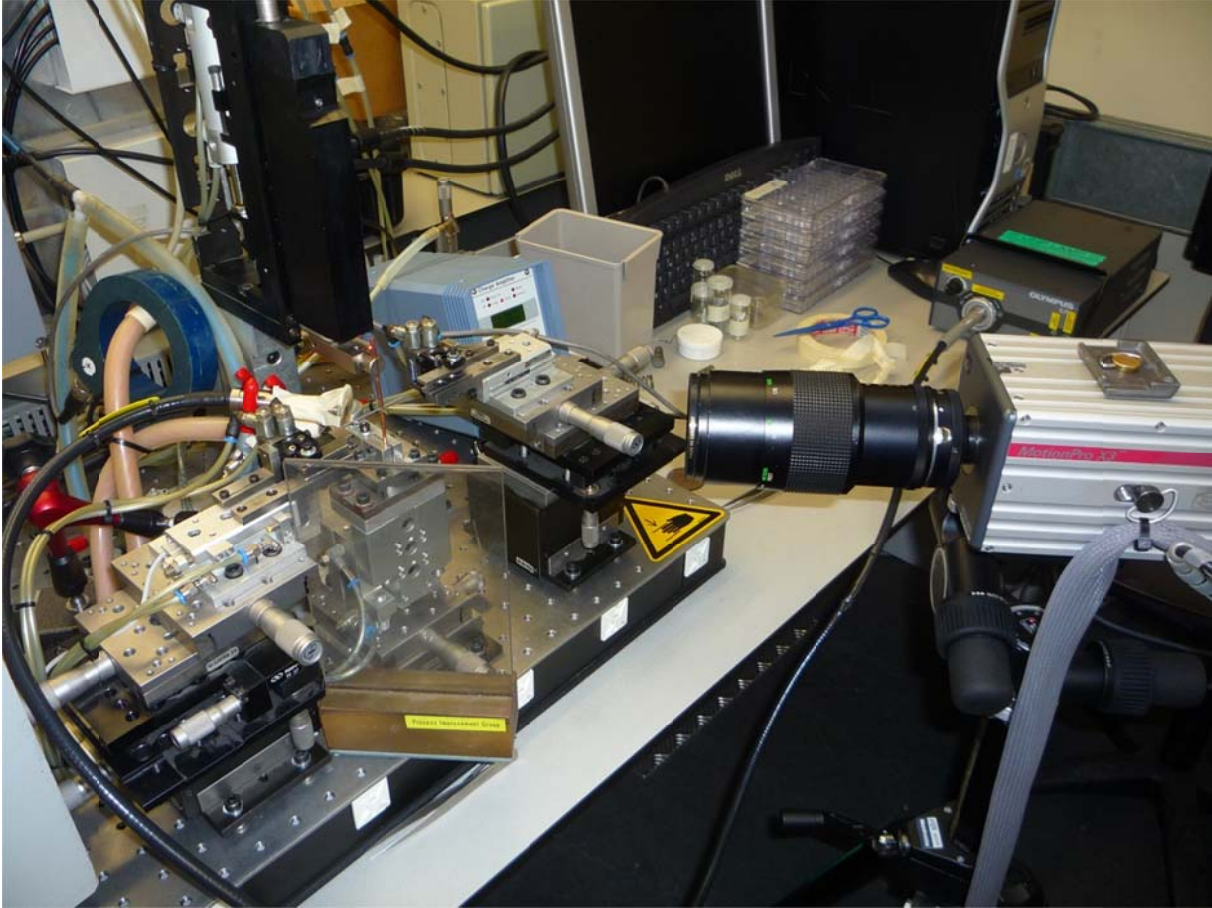


Figure 5-21 Explosion test setup with counter LED lighting

5.5 Stick – Slip Test

Stick-slip is the phenomenon where two objects sliding over each other spontaneously show a halting or bouncing movement. The cause of the latter lies in the fact that friction occurs between two sliding surfaces. The force necessary to overcome the frictional force is higher when the object is not moving (static friction) in comparison with the object effectively moving (kinematic friction).

In the case of a pneumatic cylinder it is considered that when the input pressure is sufficient to conquer the static friction, the piston will initiate movement. (friction force is then opposed to the movement direction)

At that specific moment, the friction coefficient changes from its static to its kinematic condition, thus reducing the friction coefficient that in turn leads to a sort of “balance in force”. The latter will initiate an accelerated movement of the piston until the moment that pressure drops below the amount needed for conquering friction, stopping movement. In a well built pneumatic cylinder, air supply will be sufficient to avoid the repeated occurrence of stick-slip effects.

However, depending on the response of the control valve used and the supplied input pressure, it occurs and it will lead to the halting movement. The response velocity of the control valve will define the response time of the air supply network to a drop in pressure.

On the other hand, the supplied input pressure is very important, the higher the input pressure, the higher the pressure on the piston seals, increasing static friction force and increasing the risk of stick-slip.

5.5.1 Test setup for stick-slip test

(see Figure 5-22)

To enable stick-slip tests on a resistance welding machine, the lower electrode assembly of the machine is replaced by a rubber bellows (Pirelli Thorpress air actuator). Compressed air is supplied from the main network by means of a pressure regulator at a predefined pressure level and monitored by means of a Keller 21S pressure transmitter, mounted in a T-joint in the supply line and measured with our data-acquisition system. Pressure in the welding cylinder of the moving welding head is set by means of the pressure regulator of the welding machine in steps of 1 bar, the latter controlled by a second Keller 21S pressure transmitter. Force between the moving electrode and the supporting bellow is measured by means of a Miyachi MM601-A load cell.

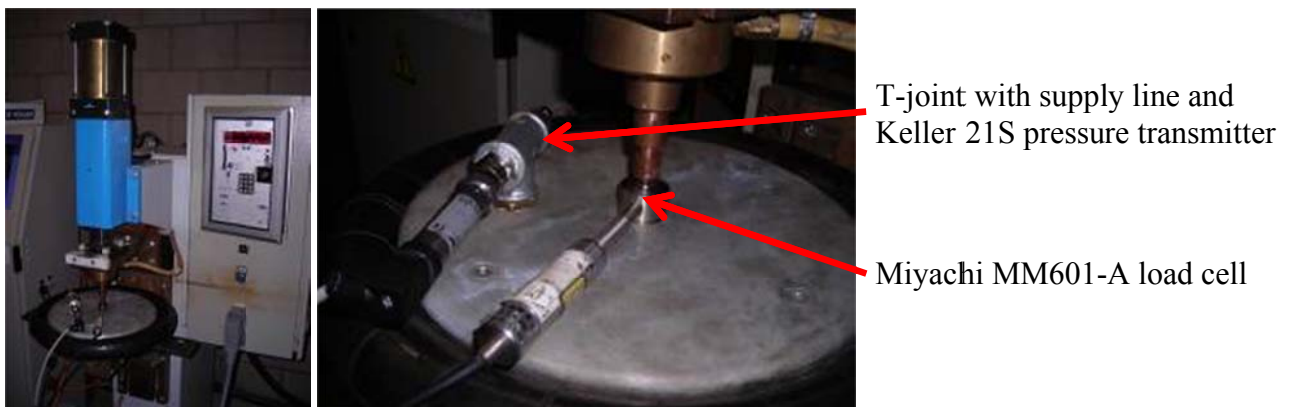


Figure 5-22 Test setup for stick-slip measurements

5.5.2 Test procedure stick-slip measurements

A predefined input pressure is set on the machines welding cylinder, the latter forcing the moving electrode downwards to apply a force on the supporting bellows. The Miyachi load cell is placed between electrode and bellows. Subsequently, the pressure in the bellows is increased to the point where the bellows delivers sufficient force to move the electrode upwards again. When this occurs, pressure is no longer increased. As a next step, pressure in the bellow is lowered smoothly until the cylinder-electrode combination comes into balance.

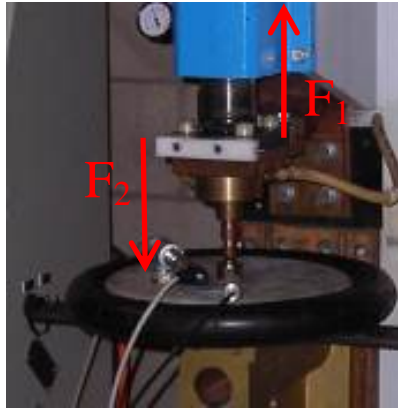


Figure 5-23 Test procedure for stick-slip measurements

Subsequently, the machine welding head and cylinder are manually pushed upwards and smoothly lowered again, followed by recording the supporting force.

In a next step, we push the welding head and cylinder downwards and release it, followed by recording the supporting force again (see Figure 5-23). This procedure is repeated for different pressure levels in the welding head cylinder between 1 and 6 bar.

5.5.3 Processing of results

The difference between the measured forces (piston pushed up and down) is divided by two because we measure around an equilibrium point and we have interest in the difference in respect of this equilibrium situation. The values obtained in this way give us the static friction force:

$$F_{w (static)} = \frac{(|F_1 - F_2|)}{2}$$

5.6 Stick-slip test with application of lateral force

5.6.1 Test setup

The same test setup as used in paragraph 5.5.1 is used, extended with a facility to enable the application of a lateral force on the moving welding heads electrode. The practical setup of the latter can be seen in Figure 5-24 below.



Figure 5-24 Application of lateral force on welding head

Lateral force is applied by means of a mass hanging on a string over a guiding roll and attached to the moving welding electrode.

5.6.2 Test procedure

Identical to 5.5.2

5.6.3 Processing of results

Identical to 5.5.3

5.7 Test methodology on different machines tested

5.7.1 AWL machine

The AWL multi-purpose spot/projection welder is a machine equipped with a rather particular construction of its moving welding head.

The moving welding head actually is composed of two masses, coupled with a compression spring coupling between actuator piston mass and moving welding head slide assembly mass. The coupling compression spring is surrounded by a compression limiter, the latter enabling for setting the compression force range of the spring coupling. (see Figure 5-25)

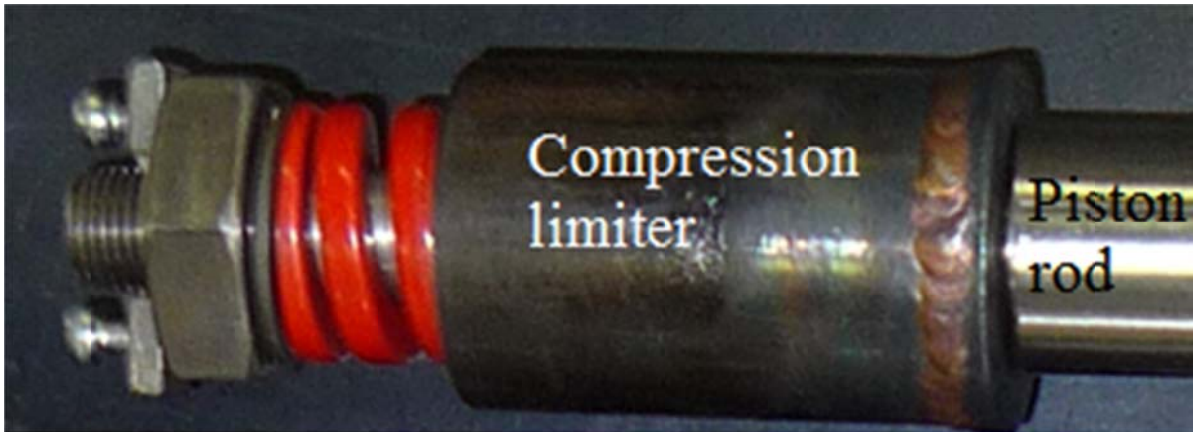


Figure 5-25 AWL moving welding head coupling system (spring and compression limiter)

Its spring constant was tested on an Instron compressive test bench and was measured as $k = 165\text{N/mm}$. Both the upper actuator piston rod and the lower hollow shaft of the slide are connected by means of the nut (and its securing locking screws) on the left of Figure 5-25.

This nut also serves to set the pre-stress level of the coupling spring, in this case, with a spring compression of 4mm, there is a pre-stressing force of 660N on the spring. The remaining available travel that can be further compressed is 14mm, yielding the maximal force at which the limiter contacts the lower slide of 2970N.

Between 660N and 2970N, the force exerted by the piston rod on the lower slide is transferred through the spring, loading the lower slide with the actuator force, without adding its mass to it. In this range, piston rod assembly and lower slide and electrode assembly move as if they were separated. Below 660N and above 2970N, all moving parts (piston rod assembly + lower slide and electrode assembly) move as one single mass actuated by the actuator force.

This spring coupling was installed as a standard feature in these multi-purpose spot/projection welding machines to slightly improve follow-up characteristics of the welding head towards projection welding applications in the lower actuator force range of the machine. It however is surely subject for improvement since the reduced mass is still the highest in the assembly instead of the other way around.

By increasing the compressing distance of the spring, the operating range where the spring is active will evenly increase. But most of all, weight reduction of the lower assembly will lead to improved behavior in addition to the reduced friction.

Figure 5-26 below shows a schematic block diagram representing the moving welding head with its degrees of freedom and limitations.

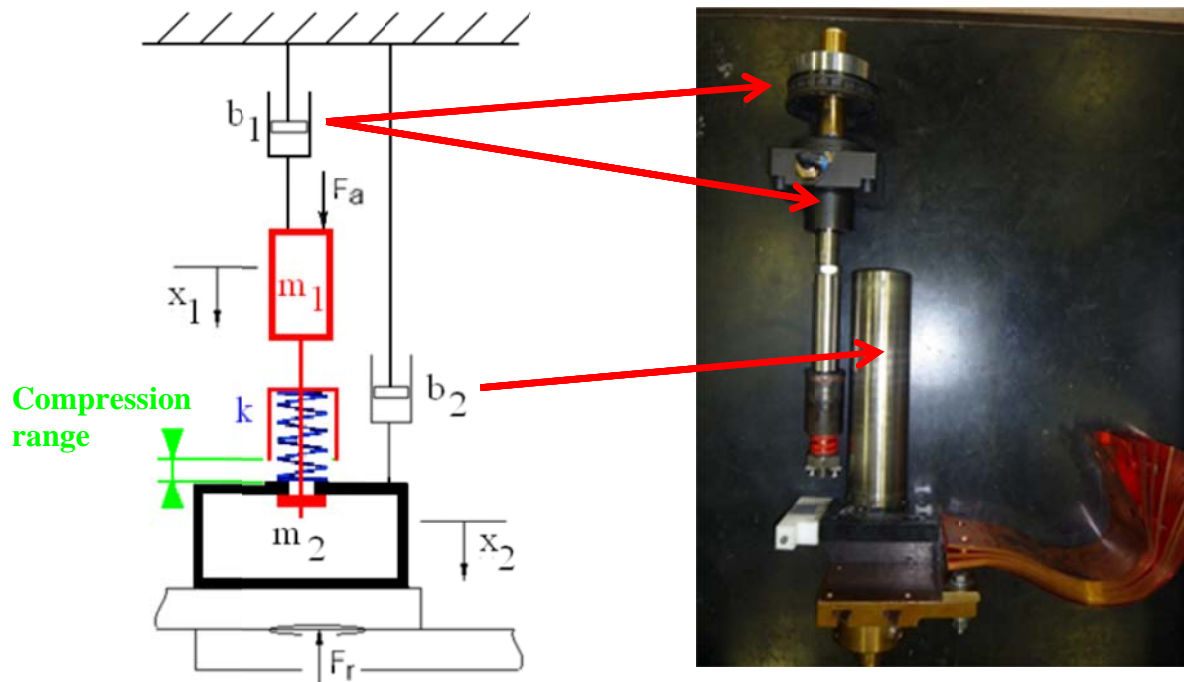


Figure 5-26 Moving welding head schematic block diagram (left) + corresponding components (right)

In Figure 5-26 above, the block diagram contains the following elements:

- m_1 = lumped mass of pneumatic actuator piston seal, piston rod, compression limiter and securing nut.
- b_1 = damping due to friction between piston seal and cylinder wall + damping due to friction in piston rod bearing + viscous damping in air feed and bleed system.
- x_1 = displacement of lumped mass m_1 .
- k = spring constant of coupling spring.
- F_a = applied actuator force
- m_2 = lumped mass of moving welding head slide + electrode holder + electrode assembly + flexible current lead.
- b_2 = damping due to friction between moving welding head slide and its bearing.
- x_2 = displacement of lumped mass m_2 .

All the testing methodology and all test procedures developed and described in this work aim to produce characterising mechanical machine values that allows the user to model its behaviour in a ‘black-box-approach’. The moving welding head thus is represented by a single mass-damper system, actuated at a specific actuator force (according to section 5.1). The AWL machines’ physical moving welding head setup as described above should therefore result in different mechanical behaviour at different actuator force ranges, due to the coupling spring used.

5.7.1.1 Free fracture tests

Four groups of five fracture tests each at four different actuator force levels (inside and outside of the working range of the compressing spring coupling in the welding head assembly) are performed to evaluate the accuracy and effectiveness of the step function

imposing tests and subsequent data processing procedure to reveal the different mechanical behaviour due to the spring coupling present.

Or in other words: “Will the step function imposing test with its according data processing procedure result in different lumped masses calculated?”

Table 5-1 below gives the setup for the step function imposing free fracture test following the test procedure described in section 5.3.1 and appendix C.

Fracture pin breaking force [kN]	Fracture pin diameter [mm]	Fracture pin length [mm]	Support distance [mm]
Range A ~0,75kN	2,5	40	27
Range B ~1,4kN	3	50	32,5
Range C ~3kN	4	40	32,5
Range D ~5kN	4	60	25

Table 5-1 Test setup for free fracture tests on AWL machine

Values for fracture pin breaking force are chosen in the four ranges mentioned above, with Range A on the lower boundary of the working range of the spring coupling, Range B in the middle of the working range of the spring coupling, Range C on the upper boundary of the working range of the spring coupling and finally range D completely outside of the working range of the spring coupling.

This tests are performed on the welding head twice, with the coupling spring present in the welding head assembly, and with the coupling spring removed from the welding head assembly.

5.7.1.2 Explosion tests

To evaluate the accuracy and effectiveness of the exploding button and exploding ball test as step function imposing test, two series of exploding button and exploding ball tests will be performed.

In the first series of tests, to enable evaluation of the useful application range of the explosion tests in machine heat setting, both exploding button and exploding ball tests will be executed at five different ranges of machine “heat setting (HS)”. The latter is the setting on the machines’ control box, representing the energy level to be added to the welding application in between the welding electrodes. HS is expressed as a percentage of the maximum setting that can be made on the machine.

Heat setting levels to be evaluated are 40%, 45%, 50%, 75%, 99% (= maximum setting).

The actuator force setting is set identical for all these tests at 1,65kN inside the working range of the spring coupling present in the moving welding head assembly.

In the second series of tests, explosion tests at 99% HS are performed at six different actuator force levels between 0,4kN and 1,8kN, both with and without the spring coupling present in the moving welding head assembly.

Table 5-2 below gives the setup for the step function imposing exploding test following the test procedure described in section 5.3.2.

		Actuator force setting [kN]							Heat setting [%]					
Series 1	Spring	Button	1,65							40	45	50	75	99
		Ball	1,65							40	45	50	75	99
Series 2	Spring	Button	0,4	0,7	1	1,2	1,6	1,8	99					
	No spring	Button	0,4	0,7	1	1,2	1,6	1,8	99					
Bearing ball: 1,5mm diameter					Button of 1,2mm x 1.2mm diameter (17% Cr)									

Table 5-2 Test setup for explosion tests on AWL machine

5.7.1.3 Fracture tests with application of current

Two series of twenty fracture tests are conducted on the AWL machine at an actuator force setting of 0,9kN with and without the application of a welding current of 10kA, with the test procedure described in section 5.3.1.2.

Table 5-3 below gives the setup for the tests to evaluate the influence of current on fracture tests.

		Actuator force setting [kN]				Current flowing	
Series 1	0,9				No current		
Series 2	0,9				10kA		
	Fracture pin breaking force	~0,9kN					
	Fracture pin diameter [mm]	2,5					
	Fracture pin length [mm]	50					
	Support distance [mm]	32,5					

Table 5-3 Test setup for fracture tests with application of current

5.7.1.4 Fracture tests with application of lateral force

To enable the influence of a lateral force acting on the moving welding head on its mechanical behavior, three series of tests will be performed.

First, with the spring coupling present in the moving welding head assembly, a fracture test at 2,5kN actuator force with application of 50N of lateral force on the welding head, as described in section 5.3.1.3, and a fracture test at an identical actuator force without application of any lateral force on the welding head.

Second, with the spring coupling present in the moving welding head assembly, a fracture test at 3,3kN actuator force with application of 100N of lateral force on the welding head and a fracture test at identical actuator force without application of any lateral force on the welding head.

Third, a fracture test at 5kN actuator force without application of any lateral force on the welding head with and without the coupling spring present in the moving welding head assembly.

Table 5-4 below gives the setup for the tests to evaluate the influence of a lateral force acting on the moving welding head on the fracture tests.

		Actuator force [kN]	Lateral force [N]	
Series 1	Spring	2,5	50	
	Spring		0	
Series 2	Spring	3,3	100	
	Spring		0	
Series 3	Spring	5	0	
	NO spring		0	
Fracture pin breaking force [kN]	Fracture pin diameter [mm]	Fracture pin length [mm]	Support distance [mm]	
~2,5kN	3	40	20	
~3,3kN	4	40	27	
~5kN	4	60	25	

Table 5-4 Test setup for fracture tests with application of lateral force

5.7.1.5 Stick – slip test

To enable the influence of the stick-slip effect on mechanical behaviour of AWL machines' moving welding head, a series of friction measurements are set up, incorporating the effect of a lateral force acting on the welding head. Table 5-5 below lists the test setup following the procedures described in sections 5.5 and 5.6.

Actuator pressure [bar]	Actuator force [kN]	Lateral force on welding head [N]			
0	0	0	25	50	75
1	0,73				
2	1,47				
3	2,22				
4	2,96				
5	3,70				
6	4,44				
7	5,19				

Table 5-5 Test setup for friction measurements on AWL machine

5.7.1.6 High speed camera evaluation

In several of the tests described above, high speed camera recording is used, together with data-acquisition of electrical and mechanical parameters, in order to allow for evaluation of fracture, exploding ball and button tests and influence of current flowing on the machines' mechanical behaviour.

5.7.2 PECO roll membrane machine

To define the representative machine parameters (mass m and damping factor b) of this machine equipped with this specific type of actuator in the moving welding head, a series of fracture tests will be performed on it.

Table 5-6 below gives the setup for the step function imposing free fracture test following the test procedure described in section 5.3.1 and appendix C.

Fracture pin estimated breaking force [kN]	Fracture pin diameter [mm]	Fracture pin length [mm]	Support distance [mm]
~1,06	2,5	40	20
~1,11	2,5	45	25
~1,14	2,5	50	25
~1,40	3	50	32,5
~1,64	3	40	32,5
~1,82	3	50	25
~2,66	3	40	20
~2,87	4	40	32,5
~3,45	4	40	27
~3,73	4	40	25
~3,76	4	60	32,5

Table 5-6 Test setup for free fracture tests on PECO roll membrane machine

5.7.3 ARO multi-purpose spot/projection welder (pneumatic)

5.7.3.1 Fracture tests

To define the representative machine parameters (mass m and damping factor b) of this machine equipped with this specific type of actuator in the moving welding head at different actuator load levels, a series of fracture tests will be performed on it.

Table 5-7 below gives the setup for the step function imposing free fracture test following the test procedure described in section 5.3.1 and appendix C and for the step function imposing explosion tests following the test procedure described in section 5.3.2.

Fracture tests	Fracture pin estimated breaking force [kN]	Fracture pin diameter [mm]	Fracture pin length [mm]	Support distance [mm]
	~2,13	3	40	25
	~3,45	4	40	27
Explosion tests	Actuator force setting [kN]	Heat setting [%]		
	1,6	99		
	1,6	99		
	1,6	99		
	1,6	99		
	1,6	99		
	2	99		
	2	99		
	2	99		
	2	99		
	3	99		
	3	99		

Table 5-7 Test setup for free fracture and explosion tests on ARO pneumatic

5.7.3.2 High speed camera evaluation

High speed camera recording is used, together with data-acquisition of electrical and mechanical parameters, in order to allow for evaluation of fracture, exploding wire and button tests.

5.7.4 Mc Gregor μ -resistance welding head

5.7.4.1 Explosion tests

To evaluate the accuracy and effectiveness of the exploding button test as a step function imposing test and to check its use on a μ -resistance welding head working at extremely low actuator force settings, a series of eight exploding button tests, using Fronius Deltaspot process tape (single sided copper plated stainless steel) as intermediate layers.

The power source used to vaporise the button is a Myiachi dual pulse capacitor discharge source, capable of delivering a maximal energy pulse of 250J at its full heat setting of 100%. Table 5-8 below gives an overview of the setup for the explosion tests to perform on the μ -resistance welding head.

Actuator force setting [N]	Heat setting [%]
50	100
Button of 0.8mm x 1.2mm diameter (17% Cr)	

Table 5-8 Test setup for exploding button tests on Mc Gregor μ -resistance welding head

5.7.4.2 High speed camera evaluation

High speed camera recording with integrated and coupled data-acquisition is used to allow for evaluation of the step function imposing test using buttons as elements to explode in combination with intermediate layers. Especially the accuracy of the test setup and procedures described in this work when applying it to a μ -welding head at the extreme low actuator force levels used here will be studied.

6 Results

6.1 Processing of Kinematical measurements

Signals were recorded with the Dewetron data acquisitions standard software “Dewesoft” at a sample rate of 20000 samples/s, from where they were exported to Flexpro spreadsheet data processing software. The examples below all come from measurements on an AWL multi-purpose spot/projection welder equipped with a pneumatic actuator and a spring coupling or follow-up system integrated in the hollow vertical slide of the upper welding head.

In Figure 6-1 below is a Dewesoft screenshot showing the measured air pressure in the welding head (blue), the measured welding head velocity (light green) and the air pressure in the welding head cylinder pressure release line (dark green). The interesting part of these curves is located in the area marked in red, where fracture of the pin takes place, resulting in a drop in the welding head cylinder supply pressure, an increase in welding head velocity and an increase in welding head cylinder release line pressure due to the upper welding head moving down towards the stationary welding head.

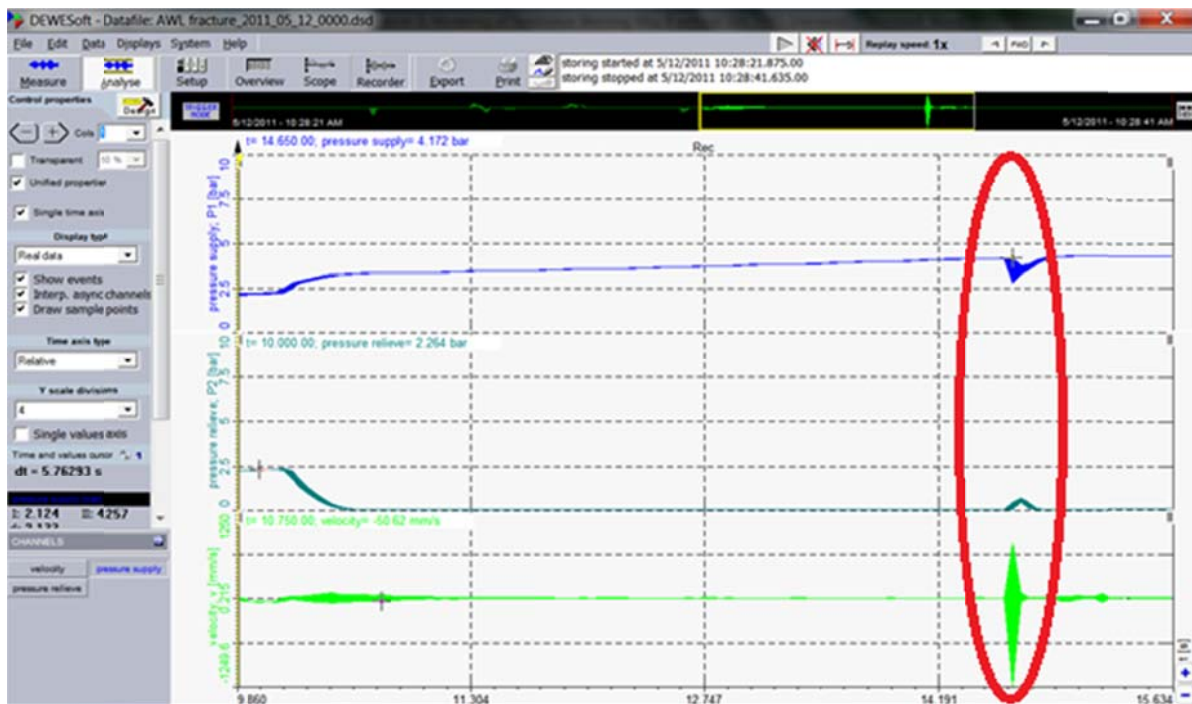


Figure 6-1 Screenshot of measured signals in a fracture test

In Figure 6-1, the pressure signal clearly shows the manual increase in pressure by means of the welding machines’ pressure regulator, thus enabling the fracture pin to bend while allowing the welding head to stop moving prior to fracture. This leads to test results with an initial welding head velocity as closely to zero as possible.

Figure 6-2 shows a Dewesoft screenshot of a zoom, starting at the moment of fracture, and stopping just before the moving welding head collides with the stationary welding head. The latter zoom actually ensures that only data relevant for further processing is exported to the data processing software. In the mean time this procedure enables the exported datasets to stay concise and of small size.



Figure 6-2 Screenshot of zoom at point of fracture

Notice in Figure 6-2 that the welding heads velocity is constantly increasing to more than 1250mm/s (upper measuring limit of the laser vibrometer used), while supply air pressure in the welding head cylinder remaining nearly constant over the same time span. Air pressure in the cylinder release line remains zero until after the maximal welding head displacement. These signals are subsequently exported to Flexpro spreadsheet data processing software, resulting in the following graphs (Figure 6-3 and Figure 6-4).

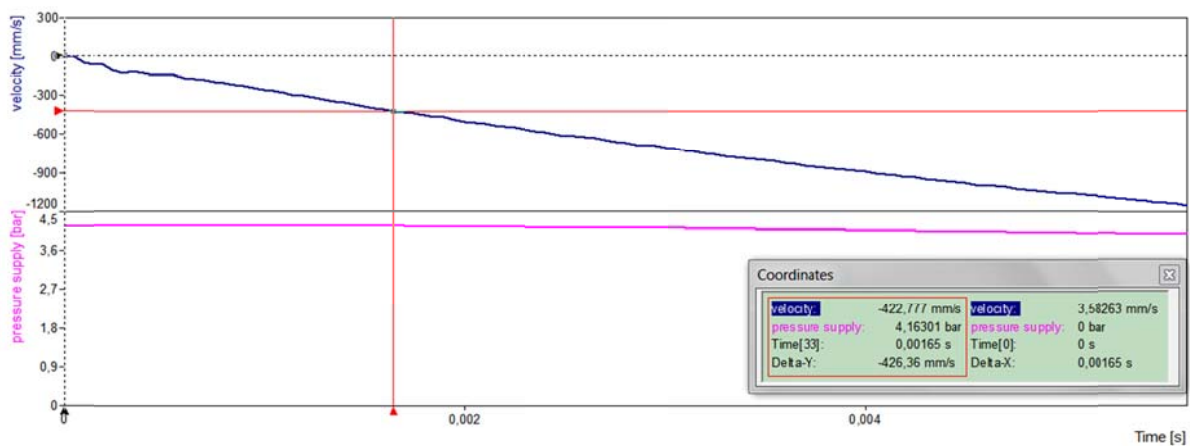


Figure 6-3 Velocity and pressure signal from fracture in Flexpro

Figure 6-3 above shows the fragment in time cut away from the measured signal as exported into the Flexpro spreadsheet data processing software. The according datasets can subsequently be processed further for measuring and evaluation, in Flexpro or in MS Excel, depending on the choice of export destination made in the Dewesoft data acquisition software.

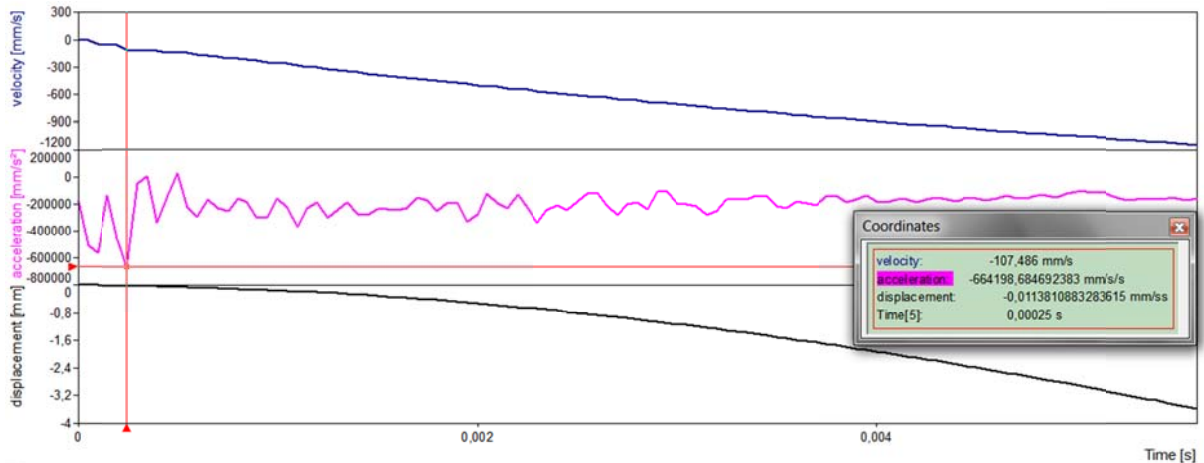


Figure 6-4 Velocity signal, calculated acceleration and displacement signals in Flexpro

In Figure 6-4 above, the blue velocity signal is both derived and integrated, resulting in the calculated welding head acceleration signal (purple signal) and the calculated welding head displacement signal (black signal). The coordinate window on the right displays the actual values of the three signals (one measured and two calculated) at the time point indicated by the red cursor.

Note the two peaks in the acceleration signal at the moment of fracture. The initial acceleration values at the start of movement by the welding head result from elastic deformation of every element above the upper electrode supporting the actuator force, including the upper part of the machine frame and of a transient vibration in the machine following the extreme abrupt change in support initiated by a fracture test. The latter is obvious when experiencing a live fracture test and will show clearly when viewing a video recording including the audio signal of a fracture test. This results in a welding head velocity value of 107mm/s, reached in a time span of 0.00025s and covering a displacement of 0.0114mm. The latter gives a mean acceleration value reached over this very short displacement of about 430m/s². After this start in displacement at high acceleration, acceleration of the complete lumped mass of the welding head stabilizes around 250m/s² in the first part of the velocity curve and later on gradually decreases as damping effects increase at higher velocity values.

For clarity, this phenomenon is completely independent of the spring coupling between the machines piston rod assembly and its vertical slide underneath. With the spring coupling removed and with both elements solidly attached to one another, the same short high accelerations occur as a response to a fracture test.

6.2 AWL machine

6.2.1 Free fracture tests

Figure 6-5 below shows an overview in Flexpro of welding head velocity responses of twenty fracture tests conducted with three different fracture pin diameters at two support distances on an AWL wp 63 r1 multi-purpose spot/projection welder with pneumatic actuation, yielding four ranges of fracture forces for further processing.

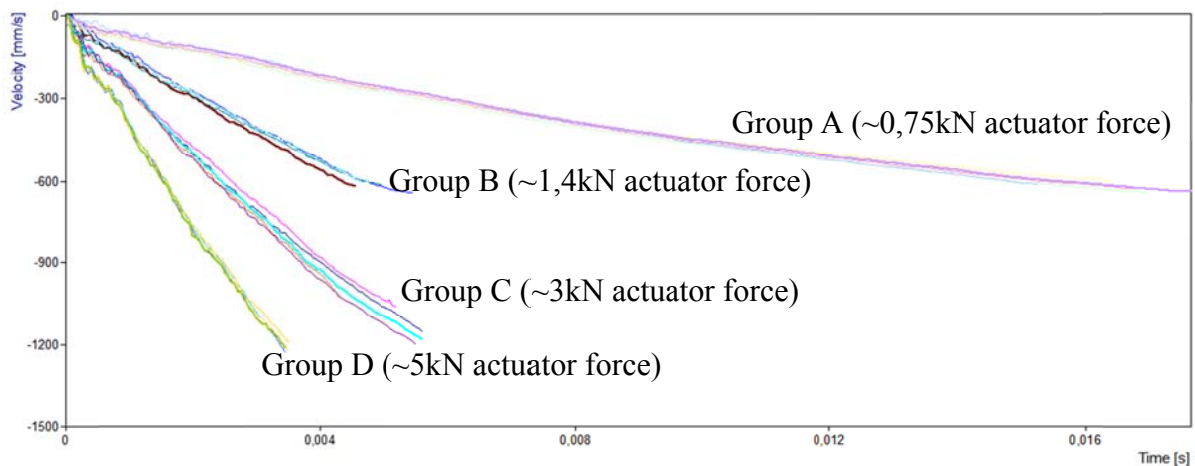


Figure 6-5 AWL welding head velocity signals as response to fracture tests

Figure 6-6 to Figure 6-9 below show the velocity signals of four groups of each time five tests conducted with identical boundary conditions of pin length, pin diameter and pin support distance.

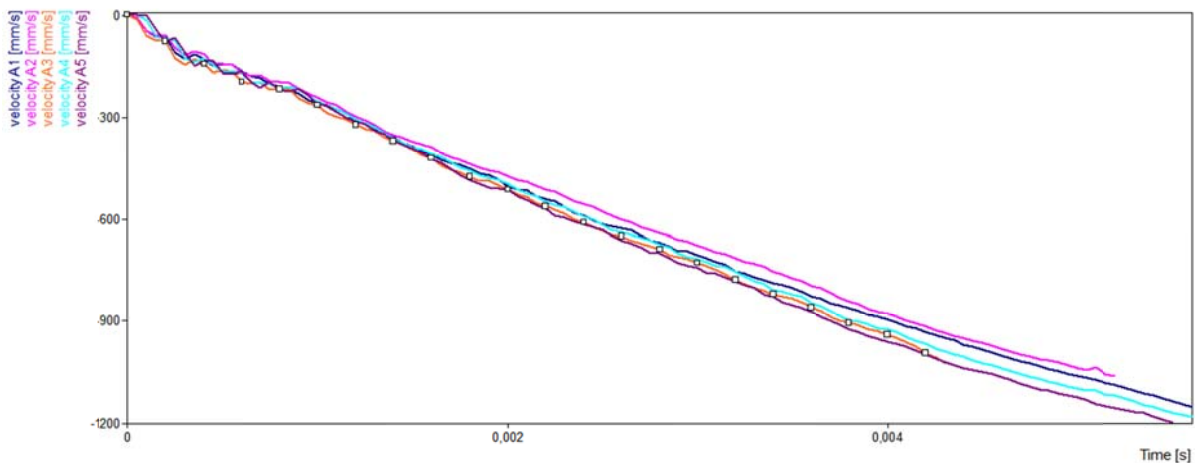


Figure 6-6 AWL fracture test velocity signals group A (~0,75kN actuator force)

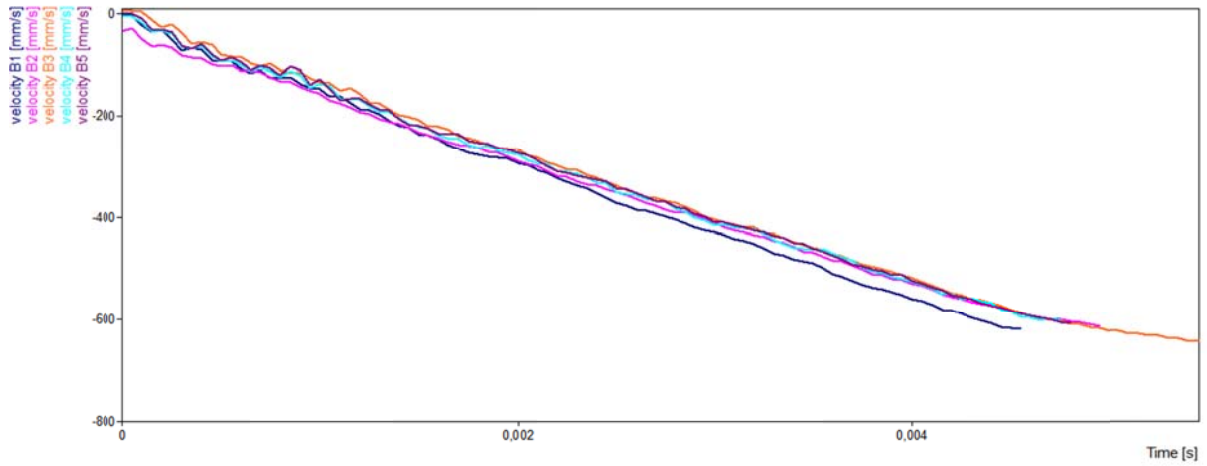


Figure 6-7 AWL fracture test velocity signals group B (~1,4kN actuator force)

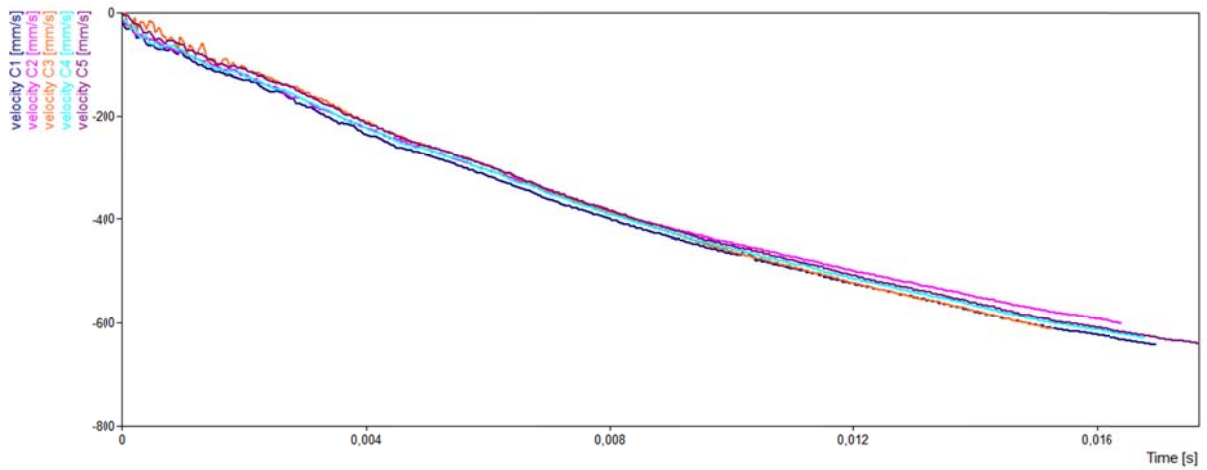


Figure 6-8 AWL fracture test velocity signals group C (~3kN actuator force)

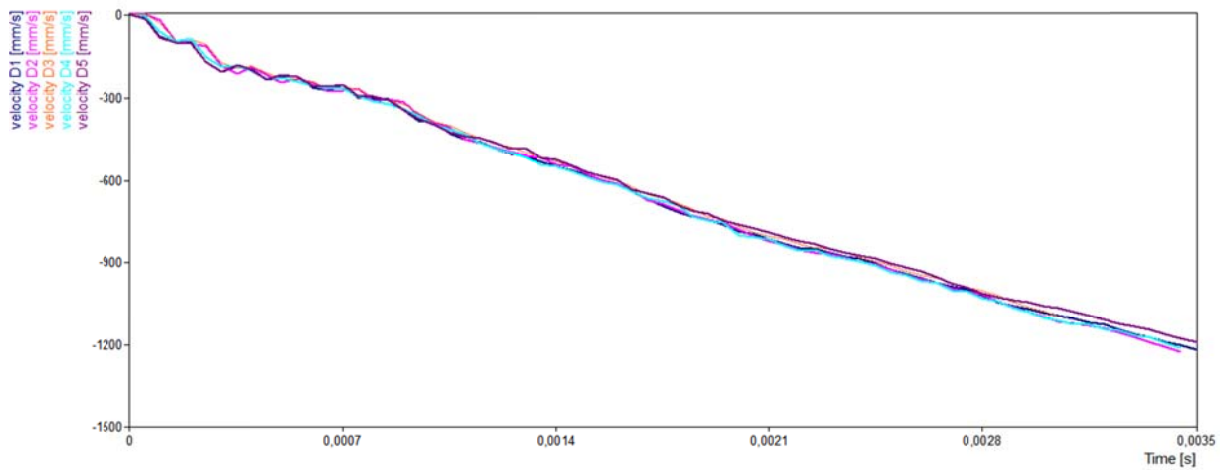


Figure 6-9 AWL fracture test velocity signals group D (~5kN actuator force)

As you will notice, these curves per group are nearly identical in shape and only differ slightly in slope due to the force level at the moment of fracture slightly differing.

Table 6-1 below shows results after processing the signals from Figure 6-6 to Figure 6-9 as described in the data processing procedure in Appendix D.

This includes two sets of analyses. One includes the effect of the spring which is normally present in the machines' welding head, while the second doesn't.

		Measured values	Calculated values	
		Breaking force	Mass	Damping coefficient
No spring mounted		F [N]	m [kg]	b [kg/s]
Group A ~ 0,75kN force	1	720	12.5	845
	2	730	11.9	822
	3	741	12.2	827
	4	752	11.8	929
	5	775	11.7	914
Group B ~ 1,4kN force	1	1393	12.2	898
	2	1448	12.4	1059
	3	1473	11.9	969
	4	1353	12.1	930
	5	1354	11.8	900
Group C ~ 3kN force	1	3165	12.1	1306
	2	2714	12.3	1086
	3	2943	13.5	968
	4	3333	12.6	1238
	5	3115	12.0	1314
Group D ~ 5kN force	1	3941	12.0	1329
	2	5574	11.3	2187
	3	5167	12.6	1651
	4	5225	12.0	1798
	5	5257	12.0	1996
Spring mounted		Mean Mass	12.1	
Group A ~ 0,75kN force	1	772	10.8	943
	2	722	11.2	865
	3	782	11.7	833
	4	758	11.8	835
	5	748	11.5	834
Group B ~ 1,4kN force	1	1521	9.5	673
	2	1364	10.0	465
	3	1468	9.7	765
	4	1406	9.6	594
	5	1483	10.0	640
Group C ~ 3kN force	1	2836	11.0	978
	2	3458	12.3	1144
	3	3456	12.6	1186
	4	3576	12.5	1239
	5	3086	11.1	1254
Group D ~ 5kN force	1	5164	11.6	1668
	2	5300	12.6	1257
	3	5167	12.4	1219
	4	5222	11.9	1539
	5	5022	11.6	1616
Mean Mass out of working range spring			12.1	

Table 6-1 Results fracture tests on AWL multi-purpose spot/projection welder

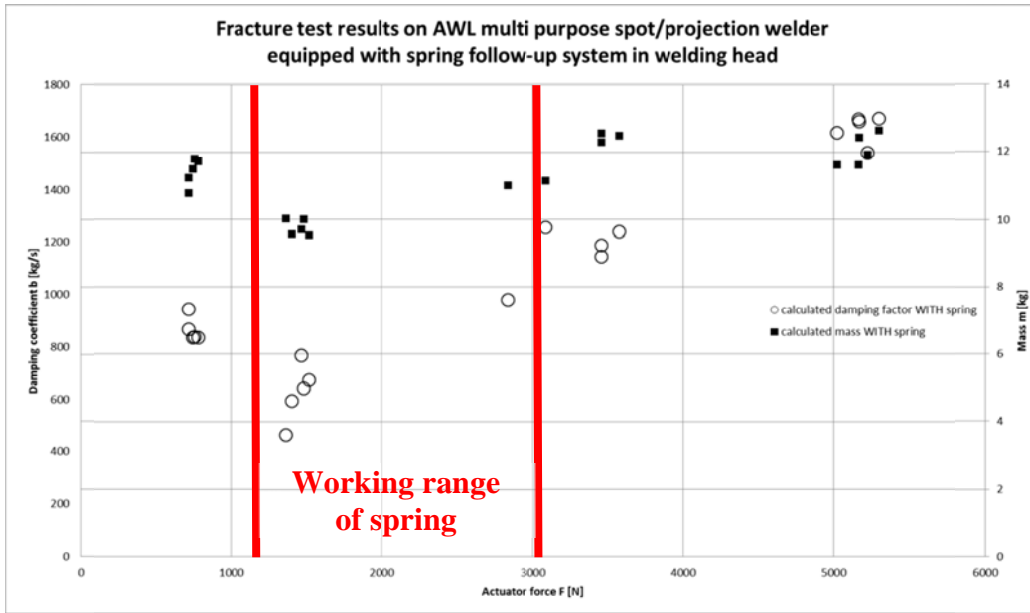


Figure 6-10 Fracture test results AWL equipped WITH spring

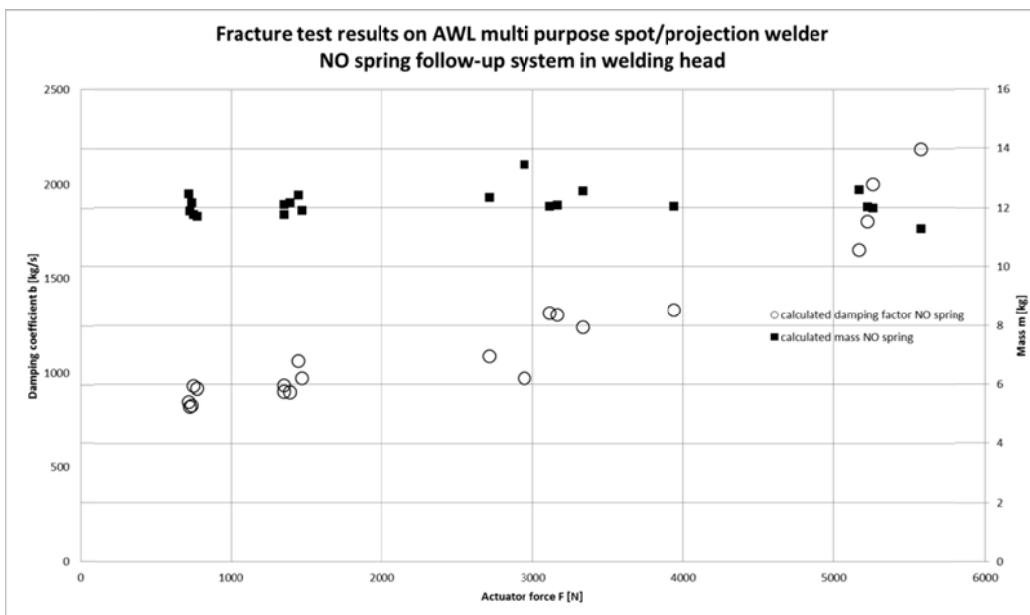


Figure 6-11 Fracture test results AWL NO spring

It is clear from the results in Table 6-1 and Figure 6-10 and Figure 6-11 that the feature of the spring coupling between the AWL machines actuator piston rod assembly, the latter weighing exactly 3.02kg and having a working range, roughly within 700N and 3000N is effective within this range of actuator forces. The calculated lumped mass drops from the total lumped mass of 12.12kg of the actuator piston rod assembly ($3.02\text{kg} + 4.58\text{kg} + 4.52\text{kg} = 12.12\text{kg}$) to the lower 9.1kg of only the vertical slide and electrode assembly.

The damping coefficient drops evenly in that working range to lower values corresponding with the lower friction between the hollow shaft of the vertical slide and its sliding bearing. Friction between the upper piston seals does not influence damping in this working range.

Figure 5-25 shows the coupling spring mounted on the actuator piston rod assembly and limited in its compression by a cylindrical stop around it.

Its spring constant was tested on an Instron compressive test bench and was measured as $k = 165\text{N/mm}$. Both the upper actuator piston rod and the lower hollow shaft of the slide are connected by means of the nut (and its securing locking screws) on the left of Figure 5-25. This nut also serves to set the pre-stress level of the coupling spring, in this case, with a spring compression of 4mm, there is a pre-stressing force of 660N on the spring. The remaining available travel that can be further compressed is 14mm, yielding the maximal force at which the limiter contacts the lower slide of 2970N.

Between 660N and 2970N, the force exerted by the piston rod on the lower slide is transferred through the spring, loading the lower slide with the actuator force, without adding its mass to it. In this range, piston rod assembly and lower slide and electrode assembly move as if they were separated. Below 660N and above 2970N, all moving parts (piston rod assembly + lower slide and electrode assembly) move as one single mass actuated by the actuator force.

This spring coupling was installed as a standard feature in these multi-purpose spot/projection welding machines to slightly improve follow-up characteristics of the welding head towards projection welding applications in the lower actuator force range of the machine. It however is surely subject for improvement since the reduced mass is still the highest in the assembly instead of the other way around.

By increasing the compressing distance of the spring, the operating range where the spring is active will evenly increase. But most of all, weight reduction of the lower assembly will lead to improved behavior in addition to the reduced friction.

6.2.2 Explosion Test

Figure 6-12 and Figure 6-13 below both show an overview in Flexpro of twenty exploding button and twenty exploding ball tests conducted at a single welding force setting varying between 1638N and 1694N for evaluation of both tests. The lines are each time the average of four tests conducted at identical heat settings. Tests were performed with five current settings between 40% and 99% HS (heat setting) on the machines control panel. In the same graph is the velocity response of a single fracture test conducted at 1523N for visual comparison. The welding head of the AWL machine was equipped with the spring coupling between actuator rod and lower slide.

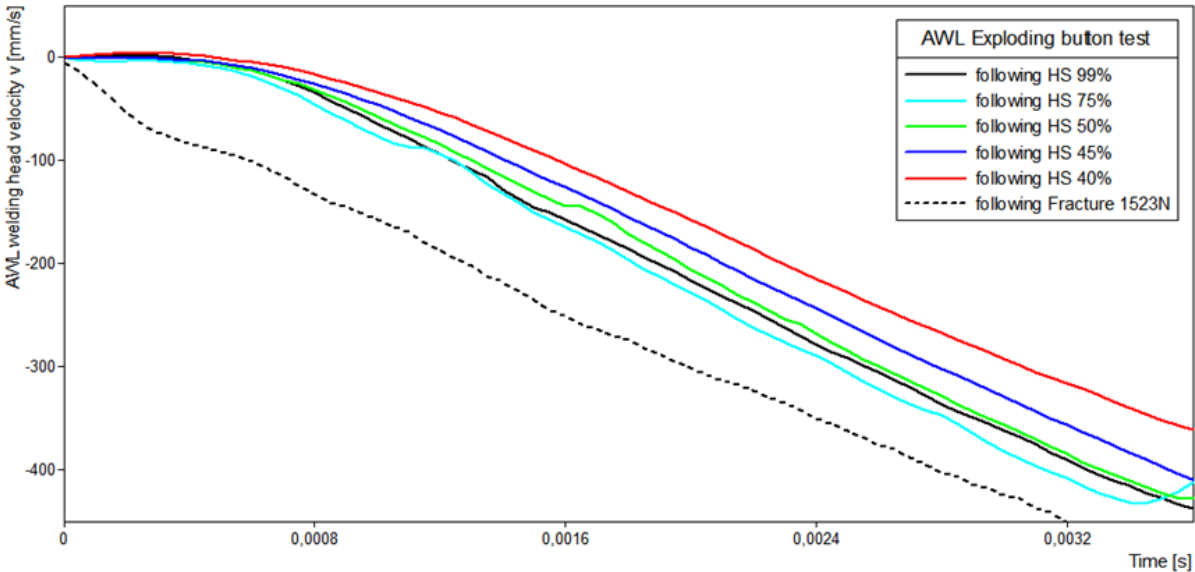


Figure 6-12 AWL welding head velocity signals as response to exploding button tests

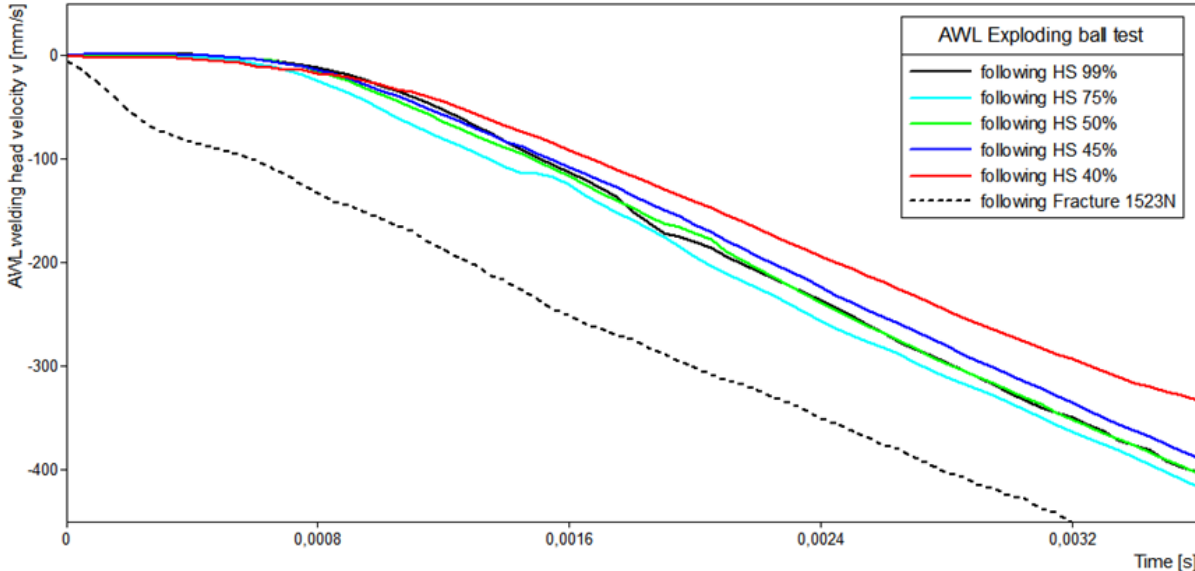


Figure 6-13 AWL welding head velocity signals as response to exploding ball tests

Notice the same slope in all the curves from the exploding button tests (Figure 6-12), indicating that power supplied to the metallic buttons to melt and vaporise them is sufficient to remove support faster than the welding head is capable of following.

In Figure 6-13 however, at the lowest heat settings of 40% slope of the velocity curve (the upper red curve in the figure) nearly matches that of the black coloured (dotted) fracture test that resulted from a welding head actuator force of nearly 100N less than the explosion tests. Also interesting is the time shift in the moment of velocity starting to increase following current flow throughout the button or ball. In Table 6-2 below, calculated lumped mass and damping coefficients are calculated for a series of exploding ball and exploding button tests within a limited range of actuator forces, the latter measured by means of a Keller piezo-resistive pressure sensor inside the actuator piston pressure supply line and calibrated by means of a Myiachi load cell between the electrodes. Actuator force is calculated from the measured pressure in the actuators supply line as follows: $F = P [\text{bar}] * 742.23 - 10.238 [\text{N}]$, following load tests at different actuator pressures.

Explosion tests AWL		Measured values		Calculated values			
		Actuator force		Mass	Damping coefficient		
	Heat Setting [%]	F [N]	m [kg]	b [kg/s]			
Spring	99	Button	1677	9.9	1092		
				1710	9.4	1165	
				1758	10.5	909	
			1690	10.4	682		
			1412	9.9	969		
			1902	10,0	615		
			1726	9.4	1238		
		75		1681	10.2	826	
				1744	9.3	1200	
				1658	10.2	924	
				1737	9.6	1540	
		50		1675	9.4	1008	
				1677	10.6	807	
				1671	10.2	584	
				1672	10.8	230	
			1710	10.4	662		
		99	Ball	1667	9.1	1384	
					1671	10.5	324
					1684	9.7	1191
				1694	10.3	793	
	75			1678	9.7	936	
				1674	10.5	303	
				1667	10.1	781	
				1663	9.9	1059	
				1733	9.1	1589	
	50			1663	9.9	706	
				1682	10.2	703	
				1681	10.0	833	
				1681	10.1	693	
			1658	10.3	601		
			1681	10.3	808		
		1680	10.9	442			
		1683	9.5	1094			

Table 6-2 Results exploding ball & button tests on AWL multi-purpose spot/projection welder

Notice that the actuator force range tested in is situated exactly in the working range of the welding heads coupling spring, leading to values for lumped mass that correspond to those found by means of the fracture tests. On this specific AWL machine, the 63kVA of available power is insufficient to conduct explosion tests at actuator force levels of more than 3000N. The latter leads to calculated values for lumped mass much higher than the weighed masses of the welding heads components. Due to insufficient heating by lack of available power, velocity of plastic deformation of ball and button elements are measured instead of the welding head velocity as a response to the welding heads reaction force completely disappearing.

These results are graphically displayed in Figure 6-14 and Figure 6-15 below.

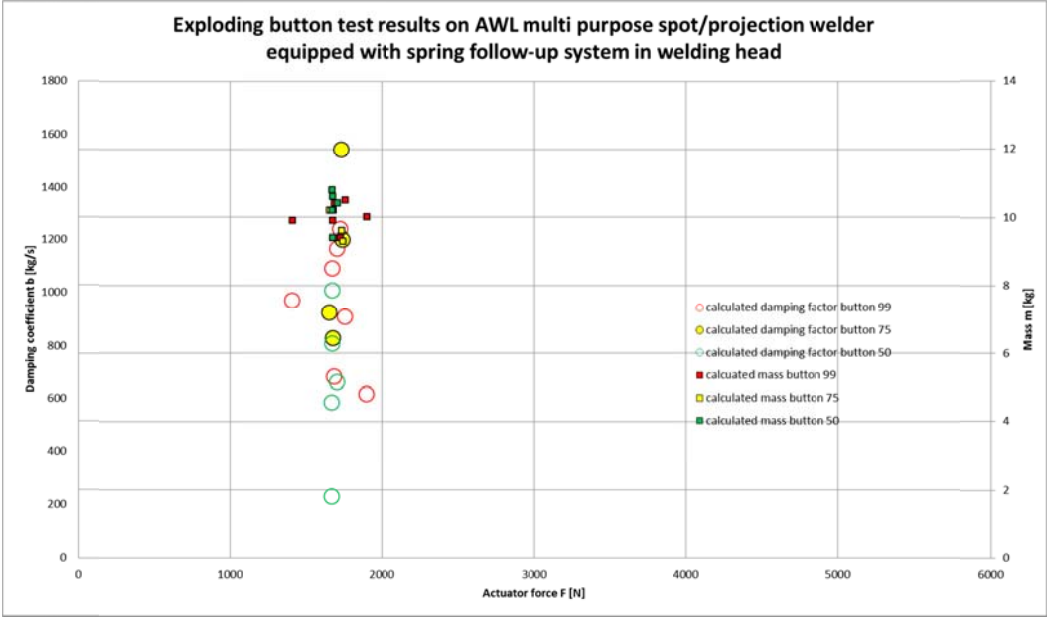


Figure 6-14 Exploding button test results AWL equipped WITH spring

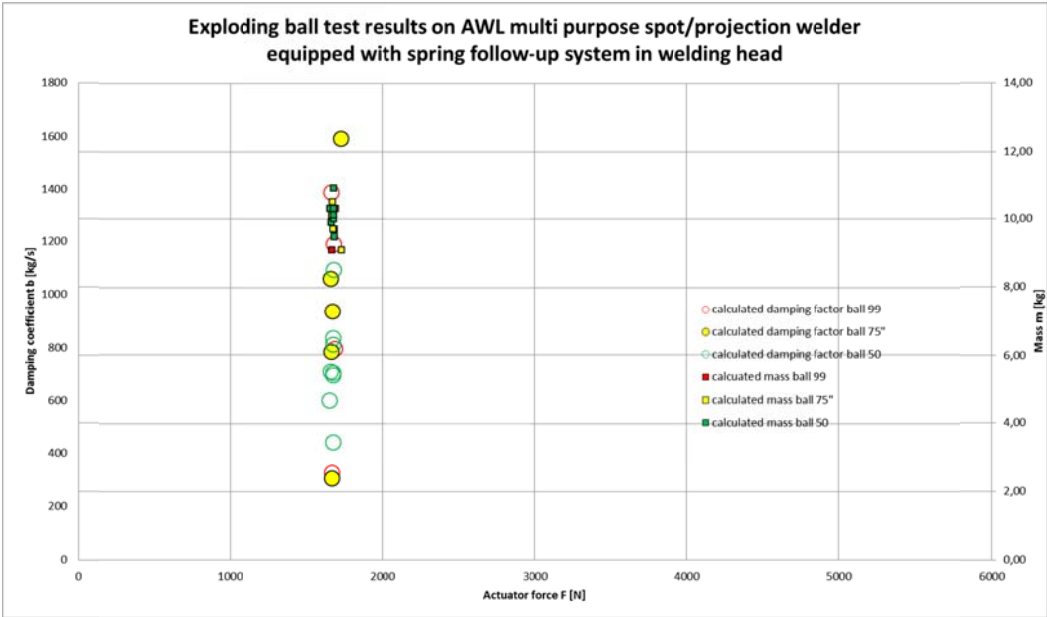


Figure 6-15 Exploding ball test results AWL equipped WITH spring

It is apparent from the graph that, in the actuator force range the explosion tests were conducted (in the middle of the working range of the spring coupling), the calculated masses correspond very well with those found using the same procedure in free fracture tests.

Also apparent are the large differences between damping factors calculated from these test signals. It has to be considered what causes these large differences emerging from quasi identical tests.

It is apparent that consistent damping values are obtained in the free fracture test due to the large displacement. In contrast in the exploding ball/button test, the displacement is small and this results in very large scatter in calculated damping.

In practice, the large displacements made in the free fracture test are never achieved in a real weld. Hence, the calculated damping from free fracture tests has little relevance.

Figure 6-16 below displays a free fracture test and an exploding button test both conducted on the AWL machine at comparable actuator loads.

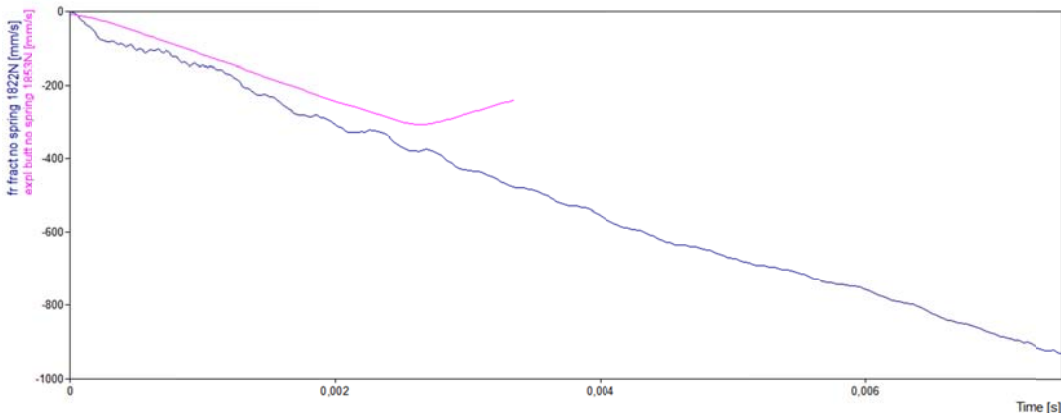


Figure 6-16 Comparison AWL velocity response to free fracture and exploding button test

At first, it is clear from the graphs that an explosion test initiates a far more gentle increase in welding head velocity compared with the very abrupt increase in welding head velocity by a free fracture test, the latter initiating a significant amount of vibration into the machine.

Secondly, the displacements made during both tests are far from comparable, explosion tests leading to welding head displacements in the order of 0 to 1mm (being realistic values for micro resistance welding applications as for a majority of macro applications as well), fracture tests on the other hand lead to welding head displacements of several mm up to even more than a cm (see Figure 6-17).

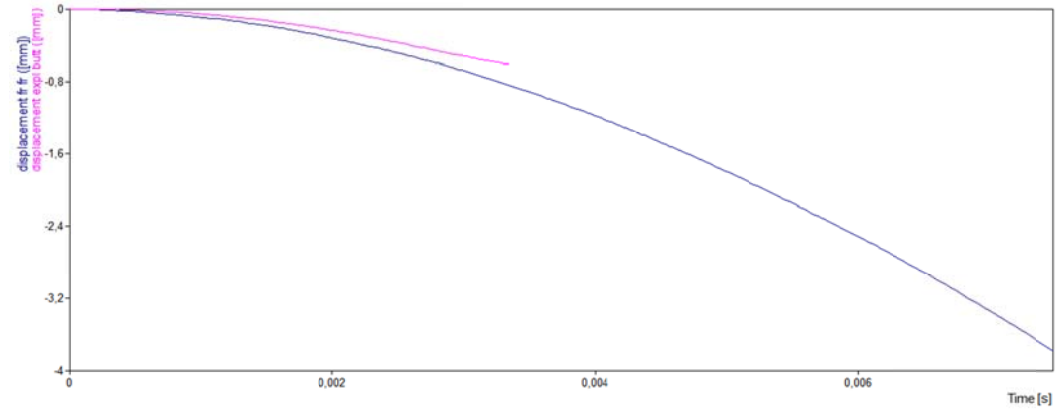


Figure 6-17 Comparison AWL displacement response to free fracture and exploding button test

From the velocity signal following an explosion test in Figure 6-16 it shows that it has a nearly linear shape in comparison with the decrease in velocity built up due to damping following a fracture test. As damping effects only take place at increasing welding head velocities that are nearly impossible to be reached with an explosion test, calculated lumped mass and damping factor of the welding head under study by means of the calculation sheet used for processing the free fracture tests has to be interpreted with caution.

A far more realistic way of processing measured results is in using Newton's second law of motion.

Subsequently, a series of exploding button tests were performed on the same AWL multi-purpose machine at its maximum heat setting of 99%, at different actuator force levels and with and without the coupling spring installed in the actuator assembly (see Figure 6-18 and Figure 6-19).

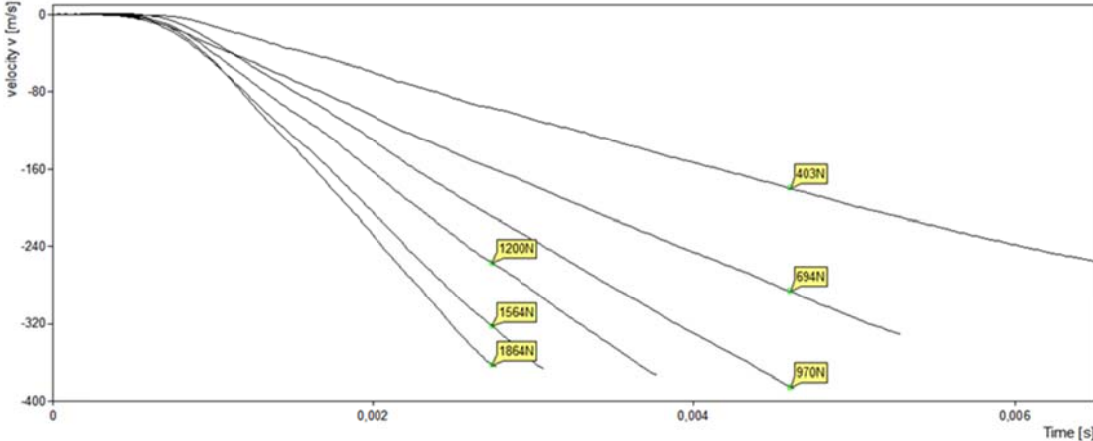


Figure 6-18 AWL velocity response to exploding button test WITH spring mounted

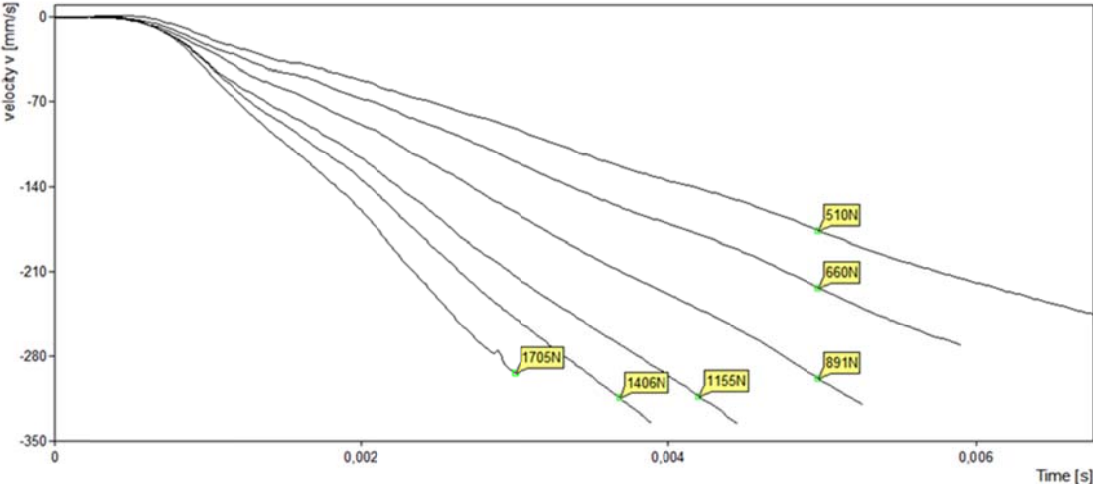


Figure 6-19 AWL velocity response to exploding button test NO spring mounted

The actual measured (weighed) masses of the composing elements are as follows:

- Spring mounted: 12.12kg total
 - 3.02kg actuator piston rod assembly mass (including spring)
 - 4.58kg lower slide and mounting plate
 - 4.52kg electrode assembly
- to be increased with dynamically acting part of mass of flexible current lead (3.88kg)
- Spring not mounted (spring replaced with washers for dimensions): 12.004kg total
 - 2.904kg actuator piston rod assembly mass – 0.185kg (spring)
+ 0.069kg (washers)
 - 4.58kg lower slide and mounting plate
 - 4.52kg electrode assembly

to be increase with dynamically acting part of mass of flexible current lead (3.88kg)

This compares to the calculated effective lumped masses from the different fracture and explosion tests conducted and displayed in Table 6-1, Table 6-2 and Table 6-3.

In Figures Figure 6-20 to Figure 6-23 below are the individual welding head velocity curves as a response to exploding button test, conducted at maximum electrical power setting of the AWL machine and conducted with the spring coupling removed from the welding head.

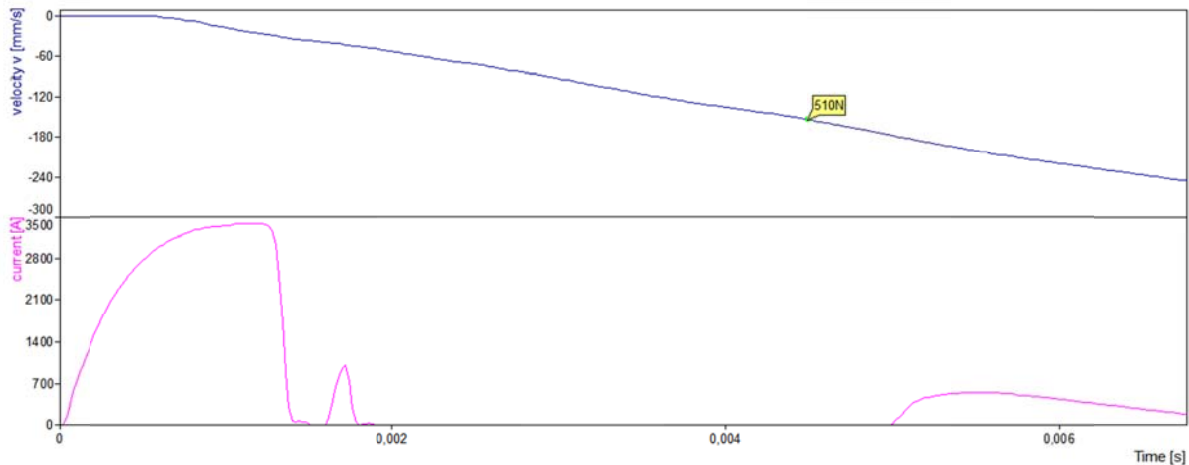


Figure 6-20 Velocity and current signal, NO spring, 510N

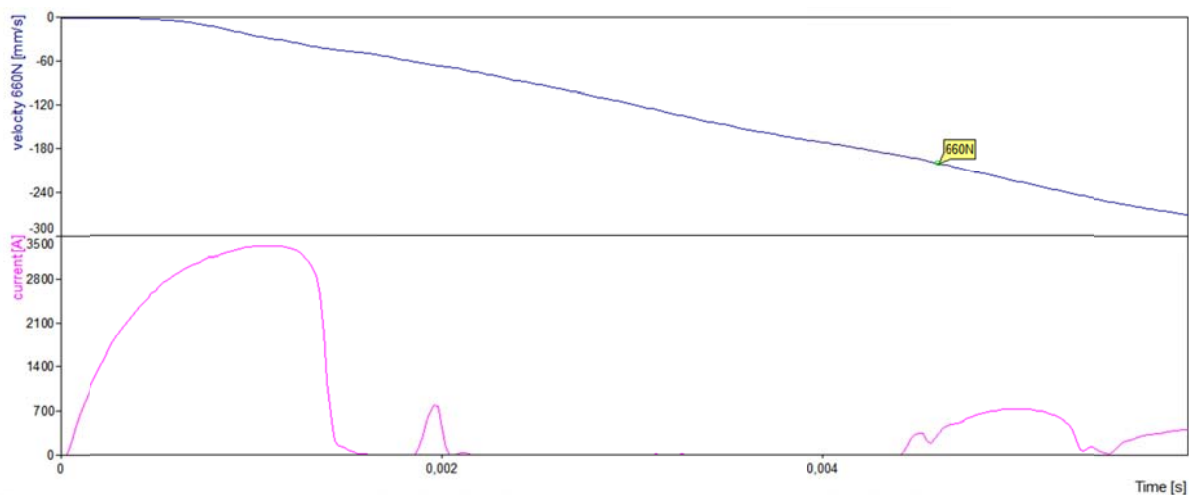


Figure 6-21 Velocity and current signal, NO spring, 660N

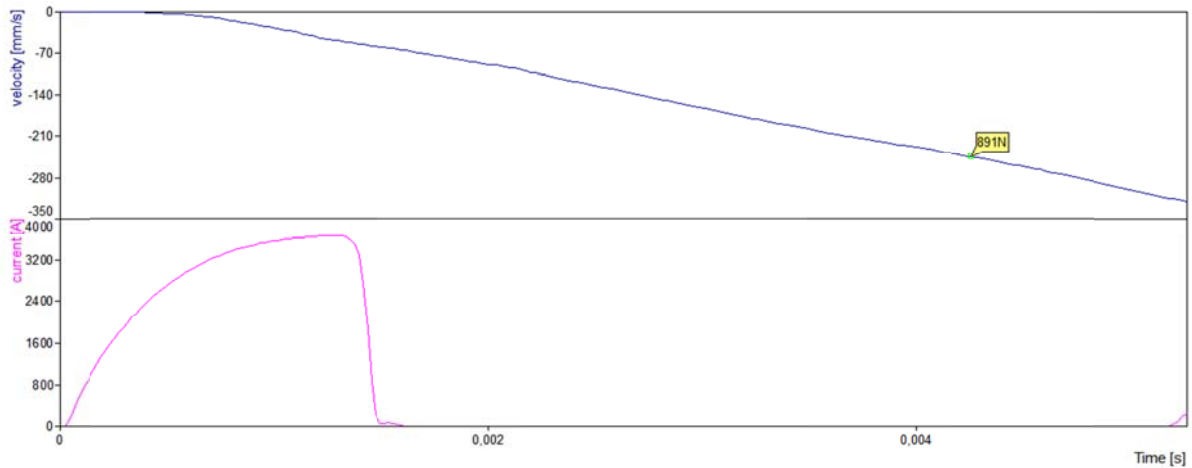


Figure 6-22 Velocity and current signal, NO spring, 891N

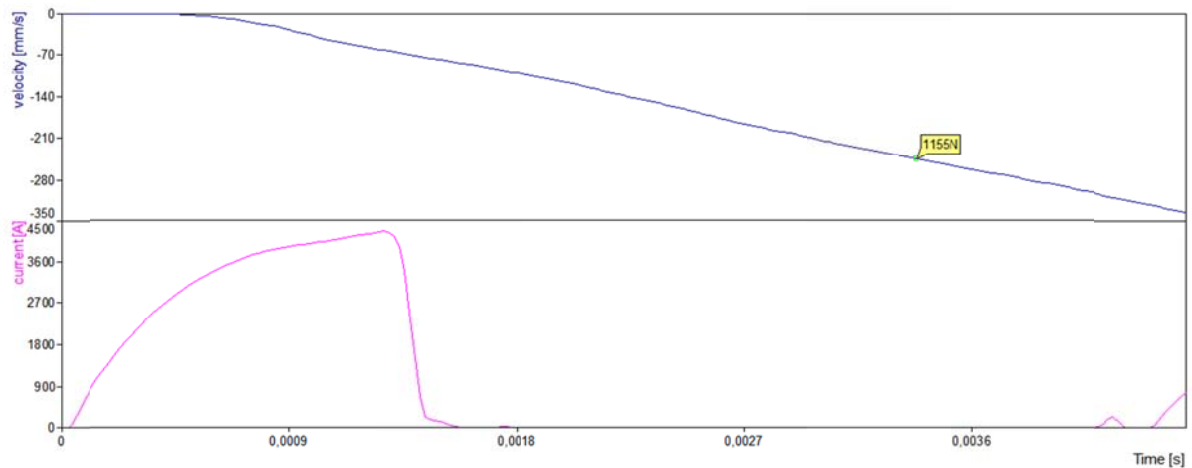


Figure 6-23 Velocity and current signal, NO spring, 1155N

Important remarks to be made with these test results:

- the welding head was dismantled a few times in order to remove and re-install the coupling spring. The tests results in Table 6-3 below conducted with spring were made with the spring installed without pre-stressing it, the latter explaining the reduced values for mass at the lowest force levels.
- the test results in Table 6-3 below conducted without the coupling spring installed were made with the nut securing the connection between piston rod and lower slide tightened too firmly, locking the spring washer in between subsequently leading to increased friction due to less optimal alignment. The slightly higher results for calculated masses can be explained as due to lower effective actuator forces in respect of the piston supply pressure.
Ratio between actuator pressure and effective force load could not be measured since the actuators assembly was taken apart and assembled with the spring coupling included again prior to data processing.

In Table 6-3 below is an overview of the 16 exploding button tests conducted and their velocity responses presented in Figure 6-18 and Figure 6-19.

	Measured values		Calculated values	
	Actuator force		Mass	Damping coefficient
	F [N]	m [kg]	b [kg/s]	
With spring	403	9.0	382	
	694	9.2	275	
	970	9.0	365	
	1200	9.5	205	
	1564	10.2	-207	
	1864	10.8	-614	
	2161	12.6	-2254	
	2388	12.5	-1739	
No Spring	510	13.2	-234	
	660	14.6	-645	
	891	14.5	-552	
	1155	14.0	-283	
	1406	15.1	-799	
	1705	15.9	-2142	
	2087	15.9	-1106	
	2513	14.1	776	

Table 6-3 Results exploding button tests on AWL machine with and without spring mounted

Processed results are also displayed in Figure 6-24.

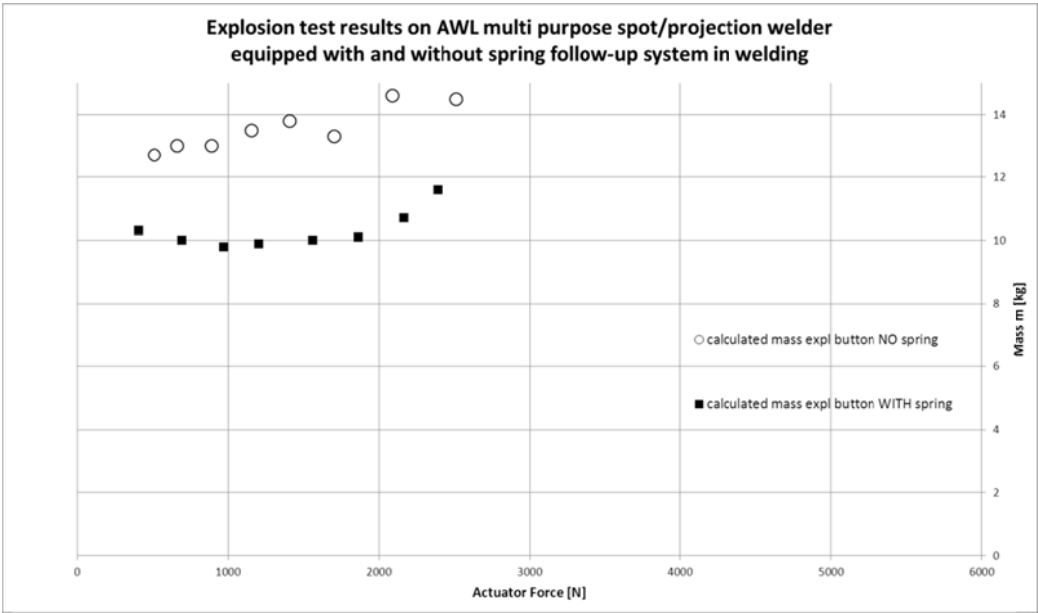


Figure 6-24 Exploding button test results AWL equipped with and without spring

6.2.3 Comparison of fracture and explosion test

In order to allow comparison between both tests, Figure 6-25 below shows the recorded velocity signals with identical actuator force with 1st an exploding button test conducted with 99% of heat setting on the machine (blue signal), 2nd and exploding button test conducted with 75% of heat setting on the machine (green signal) and 3rd a free fracture test (red signal).

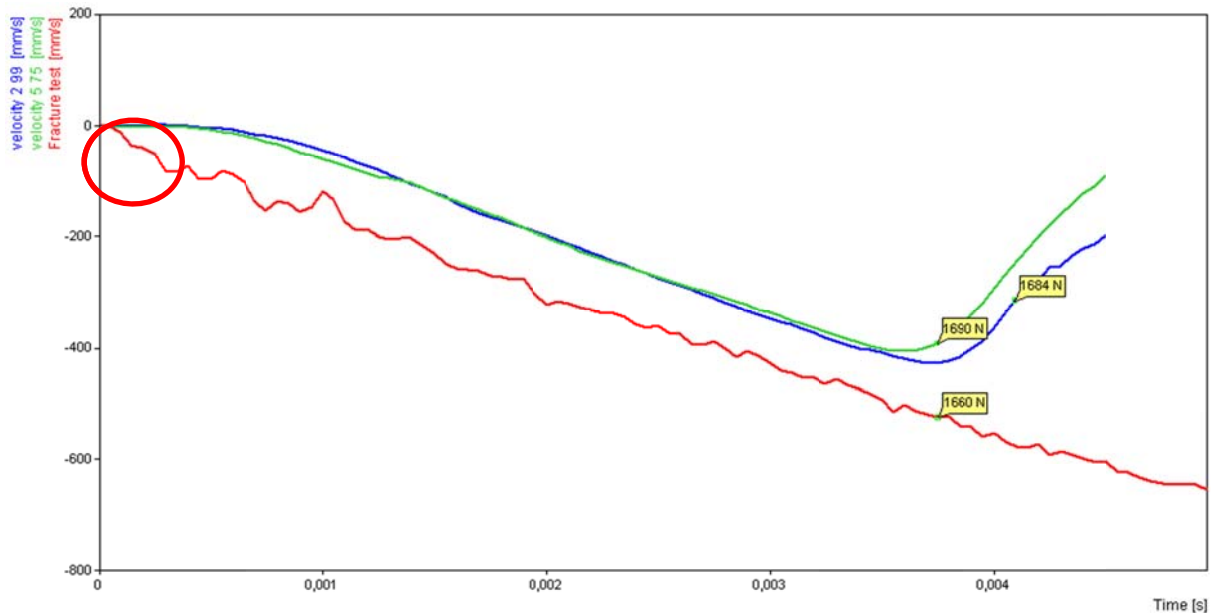


Figure 6-25 Velocity response on fracture and explosion tests

These signals are very representative for all fracture and explosion tests and it shows clear that the fracture test imposes a very aggressive sudden change in reaction force by the lower welding head. The latter inducing a lot of vibration into the machine, both in the fixed but obviously also in the moving welding head.

Bearing in mind the physical construction of this specific welding head, with a spring coupling between actuator piston rod and the machines' lower slide, these vibrations cause more friction, leading to the slightly lower value of acceleration that can be observed in the different slope of the curves.

The two explosion test responses (blue and green signals in Figure 6-25) clearly demonstrate the very smooth onset of motion of the welding head.

Note also the extreme slope of the fracture test response in the first 0.3ms (see red marking on the figure), representing an acceleration value that is significantly higher than what is physically achievable with Newton's second law in a linear motion with the given actuator force.

This behaviour that is consistently present in all fracture test velocity responses of the welding head can only be explained physically through sudden release of all energy stored in elastic deformation of components in the upper welding arm and moving electrode assembly.

6.2.4 General motion of welding head

Given the difference between the welding heads' velocity response to explosion and fracture tests, motion of the complete welding head was examined. Motion of both the moving welding head assembly and the cylinder housing was measured during manual actuation and during fracture tests.

In unloaded condition, the moving welding head assembly has a play of 0.2mm. Figure 6-26 below shows the lateral displacement of the moving welding heads' mounting plate under manual actuation from its rest position to its most outward position in one direction (by pulling). In the other direction, the same displacement can be measured (by pushing). This play of 0.2mm explains why there is nearly no friction what so ever between the vertical slide and its bearing, apart from the friction caused due to the grease between slide and bearing.

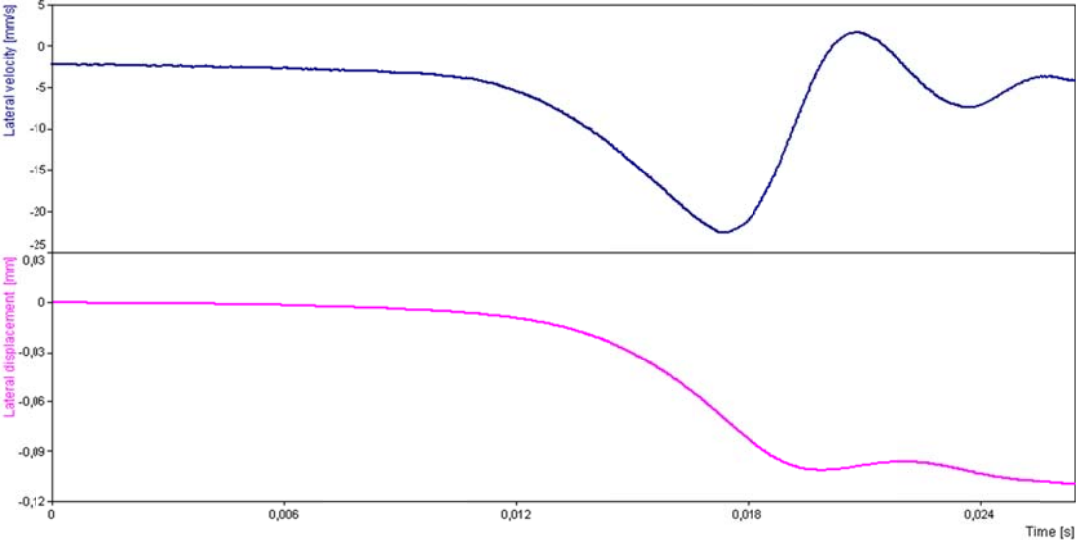


Figure 6-26 Lateral (horizontal) displacement of moving welding head assembly, manual actuation

Furthermore, in order to verify the cause of the high acceleration values observed in the first 0.3ms of the velocity responses of all fracture tests, the lateral displacement of the moving welding head's mounting plate was measured during a fracture test. (see Figure 6-27 below)

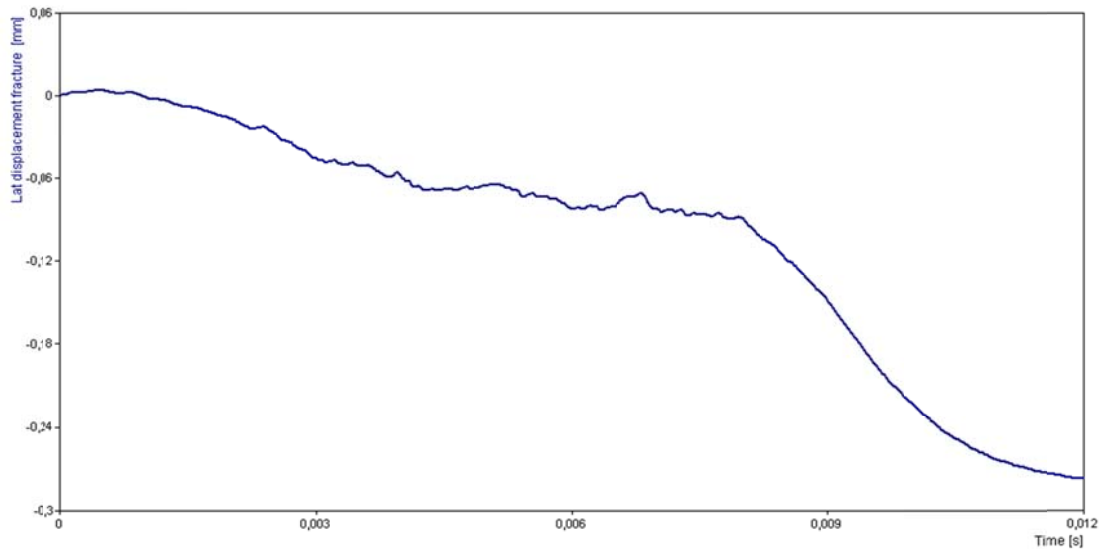


Figure 6-27 Lateral (horizontal) displacement of moving welding head assembly, fracture test at 2677N

From this measurement, it shows that there is nearly no lateral motion made by the moving welding heads' assembly in the first milliseconds.

Lateral motion of the welding cylinder body was then measured (see Figure 6-28 below).

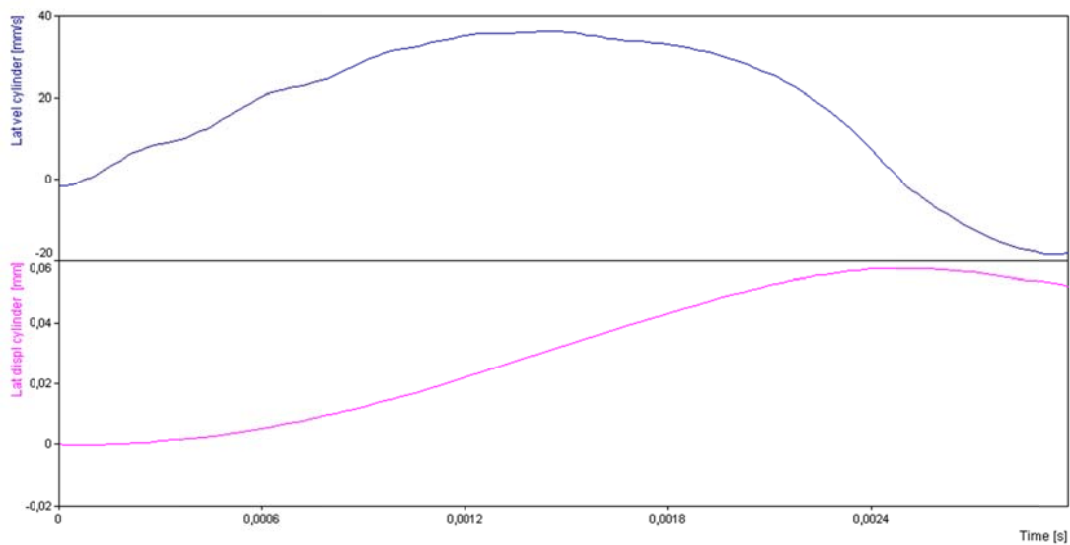


Figure 6-28 Lateral (horizontal) motion of upper part of welding cylinder, fracture test at 2930N

Additionally, the vertical downward motion of the welding cylinder was measured (see Figure 6-29 below)

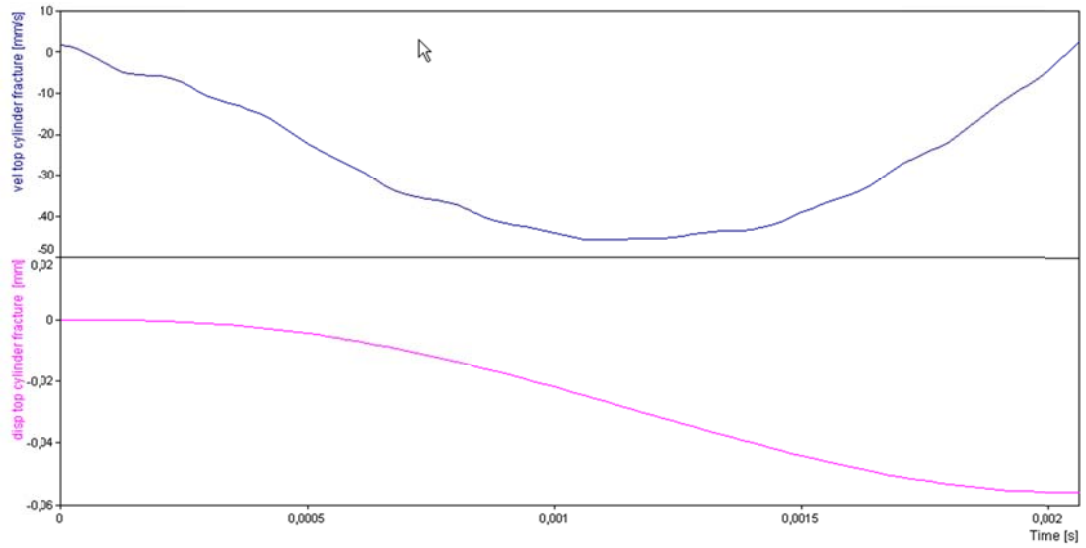


Figure 6-29 Downward (vertical) motion of upper part of welding cylinder, fracture test at 4888N

6.2.5 Influence of current on machine behavior

In the graphs of Figure 6-19 one can already notice a different slope in the velocity responses of the AWL machines welding head on the lower force ranges.

In Figure 6-30, is the velocity response to an exploding button test conducted on the AWL machine without the coupling spring in the welding head assembly at a piston pneumatic pressure of 1.21bar normally matching with a force level of 891N. The areas of interest to have a look at the slopes are marked with green.

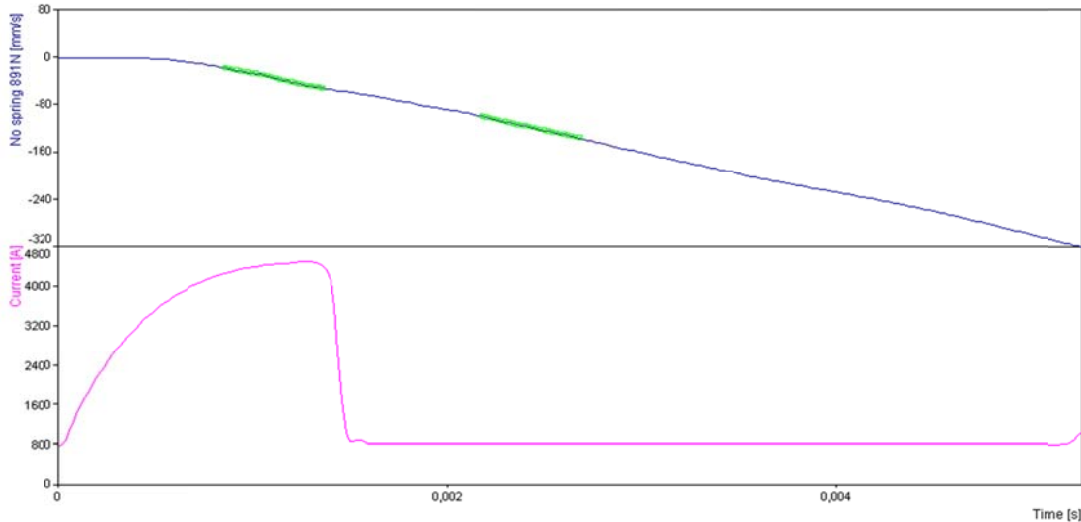


Figure 6-30 Slopes in AWL velocity response to explosion test at 891N, NO connecting spring

In Figure 6-31, is a graph from the same test of both velocity response signal and current signal during the test.

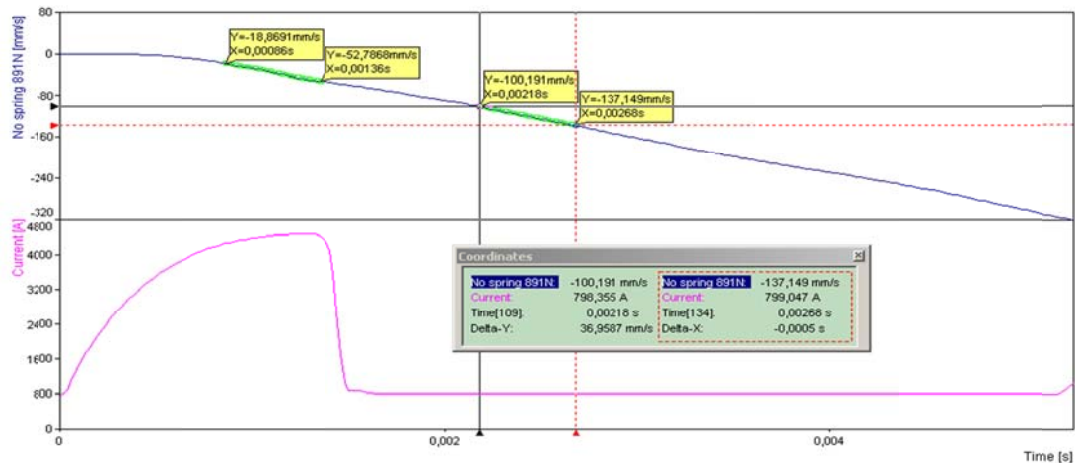


Figure 6-31 AWL velocity response to explosion test at 891N, NO connecting spring

Note that the difference in slope in the velocity signal immediately following the abrupt stop of conduction when the supporting element explodes. Acceleration values in both areas marked green as well as the corresponding loss in actuator force causing the difference in acceleration value, are given in Table 6-4 below.

a_1 [m/s ²] (current flowing)	a_2 [m/s ²] (current interrupted)
67.84	73.73
Δ acceleration = 5.89m/s ²	
Δ actuator force with mass of 13kg = 76.57N	

Table 6-4 Δ acceleration explosion test 891N, no spring

The same procedure is followed for the explosion test conducted at 1406N (Figure 6-32) and results are displayed in Table 6-5.

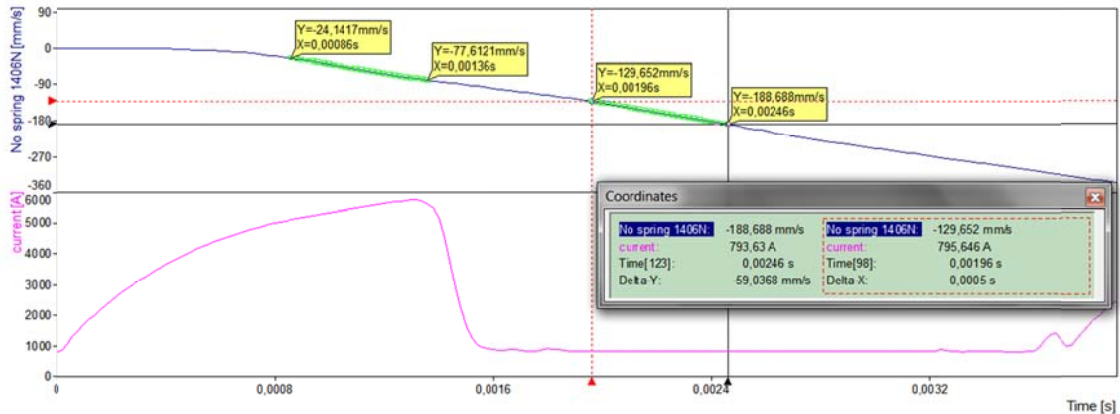


Figure 6-32 AWL velocity response to explosion test at 1406N, NO connecting spring

a_1 [mm/s ²] (current flowing)	a_2 [mm/s ²] (current interrupted)
106.94	118.08
Δ acceleration = 11.14m/s ²	
Δ actuator force with mass of 13kg = 145N	

Table 6-5 Δ acceleration explosion test 1406N, no spring

Acceleration value in both areas marked green is respectively 106.941m/s² and 118.074m/s² or a Δ acceleration of 11.13m/s².

Bearing in mind that we accelerate a mass of 13kg, this brings us with a Δ in actuator force of 145N.

Results for the explosion test conducted at 1705N (Figure 6-33) are displayed in Table 6-5.

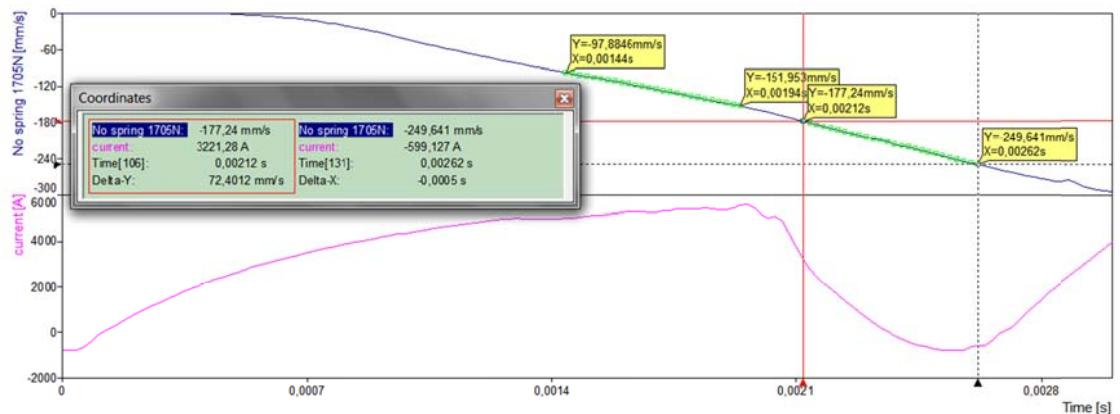


Figure 6-33 AWL velocity response to explosion test at 1705N, NO connecting spring

a_1 [mm/s ²] (current flowing)	a_2 [mm/s ²] (current interrupted)
108.14	144.20
Δ acceleration = 36.1m/s ²	
Δ actuator force with mass of 13kg = 469N	

Table 6-6 Δ acceleration explosion test 1705N, no spring

The same procedure is followed for the explosion test conducted at 694N WITH the spring coupling present in the actuator assembly (Figure 6-34) and results are displayed in Table 6-7.

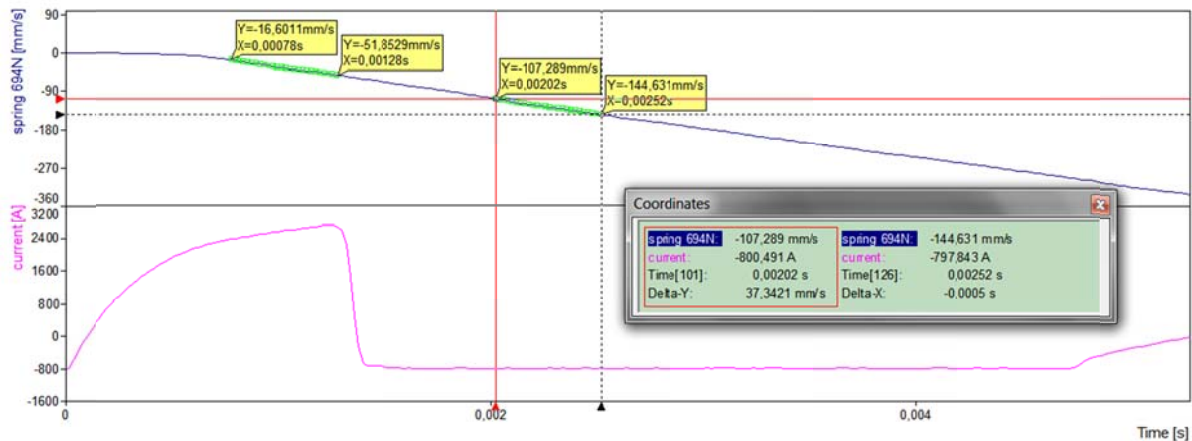


Figure 6-34 AWL velocity response to explosion test at 694N, WITH connecting spring

a_1 [mm/s^2] (current flowing)	a_2 [mm/s^2] (current interrupted)
70.50	74.68
Δ acceleration = 4.18 m/s^2	
Δ actuator force with mass of 9.5kg = 39.71N	

Table 6-7 Δ acceleration explosion test 694N, with spring

Results for the explosion test conducted at 1564N WITH spring coupling in the actuator assembly (Figure 6-35) are displayed in Table 6-8.

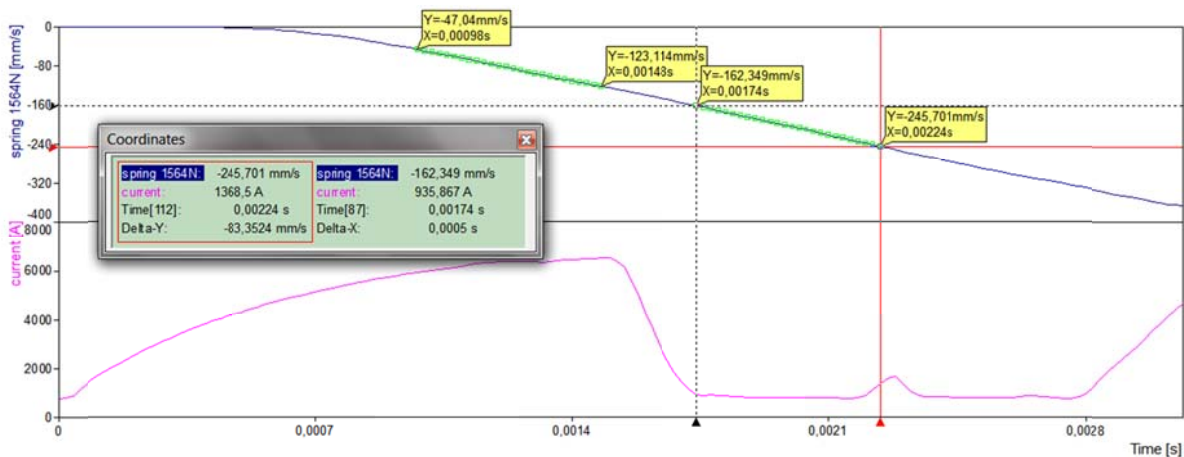


Figure 6-35 AWL velocity response to explosion test at 1564N, WITH connecting spring

a_1 [mm/s^2] (current flowing)	a_2 [mm/s^2] (current interrupted)
152.15	166.7
Δ acceleration = 14.55 m/s^2	
Δ actuator force with mass of 9.5kg = 138N	

Table 6-8 Δ acceleration explosion test 1564N, with spring

Results for the explosion test conducted at 1864N WITH spring coupling in the actuator assembly (Figure 6-36) are displayed in Table 6-9 Δ acceleration explosion test 1864N, with spring.

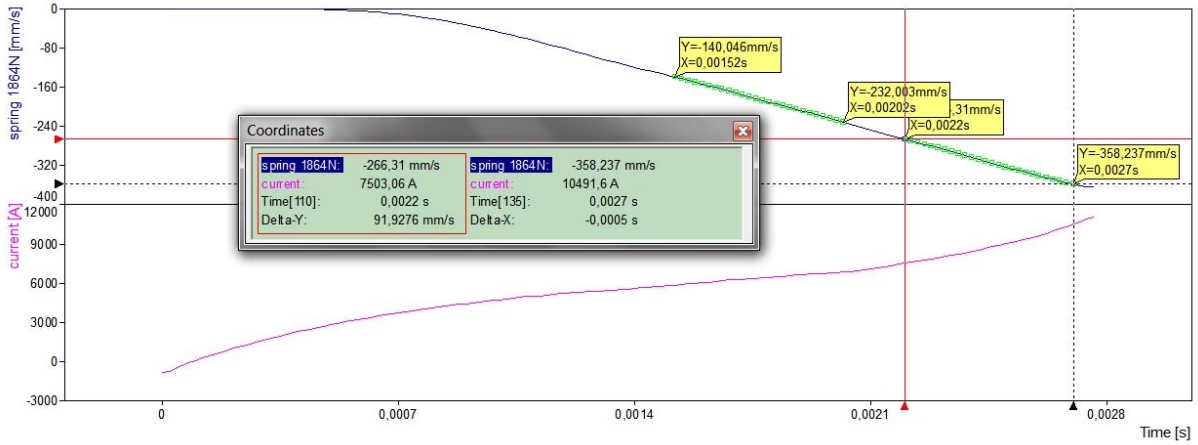


Figure 6-36 AWL velocity response to explosion test at 1864N, WITH connecting spring

a_1 [mm/s ²] (current flowing)	a_2 [mm/s ²] (current flowing)
187.12	187.96
Δ acceleration = 0.84m/s ²	
Δ actuator force with mass of 9.5kg = 8N	

Table 6-9 Δ acceleration explosion test 1864N, with spring

Results of the reduction in actuator force caused by the welding current in the AWL machine with the coupling spring mounted and removed are displayed in Figure 6-37 below.

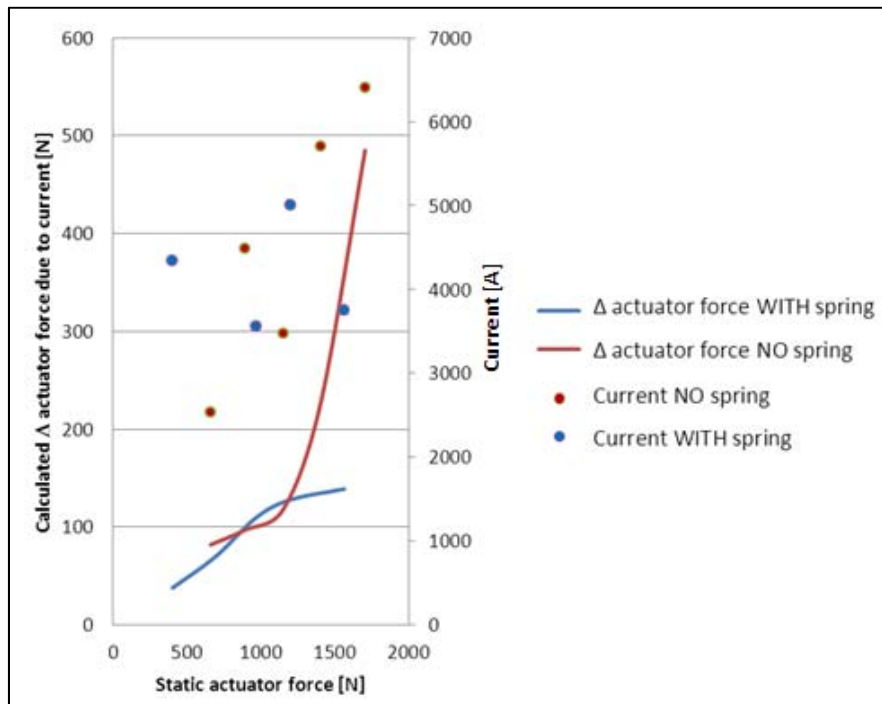


Figure 6-37 Reduction in actuator force caused by the welding current following explosion tests

6.2.6 Fracture tests with application of current

In Figure 6-38 below are the moving welding head displacement responses on a fracture tests, conducted with 898N actuator load and with the application of a welding current of 10kA for the blue graph and a fracture test conducted ‘dry’ (without any current flowing through the machines’ secondary circuit) with 916N actuator load for the pink graph.

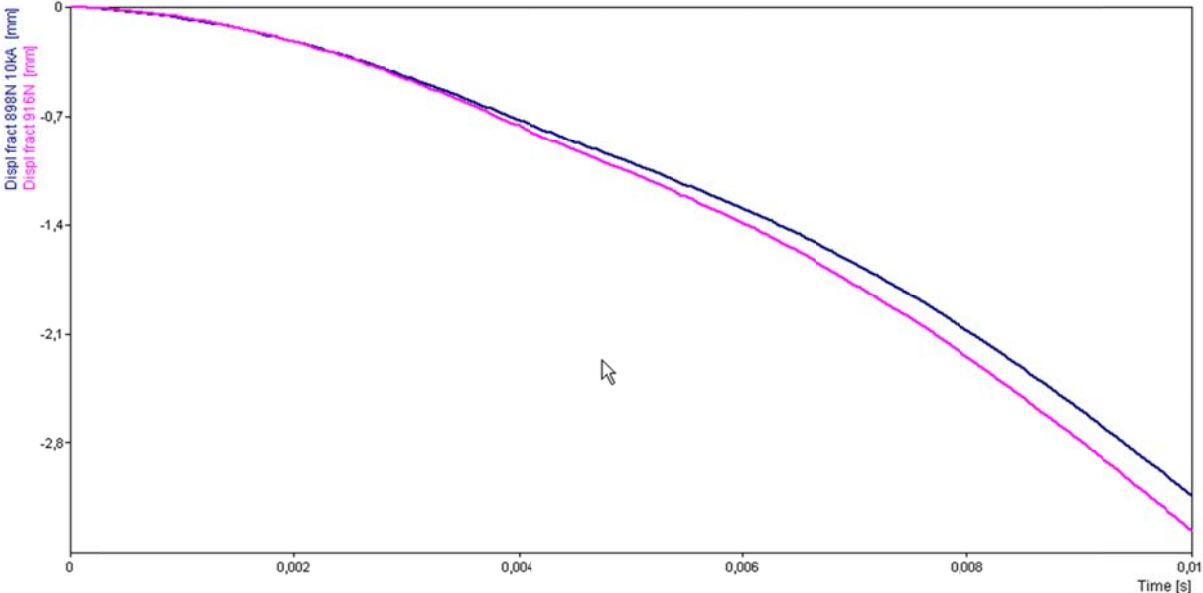


Figure 6-38 Displacement responses fracture tests 900N with and without application of current

There is a significant difference in slope noticeable leading to a difference in displacement made after 0.01s of 0.226mm.

In Figure 6-39 below, it shows that the decrease in slope takes place during the moments that current is flowing and restores as soon as current flow stops.

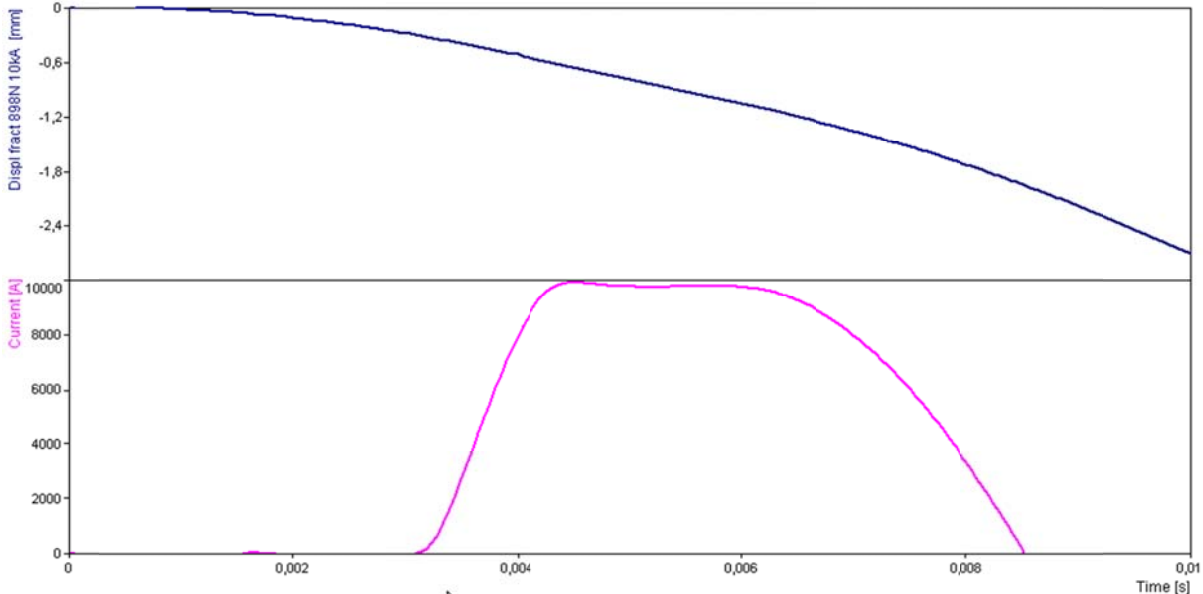


Figure 6-39 Displacement response fracture test 898N including current signal

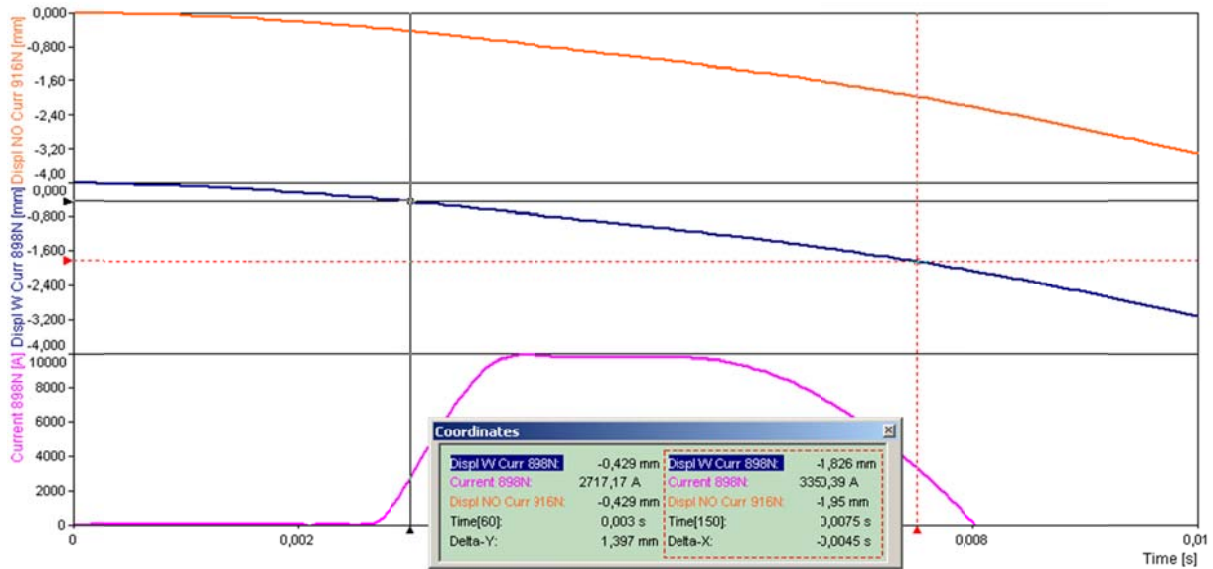


Figure 6-40 Measuring displacement responses with and without current flowing

In Figure 6-40 above, difference in displacement between the two displacement response signals is measured after an elapsed time of 0.0075s, the difference in displacement is of 0.125mm. If we would compare both displacement signals as being motions with constant acceleration, it would give us:

$$s (\text{displacement}) = \frac{1}{2} \cdot a \cdot t^2$$

$$0.125\text{mm} = \frac{1}{2} \cdot a \cdot (0.0075)^2$$

Which in this case would give a difference in acceleration Δa of 4.4m/s²

The difference in actuator force of 18N would already cause a theoretical difference in acceleration of the welding heads lumped mass (9.5kg) of 1.9m/s², leaving us with an approximated decrease in acceleration of 2.6m/s². The latter decrease in acceleration corresponding to a decrease in actuator force in the order of 24N.

6.2.7 Fracture tests with lateral force

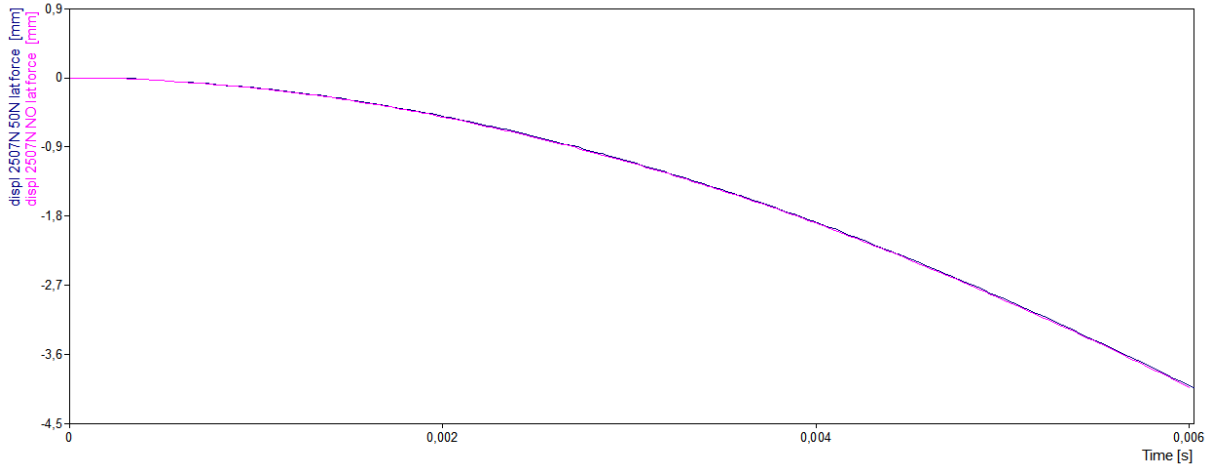


Figure 6-41 Displacement responses fracture test 2507N with and without lateral force on welding head

Considering the difficulty to have a fracture pin break at fully identical loads, it takes about 50 fracture tests to obtain a pair of identical actuator loads at the moment of fracture.

The displacement responses in Figure 6-41 follow a fracture test conducted with an actuator load of 2507N without any lateral force acting on the moving welding head on the one hand (blue graph) and on the other hand a fracture test conducted with an actuator force of 2705N with a lateral force of 50N acting horizontal and away from the welding window on the moving welding head.

As is noticeable, the displacement curves are very close to one another.

When measuring after an elapsed time of 0.005s, the difference in displacement is of 0.016mm. If we would compare both displacement signals as being motions with constant acceleration, it would give us:

$$s (displacement) = \frac{1}{2} \cdot a \cdot t^2$$

$$0.016mm = \frac{1}{2} \cdot a \cdot (0.005)^2$$

What in this case would give a difference in acceleration Δa of 1.28m/s²

Given a welding head mass from the fracture or explosion tests of 9.5kg, Newton’s second law would lead us to a difference in actuator force ΔF of 12N

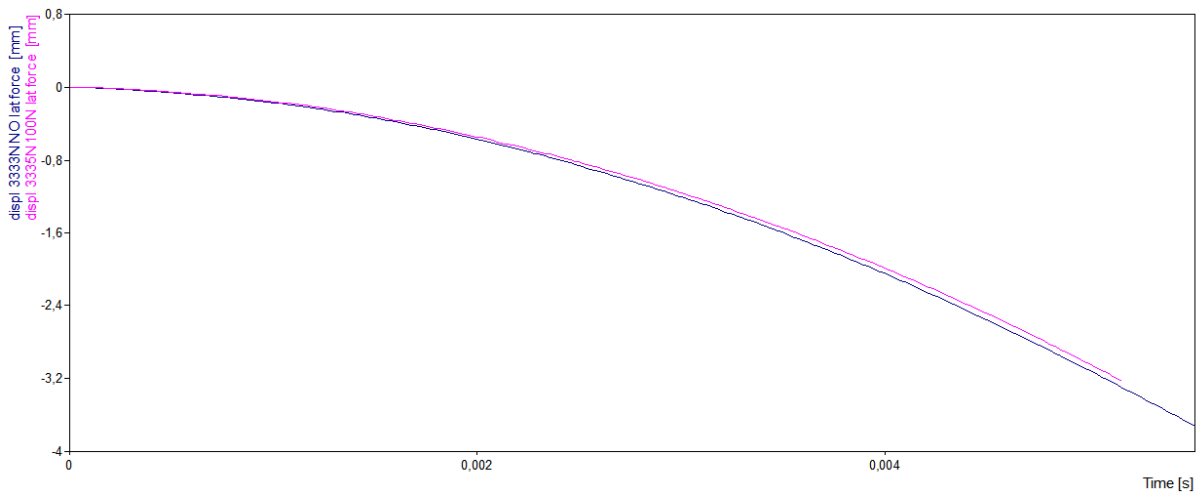


Figure 6-42 Displacement responses fracture test 3333N with and without lateral force on welding head

The displacement responses in Figure 6-42 follow a fracture test conducted with an actuator load of 3333N without any lateral force acting on the moving welding head on the one hand (blue graph) and on the other hand a fracture test conducted with an actuator force of 3335N with a lateral force of 100N acting horizontal and away from the welding window on the moving welding head.

As is noticeable, the displacement curves are very close to one another.

When measuring after an elapsed time of 0.005s, the difference in displacement is of 0.072mm. If we would compare both displacement signals as being motions with constant acceleration, it would give us:

$$s (\text{displacement}) = \frac{1}{2} \cdot a \cdot t^2$$

$$0.072\text{mm} = \frac{1}{2} \cdot a \cdot (0.005)^2$$

What in this case would give a difference in acceleration Δa of 5.76m/s^2

Given a welding head mass from the fracture or explosion tests of 9.5kg, Newton's second law would lead us to a difference in actuator force ΔF of 52N

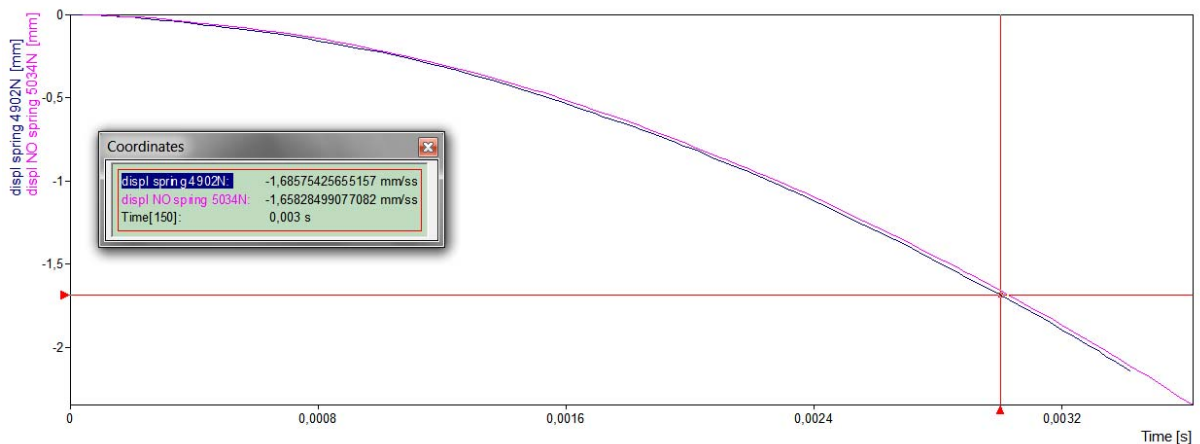


Figure 6-43 Displacement responses fracture test 5000N spring/NO spring in actuator assembly and without lateral force on welding head

The displacement responses in Figure 6-43 follow a fracture test conducted with an actuator load of 4902N with the coupling spring mounted in the actuator piston assembly (blue graph)

and one with an actuator load of 5034N and without the coupling spring mounted. Both responses result from a fracture test without any lateral force exerted on the moving welding head.

As is noticeable, even with 132N less in actuator force, the response with the spring mounted is better in comparison with the one where the spring is not mounted.

When measuring after an elapsed time of 0.003s, the difference in displacement is of 0.027mm. If we would compare both displacement signals as being motions with constant acceleration, it would give us:

$$s (\text{displacement}) = \frac{1}{2} \cdot a \cdot t^2$$

$$0.027\text{mm} = \frac{1}{2} \cdot a \cdot (0.003)^2$$

What in this case would give a difference in acceleration Δa of 6m/s^2

Given a welding head mass from the fracture or explosion tests of 9.5kg, Newton's second law would lead us to a difference in actuator force ΔF of 57N to be added with the initial difference in actuator force of 132N = 189N

6.2.8 Stick – Slip test

Results of friction measurements are given in Table 6-10 Results stick-slip measurements on AWL and Figure 6-44 below.

Lateral force [N]				Actuator Pressure [bar]	Actuator Force [N]
0	25	50	75		
96	110	124	138	0	0
104	112	128	140	1	732
106	122	136	148	2	1474
114	128	140	158	3	2216
150	160	170	198	4	2959
198	216	230	256	5	3701
288	292	296	300	6	4443
348	352	356	362	7	5185

Table 6-10 Results stick-slip measurements on AWL

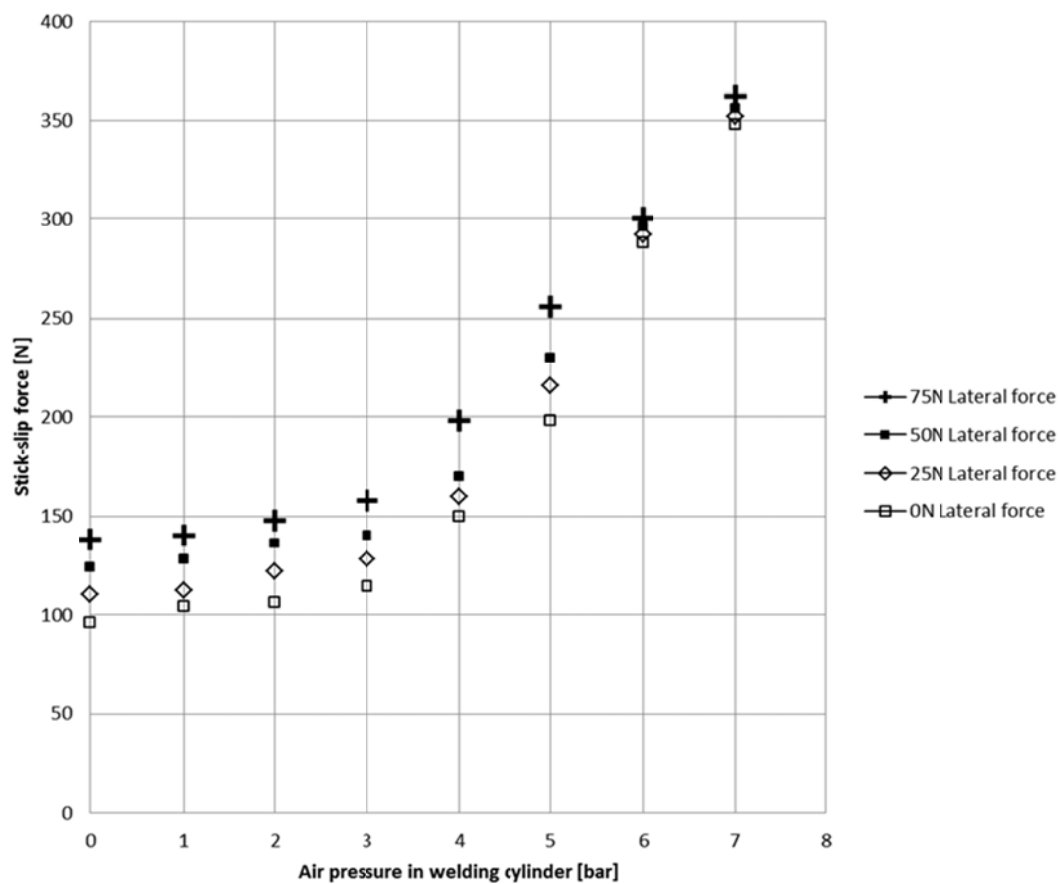


Figure 6-44 Results stick-slip measurements on AWL multi purpose spot/projection welder

6.2.9 High speed camera evaluation

To increase the level of understanding in what physically happens during a fracture test as well as the behaviour of materials during an explosion test, high speed camera evaluations were made on the AWL machine.

In Figure 6-45 below is a photograph of an exploding button test conducted on an AWL multi-purpose spot/projection welder taken at the exact moment that material of the 17% Chromium button and the AISI 304 intermediate layers is projected away due to the vaporising of material by overheating.

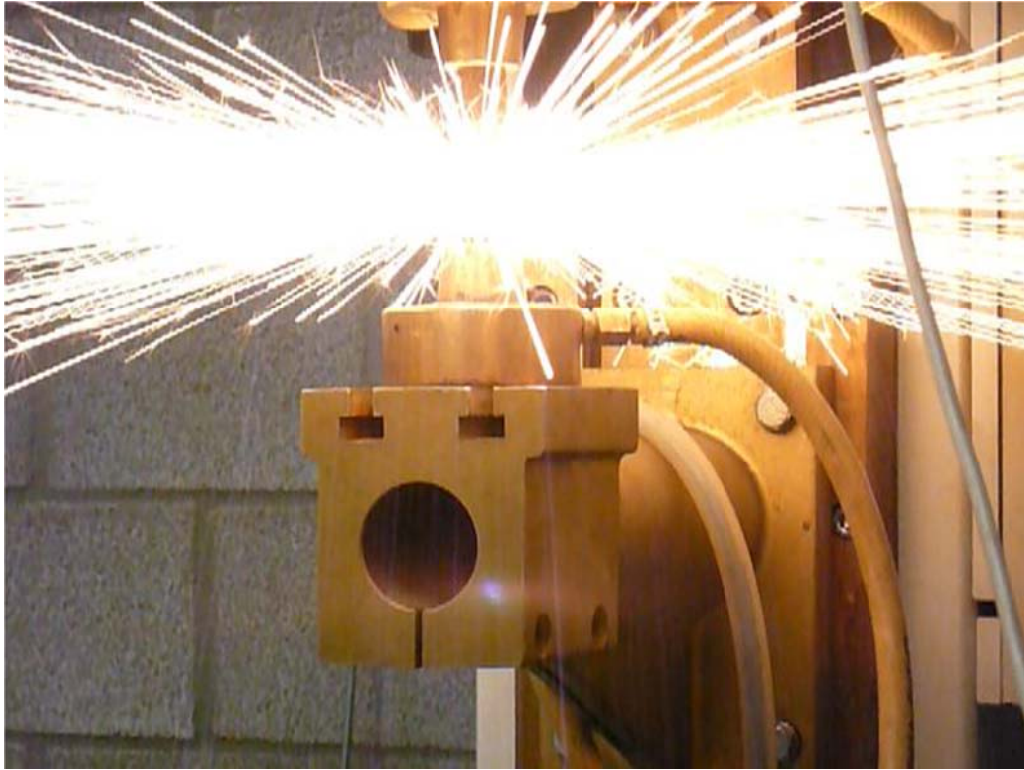


Figure 6-45 Photo of material splashing away during exploding button test on AWL

In Figure 5-9 and Figure 5-10, a sequential overview is given of a selection of frames from high speed recording of a fracture test revealing the substantial level of bending prior to fracture, the rupture of a fragment, immediately followed by the fracture of the pin. The latter immediately initiating the disappearance of reaction force, leading to the response of the moving welding head.

On the other hand, explosion tests were conducted on this machine, both with and without intermediate layers, with ball bearing elements, wire piece and wire button elements to explode.

6.2.9.1 Exploding ball test

In Figures Figure 6-46 to Figure 6-49 below, a sequential overview is given of a selection of frames from an exploding ball test conducted with an actuator force of 918N, a ball bearing of 1.5mm diameter and maximal electrical power available. Notice that liquid material stays in between the additional layers throughout the complete downward motion of the welding head. (marked with red circles and red arrows on the four figures)

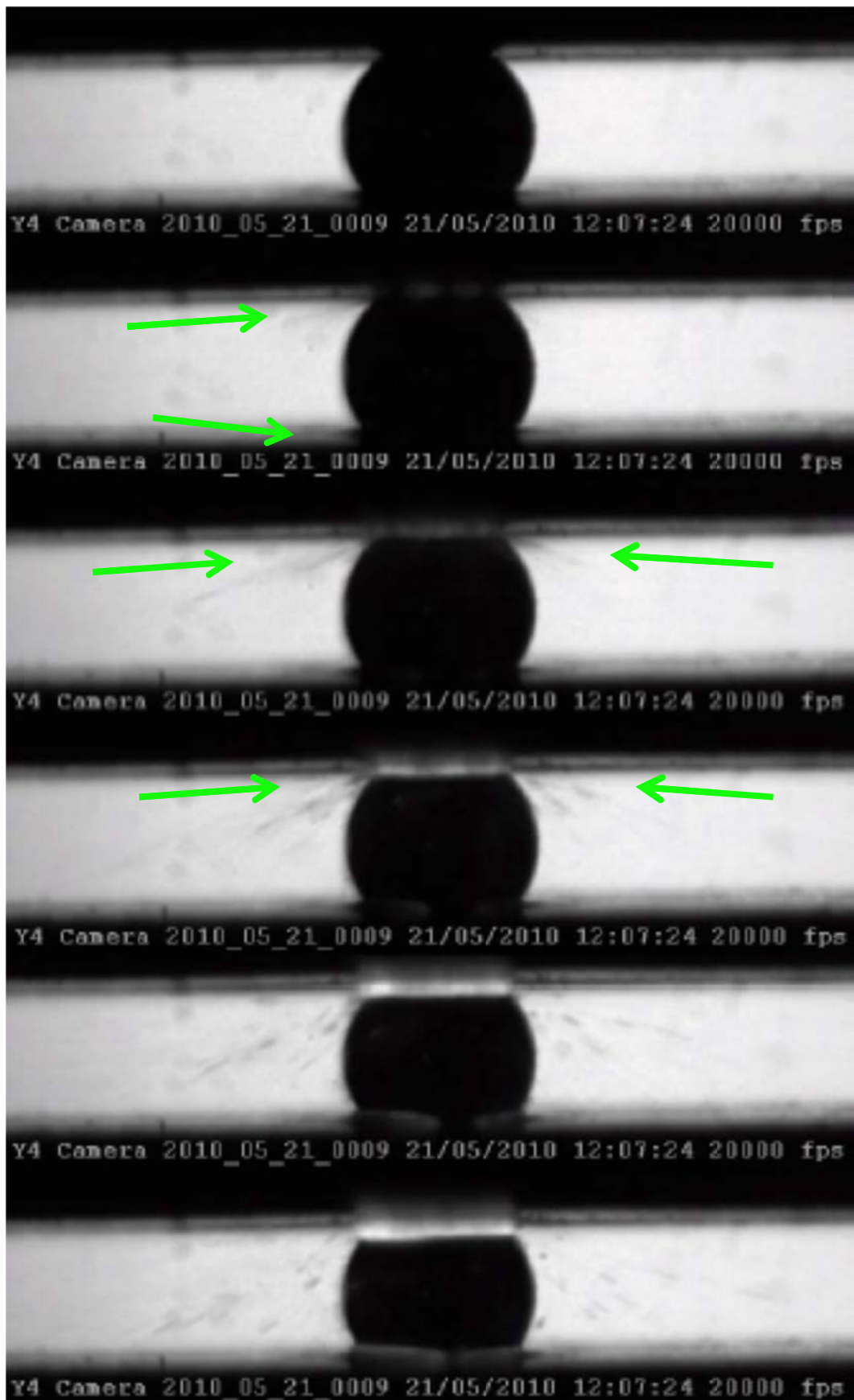


Figure 6-46 Exploding ball test AWL (part 1)

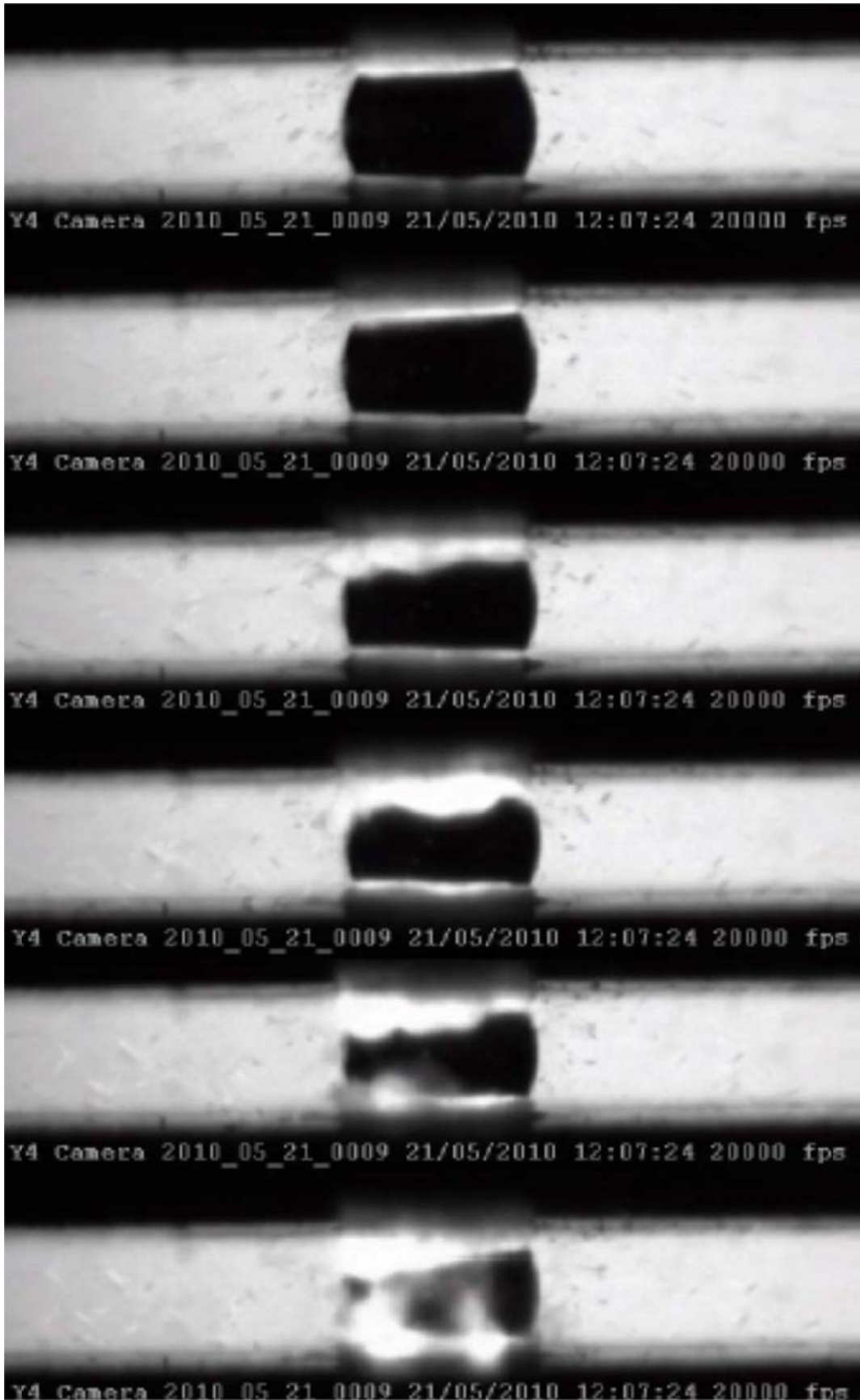


Figure 6-47 Exploding ball test AWL (part 2)

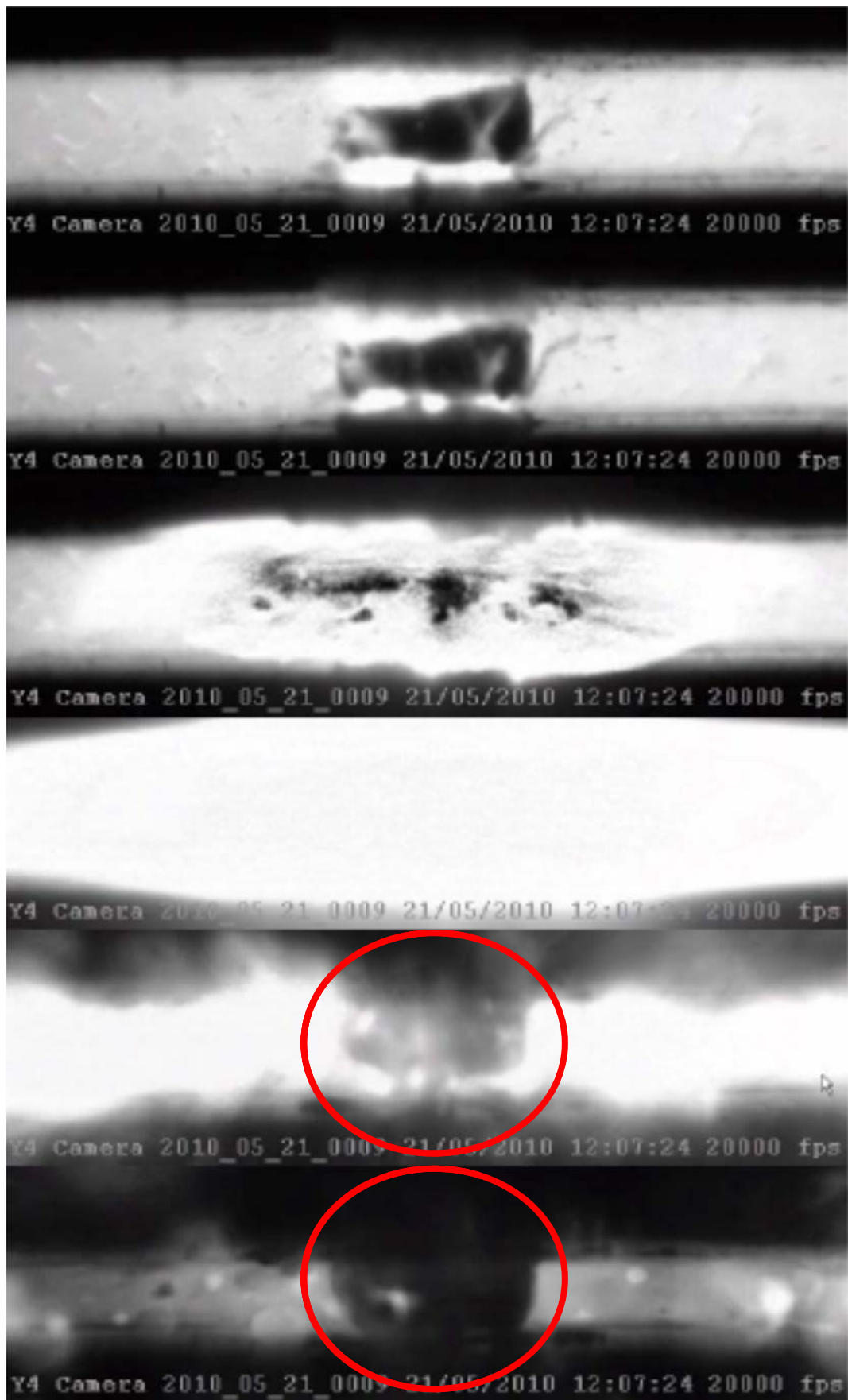


Figure 6-48 Exploding ball test AWL (part 3)

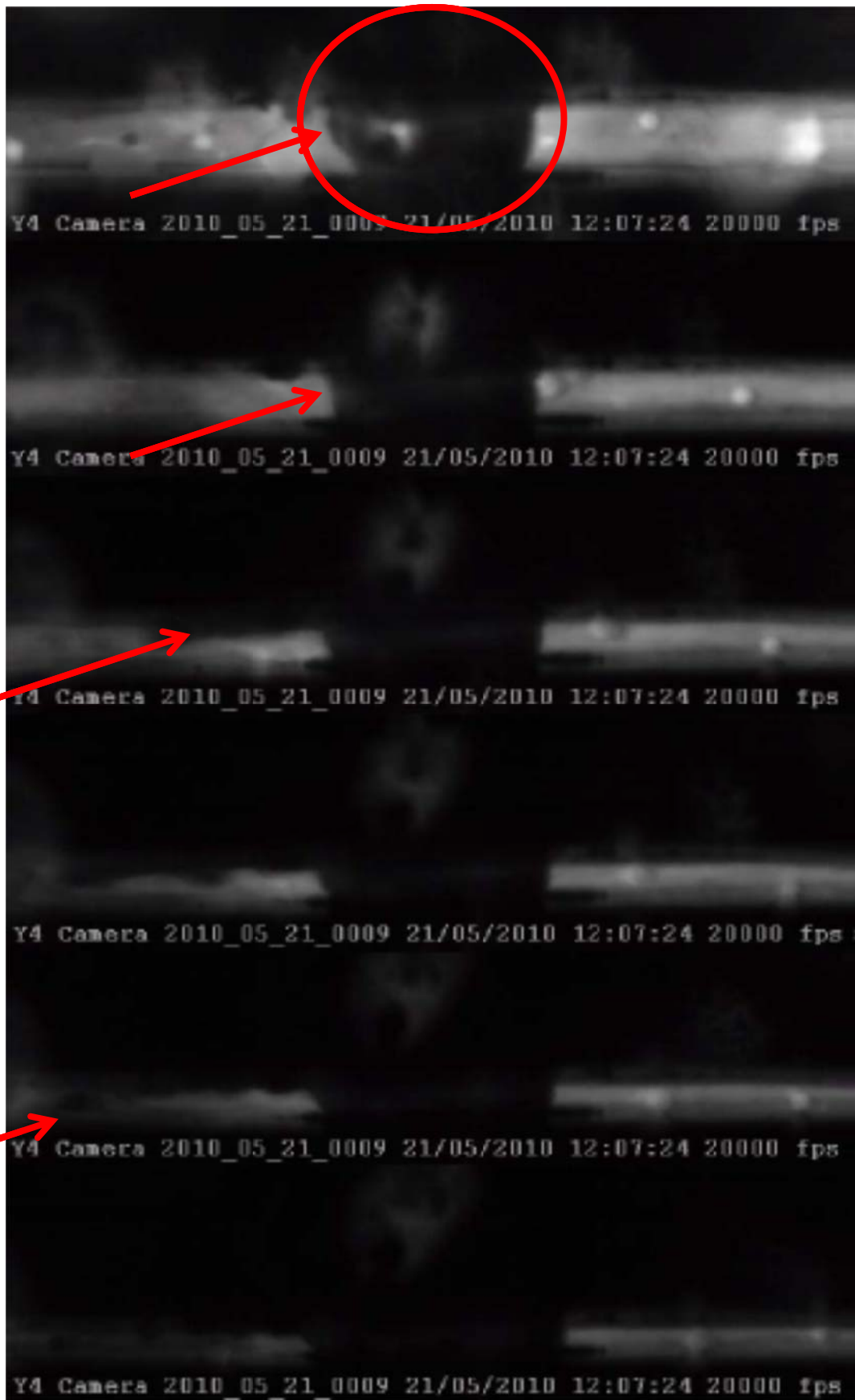


Figure 6-49 Exploding ball test AWL (part 4)

The welding head velocity response signal and the initiating current causing the step function to take place corresponding with the frames given in Figure 6-46 to Figure 6-49 are displayed in Figure 6-50 below and Figure 6-51, a zoom of the latter.

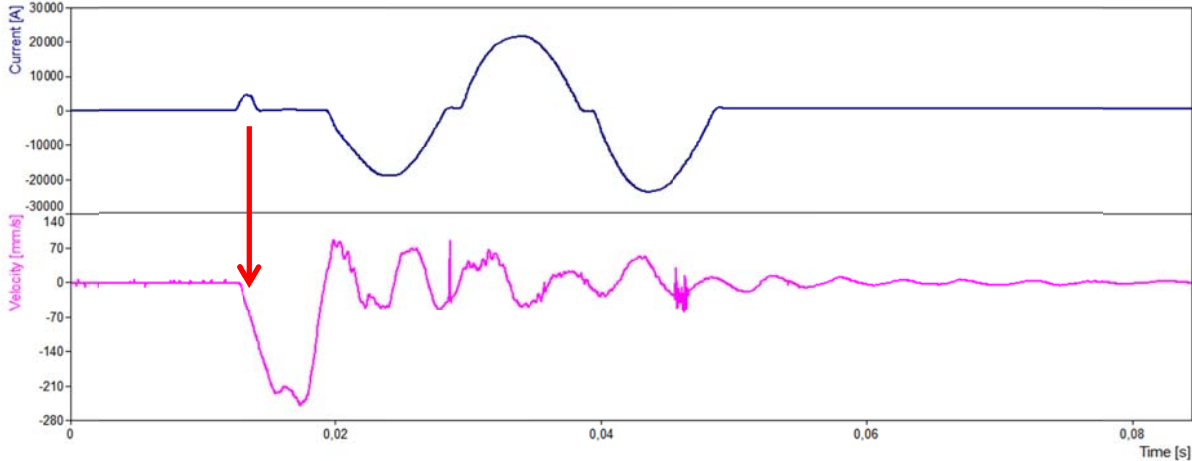


Figure 6-50 Current and velocity signal from exploding ball test on AWL

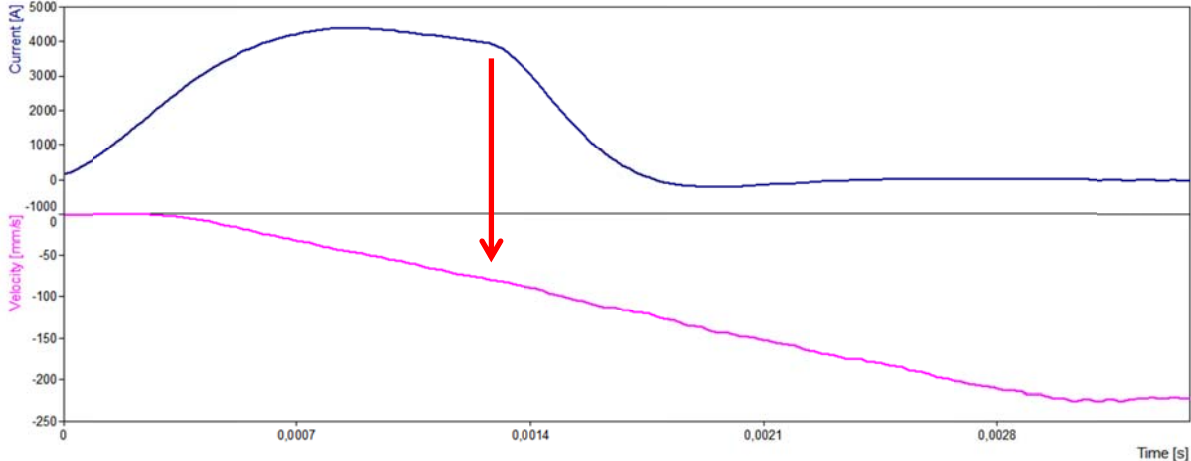


Figure 6-51 Current and velocity signal from exploding ball test on AWL (zoom)

It is clear from these graphs that there is no conduction from the moment where the explosion occurs (marked with the red arrows in Figures Figure 6-50 and Figure 6-51) until complete setdown of the electrodes, whereas from the high speed images one would tend to conclude that conduction remains with only a short interruption. Maximum welding head velocity reached with the explosion of this 1.5mm diameter ball bearing is 224mm/s, in a time period of 0.00277s, giving a mean acceleration value of 81m/s².

The intermediate layers have a large influence in the phenomenon of current interruption, since they allow the element to explode to ‘dig’ into the surrounding stainless layers (marked with the green arrows in Figure 6-46 and going on until the moment of explosion). Material actually is sprayed away sideways, creating a cavity in the intermediate layers. The latter effect creates space for the remains of the exploding element, in this case a ball bearing, to sink into both the intermediate layers. At a certain stage (third image of Figure 6-48), bulk

heating of the ball bearing causes it to partially vaporise, creating excessive expulsion of material, both from the intermediate layers as the ball bearing.
Notice also that free motion is enabled from the moment that melting takes place.

The latter 'digging' is visible in Figure 6-52 below in a metallographic cross-section throughout the resulting intermediate layers, squeezed together after the explosion test.

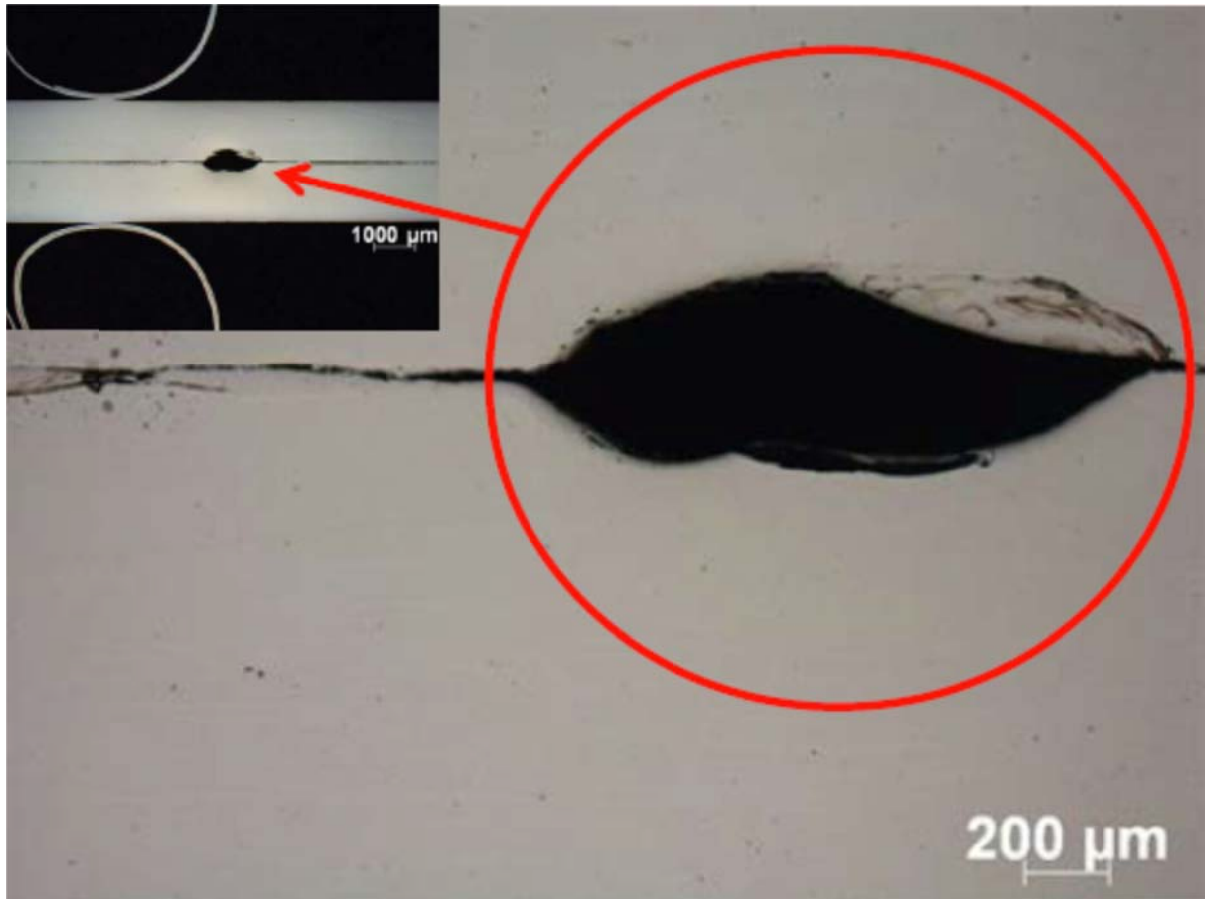


Figure 6-52 Cross-section through intermediate layers after explosion test (ball bearing)

One can notice some remaining solidified material that was not expelled due to the vaporising of material still present in the resulting cavity.

6.2.9.2 Exploding button test

In Figures Figure 6-53 to Figure 6-57 below, a sequential overview is given of a selection of frames from an exploding ball test conducted with an actuator force of 918N, a button of 1.2mm sliced from a 17% Chromium filler wire of 1.2mm diameter and maximal electrical power available. Notice the digging in is more pronounced in the first frames and that all liquid material is expelled from between the additional layers throughout the complete downward motion of the welding head.

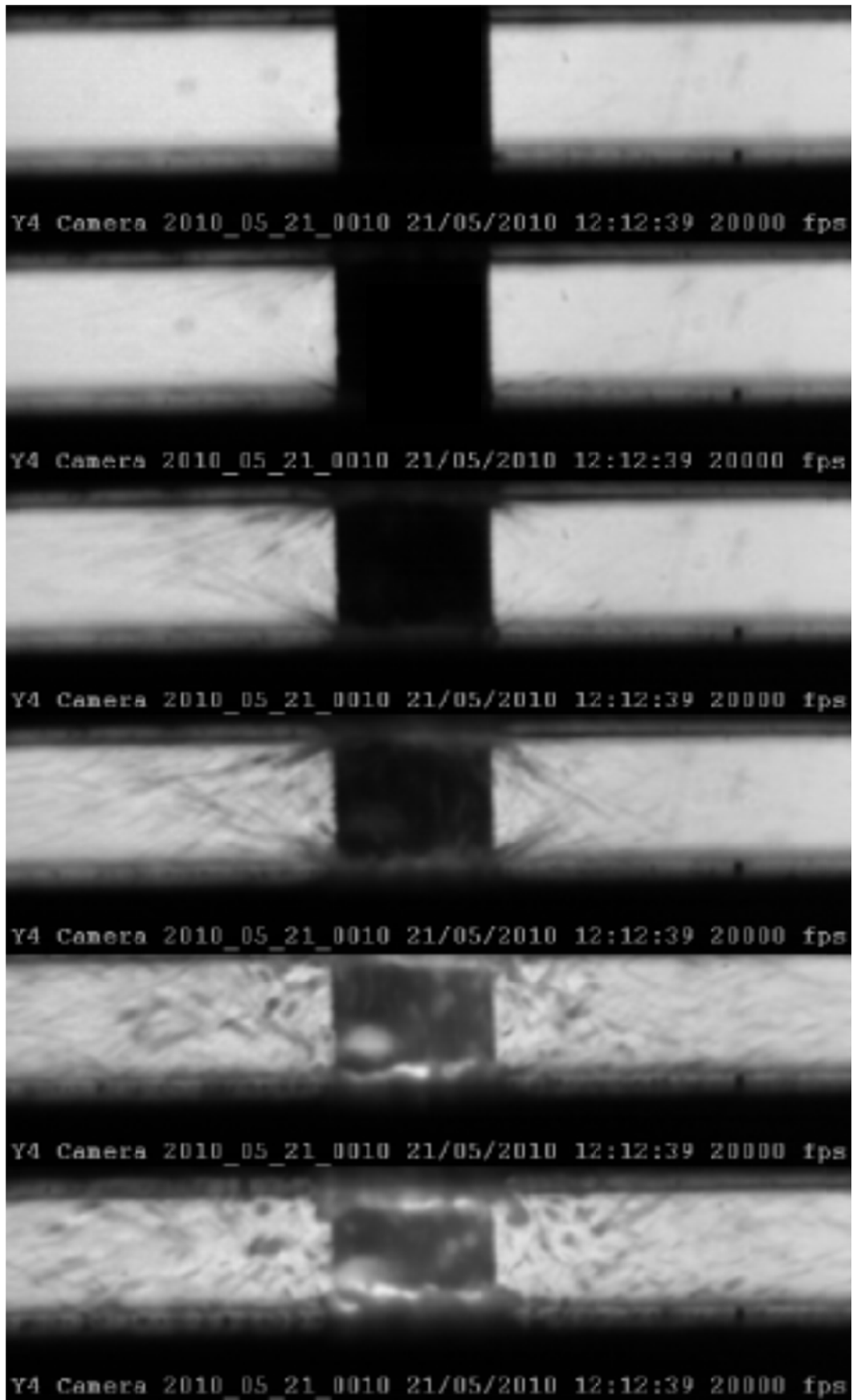


Figure 6-53 Exploding button test AWL (part 1)



Figure 6-54 Exploding button test AWL (part 2)

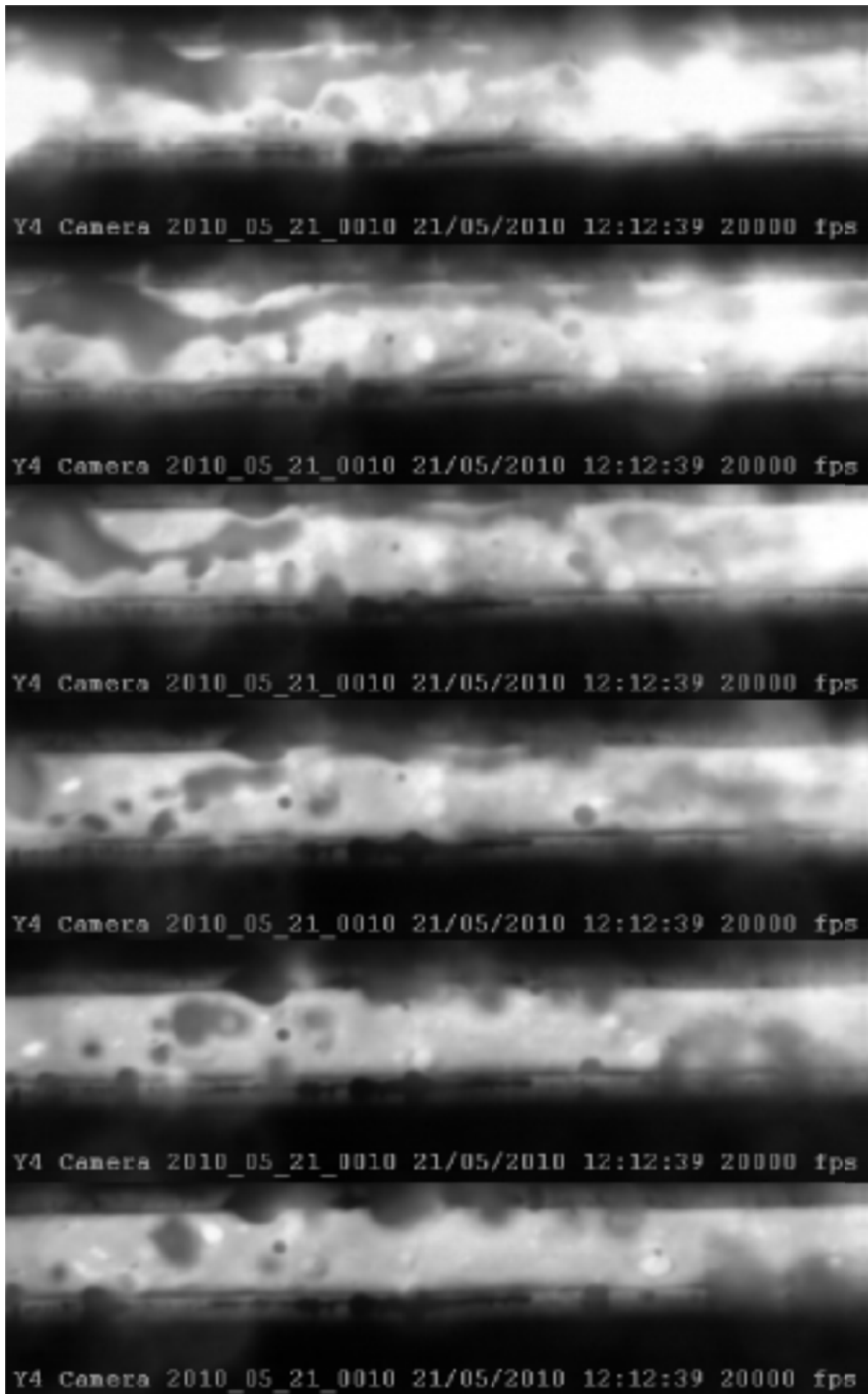


Figure 6-55 Exploding button test AWL (part 3)

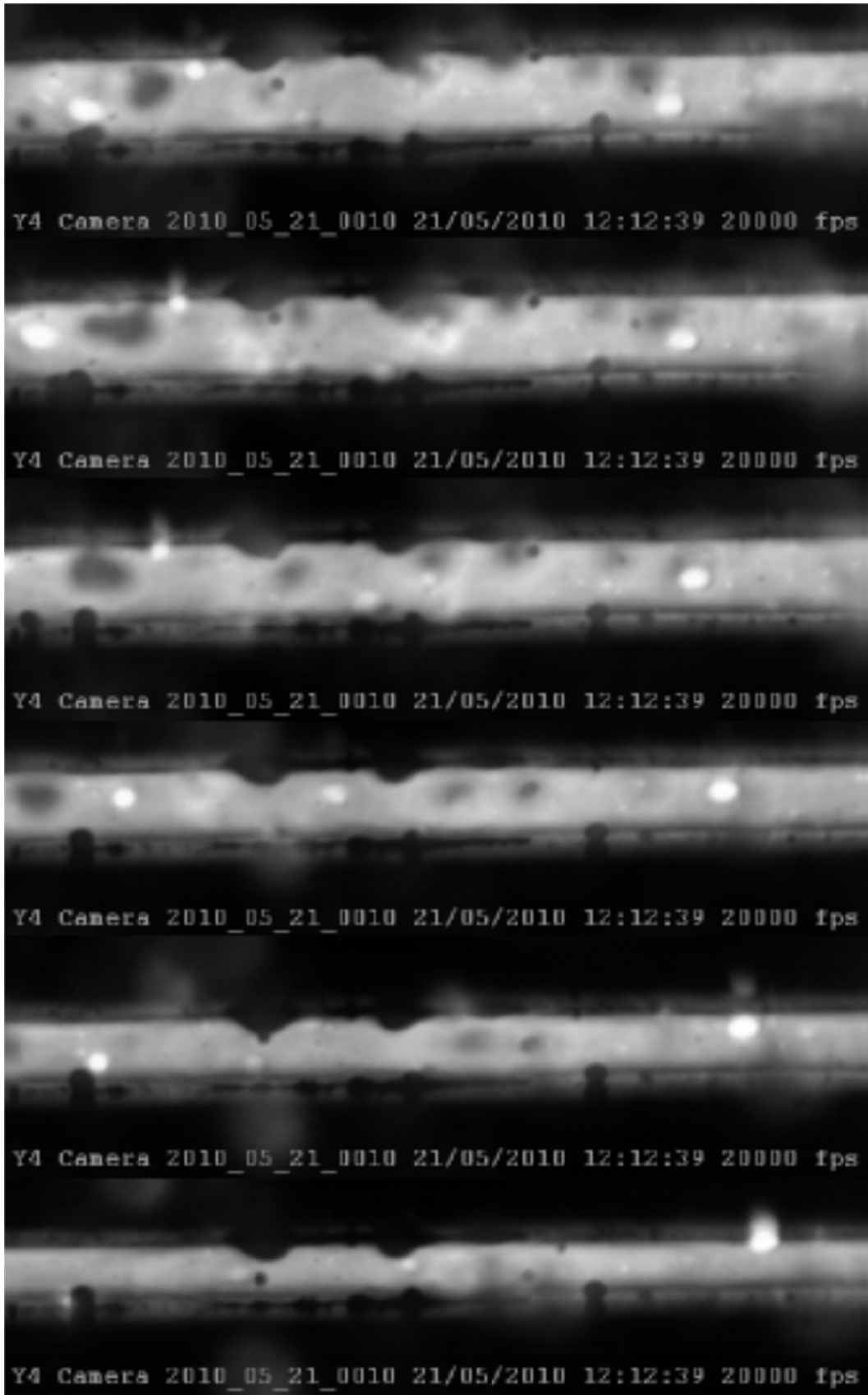


Figure 6-56 Exploding button test AWL (part 4)

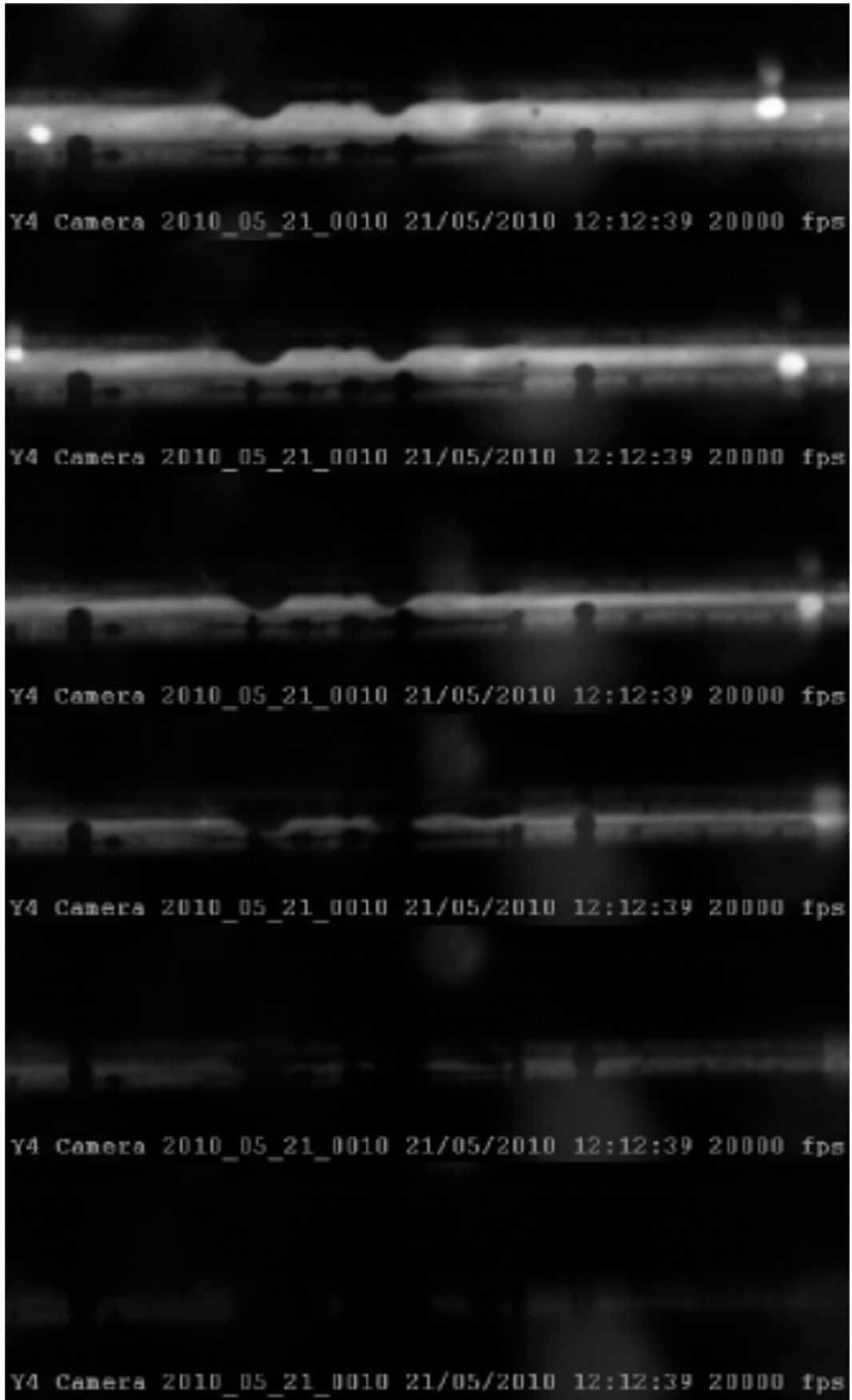


Figure 6-57 Exploding button test AWL (part 5)

The welding head velocity response signal and the initiating current causing the step function to take place corresponding with the frames given in Figures Figure 6-53 to Figure 6-57 are displayed below in Figures Figure 6-58 and Figure 6-59, a zoom of the latter.

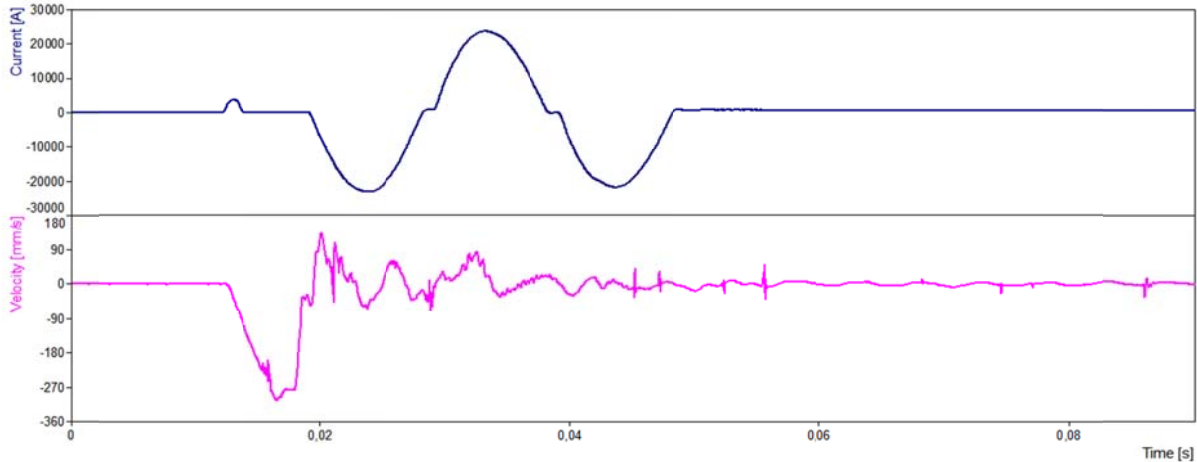


Figure 6-58 Current and velocity signal from exploding button test on AWL

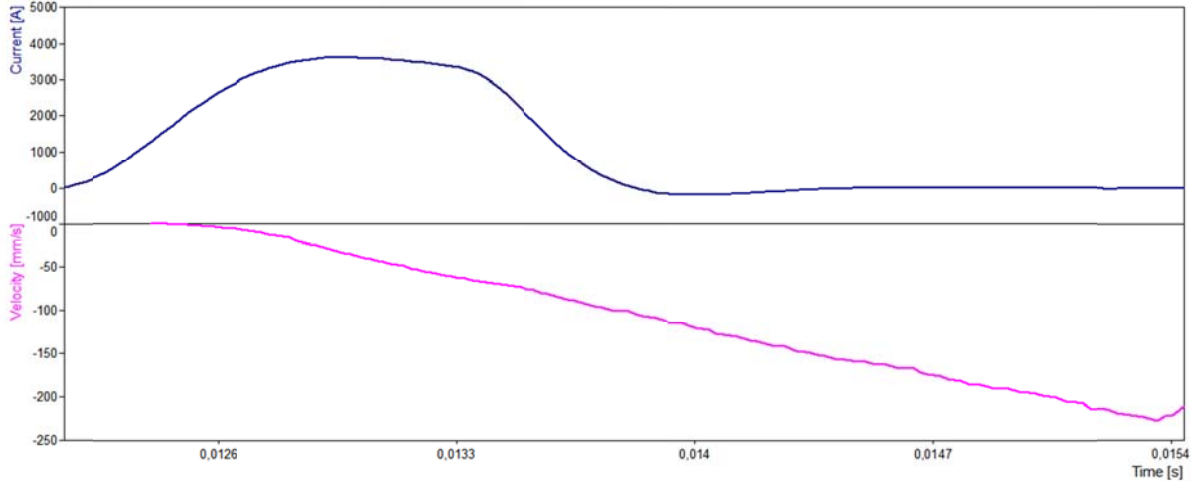


Figure 6-59 Current and velocity signal from exploding button test on AWL (zoom)

It shows clear from these graphs that also with the exploding button test, there is completely no conduction from the moment on where the explosion occurs until complete setdown of the electrodes, what is also obvious from the high speed images in Figure 6-53 to Figure 6-57 above. Maximum welding head velocity reached with the explosion of this 1.2mm thick button, sliced of 1.2mm diameter 17% Chromium steel filler wire is 224mm/s, in a time period of 0.00277s, giving a mean acceleration value of 81m/s², identical with the value reached with the ball bearing test at the same actuator load.

The ‘digging-in’ in the surrounding stainless steel layers also takes place with the buttons before exploding. Material actually is sprayed away sideways, also creating a cavity in the intermediate layers, comparable with what happens with the exploding ball test. The latter effect creates space for the element to explode, in this case a Chromium steel button. At a certain stage, bulk heating of the button material causes it to partially vaporise, creating excessive expulsion of material, both from the intermediate layers as the button element. Notice also that free motion is enabled from the moment that melting takes place.

The ‘digging’ with this exploding button test is visible in Figure 6-60 below in a metallographic cross-section throughout the resulting intermediate layers, squeezed together after the explosion test.



Figure 6-60 Cross-section through intermediate layers after explosion test (button)

One can notice the less curved cavity created by the more straight upper and lower surfaces of the button in comparison with the cavity created by the exploding ball test in Figure 6-52.

6.3 PECO roll membrane machine

The Peco – Messer Griessheim resistance welder, equipped with a rather unique pneumatic roll membrane actuator in its moving welding head has been used previously by Philips Lighting in Turnhout, Belgium for cross wire welding in lamp production..

Fracture tests and measurements performed during the period when this machine was available in 2005.

In Table 6-11 and Figure 6-61 below is an overview of the results of fracture tests made at different actuator load levels conducted on it.

Measured values	Calculated values	
Actuator force	Mass	Damping coefficient
F [N]	m [kg]	b [kg/s]
1164	8.3	703
1321	8.1	834
1373	8.2	1172
1446	8.2	1164
1579	8.1	734
1632	8.2	1349
2996	8.4	557
3031	8.2	868
3541	8.3	979
3679	8.3	837
3875	8.2	1164

Table 6-11 Results fracture tests on PECO roll membrane

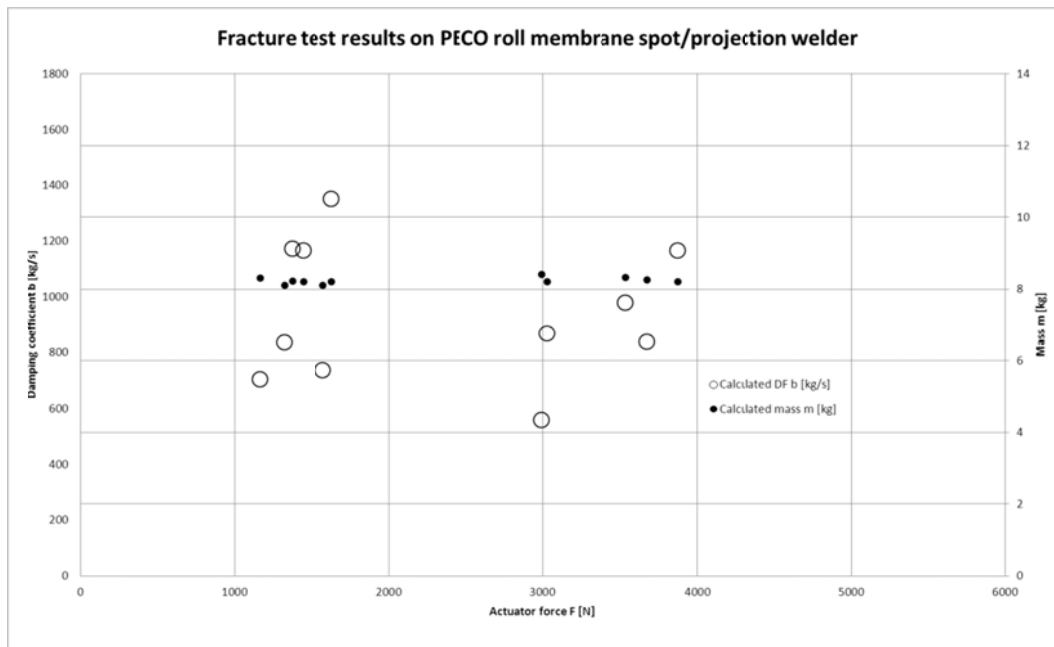


Figure 6-61 Fracture test results on PECO roll membrane machine

6.4 ARO multi-purpose spot/projection welder (pneumatic)

6.4.1 Fracture and explosion tests

Processed results from velocity responses to the step function imposing tests are given in Table 6-12 below and graphically displayed in Figure 6-62 below.

Measured values	Calculated values		
	Actuator force	Mass	
F [N]	m [kg]	b [kg/s]	
2298	20.9	727	Fracture
3331	20.9	1390	Fracture
2083	21.4	1051	Explosion
2066	21.9	1247	"
2004	21.7	1266	"
2189	22.2	972	"
3309	21.6	1466	"
3208	20.9	1616	"
3251	21.6	1658	"
1617	21.0	591	"
1757	21.4	962	"
1622	20.9	1052	"
1623	21.0	707	"
1563	21.0	638	"
2769	21.0	1242	"

Table 6-12 Results fracture- and exploding wire tests on ARO pneumatic

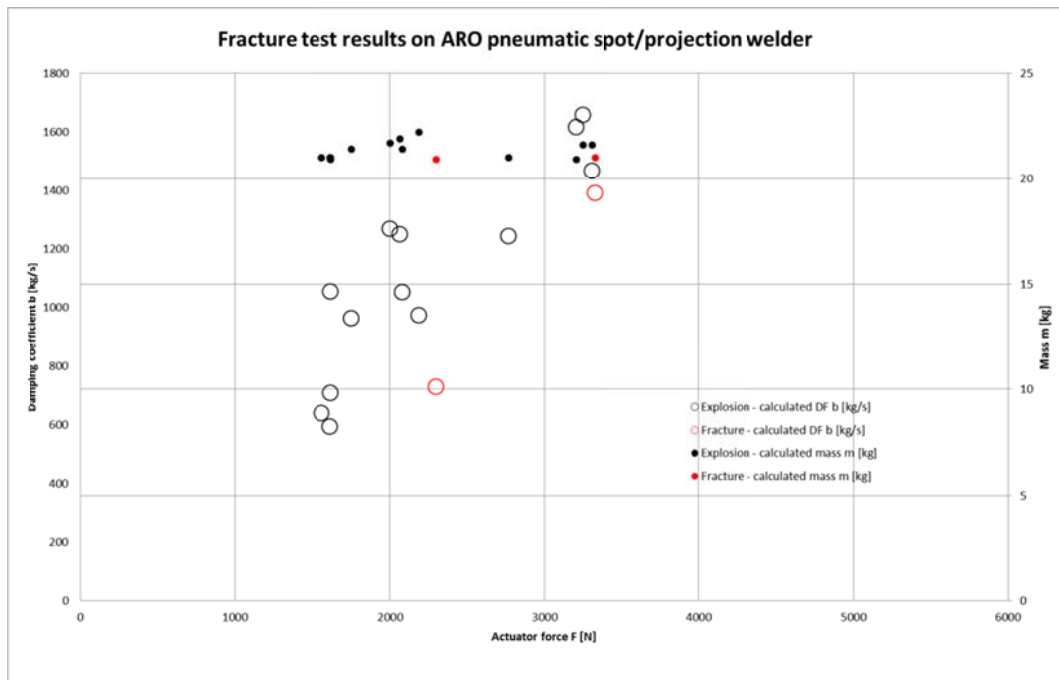


Figure 6-62 Processed results fracture and explosion tests on ARO pneumatic

The explosion tests were carried out with wire elements and without intermediate layers between the electrodes and the element to explode.

Evaluations were made on the use of different materials and different shapes for the elements to explode. An example is given in Figure 6-63 below, giving acceleration values reached for AISI 304 diameter 1mm welding filler wire in wire piece lengths of 5mm placed without any intermediate layers between the copper electrodes at different loads and loaded with different current values on the welding machine under study.

It can be noticed that at a given actuator load value, there is a current value where the resulting acceleration value tends to stabilise.

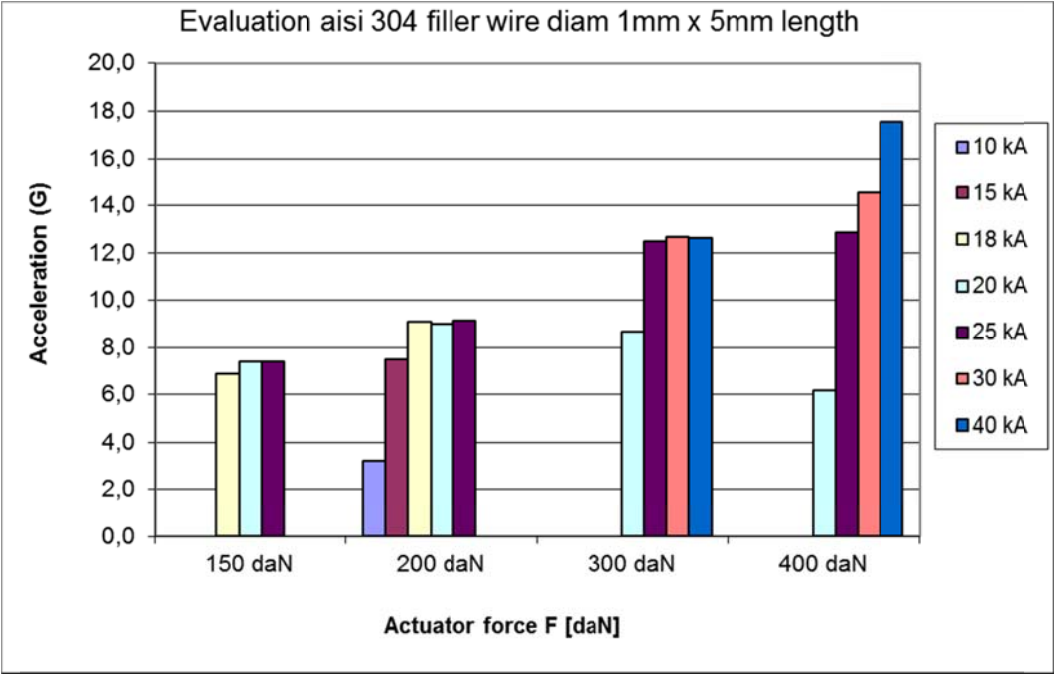


Figure 6-63 Evaluation of 5mm x 1mm diameter AISI 304 filler wire as exploding element

On the image above, it is apparent that the available power source on this ARO machine, at an actuator load of 4000N is possibly insufficient to impose a step in the load from full reaction force to 0N reaction force. The three left bars in the graph at 4000N are the result of measuring the velocity of plastic deformation of material from the exploding element due to insufficient heating.

Optimal to use is the 'button'-type element rather than the 'wire'-type element. Use of 'ball-bearing' elements results in identical acceleration values as the 'button'-type element with the restriction of it being extremely difficult to position and maintain positioned before closing of the electrodes.

Use of intermediate layers increasing contact resistance and supplying material for the exploding elements to 'dig' in is a technical improvement and saves the electrodes.

To ensure that the machine's maximum acceleration is measured in an explosion test, one should ensure that current is interrupted during the explosion. In that way, there is certitude of complete removal of electrode support. The latter is not a necessity, since high speed camera evaluation revealed that liquefied material from the element to explode is not hindering motion.

6.4.2 High speed camera evaluation

Setup for making high speed video recordings on the ARO machine is visible in Figure 6-64 below.

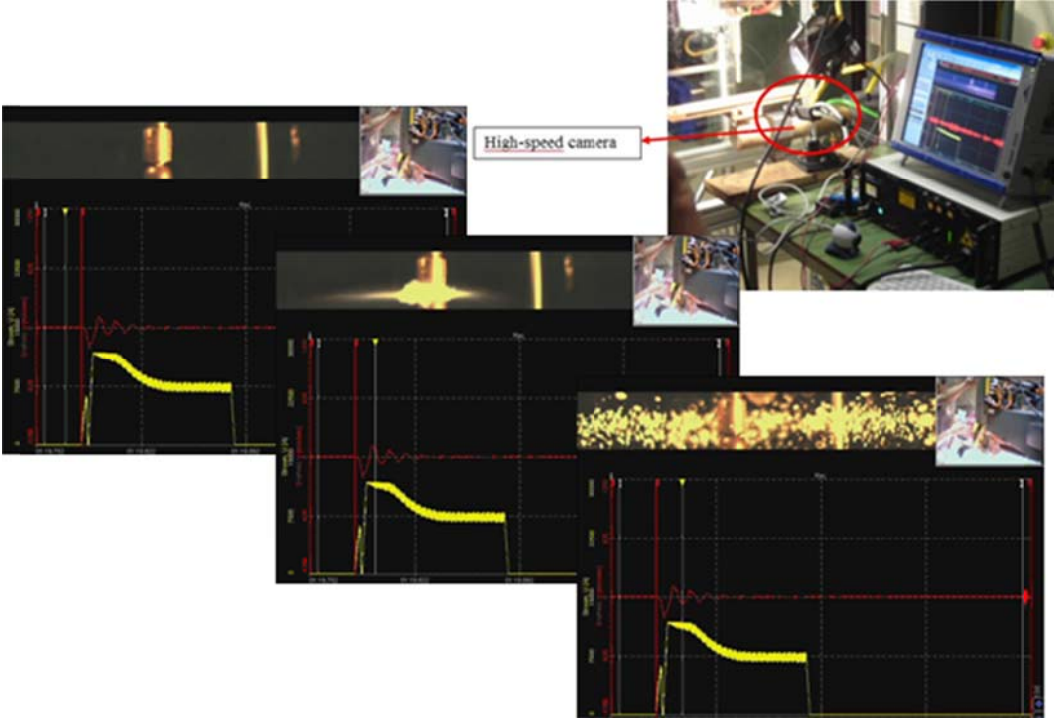


Figure 6-64 Setup for high speed video recording on ARO pneumatic



Figure 6-65 Positioning of wire and button without intermediate layers

In Figure 6-65 above, the positioning of a wire or button on the welding electrodes without intermediate layers can be seen.

In Figures Figure 6-66 and Figure 6-67 below are the sequential frames taken from an exploding button test without the use of intermediate layers, made on an ARO pneumatic spot/projection welder. Images are taken from a distance in order to get a clear overview of an explosion.

The first three frames display the ‘digging’ effect into the copper electrodes, in the fourth frame the button explodes due to excessive bulk heating and its material is expelled in a radial cloud of molten particles driven by vaporised material, the latter visible as a white cloud.

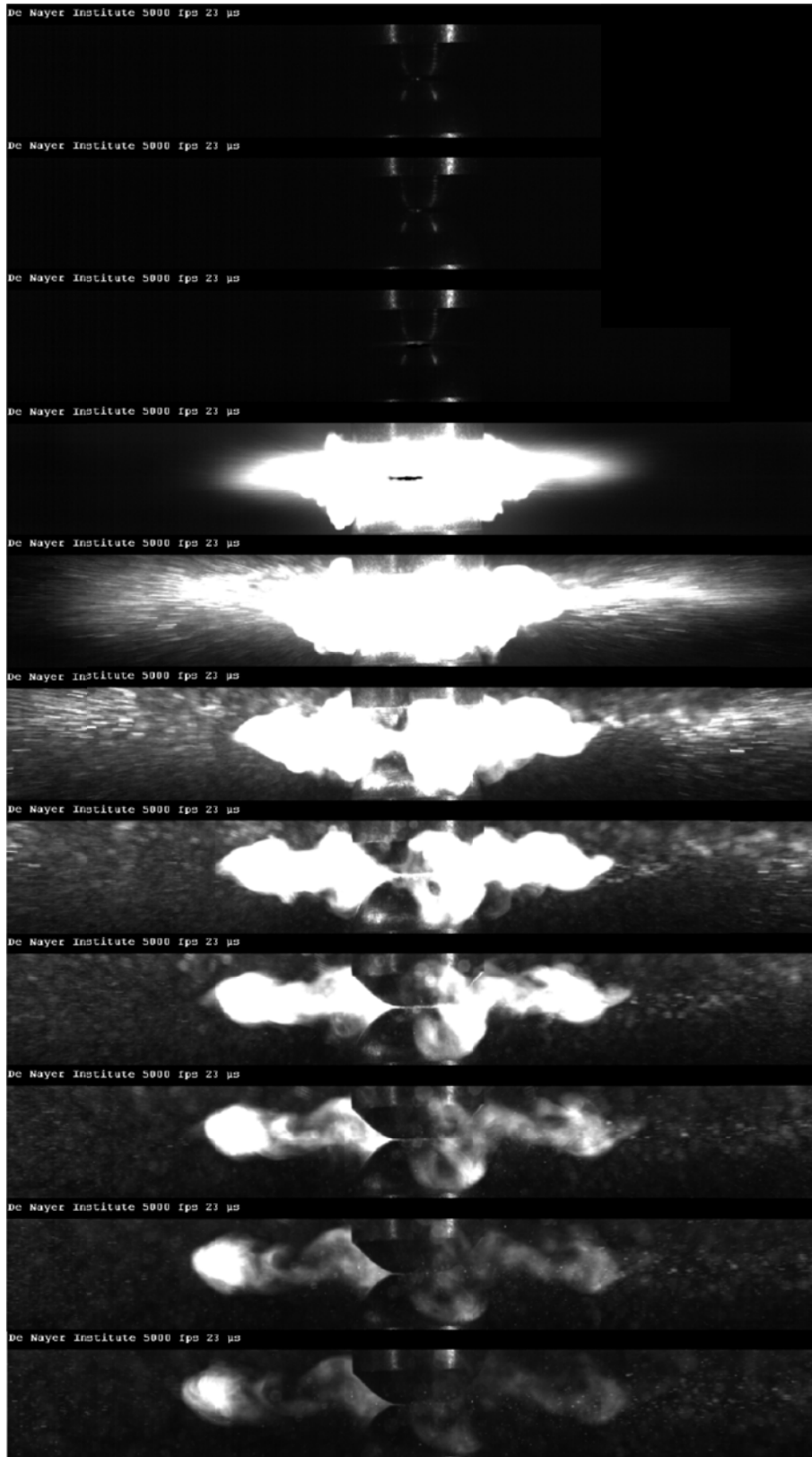


Figure 6-66 Exploding button test ARO pneumatic, no intermediate layers (part 1)

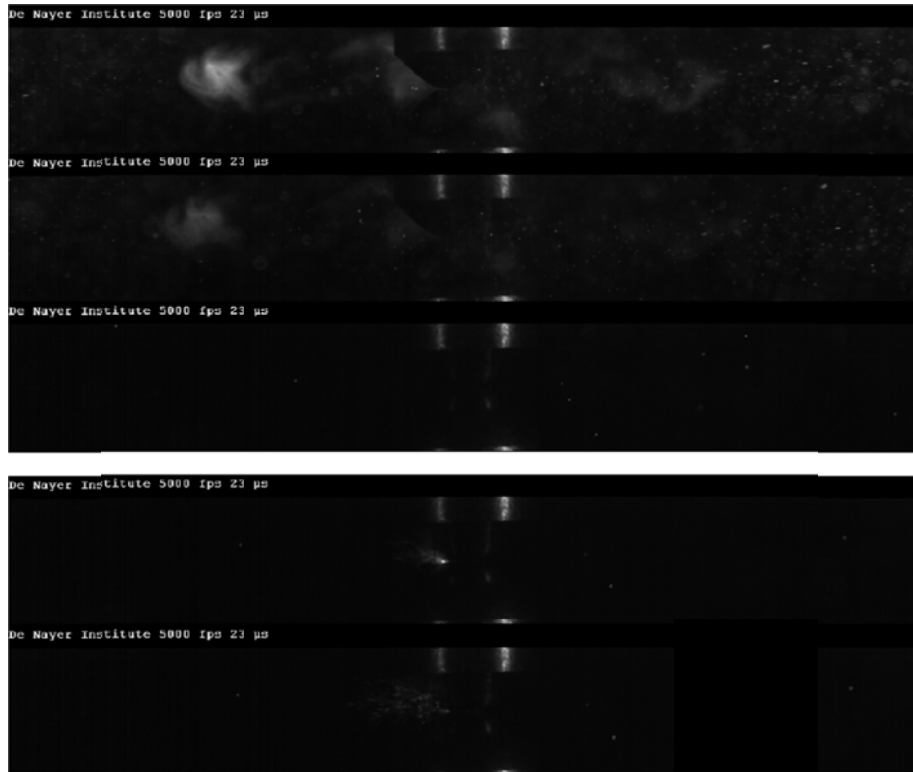


Figure 6-67 Exploding button test ARO pneumatic, no intermediate layers (part 2)

Notice that in Figure 6-67 above, there is a substantial time gap between the upper three frames and the two last frames. Due to the impact from the upper moving electrode against the lower fixed on, a vibration is initiated, resulting in bouncing of the electrodes. The last two frames show a secondary explosion, caused by the welding current still flowing in combination with reduced electrode pressure due to this bouncing effect.

6.5 Mc Gregor μ -resistance welding head

6.5.1 Explosion tests

Explosion tests have been conducted in combination with high-speed camera evaluations on this small standard opposed welding head pneumatic module, equipped with a Unitek Myiachi dual pulse capacitor discharge power source.

The welding head is pneumatically loaded, enabling a pneumatic piston to move to the end of its stroke while loading a calibrated spring. Spring used in these tests was set for a load of 50N. Instead of the stainless steel intermediate layers used to test on the larger welding machines, this test was made with 'process tape' normally used on a Fronius Deltaspot welding machine.

Results are given in Table 6-13 and Figure 6-68 below.

Measured values	Calculated values	
Actuator force	Mass	Damping coefficient
F [N]	m [kg]	b [kg/s]
50	0.137	19
46	0.145	10
50	0.130	9
48	0.139	7
50	0.132	11
58	0.132	27
48	0.130	29
50	0.131	16

Table 6-13 Results explosion tests on Mc Gregor μ -resistance welding head

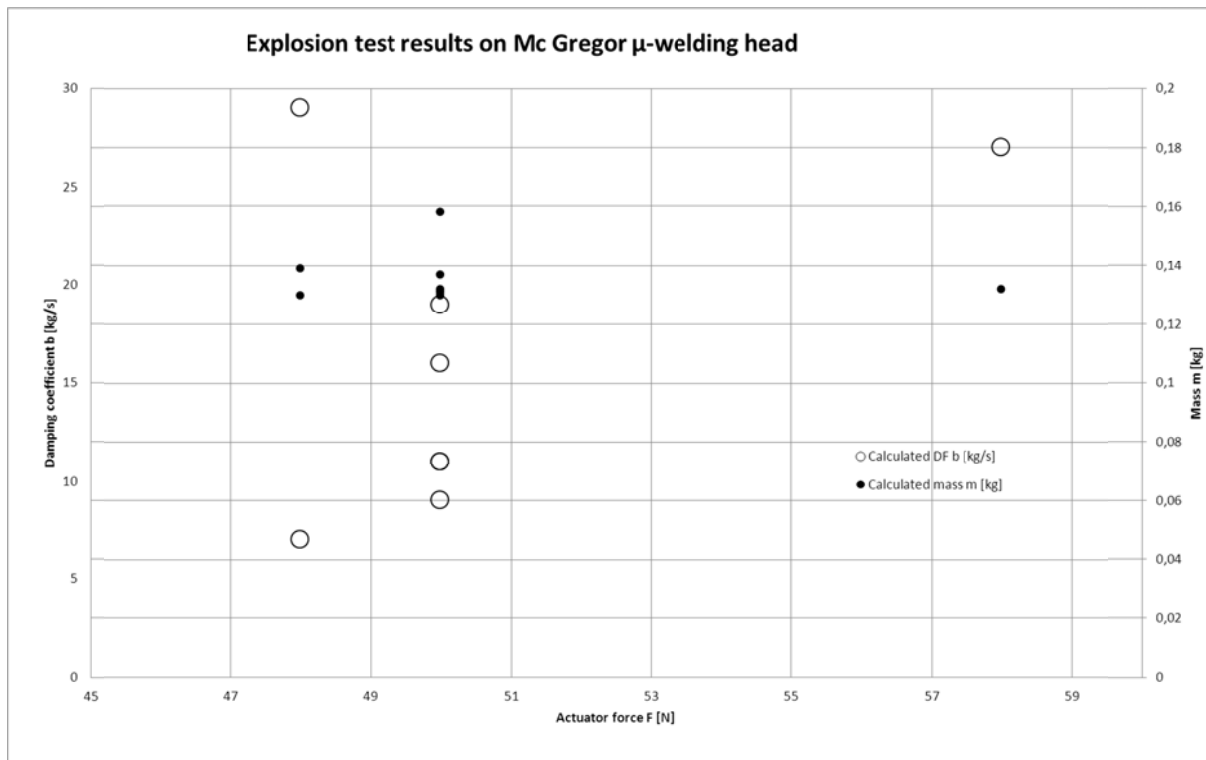


Figure 6-68 Processed results explosion tests on Mc Gregor μ -welding head

6.5.2 High speed camera evaluation

The Mc Gregor welding head evaluated here is the company standard at the Philips Lighting production plant in Turnhout, Belgium. There are hundreds of these machines implemented in highly automated production machines, all assembling micro cross-wire metal components for HID (High Intensity Discharge) lamps. This company produces between 30 and 40% of all HID lamps and this micro welding machine is representative for equipment used in the μ -resistance welding application field. Measurements were made in this company using an IDT HS camera with integrated and coupled data acquisition system. This provides synchronisation between measured current, resulting welding head displacement and the physical phenomena taking place during an explosion test.

Set up for high speed video recording on this specific machine can be seen in Figure 6-69 below.

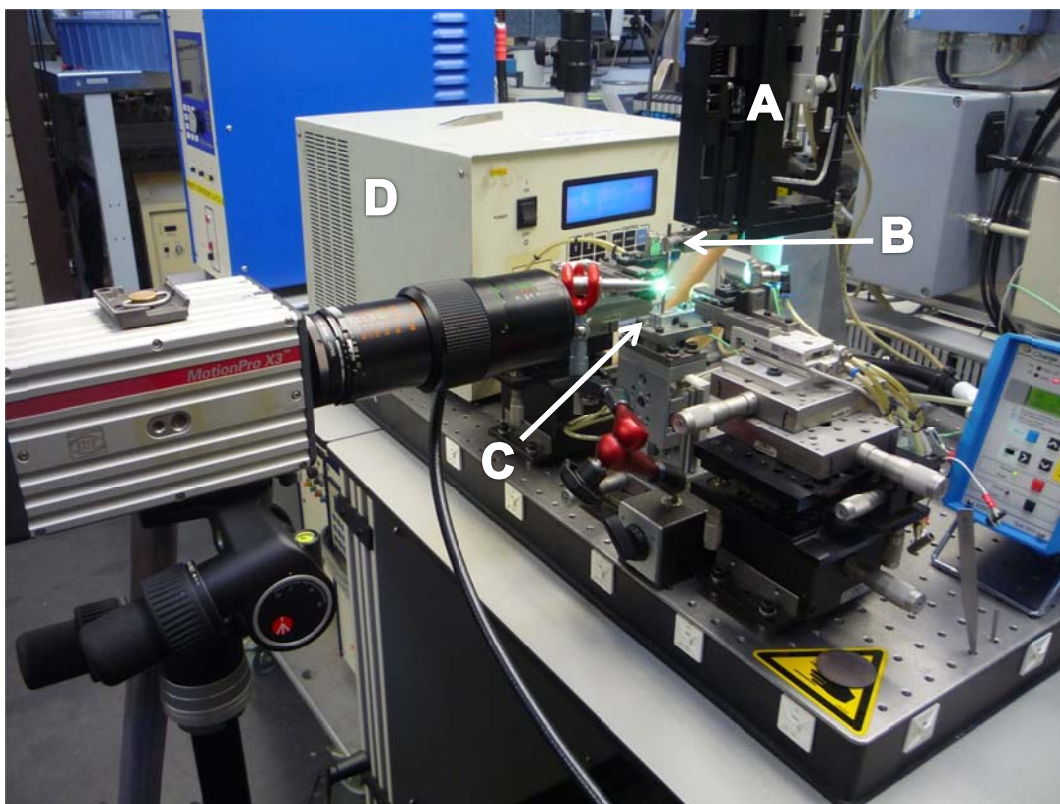


Figure 6-69 High speed video recording setup for exploding button test on Mc Gregor machine

Notice the Mc Gregor welding heads' pneumatic and spring actuated actuator (A), the moving welding head with the upper electrode (B), the fixed lower electrode (C) and the capacitor discharge power supply used (D).

Supplementary side and back lighting is used in order to avoid overexposure when the explosion takes place. (bright green spot between the electrodes) Protecting glasses are used both before the objective of the camera and before the fiberglass used for the illumination.

In Figures Figure 6-70 to Figure 6-75 below are sequential frames taken from an exploding button test.

Button of 0.8mm x 1.2mm diameter (17% Cr), 50N actuator load, intermediate layers.

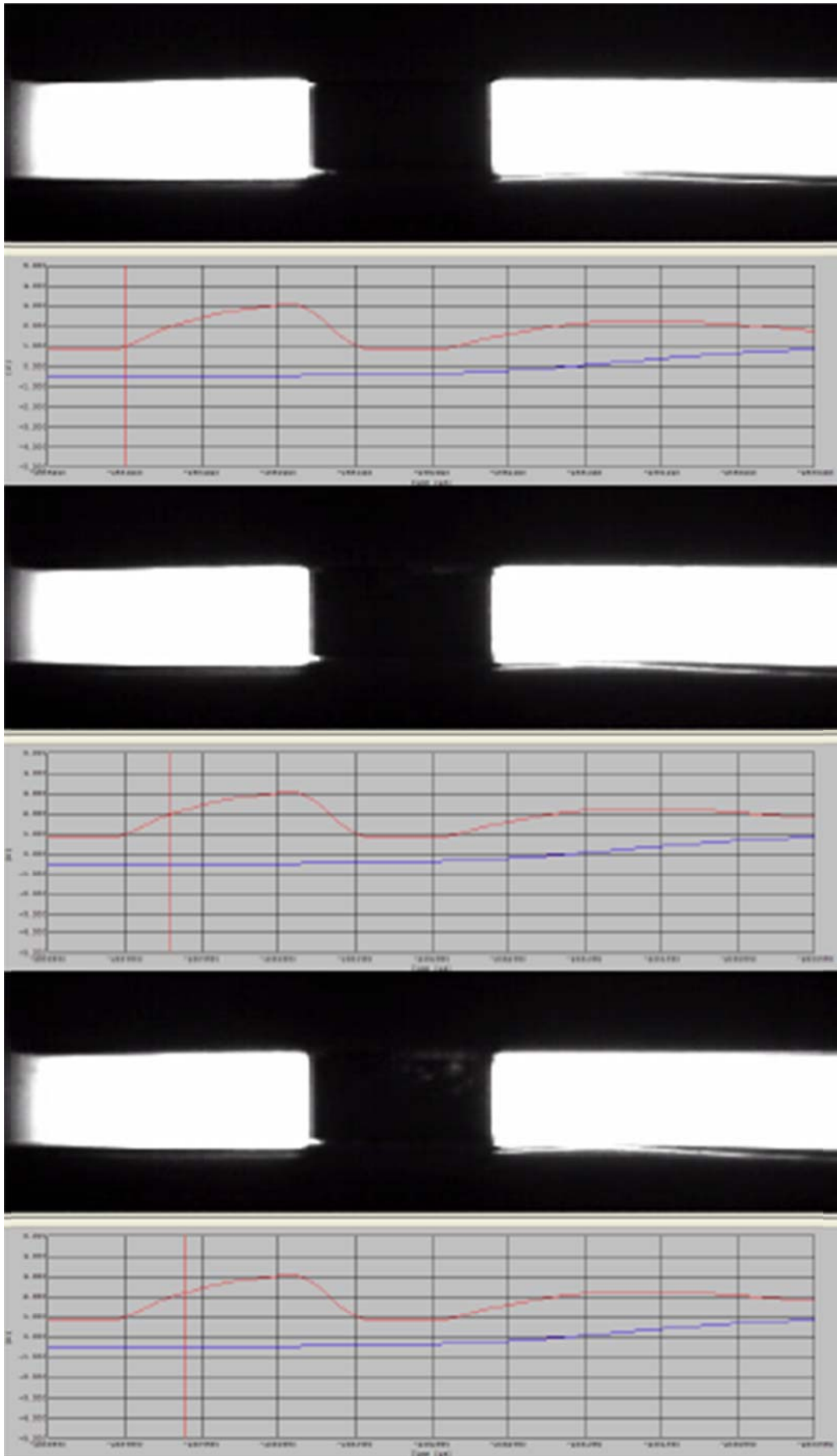


Figure 6-70 Exploding button test on Mc Gregor (part 1)

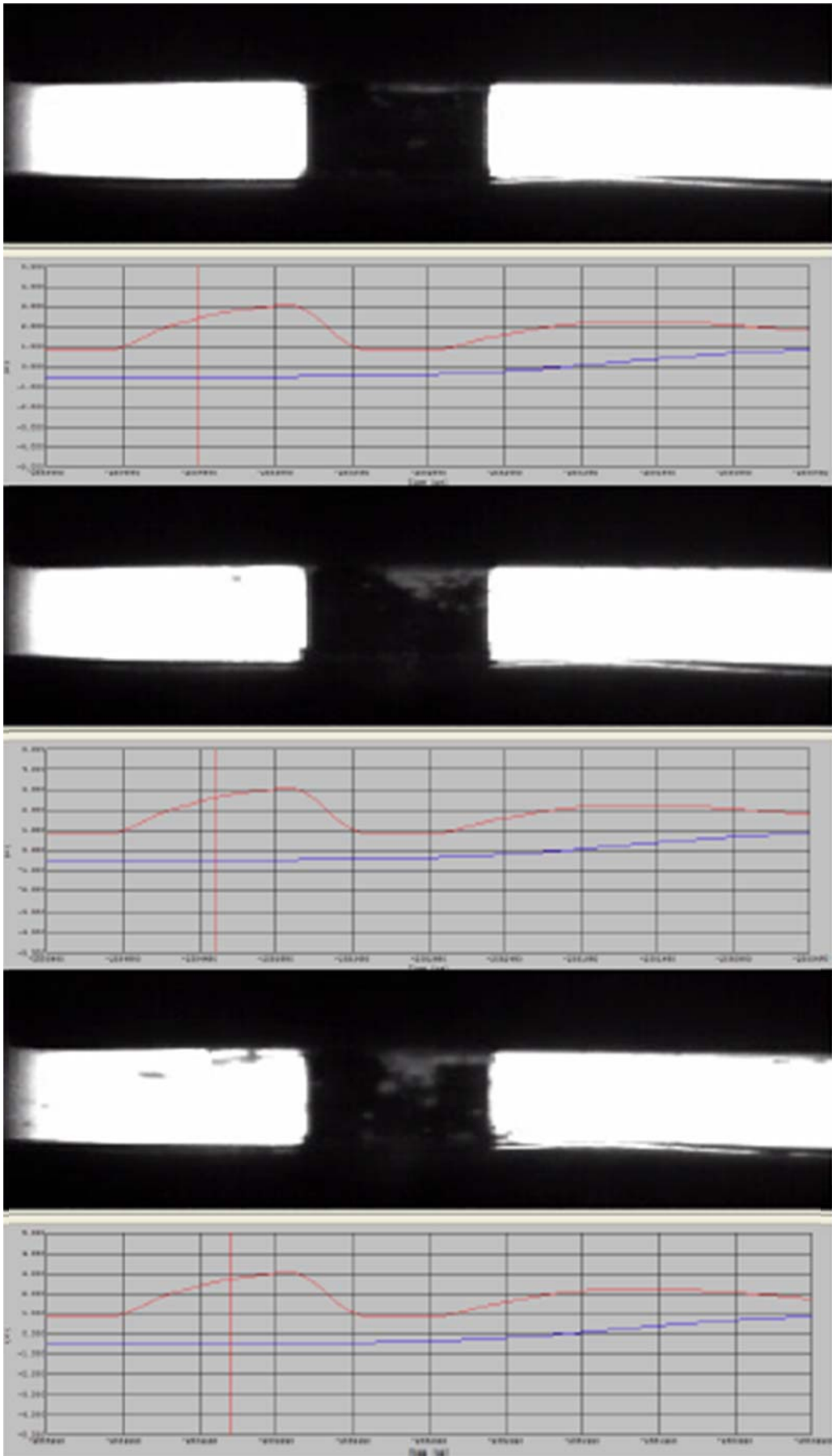


Figure 6-71 Exploding button test on Mc Gregor (part 2)

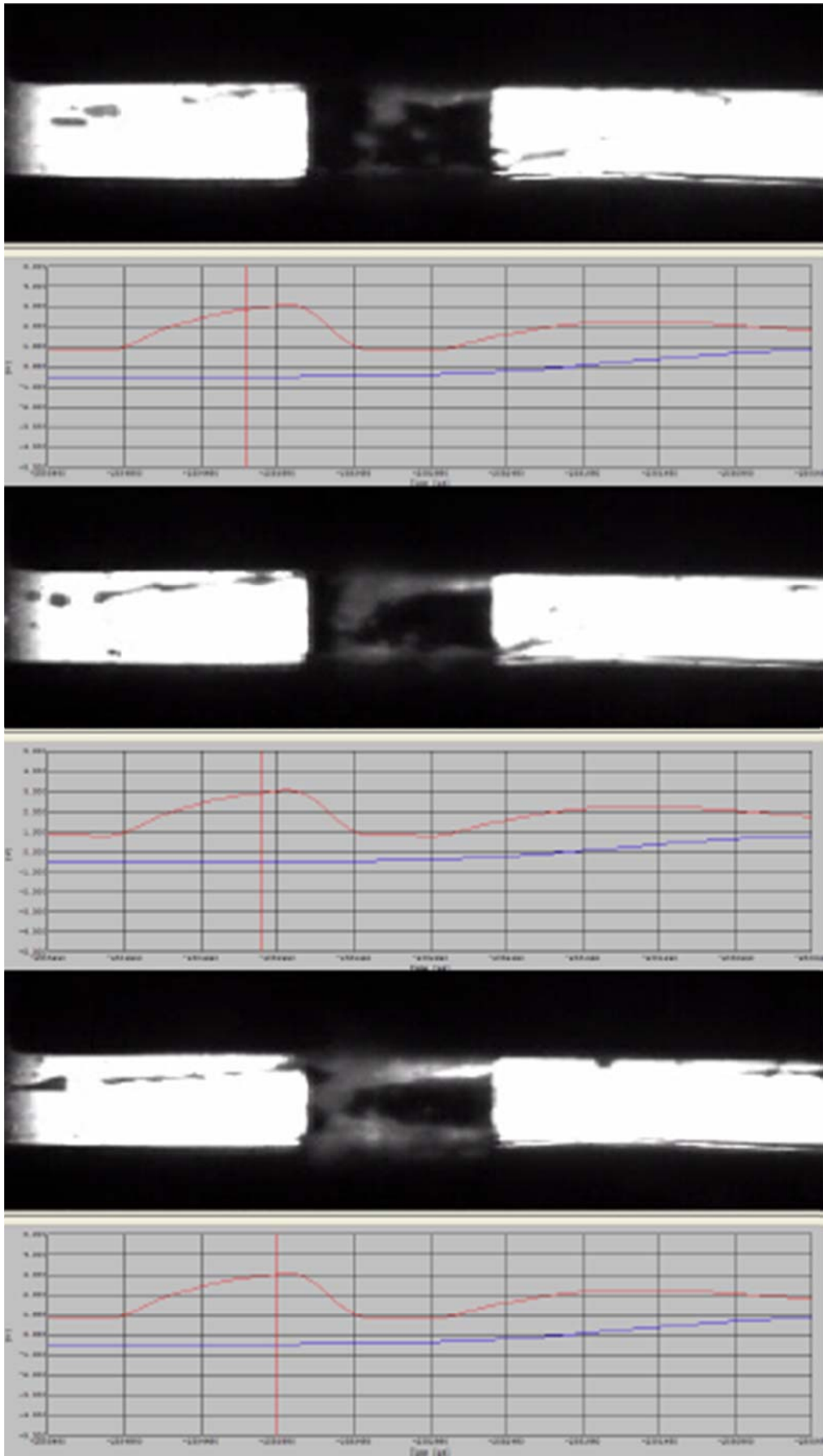


Figure 6-72 Exploding button test on Mc Gregor (part 3)

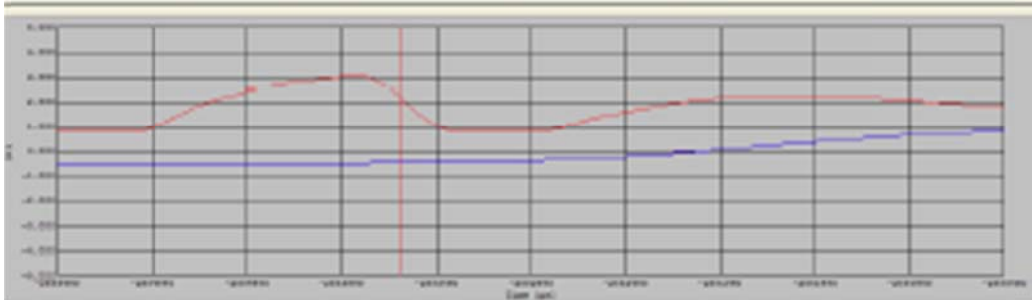
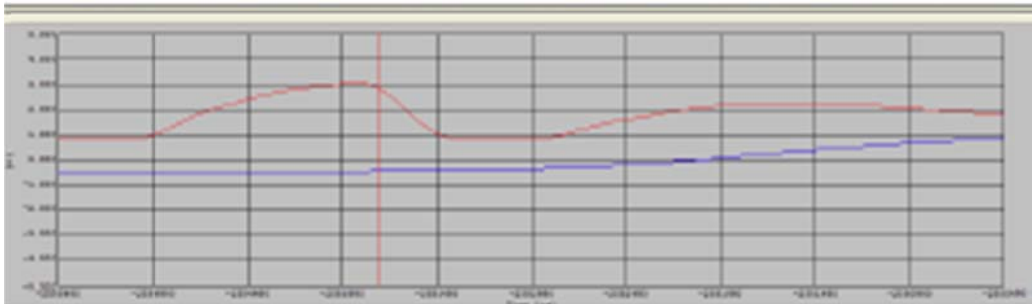
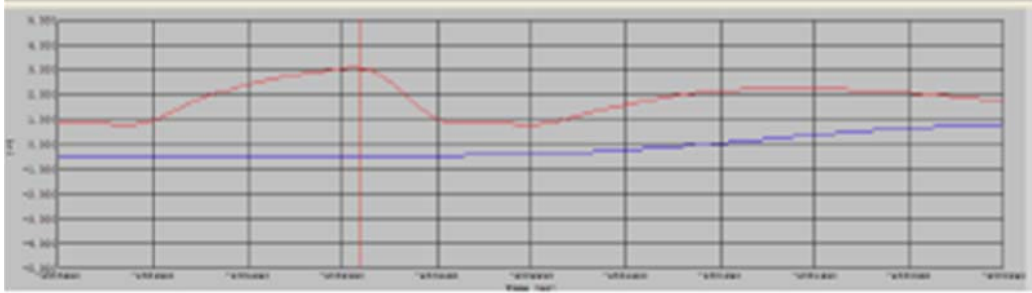


Figure 6-73 Exploding button test on Mc Gregor (part 4)

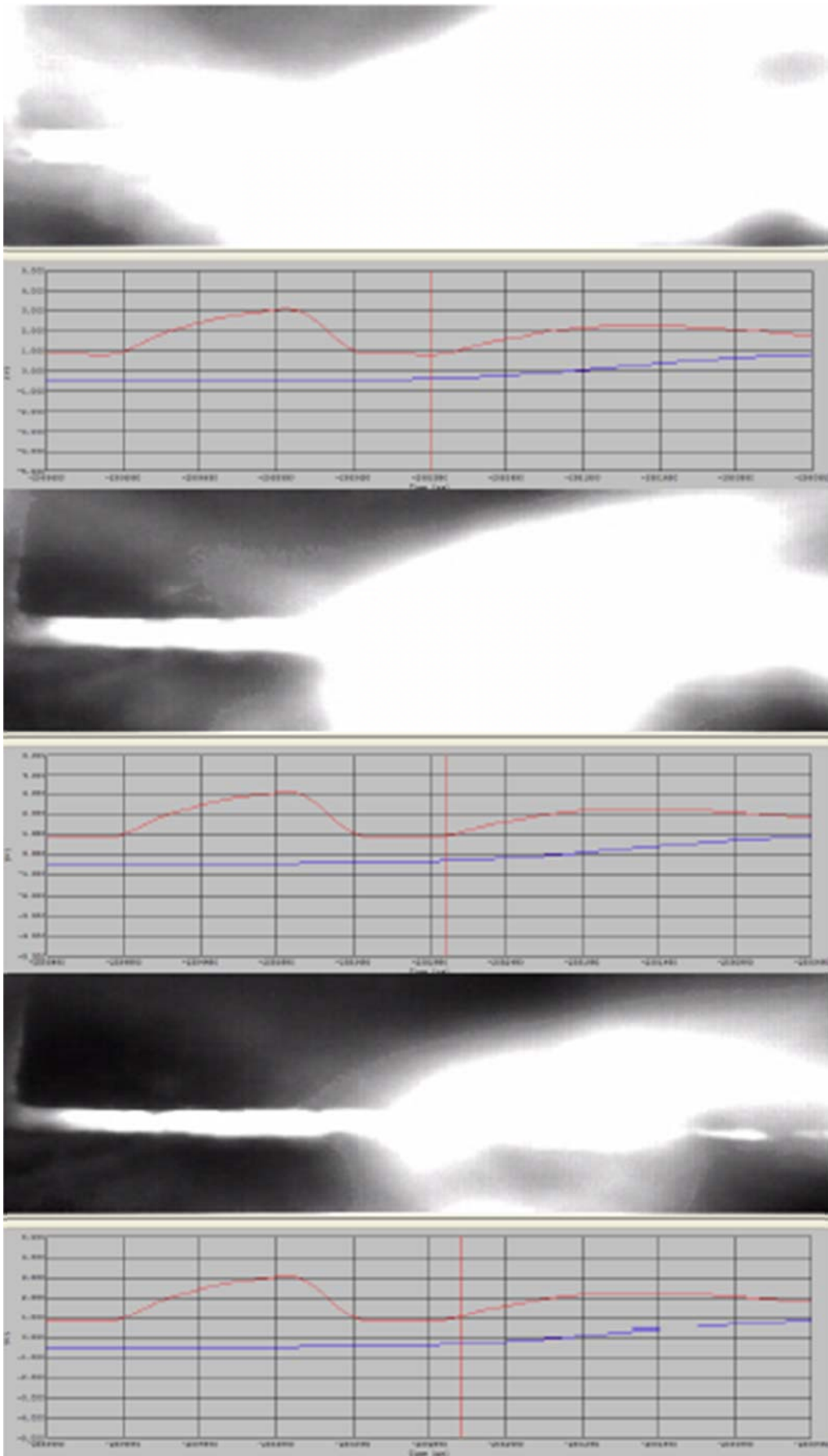


Figure 6-74 Exploding button test on Mc Gregor (part 5)

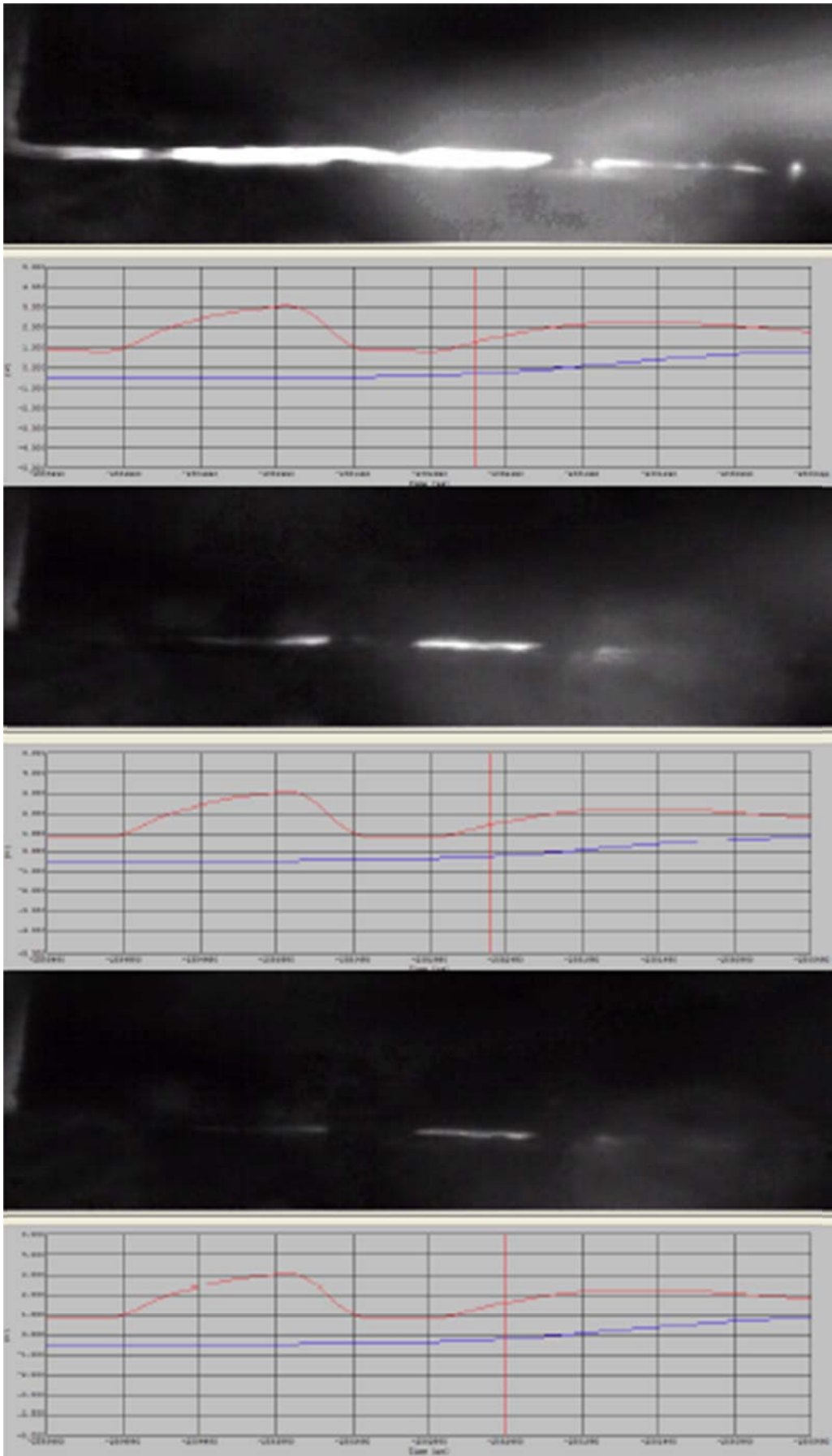


Figure 6-75 Exploding button test on Mc Gregor (part 6)

Welding head velocity response signal and the initiating current causing the step function to take place corresponding with the frames given in Figures Figure 6-70 to Figure 6-75 are displayed below in Figure 6-76 and Figure 6-77, a zoom of the former.

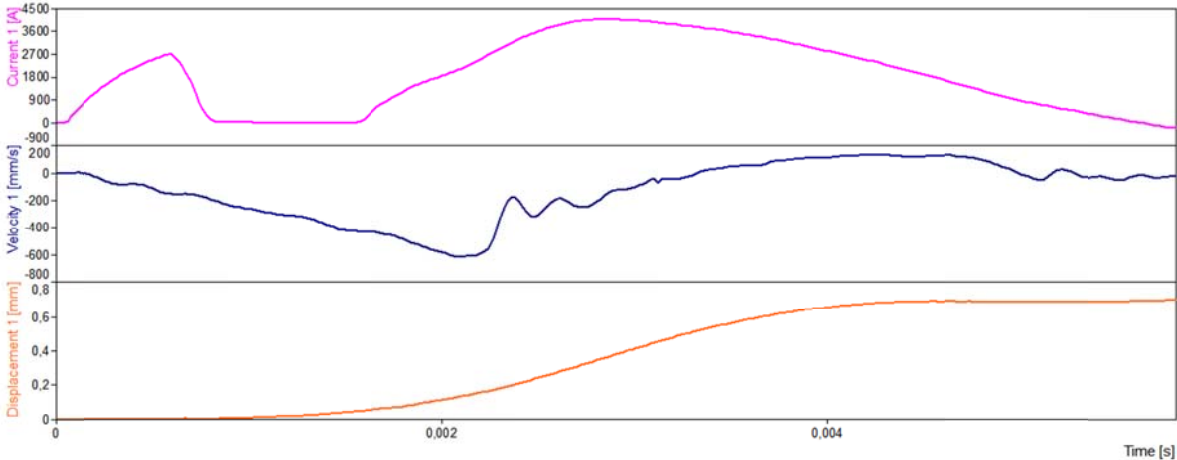


Figure 6-76 Current, velocity and displacement signal from exploding button test on Mc Gregor

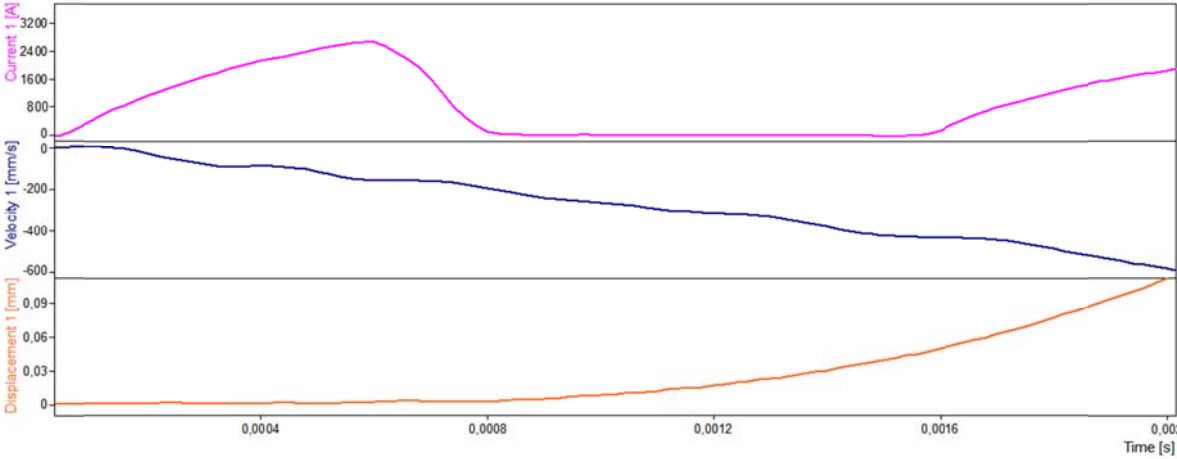


Figure 6-77 Current, velocity and displacement signal from exploding button test on Mc Gregor (zoom)

It is clear from these graphs that no conduction due to the button occurs, from the moment on where the explosion takes place until nearly complete setdown of the electrodes. The latter shows from the high speed images in Figure 6-70 to Figure 6-75 above. The fact that conduction is restored before complete setdown of the electrodes is due to the use of the Fronius Deltaspot process tape used as intermediate layer. (see Figure 6-78 below)

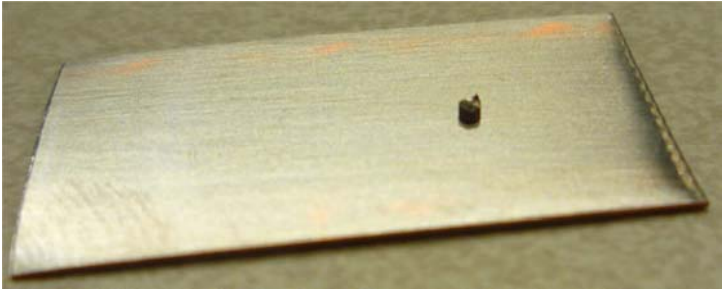


Figure 6-78 Fronius Deltaspot process tape with 0.8mm x 1.2mm diameter button

This process tape offers the advantage that it is made of Copper plated AISI 304 stainless steel with the Copper plating removed from one side. The latter initiating less heating on the side of the electrodes (when it is introduced with the copper plating towards the electrodes) and initiating increased heating in the contact with the Chromium steel button in between. Other very important advantages of this process tape is the availability at low prices and the possibility to cut it to a suitable size with normal scissors.

A disadvantage when manipulated is the loss of full flatness (visible in Figure 6-78 above and Figure 6-79 below), the latter causing current flowing between the intermediate layers when they touch before complete setdown of the electrodes.

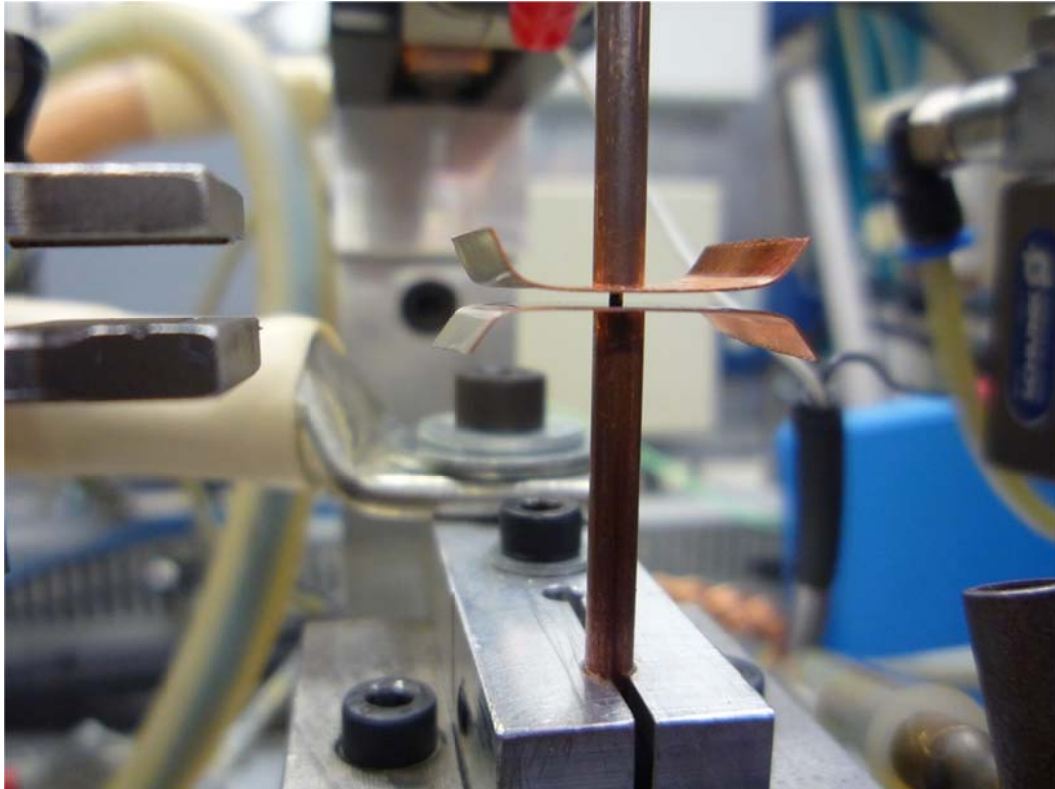


Figure 6-79 Button and intermediate layers positioned between electrodes on Mc Gregor

This phenomenon is also visible in the high speed recording images in Figure 6-74 and Figure 6-75 where you can notice the intermediate layers (the black areas above and below the gap where the button disintegrated) no longer being positioned completely horizontal. Maximal welding head velocity reached with the explosion of this 0.8mm thick button, sliced of 1.2mm diameter 17% Chromium steel filler wire is 608mm/s, in a time period of 0.00192s, giving a mean acceleration value of 317m/s² with an measured actuator load of 46N.

When considering this as a motion with constant acceleration, Newton's second law of motion would give us a calculated mass of 0.145kg.

Comparing this with test 2 from Table 6-13 above gives us identical values. Indeed, the damping values are of an order to allow them to be neglected.

The 'digging-in' in the surrounding stainless steel layers also takes place with the buttons before exploding. Material actually is sprayed away sideways, creating a cavity and sometimes even a hole in the intermediate layers. The latter effect creates space for the element to explode, in this case a Chromium steel button.

Notice also that free motion is enabled from the moment that melting takes place.

6.6 ARO Servo electric

Without full access to this machine and its control system, it is impossible to perform fracture or explosion tests on it and draw conclusions from them.

6.7 Overview of results per machine tested

Please find in Table 6-14 below an overview of the calculated machine data with their 95% confidence intervals as they were calculated following fracture and explosion tests on each machine tested and using the data processing procedure as described in Section 5.2 and in detail in Appendix D.

Values for damping factors are not given since these are dependent on friction, highly influenced by the specific force level at which the (fracture) test is performed. The latter shows clearly from the results in Section 6.

	Calculated mass [kg]	(95% CI)
AWL multi purpose spot/projection welder		
Fracture, no spring in system	12,15	(11,95-12,34)
Fracture, outside working range spring	11,98	(11,71-12,25)
Fracture, inside working range spring	10,58	(10,04-11,12)
Exploding button, inside working range spring	9,89	(9,66-10,13)
Exploding ball, inside working range spring	9,88	(9,55-10,21)
PECO Messer Griessheim roll membrane welder	8,23	(8,18-8,28)
ARO multi purpose welder (pneumatic)	21,35	(21,13-21,58)
Mc Gregor μ-resistance welding head	0,135	(0,131-0,138)

Table 6-14 Overview of machine data on all machines tested

7 Discussion

In this chapter, discussion of results generated during the present work as well as their comparison to other published data is included. It is divided into four sections:

a) use of different step function imposing tests and machine evaluations

Use of the fracture and explosion test procedures and their resulting machine specific data is expected to contribute to more detailed and correct data input into Finite Element Analysis software. The latter resulting in more realistic output that mimic reality more closely.

The degree of realism in the presented model and its supporting procedures is compared with previous published work.

b) importance of machine specific phenomena like ‘stick-slip’, viscous damping and even the welding current itself on machine mechanical behaviour will be analysed and discussed. Understanding the influence of the specific make of a resistance machines welding head on behaviour will allow for a more correct choice of machine towards a specific welding application.

c) machine follow-up improving devices

Mechanical machine response during the follow-up stage in projection welding can deliberately be adapted to a specific welding application. Practical design solutions will be proposed.

d) alternative design geometries for projection embossments

Improved weldability as well as properties of the joint after welding can be achieved by using alternative geometrical projection designs. The latter in the meanwhile patented and fully implemented in windscreen wiper design as well as in high-end cookware;

7.1 Step function imposing tests and machine evaluations

There are undisputable differences between the fracture and the explosion test that result in a potential shifted application field for both tests in practice. Also the degree of difficulty to install and/or conduct the test on a specific machine is discussed.

Adoption of the test in International Standards like ISO 669 like for instance in its Annex A ‘Dynamic mechanical behaviour’ would be advisable.

7.1.1 Fracture test

This test offers the possibility in combination with the model presented in this thesis to make machine evaluations and calculate machine specific data that in turn enables more realistic numerical simulations of a resistance welding application on specific machines.

It is a simple test, capable of imposing an aggressive step function on the mechanically loaded welding heads from normal load to zero load.

The test in its closed canister design is completely safe and uses standard and low cost dowel pins or alternative brittle breaking elements.

Measurements made during fracture tests on different machines in Chapter 6 reveal that this test in combination with the processing procedure presented in this thesis enables the

calculation of the lumped mass of the moving welding head following a single or at maximum a few tests.

Following the tests conducted on the AWL standard spot/projection welder under study in this work (see 6.2 AWL machine), it is clear that this test is capable of determining damping characteristics of a machine at a wide variety of different actuator loads.

This evaluation is possible due to the large displacements automatically made by the moving welding head in response to the step function that this specific test imposes on the machine. Displacements in the order of a cm or even more are normal as a response to a fracture imposed. This is in contrast to what happens in reality as soon as a welding head comes in motion, attempting to follow the decreasing reaction force against the actuator force when workpieces collapse under heating. Displacements in the order of a few tenths of a mm to a few mm at maximum are of a more realistic level considering the large majority of welding applications. However, in projection welding of hollow components, like cross-tube welding or in projection welding of materials with lower Elasticity Moduli, larger displacements occur.

The fracture test allows us to make a complete evaluation of the mechanical properties of a resistance welding machine's moving welding head in full accordance with the theoretical approach of pneumatic actuators by Gould [23], [21]. The latter is very interesting for general understanding of all machines where the welding force necessary is generated through an actuator that is driven at nearly constant force. This is the case for all fully pneumatic actuators and for actuators where an actuator (pneumatic, hydraulic, electro-mechanic or piezzo-electric) with a bi-stable state (on or off) loads a spring actuator when it is in its on state, under condition that the spring is well-chosen in order not to drop too much force during the displacements due to be made during welding.

The theoretical model used copes well with reality as is proven by the calculated results using the processing procedure developed in this work. Calculated lumped masses are very realistic and close to weighing results of the dismantled physical components of the welding head tested. Calculated damping coefficients are also realistic and follow the same tendency as frictional measurements.

Disadvantageous in the use of the fracture test is the introduction of a significant shock to the machine frame, the machine arms, the moving welding head as well as in the machines' foundation. This leads to a lot of vibrations that are effectively measured along with the response signals. These vibrations do not jeopardize the calculated results as such, they however highly influence the regression coefficients obtained when calculating the model results.

The major disadvantage in the use of the fracture test is however the issue of the large scatter on the force level at which the fracture effectively takes place. This necessitates the application of a force measurement system on all fracture tests made, in order to enable correct calculation of mass and damping factor in processing afterwards. Additionally it needs to be mentioned that the fracture test is not applicable on micro welding machines due to its physical dimensions.

Using the fracture test in its open design requires safety precautions to be made before conducting the test in order not to harm personnel or damage equipment with the ejected fracture pin. These particles are projected away and reach very high velocities, making them dangerous projectiles that can travel several metres.

Although small versions of the test were made and used, application of the test on a micro-welding machine is very difficult to impossible due to lack of stable breaking elements.

7.1.2 Explosion test

This test, reported earlier as an easy means for hands-on machine comparison [24] at TWI and British Steel [25] and proposed by Gould [23] in his so-called ball model describing the follow-up process of a resistance welding machine, offers the possibility in combination with the model and processing procedure presented in this thesis to make machine evaluations and calculate machine specific data. The latter data subsequently enable more realistic numerical simulation of resistance welding applications.

It is a very simple test, capable of imposing a step function on the mechanically loaded welding heads from normal load to zero load and all of this without imposing vibration in the machine frame, its arms, its welding head nor in the machine foundation.

The test is completely safe when simple shielding by means of a piece of cardboard or an alternative is used. It can be operated with standard ball bearing elements or with custom made buttons that can be cut to the required dimensions from low-cost standard welding filler wire.

The test setup for an explosion test is so simple that nothing on the machine to be tested needs to be dismantled or replaced. The element to explode is placed between a sandwich of two intermediate conductive layers and introduced between the machine's electrodes, followed by the execution of the test. The power source of the machine under study itself delivers the energy necessary for heating and vaporising parts of the element to explode and its surrounding intermediate layers.

Measurements made during explosion tests on different machines in Chapter 6 reveal that this test in combination with the processing procedure presented in this thesis enables calculation of the lumped mass of the moving welding head following a single or at maximum a few tests.

In contrast with the fracture test, this test does not allow for imposing a step function on a machines' welding head that results in large displacements. Nevertheless, it allows for realistic displacements that mimic those made in the vast majority of projection welds. The fact that the extreme case of a splash weld is highly surpassed by this test, still resulting in very smooth kinematic responses by the welding head without introducing vibrations into the machine, is certainly an advantage.

Hence, machine behaviour as response to the worst case scenario in projection welding can be measured. As a matter of fact, previous publications [19], [20], [21], resulted in a boost in understanding of the welding process, but they all describe follow-up over large displacements, the latter enabling for welding head velocities to increase to extreme values never reached during real welding. However, reference [18] advises to use a real circular projection and have this heated above the expulsion limit to make machine evaluations.

Following the tests conducted on the AWL standard spot/projection welder under study in this work (see 6.2 AWL machine), it is obvious that the use of this test, followed by the data processing procedure presented in this work is to be made with the necessary precaution and with sound knowledge. Since the response signals only cover very small displacements not leading to high welding head velocities, it follows that damping effects as they are described by others [19], [20], [31], [34], [35], [23] are very difficult to be calculated and resulting in realistic and useable values.

It also needs to be mentioned that the explosion test can be executed to a certain actuator force level, depending on the energy the machine's power source can supply. High actuator loads will decrease contact resistances between the intermediate layers and the element to explode, leading in extremis to plastic deformation of the element rather than melting and vaporising it. All of this should not pose a problem, since the welding heads' lumped mass can be calculated at low actuator force levels and accelerations subsequently can be calculated at different actuator load levels. Calculated lumped masses are very realistic and close to

weighing results of the dismantled physical components of the welding heads tested. Results from tests on a Mc Gregor micro-welding head confirm the ease of use of this test in practice and have proven reliability considering the agreement between calculated mass by testing and the weighed values of the latter.

7.2 Measurements on AWL machine

7.2.1 Fracture and explosion tests

Results from fracture tests actually resulted in uniform values for calculated lumped mass of the moving welding head components in the lower actuator force values and with values above 3kN. However, within the 0.6kN to 3kN range, results deviated from the weighed values on the machine itself. Hence a quest for design drawings from the welding head followed without result at the constructor, resulting in the complete dismantling of the welding head. The latter revealing the presence of a spring coupling between actuator piston and moving welding head slide assembly, surrounded by a compression limiter, the latter enabling for setting the compression force range of the spring coupling. (see Figure 5-25)

Figure 5-26 shows a schematic block diagram representing the moving welding head with its degrees of freedom and limitations.

It must be mentioned that the fracture and explosion tests executed on the AWL machine revealed the typical construction of this specific welding head.

Fracture tests also show that a feature of this spring coupling is to disengage the piston with its seals and the piston rod with its additional mass from the rest of the moving welding head components. This alters machine behaviour favourably within the force range of the coupling spring.

7.2.2 Influence of current on machine behaviour

Explosion tests carried out on the AWL multi-purpose pedestal spot/projection welder revealed the influence of current flow on acceleration values measured. Welding current causing changes in welding force due to Lorentz forces generated were already mentioned in previous research by Williams [25], and others [36] and more recently confirmed in tests performed by Wu [37].

In the schematic representation of the secondary current path of a resistance welding machine in the right image of Figure 2-14 [37], Wu draws the directions of welding current and the directions of resulting Lorentz forces acting on the conductors. Two major influences can be noticed:

- a) Forces F_1 , acting on the horizontal conductors and directed outward from the welding window;
- b) Forces F_2 , acting on the vertical conductors and acting outward from the welding window;

Forces a) act immediately opposite to the normal actuator force thus decreasing the latter, explaining the decrease in acceleration from the welding head as soon as current is flowing and an immediate increase in acceleration from the welding head as soon as current is interrupted when the conducting button vaporises.

Forces b) act sideways on the moving welding head, thus in the explosion tests and the fracture tests with the application of current, they do not result in more friction in the force range where the coupling spring between actuator piston rod and lower slide is active (between 0.6kN and 3kN), thus inducing no influence on actuator force and acceleration in

this working range. These forces however have a significant influence leading to increased friction out of the working range of the coupling spring or even more pronounced in the tests conducted with the spring coupling removed from the moving welding heads' assembly.

Note in Figure 6-37 that dismantling the welding head and removing the spring alters the influence that welding current has on reduction of the actuator force. The latter can only be explained by the increased friction present at the higher actuator forces. This is understandable considering the construction of the actuators' piston seal (see Figure 7-1). The latter is made with an angular lip squeezed progressively against the actuators' cylinder wall.

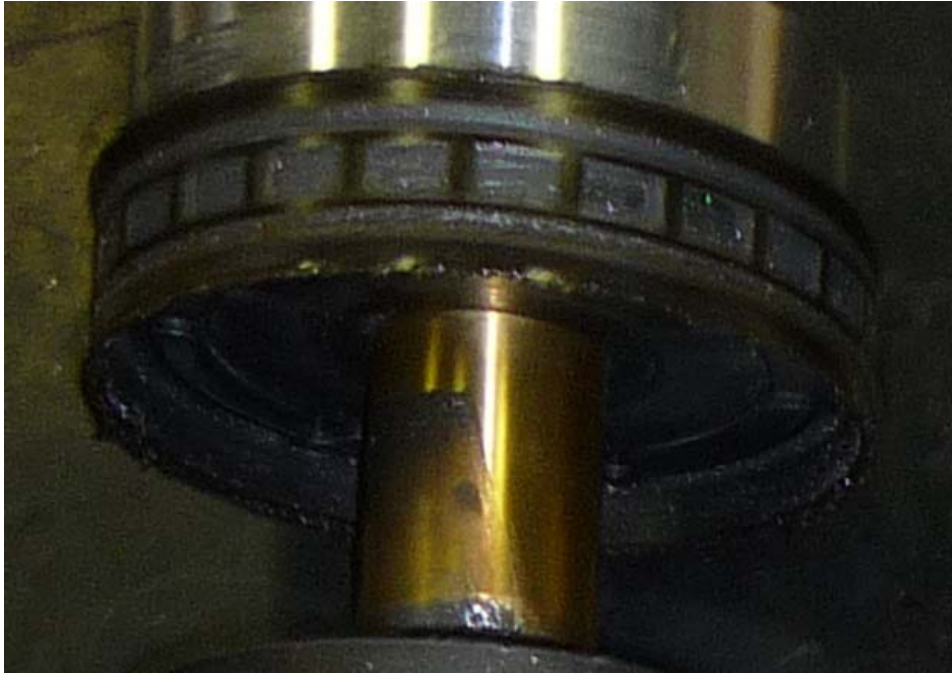


Figure 7-1 AWL piston seal

Fracture tests with the application of current during the test reveal that current indeed reduces acceleration of the welding head as long as current flows.

Following the definition of Lorentz forces,

$$F = \frac{\mu I_1 I_2 L}{2\pi a} \text{ [Nm}^{-1} \text{]}$$

Giving in the case of the fracture test in Figure 6-38 with length of upper conductor welding head (part of throat depth) = 0.26m and throat gap (or separation) = 0.18m:

$$F = \frac{2 \cdot 10^{-7} \cdot 10000^2 \cdot 0.26}{0.18} = 29\text{N}$$

This value is certainly of the same order as the loss of force causing the decrease in acceleration leading to the difference in displacement as seen in Figure 6-38. Lorentz forces will also cause the moving welding head to be loaded with a force faced outwards, with the dimensions of throat depth = 0.3m and length of electrode assembly = 0.12m:

$$F = \frac{2 \cdot 10^{-7} \cdot 10000^2 \cdot 0.12}{0.3} = 8\text{N}$$

7.2.3 Fracture tests with application of lateral force

From these tests, simulating Lorentz forces acting lateral and outwards on the moving welding head seen in Figure 6-41, we conclude that no significant influence can be measured in the actuator force range (0.6kN to 3kN) where the coupling spring disengages the piston and piston rod from the lower slide.

Tests conducted with an actuator force outside of the working range of the coupling spring, as seen in Figure 6-42, reveal a measureable influence due to increased friction between piston seal and actuator cylinder wall. Removing the coupling spring from the actuator assembly increases the influence as seen in Figure 6-43. However, when the forces used to impose a lateral load on the welding head to examine the influence were increased to over 100N, (exceeding Lorentz forces that might act in the lateral direction on the welding head realistic by over a factor 10), there is no further effect

The Lorentz forces act both laterally and axially and the axial effect in this AWL machine setup has a more significant influence.

7.2.4 Stick – slip test

Much research in the past focussed on specific machine properties and their influence on machine behaviour [31], [34], [35], [26], [27], others focussed on the influence of these properties on weld quality and electrode life [6], [7], [30], [31]. Dupuy [38] concludes from his tests on five different pneumatically actuated machines that stick – slip influences machine follow-up behaviour.

In the tests conducted in the present work, the pneumatic actuated moving welding head of the AWL machine was forced in equilibrium at different actuator loads by means of inflating a rubber bellows. Afterwards, the moving welding head was manually displaced upwards, immediately followed by recording the actuator force. Subsequently, the moving welding head was manually forced downwards, again followed by recording the actuator force.

The results give us the static friction of the welding head at different actuator loads. Kinematic friction is generally accepted in engineering machine construction guides, to have values of 10 to 20% lower than the static friction values.

From Table 6-10 and Figure 6-44, we conclude that the absolute value of static friction (and automatically the absolute value of kinematic friction) increases with increasing pneumatic pressure in the moving welding head actuator. Considering the physical design of the piston seal on this AWL machines' actuator, this is logical behaviour. Increased pneumatic pressure in the actuator cylinder will squeeze the sealing lips tighter to the cylinder wall, thus increasing friction.

The additional influence of lateral force will be similar at different actuator pneumatic pressures, since the lateral force will force moving welding head in the lateral direction, but always proportional to the lateral force acting on it.

When looking at the fracture test results in Table 6-1 and Figure 6-10 in combination with the stick-slip friction tests from Table 6-10 and Figure 6-44 then we conclude that damping effects in welding head motion are caused by friction rather than viscous damping in the welding cylinder.

7.2.5 High speed camera evaluation

Both exploding ball as exploding button tests were evaluated on the AWL machine by means of high speed video recording. Both test procedures using intermediate conductive layers with a high bulk resistance and high contact resistance values result in significant ‘digging-in’ by the element exploding into the intermediate layers. The latter creates a cavity capable of encapsulating remains of molten material from the exploding element that wasn’t projected away during the explosion. This effect prevents the welding current resuming before the electrodes make contact again. Exploding button tests show less tendency for molten material to remain trapped since there is a more pronounced tendency for material from the contact area ‘intermediate layer – button’ to be projected to the side instead of down and upwards.

The welding head velocity signals as a response to both these step function imposing tests (ball and button) have a very smooth course, without abrupt changes in velocity as seen in the fracture test responses.

The major practical advantage of the exploding button test is the ease of application as the button remains in place as it is introduced between the welding heads. The use of intermediate layers avoids damage to electrodes and allows us to introduce the sandwich intermediate layer – button – intermediate layer with ease between the standard electrodes mounted on a machine.

7.3 Measurements on PECO roll membrane machine

Results from fracture tests made on this machine, presented in Table 6-11 and Figure 6-61 lead to the conclusion that a welding head with this specific feature of a so-called low friction piston results in follow-up behaviour ruled by a still significantly high mass of 8kg and damping values comparable with those obtained with a standard pneumatic actuator like the one on the AWL machine. What does show as an advantage is the damping factors not increasing with increasing actuator force, as could be expected from this type of actuator. This is only advantageous when large displacements are needed, for instance in a projection welding application.

7.4 Measurements on ARO pneumatic multi-purpose machine

7.4.1 Fracture and explosion tests

Fracture and explosion test results presented in Table 6-12 and Figure 6-62 both reveal the high lumped mass of this moving welding heads’ assembly in full agreement with the weighed values of the dismantled individual components. Damping factors increase proportional with pneumatic pressure in the actuator as could be expected from this type of actuator.

It shows from these tests that this is not the optimal machine for projection welding of components that require fast follow-up at low actuator forces.

This machine was used for evaluation of wire pieces or buttons to serve as an exploding element in an explosion test. Results in Figure 6-63 reveal the necessity for sufficient welding current to apply at a given actuator force in order to measure the welding heads’ response rather than the plastic deformation of the wire or button.

7.4.2 High speed camera evaluations

These high speed video recordings were made from a distance with a zoom objective, resulting in clear macro view on material being expelled from between the electrodes. All explosion tests carried out for this occasion were conducted without the use of intermediate layers increasing heating and ‘digging’. It shows clear from the images in Figure 6-66 and Figure 6-67 that initial heating causes the ‘digging’ effect into the electrodes as also noticed in more detail and with a microscope objective on the AWL machine, followed by the overheating and vaporising of material, driving most molten material away in a horizontal plane due to the limitation made by the electrodes.

Vaporised material is clearly visible as a white cloud escaping from between the electrodes.

Interesting to notice also in Figure 6-67 is the secondary explosion occurring due to the bouncing effect of the moving welding head and the deflection of the fixed electrode.

7.5 *Mc Gregor* μ -resistance welding head

7.5.1 Explosion tests

Table 6-13 and Figure 6-68 give the processed results from explosion test made on this welding machine in-situ at the Philips plant in Turnhout Belgium and confirm why this small machine is used as a standard in hundreds of factory mechanisations. Due to the small lumped mass of the welding head, measured accurately from the processing procedure presented in this work, and in full accordance with the weighed values of the components in combination with very low damping coefficients defined, this is an extremely fast workpiece collapse follower.

This statement is to be taken literally, since a difficult cross-wire welding combination between a Molybdenum and a steel wire, that is a high melting against a low melting material, often used by Philips to evaluate the follow-up capabilities of a welding application does not explode under identical conditions used in the explosion test as is apparent from high speed recording.

7.5.2 High speed camera evaluations

High speed recording revealed the synchronisation between initiation of melting and establishment of a high acceleration value driving the moving welding head downwards.

The usefulness of Fronius Deltaspot tape as an intermediate layer is proven, offering the possibility of even higher current loading without damaging the electrodes. The use of this copper plated AISI 304 stainless steel process tape is simple and its use is highly recommended. (you can simply cut the required length from a reel with normal scissors, bend it in the shape you like to handle it with the most comfort, place the button in between and introduce the sandwich between the electrodes)

With a little attention, the disadvantage of the intermediate layers touching and conducting too early can be prevented.

7.6 ARO servo electric

Without full access to the machines' control system and its control algorithms it is impossible to even conduct fracture tests on this machine. Explosion tests work, but since the spring follow-up system, present in each of these machines was pre-installed and loaded to operate at a force level above 4kN, data obtained from explosion tests executed below this force level are not reported. Without the feature of the spring follow-up system, there remains a slow following system of the servo motor with its drive spindle, in the configuration of our laboratory machine capable of developing a maximum velocity of 200mm/s.

8 Application of testing methodology to projection welded parts

8.1 Innovative welding cycle

In the course of this PhD study, the author used both step function imposing tests and the processing procedure developed during this work on several machines and applications in industry. Since the author works in consultancy towards companies using resistance welding as joining technology, dozens of applications passed the revue in the past six years.

Through the possibilities created by the tests and procedures described in this work, realistic input of a highly mechanised Bihler resistance welding machine to weld Bosh Aero-twin® windscreen wipers was possible in Sorpas® commercial finite element code. This enabled the author to calculate the necessary ‘hold-time’ [5] to enable the C45 spring steel used for the beams of these windscreen wipers to cool down under maintained clamping by the electrodes, and just long enough to allow for post-weld heat treatment in the same single clamping operation, thus annealing the brittle heat affected zone of the eight welds made simultaneously.

Since the lumped mass m [kg] cannot be weighed straightforward, since the welding head has a pivoting design, actuated by a spring that’s driven by an hydraulic on/off actuator. Both fracture and explosion test enable for correct calculation of the lumped mass that plays in the welding head kinematics for this specific machine design.

To allow calculation of realistic temperature-time values with Finite Element modelling software, it inherently implies realistic calculation of workpiece deformations. Moreover, when calculated deformation deviates, current densities will do so as well, especially leading to unrealistic temperature time curves (see Figure 8-1).

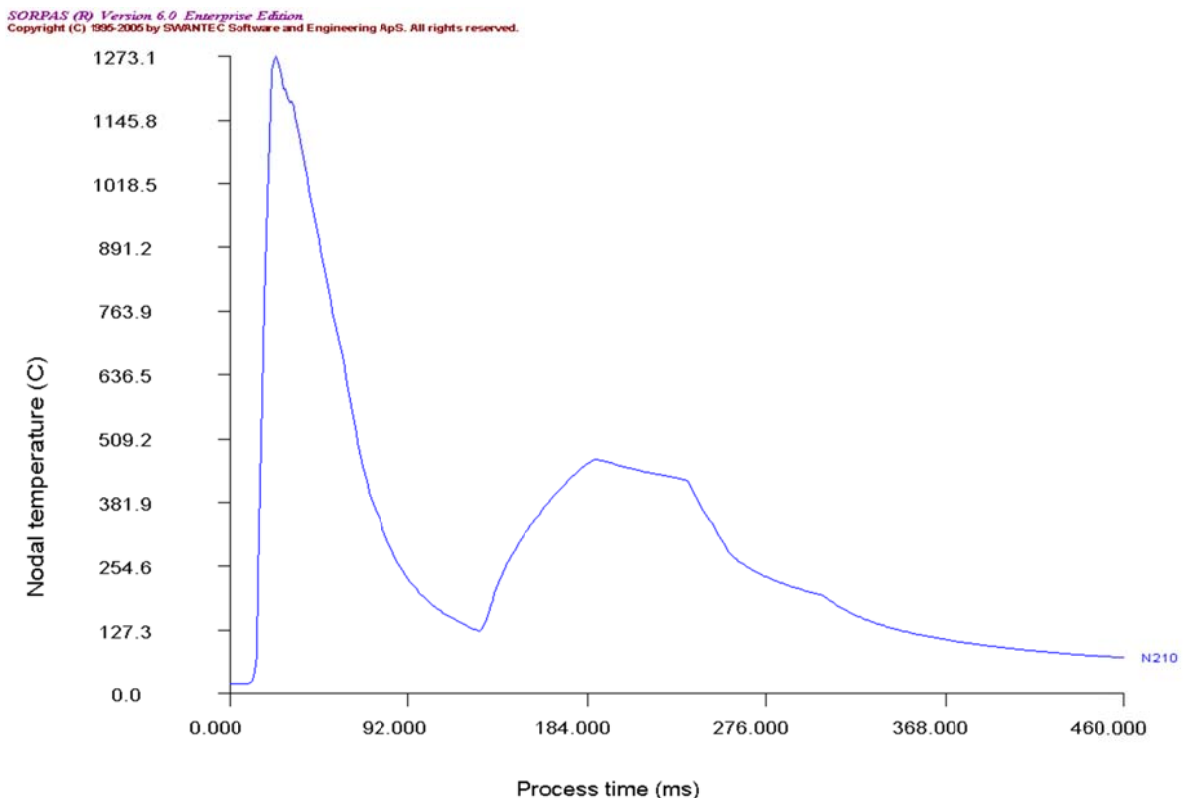


Figure 8-1 Temperature time curve of a node in the HAZ calculated with Sorpas®

The latter resulting in useless machine weld settings (see Figure 8-2) producing brittle welds.

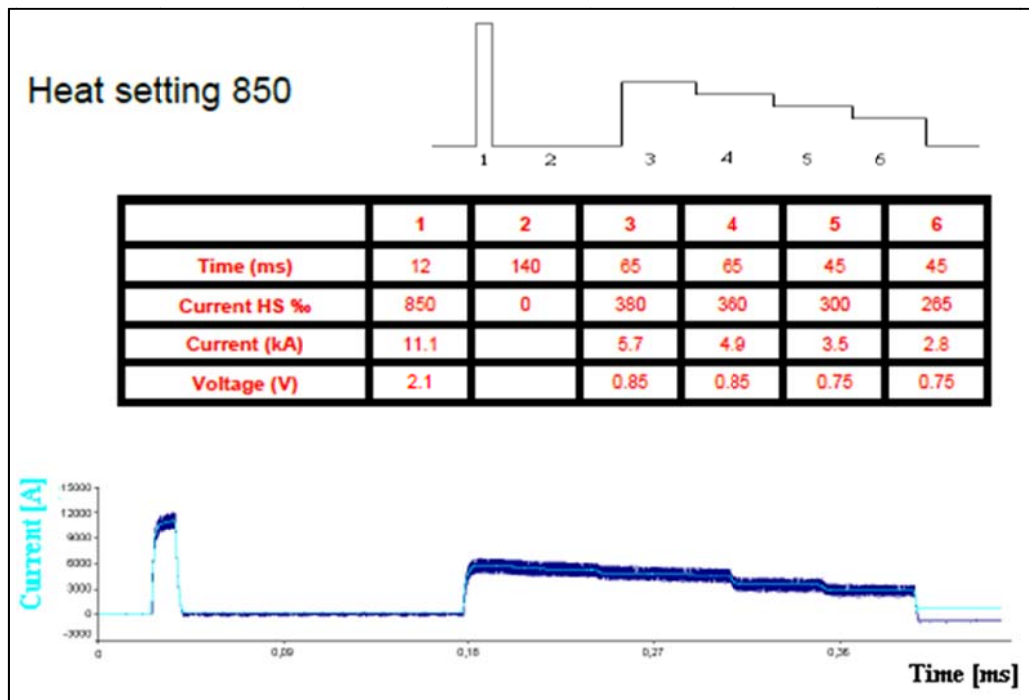


Figure 8-2 Example of machine parameter setting and resulting current flow

Correct data input results in useful temperature time curves, subsequently leading to useful machine parameter settings and sound welds (see Figure 8-3 left image). On the other hand, calculating incorrect machine parameter settings result in extremely high hardness values and unavoidable cracking in the HAZ (see Figure 8-3 right image)

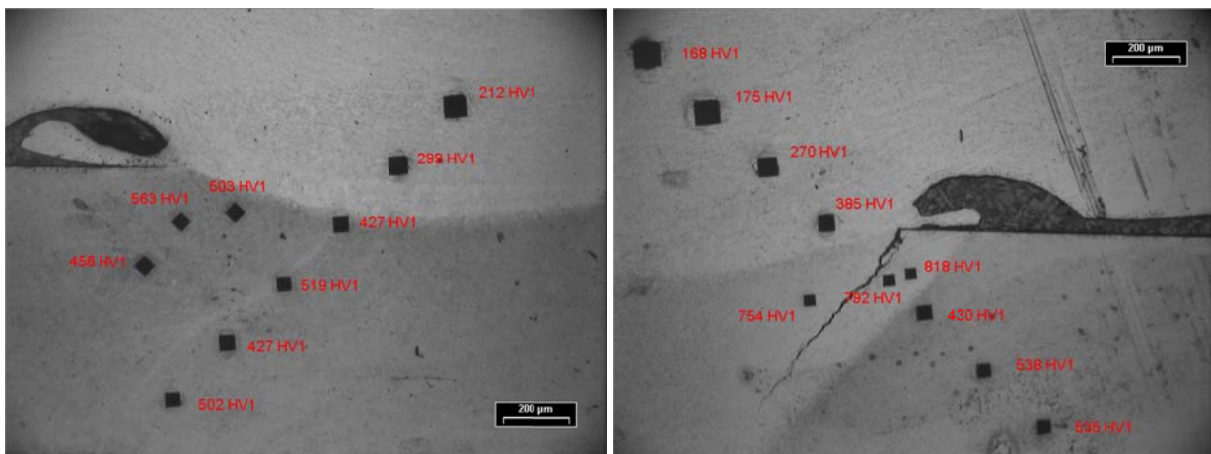


Figure 8-3 Hardness measurements, weld with good (left) and useless (right) machine parameter settings

Searching for a welding – cooling – post weld heat treatment cycle in the classical way by means of practical tests is comparable to searching for a needle in a haystack, as already commented by Gould [5]. The fact that this rather innovative welding cycle allows for post weld heat treatment to start from the hottest spots just welded and cooling down due to the higher bulk resistance of the material at these eight spots saved an enormous amount of machine capacity, thus doubling output and decimating scrap production. Previously, welds ruptured prior to the implementation of this technique in transport from a welding machine to a post weld heat treatment station. Current welding and post weld heat treatment of the eight

welds in a single windscreen wiper are performed with a floor to floor time of less than a second.

For the moment, those two machines produce finished products in one single welding – post weld heat treatment cycle, along with seven other new built machines.

8.2 Innovative projection geometry

Information available in Section 2.2, and especially data published by Harris and Riley [13] and by the ARO company [14], later confirmed and reported by Xin Sun [63], [65], in combination with the authors consultancy work at Bosch in micro-resistance welding resulted in the development of an innovative new projection geometry for use in the eight projection welds assembling the Aero-twin® windscreen wipers. This geometry, in the mean time patented DE 10 2007 012 700 A1 2008.09.18 consists of a central projection, fully surrounded by a groove, capable to receive all material squeezed out of the weld, thus maintaining the cross-sectional area of the current path through the projection. In a normal projection weld, the cross-sectional area continuously changes as the projection collapses, thus cooling the weld at constant current level.

On the other hand, this design allows for complete setdown of the two workpieces without any gap remaining. Supplementary, the groove around the projection, if well made allows for stress relief of the weld on the one hand and on the other hand creates a weaker area around the weld, thus relieving the weld and even the heat affected zone from bending stresses under dynamic loading.

All of this resulted in application of this geometry on all projection welding applications in the Bosch Aero-twin® wiper design, with significantly higher cycle test life and slam test resistance.

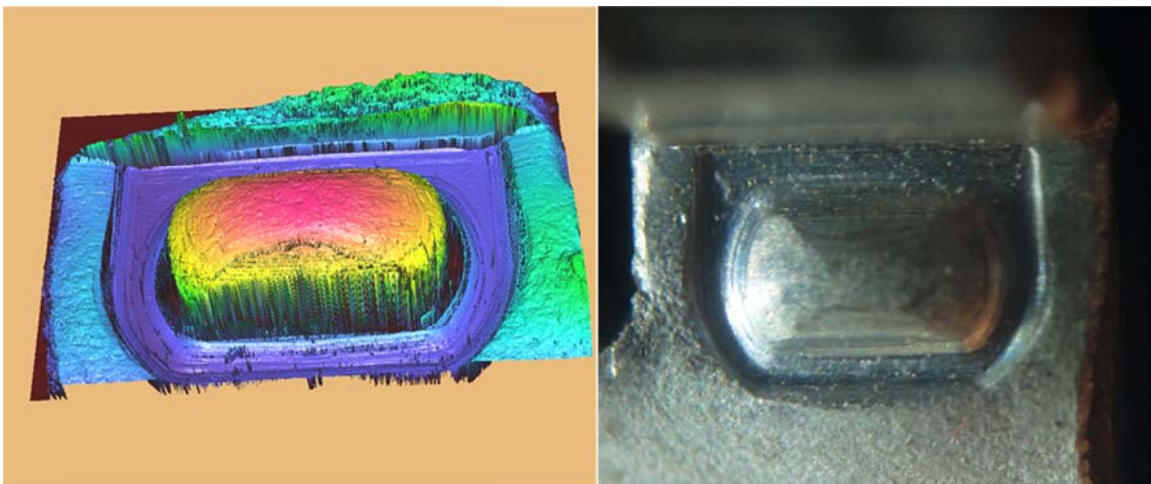


Figure 8-4 Prototype μ -surf scan (left) and series production projection (right)

Figure 8-4 above shows the μ -surf scan of a milled prototype tested in the Bosch Aero-twin wiper production on the left and the resulting mass produced projection design as patented and currently used in production.

To evaluate the influence of the sacrificial groove projection design in different materials and designs, comparative tests were made by this author. To enable mechanical testing of projection welds made with the former ‘normal’ design in comparison with welds with the contemporary ‘grooved’ design, test pieces with both geometries were produced with

dimensions as can be observed in Figure 8-5 below. Test pieces were also made in different materials.

The pink part in the figure simulates the plate material used in real welding, where the green part represents the part containing the projection.

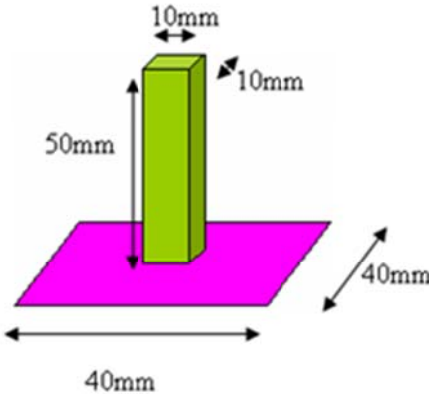


Figure 8-5 Dimensions of test pieces

To enable evaluation of the sacrificial groove in the design, comparative tests were made with an identical projection geometry apart from the groove. In Figure 8-6 and Figure 8-7 are photographs (right image is zoom of left image) of both geometries as they were machined on the bottom face of the green test pieces from Figure 8-5.

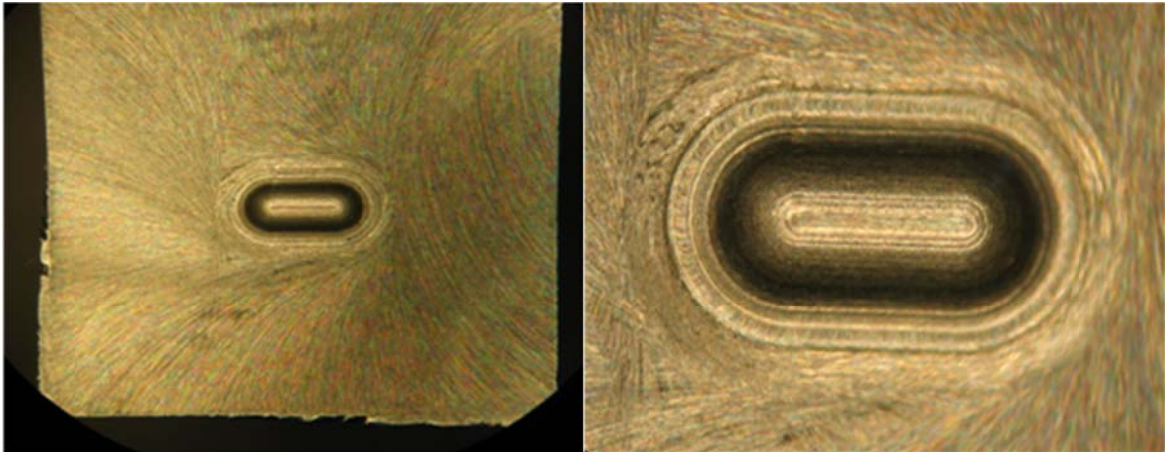


Figure 8-6 Projection design without groove

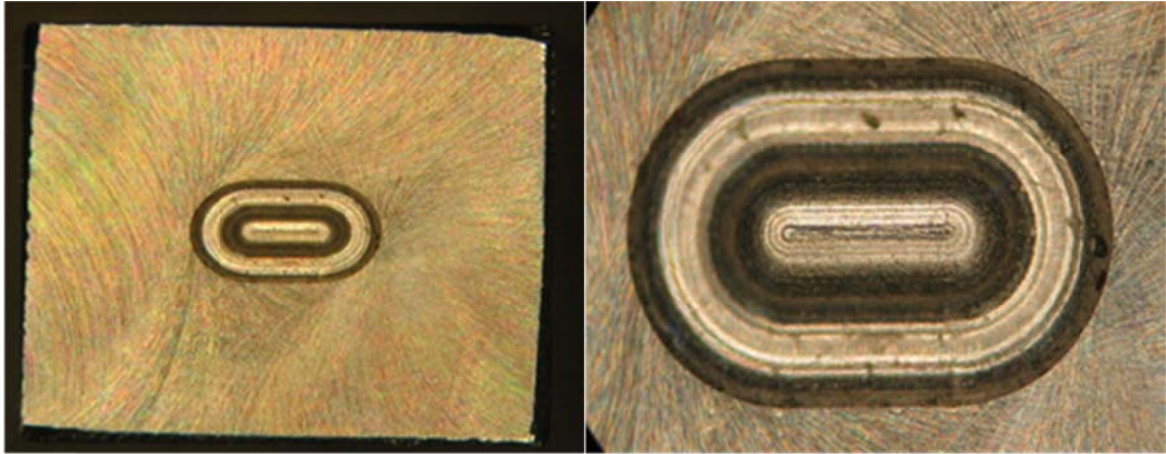


Figure 8-7 Projection design with groove

Figure 8-8 below gives a cross sectional view on the as welded geometry with a projection design without groove (left) and with groove (right).

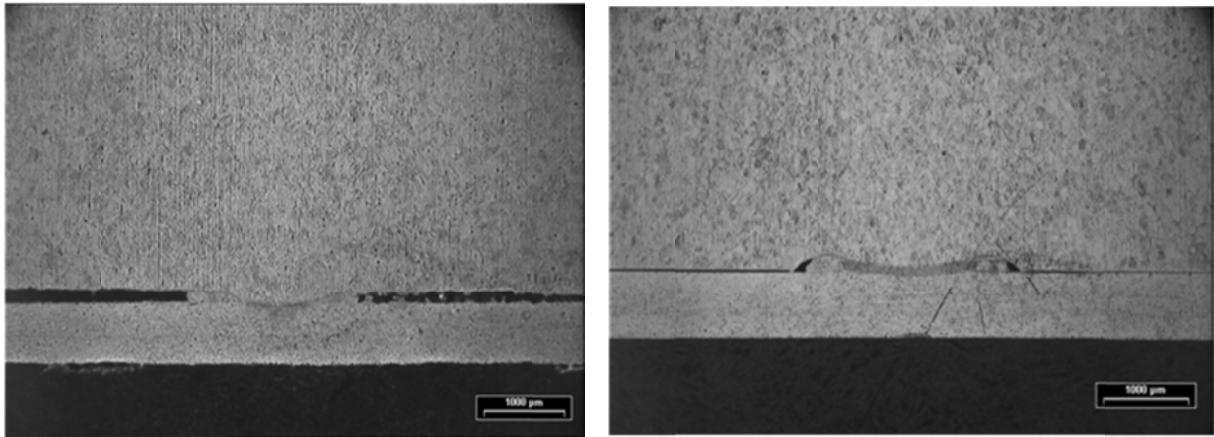


Figure 8-8 Cross-sectional geometry after welding

Furthermore, a multi-purpose clamping device (see Figure 8-9) was developed that allows mechanical testing on an Instron test bench in normal load (left), shear load (middle) and bending load (right).

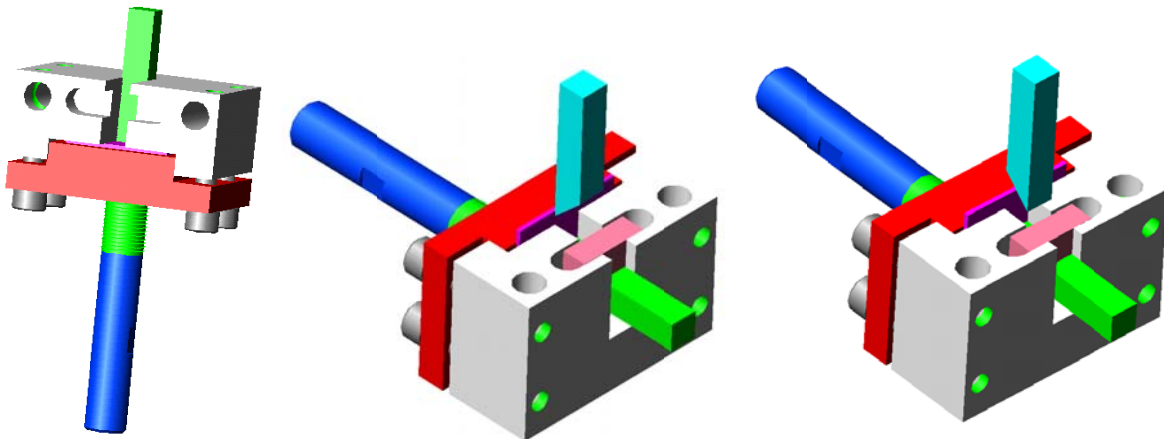


Figure 8-9 Clamping device for mechanical testing

In the mean time, the same design is implemented in the high-end series of cookware, designed by celebrated British architect John Pawson. The minimalistic design urged the author to introduce this projection design in every handle on lids, pots and pans from this series. (see Figure 8-10 below) The design with the sacrificial groove around the weld also increases the robustness of the joints.

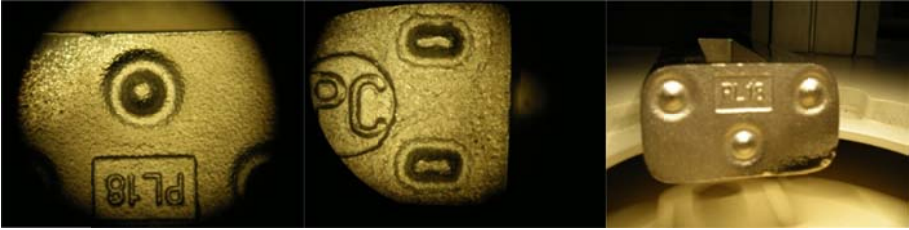


Figure 8-10 New projection design in casted stainless steel handles for cookware

9 Conclusions

- A new process model based on welding head response to a step function in actuator force and its necessary data processing procedure was developed. Welding head response signals can be recorded and both displacement or velocity response of the welding head on the imposed step function can be used as input for the data processing procedure. This enables calculation of total lumped mass of the moving welding head in combination with its damping factor.
- New and state of the art non-contact and non-invasive measuring and data-acquisition techniques and procedures were developed and tested that enable in-situ measurement of machine welding head responses to the imposed step functions. These measuring techniques also allow for assessment of a working resistance welding application in a running production environment.
- Machine specific data, related to a specific application can be measured and/or calculated and can afterwards be used as input data to enable more accurate finite element calculations of that specific welding application.
- A new test, the free fracture test, was developed to impose a step function on the welding head and hence calculation of machine parameters. This test was shown to provide accurate measurements. However, it imposes an aggressive step function (never achieved in real welding situations) which introduces vibrations.
- The explosion test was developed to more realistically simulate machine movement. This test also enables accurate calculation of effective lumped mass. Initial work utilised ball bearing elements but the final version of the test uses buttons, fabricated from welding filler wire where both the geometry and the material can be chosen. This test is straightforward and easy to use in-situ.
- The influence of Lorentz forces generated by the welding current on the force equilibrium in a resistance welding machine was examined. These forces are definitely present and alter machine behaviour. Specifically these effects can be important at low actuator force levels in combination with high current levels.
- The level of the static friction force and resulting stick-slip effects at different actuator force levels were studied and these match with the damping effects occurring during welding head response on a step function imposing test.
- High speed camera evaluations were made both of the free fracture test and the explosion tests. The latter leading to a better understanding of the physical processes taking place prior, during and after the explosion.

- An innovative new projection geometry was designed incorporating a sacrificial groove around the projection. This new geometry has major benefits in achieving full setdown with no gap left, and in maintaining stable current density and hence improve weld quality. This new technique has been used extensively in industry.

10 Recommendations for further work

- Although step function imposing test setups and procedures have been developed in this work, the author suggests that further work on optimisation might help for successful transfer to the workforce.
- Further research in the field of servo electric actuated machines, or even all types of actuators using an electronic feedback control for weld head motion would be advisable. This should however be executed with full cooperation of the machine constructor.
- Influence of current on machine mechanical behaviour could be a subject for further study.
- Explosion tests have the disadvantage that they cannot be used in the higher actuator force levels due to the decrease in contact resistance at these higher force levels in combination with insufficient available welding current from the machines' power source. It would be advisable to search for possible alternative materials or material combinations that allow for testing at higher load levels.
- Spring follow-up systems used in capacitor discharge machines to improve behaviour in projection welding deserve further attention, since this type of machines becomes more widely used in a wider variety of applications.

References

- [1] BS 3065 (2001), ISO 669 (2000), *Resistance welding - resistance welding equipment - mechanical and electrical requirements*, British Standards Institution, London.
- [2] ISO/DIS 14373.2 (2002), *Resistance welding - Procedure for spot welding of uncoated and coated low carbon steels*, British Standards Institution, London.
- [3] Kochan, A. (2004), "Volkswagen makes a success with lasers", *Assembly Automation*, vol. 24, no. 4, pp. 357-360.
- [4] Larsson, J. K. (2005), "Load Adapted Laser Weld Patterns Part 2: Crashworthiness Performance", *10th Nordic Laser Manufacturing Processes (NOLAMP) Conference*, Pite, Sweden, August 2005.
- [5] Gould, J. (1999), "Hold-time sensitivity and RSW [resistance spot welds] of high-strength steel. Weld process effects cracking", *Welding Design and Fabrication*, vol.72, no.8, pp.48-49, August 1999.
- [6] Williams, N. T. and Parker, J. D. (2004), "Review of resistance spot welding of steel sheets, Part 1: Modelling and control of weld nugget formation", *International Materials Reviews*, vol. 49, no. 2, pp. 45-75.
- [7] Williams, N. T. and Parker, J. D. (2004), "Review of resistance spot welding of steel sheets, Part 2: Factors influencing electrode life", *International Materials Reviews*, vol. 49, no. 2, pp. 77-108.
- [8] Hess, W. F. and Childs, W. J. (1947), "A Study of Projection Welding", *Welding Journal*, pp. 712s-723s.
- [9] Hess, W. F., Childs, W. J. and Underhill, R. F. (1949), "Further Studies in Projection Welding", *Welding Journal*, pp. 15s-23s.
- [10] Nippes, E. F., Gerken, J. M. and Maciora, J. G. (1950), "The Projection Welding of 0.010 and 0.020-In. Steel Sheet", *Welding Journal Research supplement*, pp. 441s-449s.
- [11] Nippes, E. F. and Gerken, J. M. (1952), "Projection welding of steel in heavy gages and in dissimilar thicknesses", *Welding Journal Research supplement*, pp. 113s-125s.
- [12] Roberts, J. E. (1956), "Resistance welding and productivity", *Welding and metal fabrication*, pp. 404-408.
- [13] Harris, J. F. and Riley, J. J. (1961), "Projection Welding Low-Carbon Steel using Embossed Projects", *Welding Journal*, pp. 363-376, April 1961.
- [14] ARO company publication (1966), "Resistance welding tubular components", *Welding and metal fabrication*, pp. 459-463.

- [15] Savage, W. F., Nippes, E. F. and Wassell, F. A. (1977), "Static Contact Resistance of Series Spot Welds", *Welding Journal*, vol. 56, no. 11, pp. 365s-370s.
- [16] Westgate, S. A. (2003), "Resistance welding - State of the art", *Welding and Cutting*, no. 5, pp. 256-260.
- [17] Westgate, S. A. (2002), "A general overview of recent developments in resistance welding", *Proceedings, 2nd International Seminar on Advances in Resistance Welding*, Aachen, Germany, November 2002.
- [18] BS EN 28167 : 1992 (ISO 8167 : 1989), "Specification for projections for resistance welding", British Standards Institution, London.
- [19] Romer, M., Press, H. and Krause, H. J. (1989), "Mechanical properties of resistance spot welding equipment and their mathematical determination (Mechanische Eigenschaften von Widerstandspunktschweisseinrichtungen ...)", *Schweissen und Schneiden*, Vol.41, no.1, pp.17-22, Jan.1989.
- [20] Romer, M., Press, H. and Krause, H. J. (1990), "Mechanical properties of resistance spot welding machines and their mathematical determination", *Welding in the World/Soudage dans le Monde*, vol.28, no.9-10, pp.190-196, 1990.
- [21] Gould, J. E. and Dale, W. (1994), "Theoretical analysis of weld head motion", *Proceedings sheet metal welding/conference VI*, October 12-14, 1994.
- [22] Feng, Z. (1997), "Analytical models for mechanical dynamics of resistance spot welding machine.", *Resistance Welding: Theory and Application Conference, American Welding Society*, October 13-16, 1997.
- [23] Gould, J. E., Feng, Z., Chou, J. and Kimchi, M. (1999), "Analytical models for the mechanical response of a resistance welding machine", *EWI Project No. 40634IRP*.
- [24] Rivett, R. M. and Westgate, S. A. (1980), "Resistance Welding of Aluminium Alloys in Mass Production", *Metal Construction*, vol. 12, no. 10, pp. 510-517.
- [25] Williams, N. T. (1996), "Factors influencing weldability and electrode life when welding coated steels in multi-welders and robotic cells", Report No. EUR 15712EN, ECSC Technical Steel Research Programme, Luxembourg.
- [26] Krause, H. J. and Lehmkuhl, B. (1984), "Measuring the dynamic mechanical characteristics of spot and projection welding machines - measured parameters, measuring procedures and initial results (Messgrößen, Messverfahren und erste Messergebnisse...)", *Schweissen und Schneiden*, vol.36, no.1, pp.18-23 (English translation of text and captions: pp.E7-E10), Jan.1984.
- [27] Krause, H. J. and Lehmkuhl, B. (1985), "A comparison of the dynamic mechanical characteristics of spot welding machines (Vergleich der dynamischen mechanischen...)", *Schweissen und Schneiden*, vol.37, no.1, pp.18-22, Jan.1985.

- [28] Satoh, T., Katayama, J. and Takafumi, N. (1988), "Effects of Mechanical Properties of Spot Welding Machine on Spot Weld Quality", *IIW Doc no III-912-88*, pp. 118-122, 1988.
- [29] Lehmkuhl, B., Press, H., Romer, M. and Weber, G. (1990), "Advances in process data acquisition and processing in resistance welding using pressure (Fortschritte in der Prozessdatenerfassung ...)", *Schweissen und Schneiden*, vol.42, no.1, pp.26-29, (English translation of text pp. E11-E13), Jan.1990.
- [30] Hahn, O., Budde, L. and Hanitzsch, D. (1990), "Investigations on the influence of the mechanical properties of spot welding tongs on the welding process (Untersuchungen zum Einfluss der mechanischen ...)", *Schweissen und Schneiden*, vol.42, no.1, pp.17-21, (English translation of text pp. E6-E8), Jan.1990.
- [31] Dorn, L. and Xu, P. (1990), "Investigations concerning the influence of the mechanical machine properties in resistance forge welding by means of a simulator (Untersuchungen zum Einfluss der mechanischen ...)", *Schweissen und Schneiden*, vol.42, no.1, pp.40-44 (English translation of text pp.E19-E20), Jan.1990.
- [32] Dorn, L. and Xu, P. (1992), "Relationship between static and dynamic machine properties in resistance spot welding (Zusammenhang zwischen statischen und dynamischen ...)", *Schweissen und Schneiden*, vol.44, no.1, pp.33-37, (English translation of text and captions pp. E19-E22), Jan.1992.
- [33] Dorn, L. and Xu, P. (1994), "Influence of the mechanical characteristics of the machine on contact resistance and dynamic resistance in spot welding (Abhängigkeit des Kontaktwiderstands und des dynamischen Widerstands beim Punkschweissen von den ...)", *Schweissen und Schneiden*, vol.46, no.1, pp.16-20 (English translation of text and captions pp. E3-E6), Jan.1994.
- [34] Tang, H., Hou, W., Hu, S. J. and Zhang, H. (2000), "Force characteristics of resistance spot welding of steels", *Welding Journal*, vol. 79, no. 7, pp. 175s-183s.
- [35] Tang, H., Hou, W., Hu, S. J., Zhang, H. Y., Feng, Z. and Kimchi, M. (2003), "Influence of Welding Machine Mechanical Characteristics on the Resistance Spot Welding Process and Weld Quality: How machine stiffness, friction, and moving mass can affect welding results", *Welding Journal*, vol. 82, no. 5, pp. 116s-124s.
- [36] Fujimoto, K., Nakata, S. and Nishikawa, M. (1997), "Design and construction of a loading system for resistance welding and its dynamic properties: optimization of the loading system in high current density spot welding with a short energizing time. First report", *Welding International (UK)*, vol. 11, no. 5, pp. 371-377.
- [37] Wu, P., Ma, Y., Han, B. and Li, F. (2006), "Analysis on electromagnetic force in resistance spot welding", *Hanjie Xuebao (Transactions of the China Welding Institution)*, vol. 27, no. 10, pp. 4-6.
- [38] Dupuy, T. (2006), "Influence of the mechanical characteristics of a pedestal spot welding machine", Proceedings, 4th International Seminar on Advances in Resistance Welding, Wells, Austria, 14-16 Novembre 2006.

- [39] Zhang, P., Zhang, H., Chen, J. and Ma, Y. (2006), "Quality monitoring of resistance spot welding based on electrode displacement characteristics analysis", *Jixie Gongcheng Xuebao (Chinese Journal of Mechanical Engineering)*, vol. 42, no. 10, pp. 176-181.
- [40] Wang, Y. B., Li, R. H. and Meng, G. X. (2011), "Experimental study on electrode displacement fluctuation characteristics during resistance spot welding", *Science and Technology of Welding and Joining*, vol. 18, no. 2, pp. 140-145.
- [41] Nied, H. A. (1984), "The Finite Element Modeling of the Resistance Spot Welding Process", *Welding Journal*, vol.63, no. 4, pp. 123s-132s, April 1984.
- [42] Gould, J. E. (1987), "An Examination of Nugget Development During Spot Welding, Using Both Experimental and Analytical Techniques", *Welding Journal*, vol. 66, no. 1, pp. 1s-10s.
- [43] Han, Z., Orozco, J., Indacochea, J. E. and Chen, C. H. (1989), "Resistance Spot Welding: a Heat Transfer Study", *Welding Journal*, vol. 68, no. 9, pp. 363s-371s, September 1989.
- [44] Tsai, C. L., Papritan, J. C., Dickinson, D. W. and Jammal, O. A. (1992), "Modeling of Resistance Spot Weld Nugget Growth", *Welding Journal*, vol.71, no. 2, pp. 47s-54s, February 1992.
- [45] Browne, D. J., Chandler, H. W., Evans, J. T. and Wen, J. (1995), "Computer simulation of resistance spot welding in aluminium: Part 1", *Welding Journal*, vol.74, no.10, pp. 339s-344s, October1995.
- [46] Browne, D. J., Chandler, H. W., Evans, J. T., Wen, J. and Newton, C. J. (1995), "Computer simulation of resistance spot welding in aluminium. Part 2", *Welding Journal*, vol.74, no.12, pp. 417s-422s, December1995.
- [47] Li, M. V., Dong, P. and Kimchi, M. (1997), "Modeling of contact resistance during resistance spot welding", *Proceedings, SCL, Low carbon steels*, 8-11 July 1997, pp. 423, San Francisco, CA, USA.
- [48] Zhang, W., Jensen, H. H. and Bay, N. (1997), "Finite element modeling of spot welding similar and dissimilar metals", *Seventh International Conference on Computer Technology in Welding*, 8-11 July 1997, pp. 364, San Francisco, CA, USA.
- [49] Zhang, W. and Kristensen, T. F. (1997), "Finite element modeling of the heat development in resistance welding", *JOM-8, The International Conference on the Joining of Materials*, 12-14 May 1997, pp. 226, Helsingor, Denmark.
- [50] Zhang, W. and Kristensen, L. (2000), "Finite element modeling of resistance spot and projection welding processes", *Ninth International Conference on Computer Technology in Welding*, 28-30 September 1999, pp. 15, Detroit, Michigan, USA.

- [51] Zhang, W. (2003), "Industrial Applications of Computer Simulation in Resistance Welding", *International Journal for the Joining of Materials*, vol. 15, no. 3, pp. 9-16.
- [52] Zhang, W. (2004), "Design and Implementation of Software for Resistance Welding Process Simulations", *SAE Transactions: Journal of Materials & Manufacturing*, vol. 112, pp. 556-564.
- [53] Santos, I. O., Zhang, W., Goncalves, V. M., Bay, N. and Martins, P. A. F. (2004), "Weld bonding of stainless steel", *International Journal of Machine Tools & Manufacture*, vol. 44, no. 14, pp. 1431-1439.
- [54] Chen, Z. and Zhou, Y. (2006), "Surface modification of resistance welding electrodes by electro-spark deposited composite coatings Part II. Metallurgical behavior during welding", *Surface and Coatings Technology*, vol. 201, no. 6, pp. 2419-2430.
- [55] Scotchmer, N. (2006), "Simulation Software Helps Automakers", *Welding Journal*, vol. 85, no. 8, pp. 47-49.
- [56] Scotchmer, N. (2007), "Reducing Resistance Welding Costs", *Welding Journal*, vol. 86, no. 2, pp. 47-49.
- [57] Scotchmer, N. (2007), "The Other Resistance Process: Cross Wire Welding", *Welding Journal*, vol. 86, no. 12, pp. 36-39.
- [58] Chan, K. R. (2008), "Save Time and Money with Resistance Welding Simulation Software", *Indian Welding Journal*, vol. 41, no. 4, pp. 60-64.
- [59] Dupuy, T. and Ferrasse, S. (1999), "Influence of the type of current and materials properties on resistance spot welding, using a finite element model", *Trends in Welding Research, Proceedings, 5th International Conference*, Pine Mountain, GA, USA, 1-5 June 1998, ASM International, pp. 610-615.
- [60] Feng, Z., Babu, S. S., Santella, M. L., Riemer, B. W. and Gould, J. E. (1998), "Modelling of resistance spot welding process", *Proceedings Taiwan International Welding Conference TIWC'98, Technology Advancements and New Industrial Applications in Welding*, National Taiwan University, Taipei, Taiwan, 7-9 Sept. 1998, pp. 235-240.
- [61] Feng, Z., Gould, J. E., Babu, S. S., Santella, M. L. and Riemer, B. W. (1999), "An incrementally coupled electrical-thermal-mechanical model for resistance spot welding", *Proceedings, 5th International Trends in Welding Research Conference*, 1-5 June 1998, Pine Mountain, ASM International, pp. 599-604.
- [62] Sudnik, V. A., Erofeev, V. A., Kudinov, R. A., Dilthey, W. and Bohlmann, H. C. (1999), "Simulation of resistance spot welding steels using SPOTSIM software", *Welding International (UK)*, vol. 13, no. 2, pp. 141-146.
- [63] Sun, X. (2000), "Modeling of projection welding processes using coupled finite element analyses", *Welding Journal*, vol. 79, no. 9, pp. 244s-251s, September 2000.

- [64] Sun, X. and Dong, P. (2000), "Analysis of aluminium resistance spot welding processes using coupled finite element procedures", *Welding Journal*, vol.79, no.8, pp.215s-221s, August 2000.
- [65] Sun, X. (2001), "Effect of projection height on projection collapse and nugget formation - a finite element study", *Welding Journal*, vol.80, no. 9, pp. 211s-216s, September 2001.
- [66] Vichniakov, A., Herold, H., Wink, H. J. and Greitmann, M. J. (2002), "Numerical simulation of resistance projection welding (Numerische Simulation von Widerstandsbuckelschweissungen)", *Praktiker*, vol.54, no.3, pp.92, 94-96, March 2002.
- [67] Robin, V., Sanchez, A. Dupuy, T., Soigneux, J. and Bergheau, J.M. (2002), "*Numerical simulation of spot welding with special attention to contact conditions*", In Book: "Mathematical Modelling of Weld Phenomena 6", Ed: Cerjak, H., Bhadeshia, H.K.D.H., Publ: Maney Publishing (for The Institute of Materials), London, SW1Y 5DB, UK.
- [68] Chang, B. H. and Zhou, Y. (2003), "Numerical study on the effect of electrode force in small-scale resistance spot welding", *Journal of Materials Processing Technology*, vol. 139, no. 1-3, pp. 635-641.
- [69] Dupuy, T. and Srikanwong, C. (2004), "*Resistance welding numerical simulation - a promising technique*", In Book: "Numerical Simulation of Welding (Revue Europeenne des elements finis) ", Ed: J.M.Bergheau, J.M., Publ: Lavoisier, F-75008 Paris, France.
- [70] Song, Q. F., Zhang, W. Q. and Bay, N. (2005), "An experimental study determines the electrical contact resistance in resistance welding", *Welding Journal*, vol. 84, no. 5, pp. 73s-76s.
- [71] Song, Q., Zhang, W. and Bay, N. (2006), "Contact modelling in resistance welding. Part 1: algorithms and numerical verification", *Proceedings of the Institution of Mechanical Engineers B, Journal of Engineering Manufacture*, vol. 220, no. B5, pp. 599-606.
- [72] Song, Q., Zhang, W. and Bay, N. (2006), "Contact modelling in resistance welding. Part 2: Experimental validation", *Proceedings of the Institution of Mechanical Engineers B, Journal of Engineering Manufacture*, vol. 220, no. B5, pp. 607-613.
- [73] Rymenant, V. P. (2002), "Testing and modelling of mechanical behaviour of welding machines", *Conference Proceedings, 2nd International Seminar on Advances in Resistance Welding*, Aachen, Germany, pp. 6-7, November 2002.
- [74] Private communication with Professor Niels Bay at 1st International seminar on the Advances in Resistance Welding, DTU, Copenhagen, October 2000.

- [75] Wu, Y. P., Zhang, W. and Bay, N. (2005), "Characterization of Dynamic Mechanical Properties of Resistance Welding Machines", *Welding Journal*, vol. 84, pp. 17s-21s, January 2005.
- [76] Chen, J. Z. and Farson, D. F. (2004), "Electrode displacement measurement dynamics in monitoring of small scale resistance spot welding", *Measurement Science and Technology*, vol. 15, no. 12, pp. 2419-2425.
- [77] DIN 8519 (1978), "*Projections for (Resistance) Projection Welding of Steel Sheet - Circular Projection, Elongated Projection and Annular Projection. (Buckel Fur Das Buckelschweissen Von Stahlblechen - Rundbuckel, Langbuckel Und Ringbuckel)*", Beuth Verlag GMBH, July 1978.
- [78] Cunningham, A. and Begeman, M. L. (1965), "A Fundamental Study of Projection Welding using High-Speed Photography", *Welding Journal*, vol. 44, no. 8, pp. 381s-384s, August 1965.
- [79] Cunningham, A. J. R. and Begeman, M. L. (1966), "Effect of Projection Height upon Weld Quality and Strength", *Welding Journal*, vol. 45, no. 1, pp. 26s-30s, January 1966.
- [80] Cunningham, A. J. R., Begeman, M. L. and Short, B. E. (1966), "An Analysis of the Nugget Formation in Projection Welding", *Welding Journal*, vol. 45, no. 7, pp. 305s-313s, July 1966.
- [81] Adams, J. V., Matthews, G. N. and Begeman, M. L. (1965), "Effect of Projection Geometry upon Weld Quality and Strength", *Welding Journal*, vol. 44, no. 10, pp. 466s-470s, October 1965.
- [82] ARO Machinery Company (1966), "Resistance Welding Tubular Components", *Welding and Metal Fabrication*, , pp. 459-463.

Appendix A - Physical properties materials used

		308L	309L	316L	430 LNb	13 % Cr 405	17 % Cr 430	S235	Hasteloy 276C
Composition weight %	C	0,02 – 0,03	< 0,03	< 0,03	< 0,03	0,08	0,12	0,17	0,01
	Mn	1,6 – 1,75	1,8	1,7	0,5	1,00	1,00	1,40	1
	Si	0,4 – 0,475	0,5	0,5	0,5	1,00	1,00		0,08
	Cr	20,25	24,0	19,0	18,2	11,5 – 14,5	16,0 – 18,0		16
	Ni	10	13,0	12,0					57
	P	0,015	0,03			0,04	0,04	0,03	
	S	0,015	0,02			0,03	0,03	0,03	
Mechanical properties	Density (kg/m ³)	7700 - 8030	8030	8027	7700	7800	7800	7800	8890
	Poisson ratio	0,27 – 0,30	0,27 – 0,30	0,27 – 0,30	0,27 – 0,30	0,27 – 0,30	0,27 – 0,30	0,27 – 0,30	
	E – Modulus (GPa)	190 - 210	200	190 - 210	220	200	200	210	205
	Tensile strength (MPa)	620	600	620	420	480	480	360	785
	Yield strength (MPa)	450	440	440	275	275	275	235	365
	Strain at fracture (%)	36	41	37	26	16	20	32	59
	Insnoering (%)	36	41	37	26	45	45	32	
Thermal properties	Coefficient of thermal expansion (($\mu\text{m}/\text{m}$). $^{\circ}\text{C}$)	17,2	15,6	15,9	10	10,8	10,4	11	11,2
	Thermal conductivity (W/m.K)	15,2	15,6	16,2	25	27	26,1	41 - 52	10,2
	Specific heat (J/kg.K)	500	502	500	460	460	460	480 - 530	427
Electrical	Electrical resistance ($\mu\Omega.\text{cm}$)	72	78	74	60	60	60		20

Table A-1

Appendix B - Theoretical Model

B.1 Model for the moving welding head

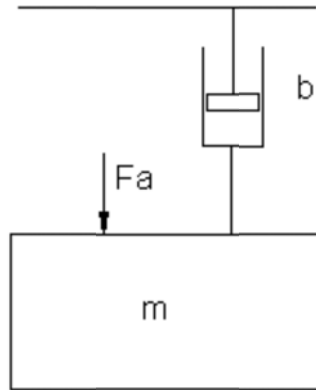


Figure B - 1 Schematical model moving electrode

Compressed air inside the welding heads actuator cilinder exerts a force ' F_a ' [N] through the piston and its piston rod on the (lumped) moving mass ' m ' [kg] of the welding head (see Figure B - 1). Movement of this mass will be slowed down by frictional effects, causing damping, represented by a damping factor ' b ' [kg/s] or [N/m/s].

During welding, the workpiece exerts a reaction force ' F_r ' [N] through the electrode on the moving mass (see Figure B - 2). This force is normally the same force that is present between the workpieces to be welded, except when for instance they are plastically deformed plate like structures that don't fit properly. In that case, a part of the compressing force is used to deform the workpieces to have them contact.

During the squeeze stange, $F_a = F_r$ applies.

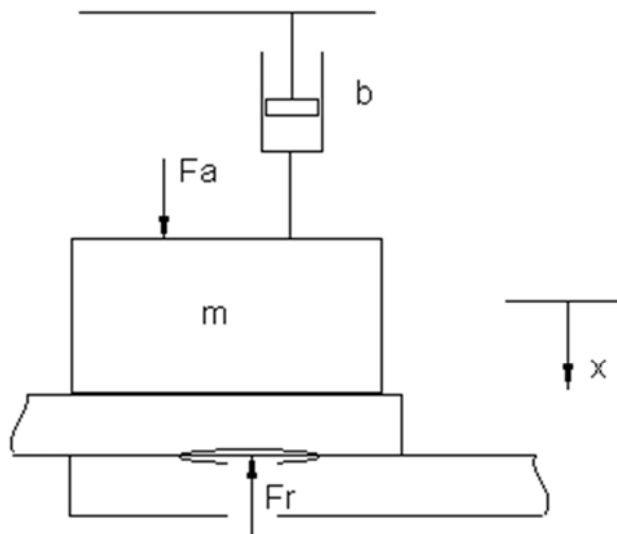


Figure B - 2 Schematical model moving welding head with reaction force of workpiece

When the weld pool is formed, reaction force ' F_r ' will decrease, leading to the mass to start moving, governed by the following equation:

$$Fa - Fr = m \frac{d^2x}{dt^2} + b \frac{dx}{dt}$$

The reaction force ' Fr ' is of metallurgical nature.

In the fracture test, reaction force ' Fr ' completely disappears ' $Fr = 0$ ', mimicking a weld that extremely overheats and explodes.

At that moment: $Fa = m \frac{d^2x}{dt^2} + b \frac{dx}{dt}$

This equation is solved using system dynamics by applying Laplace transformation where displacement is written as a function of time:

$$Fa(s) = m \cdot xs^2 + b \cdot xs \rightarrow Fa(s) = (m \cdot s^2 + b \cdot s) \cdot X(s)$$

$$\Leftrightarrow \frac{X(s)}{Fa(s)} = \frac{1}{ms^2 + bs}$$

$$\Leftrightarrow \frac{X(s)}{Fa(s)} = \frac{1/m}{s^2 + \frac{b}{m}s}$$

As mentioned above, during the fracture test, reaction force ' Fr ' will suddenly disappear due to the brittle pin breaking away. As a result, the machine actuator system is loaded with a step function. A step function is introduced in the Laplace domain by multiplying with ' $1/s$ ' leading us to:

$$\Leftrightarrow X(s) = Fa(s) \cdot \frac{1}{s(s^2 + \frac{b}{m} \cdot s)}$$

$$\Leftrightarrow X(s) = Fa(s) \cdot \frac{1}{s^2(\frac{m}{b} \cdot s + 1)}$$

Reverse transformation to the time domain: $s \rightarrow t$ leads us to:

$$\Leftrightarrow x(t) = \frac{Fa(t) \cdot m}{b^2} \cdot \left(e^{-\frac{b}{m}t} + \frac{m}{b} \cdot t - 1 \right)$$

Displacement is expressed here as a function of time. This means that starting from displacement measurements made on the moving welding head in its response to a fracture test, mass and damping factor can be calculated iterative.

Since a velocity measurement using a laser vibrometer is by far less invasive in a production environment, calculating mass and damping factor starting from a velocity signal is the more realistic and practical approach:

Instead of the actuator force symbol F_a , it is more suitable to introduce $F_{fracture}$ as the force at which fracture is initiated.

$$\frac{dx}{dt} \Rightarrow v_{th}(t) = -\frac{F_{fracture}}{b} \cdot e^{-\frac{b}{m} \cdot t} + \frac{F_{fracture}}{b}$$

$$\Leftrightarrow v_{th}(t) = -\frac{F_{fracture}}{b} \cdot \left(e^{-\frac{b}{m} \cdot t} - 1 \right)$$

When the true welding head velocity, v_w needs to be compared with the theoretical values, then initial velocity v_0 needs to be accounted for:

$$\rightarrow v_{th}(t) = -\frac{F_{fracture}}{b} \cdot \left(e^{-\frac{b}{m} \cdot (t-t_0)} - 1 \right)$$

t_0 is subsequently introduced:

$$\Leftrightarrow v_{th}(t) = -\frac{F_{fracture}}{b} \cdot \left[e^{-\frac{b}{m} \left(t - \frac{m}{b} \cdot \ln \left(-\frac{v_0 \cdot b}{F_{fracture}} + 1 \right) \right)} - 1 \right]$$

$$\Leftrightarrow v_{th}(t) = -\frac{F_{fracture}}{b} \cdot \left[e^{-\frac{b}{m} t} \cdot \left(\frac{v_0 \cdot b}{F_{fracture}} + 1 \right) - 1 \right]$$

$$\Leftrightarrow v_{th}(t) = v_0 \cdot e^{-\frac{b}{m} t} + \frac{F_{fracture}}{b} \cdot e^{-\frac{b}{m} t} + \frac{F_{fracture}}{b}$$

$$\rightarrow v_{th}(t) = -\left[\left[-\frac{F_{fracture}}{b} \cdot \left(e^{-\frac{b}{m} t} - 1 \right) \right] - \left[v_0 \cdot e^{-\frac{b}{m} t} \right] \right]$$

The minus sign in front of the formula makes the final value negative to facilitate comparison with the measured values for velocity that are negative.

B.2 Model for the fixed electrode

Most often the lower electrode in the majority of resistance welding machines.

The model looks as follows:

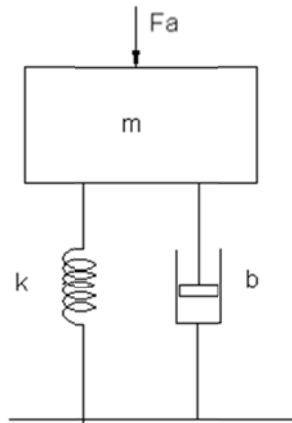


Figure B - 3 Schematical model fixed welding head

Transfert function :
$$\frac{X}{F} = \frac{1}{ms^2 + bs + k}$$

The fixed electrode is composed out of a mass 'm'. Deflection depends on the stiffness 'k' of the electrode arm. The corresponding movement or vibration that follows is dampened with a damping factor 'b'.

Since it is difficult to derive the used constants directly out of the displacement signal, they are transformed into three parameters that can be identified straightforward from the measured signal: the damping ratio ' ξ ', the natural frequency ' ω ' and 'G'.

$$\frac{X}{F} = \frac{G * \omega^2}{s^2 + 2\xi\omega s + \omega^2} \quad \text{with} \quad \xi = \frac{b}{b_c} = \frac{b}{2m\omega}$$

$$\omega = \sqrt{\frac{k}{m}}$$

$$G = \frac{1}{k}$$

Force 'F' is imposed as a step function. In the Laplace domain, a step function is proposed by deviding its value by 's':

$$X(s) = \frac{F * G * \omega^2}{s(s^2 + 2\xi\omega s + \omega^2)} = \frac{K_0}{s} + \frac{K_1}{s - p_1} + \frac{K_2}{s - p_2}$$

$$\text{with } p1 = \left(-\xi + \sqrt{\xi^2 - 1}\right)\omega_0$$

$$p2 = \left(-\xi - \sqrt{\xi^2 - 1}\right)\omega_0$$

$$K0 = \frac{F0}{k}$$

$$K1 = \frac{K0}{p1(p1 - p2)}$$

$$K2 = \frac{K0}{p2(p2 - p1)}$$

$\Downarrow s \rightarrow t$ (transfer back to the time domain)

$$x(t) = K0 + K1 * e^{p1*t} + K2 * e^{p2*t}$$

$$\Rightarrow e^{-p1*t} = e^{-\xi\omega_0 t} \left[\cos\left(\sqrt{1 - \xi^2}\omega_0 t\right) + j * \sin\left(\sqrt{1 - \xi^2}\omega_0 t\right) \right]$$

\Rightarrow

$$\Rightarrow e^{-p2*t} = e^{-\xi\omega_0 t} \left[\cos\left(\sqrt{1 - \xi^2}\omega_0 t\right) - j * \sin\left(\sqrt{1 - \xi^2}\omega_0 t\right) \right]$$

$$e^{-p1*t} = e^{-\xi\omega_0 t} [\cos A + j * \sin B]$$

$$e^{-p2*t} = e^{-\xi\omega_0 t} [\cos A - j * \sin B]$$

$$K1 = -C + jD$$

$$K2 = -C - jD$$

with

$$C = \frac{F0}{2k\omega_0^2}$$

$$D = \frac{F0 * \xi}{2k\omega_0^2 \sqrt{1 - \xi^2}}$$

$$K1 * e^{-p1*t} + K2 * e^{-p2*t} = -2C * e^{-\xi\omega_0 t} * \cos A - 2D * e^{-\xi\omega_0 t} * \sin A$$

$$= -2e^{-\xi\omega_0 t} (C * \cos(\omega_d * t) + D * \sin(\omega_d * t))$$

$$\boxed{x(t) = K0 - 2e^{-\xi\omega_0 t} (C * \cos(\omega_d * t) + D * \sin(\omega_d * t))}$$

$$\text{With } \omega_d = \sqrt{1 - \xi^2}\omega_0$$

How to find the machine variables from a step response :

It is often a hard job to find all individual machine variables on a random welding machine. It is even difficult to do so on a machine in a laboratory. So it is more obvious to derive the variables out of a step response. As an example in Figure B - 4 below the response signal to a step on a lower electrode arm.

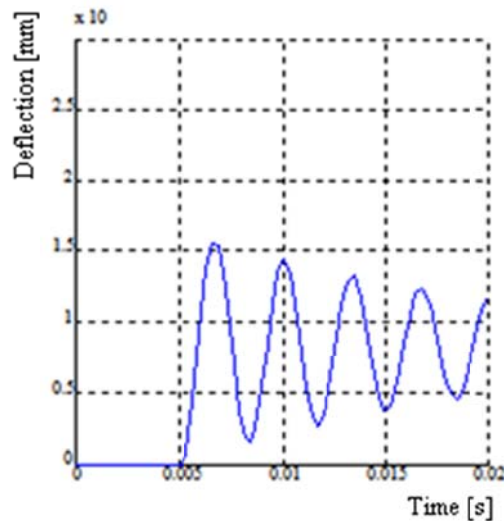


Figure B - 4 Step response fixed welding head

This step response follows equation :

$$y(t) = Ko - 2e^{-\xi\omega_0 t} (C * \cos \omega_d + D * \sin \omega_d) \quad \text{with } \omega_d = \sqrt{(1 - \xi^2)}\omega_0$$

In this equation, there are some terms to distinguish:

- the pulsating term with frequency ' ω_d '.
- the exponential function decaying in time
- the final value ' Ko '

Determination of variables can be made as follows (see Figure B - 5):

Let us suppose a step is imposed with a known force ' F_o '.

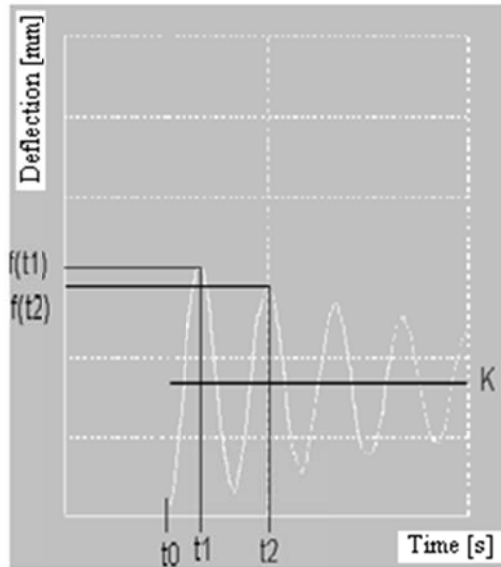


Figure B - 5 Measuring on step response fixed welding head

- K_o

⇒ Read final value K on the measured signal above

- ' ω_d '

⇒ measure : $\omega_d = \frac{2\pi}{t_2 - t_1}$

- k

⇒ $k = F_o/K_o$

- ω_o, ξ

$$f(t_1) = K_o - A * e^{-\xi\omega_o t_1}$$

$$f(t_2) = K_o - A * e^{-\xi\omega_o t_2}$$

$$\Rightarrow 1.) \quad \xi * \omega_o = \frac{\ln \frac{(f(t_1) - K_o)}{(f(t_2) - K_o)}}{(t_2 - t_1)}$$

$$2.) \quad \omega_d = \sqrt{(1 - \xi^2)} \omega_o$$

$$\Rightarrow \omega_o = \sqrt{\omega_d^2 + (\xi\omega_o)^2} \quad \text{and} \quad \xi = \frac{\xi\omega_o}{\omega_o}$$

▪ m

$$\Leftrightarrow \omega_o = \sqrt{\frac{k}{m}} \quad \Rightarrow \quad m = \frac{k}{\omega_o^2}$$

▪ b

$$\Leftrightarrow b = \xi 2m\omega_o$$

▪ G_o

$$\Leftrightarrow G_o = 1/k$$

\Leftrightarrow k, m, b or ω , ξ , G_o known.

Appendix C - Test procedure Free Fracture test

As already mentioned before, formation of a plastically deformable or molten weld pool causes workpiece support against the electrodes clamping force to partly disappear. The moving welding head will respond to this drop in reaction force by making a displacement in the direction of the workpiece. Velocity of this displacement is depending on the lumped mass of the welding head (welding head plus every auxiliary attached machine element that will have to displace as well), of the damping factor and possibly the elastic spring constant of the moving welding head. Resulting from these physical limitations, this welding head movement cannot take place infinitely fast and thus will lead to a drop in force exerted by the moving welding head on the workpieces. To analyse the latter, a theoretical model is developed within the scope of this thesis. The resulting equation of welding head displacement or velocity as a function of time contains the machine characterizing parameters lumped mass of the moving welding head m [kg] and its damping factor b [N/m/s] at a chosen preset welding force F [daN].

By means of the free fracture test, a step function is imposed on the welding heads by means of breaking of the welding head supporting pin. This step function is necessary in order to have a valid theoretical model transferred in practice. By measuring the welding heads displacement and/or velocity response to the imposed step function, sufficient data is available to subsequently calculate the characterizing machine constants m and b .

In order to measure welding head motion, measuring equipment and procedures were chosen and developed that can deliver accurate and reliable results and that can be used on such an endless pallet of different resistance welding machines in so many different production environments. Also choice of measuring equipment should be made to assure safety for operators in often highly automated production environments. The author's personal experience with significant accidents has led to a focus on safety. Noninvasive, contactless and in general more expensive measuring equipment resulted and with proven benefit. This has allowed assessment of welding applications in production plants without interfering into production in a guaranteed safe usage.

For measurement of welding head motion, a laser vibrometer was chosen, capable of measuring motion accurately from a relative large distance away from the object to measure.

The free fracture test has the purpose to apply a step function on the welding head to monitor, achieved by breaking a brittle element away from between the electrodes. Pressurizing force is built up in the force actuator until the force level for fracture is reached. At that instance, reaction force fully disappears resulting in the electrodes to move freely towards each other. This motion is measured and resulting data is processed.

Design of the fracture test needs to follow some important requirements:

- It must be compact and easy to mount on any production welding machine;
- The material to fracture (pins) must break in a brittle way in the setup;
- The test itself should have a low mass in order not to influence the lumped mass of the welding head under study;
- The test rig must retain the three remaining parts of the pin after fracture and must ensure no injury or damage is caused;

The ultimate design result is a cylindrical canister (Figure C - 1) containing supporting washers with different inner diameters that offer different supporting distances for the pins to break accordingly. After fracture, the three remaining parts of the pin stay trapped in the canister. This canister is attached to the stationary welding head. Against the moving welding head, the canisters lid is mounted, a metal disc with a hardened steel pin attached to its

underbody intended to exert the welding heads force on the center of the pin to break. The hardened steel pin used for this purpose is the same one as the metal pins used as breaking element. It is very wear resistant and thus doesn't need to be replaced often.

Inside the canister on the lower welding head, support distance for the pins to fracture can be chosen through changing the inner diameter of the supporting washer. A load cell can be mounted underneath the lower part if required.

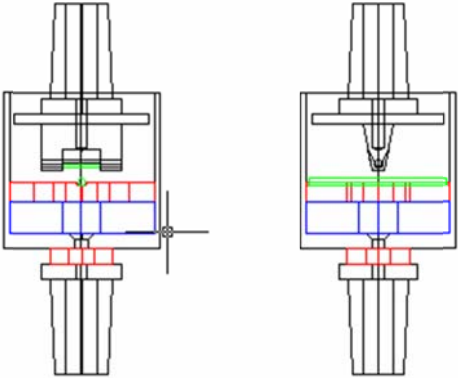


Figure C - 1 Closed canister design of free fracture test

Materials to serve as breaking elements need to break in a brittle way, thus having the reaction force transferred through the element to disappear instantly in order to be able to represent the force drop as a step function.

Material should also must be standardized to enable use of this test by others in a reproducible way. Force where fracture takes place must be known in advance and must have a range from a few daN to around 500daN. Material that can break with a few daN is needed for testing on applications in micro resistance welding while the higher levels are needed for the heavier applications.

Tests have been conducted on hardened steel pins (with and without EDM machined notches), ceramic building materials, technical ceramics and Hipped technical ceramics.

To enable evaluation of fracturing materials towards their potential usefulness and also to allow for high speed camera evaluations, the open and very flexible test rig was designed, as can be seen in Figure C - 2 below.

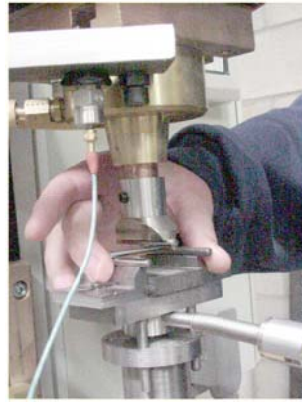


Figure C - 2 Open test set-up for fracture material evaluation

The test rig has a lower support that can be positioned to the requested value and has the possibility to insert a load cell to measure fracture force levels.

Fracture tests on hardened steel pins.

A material with low scatter on the force level at which it breaks is needed in the bending test rig as displayed in Figure C - 2 above.

Diameter of the hardened steel dowel pins used is finished to a very accurate level. They are easy to purchase in large numbers since they are standard material. The tests conducted served to examine if these pins could cope with our demands.

The tests were performed on pins that showed a breaking force well within the force level of our institute's welding machines. Results of these initial tests in the open test set-up for two sizes of dowel pins can be found below in Table C - 1 and Table C - 2.

Material: ISO 8734:1997 Dowel pins 2.5mm x 50 mm			
Support distance (mm)	25	35	42
Fracturing force (daN)	127	90	63
Sdev	8.1	2.7	4.3
Mmax (Nmm)	7938	7875	6615
σ (kN/mm ²)	5.17	5.13	4.31

Table C - 1 Steel dowel pins 2.5mm x 50mm

Material: ISO 8734:1997 Dowel pins 3 mm x 50 mm			
Support distance (mm)	25	35	42
Fracturing force (daN)	185	145	119
Sdev	10.7	3.9	8.0
Mmax (Nmm)	11563	12688	12495
σ (kN/mm ²)	4.36	4.79	4.71

Table C - 2 Steel dowel pins 3.0mm x 50mm

Remark: These results are mean values of 100 tests per material.

The fracturing forces cover a large range of the force levels to be used on the welding machines. The scatter is acceptable.

To enable comparison with pins of different at different supporting distances, I calculated the bending momentum and the stress value at fracture σ .

$$M_{\max} = F * \frac{x}{4} \qquad M_{\max} = \text{breaking momentum (Nmm)}$$

$$F = \text{fracturing force (N)} \qquad x = \text{support distance (mm)}$$

$$\sigma = \frac{32 * M_{\max}}{\pi * d^3} \qquad \sigma = \text{material fracture stress (N/mm}^2\text{)}$$

$$d = \text{pin diameter (mm)}$$

Notice the very high value for the calculated bending stress value in the order of 5000MPa. This value is however realistic considering the fact that we bend small diameters of very high strength hardened steel dowel pins with a martensitic structure. It also needs to be mentioned that each fracture follows the same physical pattern as can be observed during high speed camera evaluation of the fracture tests. (see Figure C - 3 below)

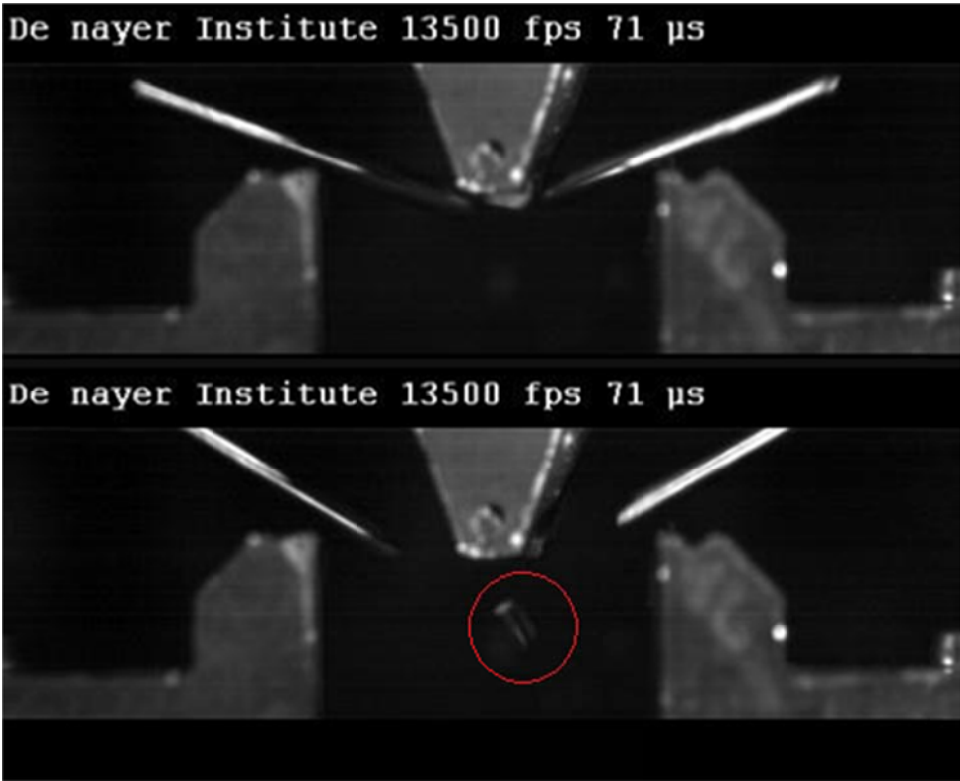


Figure C - 3 Fracture following bending load in high speed video recording

The dowel pin always displays a relevant plastic deformation prior to fracture. At the moment of fracture (upper part of Figure C - 3), a shell (visible in the red circle in the lower part of Figure C - 3 just underneath the upper support anvil) is sheared out of the top area of the pin to fracture due to compressive loading of the latter pin and this induces an impact-wise stress

increase on the remaining cross-section and is instantly followed by the fracture of the remaining pin cross-section in two elements that are projected sideways. Considering the extreme velocities of the remains of the pin and in order to ensure a guaranteed safe working environment, the fracturing device in a closed canister was designed as seen in Figure C - 1 before.

The lower support is engineered in the closed design as washers with support distances (inner diameter of the washers) of 20mm, 25mm, 27mm and 32.5mm respectively. The outer diameter is 60mm.

The results of the fracture tests in the closed canister design on steel dowel pins are summarized in Table C - 3 and they are displayed in the graph of Figure C - 4.

Dowel pin Diameter (mm)	Dowel pin Length (mm)	Supporting distance (mm)	Breaking Force (daN)
2.5	40	20	106
2.5	40	25	85
2.5	40	27	79
2.5	40	32.5	65
2.5	45	20	138
2.5	45	25	111
2.5	45	27	102
2.5	45	32.5	85
2.5	50	25	114
2.5	50	32.5	87
3	40	20	266
3	40	25	213
3	40	27	197
3	40	32.5	164
3	50	25	182
3	50	32.5	140
4	40	20	466
4	40	25	373
4	40	27	345
4	40	32.5	287
4	60	25	490
4	60	32.5	376

Table C - 3 Fracture forces for standard steel dowel pins in closed canister

This table contains all combinations of standard hardened positioning pins according to ISO 8734:1997 as they were tested in the closed canister design fracture mechanism with supporting washers. The available fracture forces cover a range from 65daN to 490daN. The test can be used safely and reliably to impose a step function in reaction force between the welding heads of a machine under study at a given force level. When a force level for a specific application is given, the choice of the dowel pin to use in combination with a supporting washer can be made quickly.

Larger pins than diameter 4mm are not used, since they would possibly damage the test equipment. Although it needs to be mentioned that it is not necessary to conduct the fracture test at higher force levels since following the theoretical model, it is possible to define the relevant machine parameters at lower force levels.

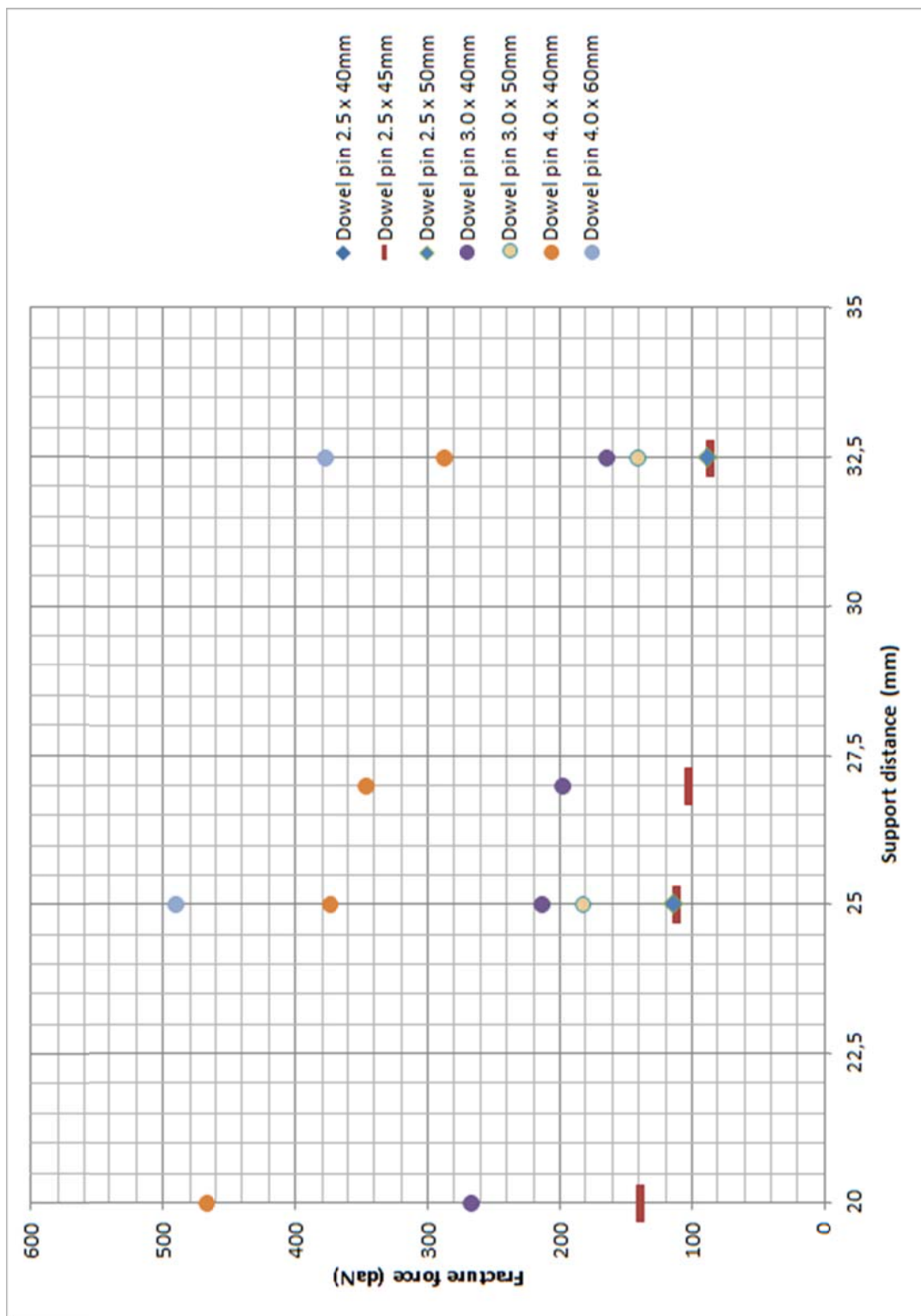


Figure C - 4 Fracture forces for standard steel dowel pins in closed canister

However, to enable testing on small machines in micro resistance welding, working with force levels below 60 daN, alternatives are needed. This issue was solved by adding a stress concentrating factor to the pins to lower their breaking force. The latter is realised by machining a notch in the middle of the dowel pin prior to fracturing it.

Fracture tests on hardened steel pins with notch

Machining of a notch is realised by means of EDM wire erosion. The result is a dowel pin breaking at force levels below 60daN. Electro erosion is an accurate machining process offering the possibility to cut a notch of defined width and depth in the middle of the dowel pins. There is very low scatter on the breaking force levels of pins with identical notch dimensions. Dowel pins were machined with a sparking gap of 0.25mm at different sparking depths. In this way, fracture tests can be conducted at force level of few daN.

Material: ISO 8734:1997 Dowel pins 1.5 x 32mm	
Support distance used: 27mm	
Notch depth (mm)	Fracture force (daN)
0	21
0.25	7.78
0.5	5.36
0.75	3.02
1	1.34

Table C - 4 Fracture forces for steel dowel pins with notch in closed canister

Remark: The results displayed in Table C - 4 and in Figure C - 5 are the mean values of 50 tests of each notched type of dowel pin. Scatter on the values within the range of 0 to 10%.

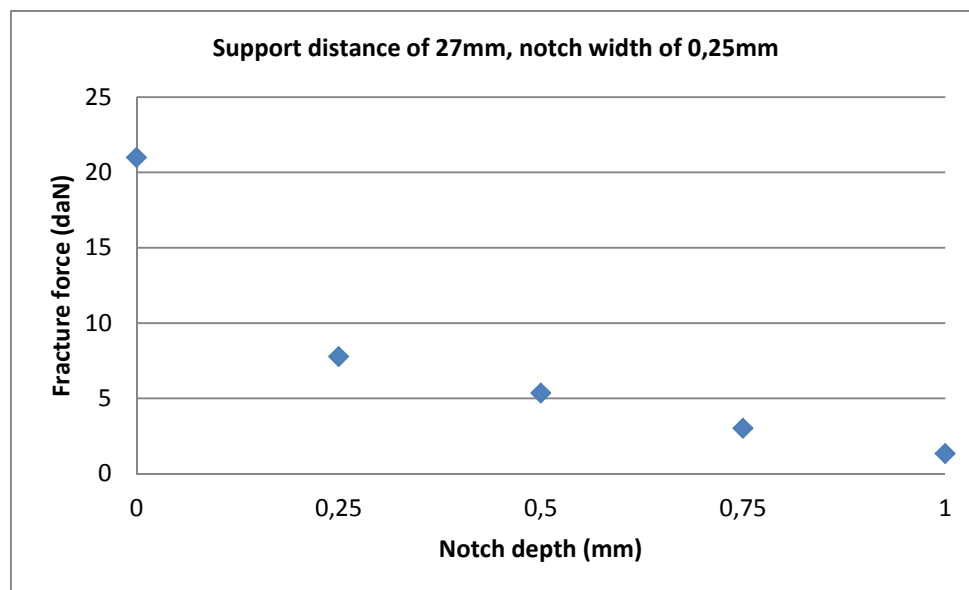


Figure C – 5 Fracture forces for steel dowel pins with notch in closed canister

Hardened steel dowel pins are suited for the purpose of this step function imposing test. At a chosen fracture force, the right dowel pin and according support washer needed can easily be selected. Force levels of nearly zero to 490daN can be used. Higher force levels are not necessary since the theoretical model is based on a motion signal instead of a force signal.

To realize the lower force levels, an accurate notch needs to be machined into the standard pins. The fracture test is relatively easy to mount on different machine designs.

Fracture tests on ceramic materials

Initially, traditional coarse ceramics (floor tiles) were tested, followed by technical ceramics (Al_2O_3 – 99.7%). Because of the high investment costs of the technical ceramics, only fracture tests with a support distance of 32.5mm have been executed.

Tests on ceramic tiles

Results on building ceramics were rather disappointing, since scatter levels on fracture forces were above 20% although extra care was taken to cut the elements to test to dimension very accurately. Another limitation is the very low range of fracture forces achievable. This would necessitate to test with unrealistic dimensions of the fracturing elements.

As a result of this, technical ceramics were evaluated.

Tests on technical ceramic bars

The tests on untreated technical ceramics proved that this was no improvement in comparison with steel dowel pins. Scatter on the fracture force is extreme due to the limited homogeneity of the ceramic material. (see Figure C - 6 below)

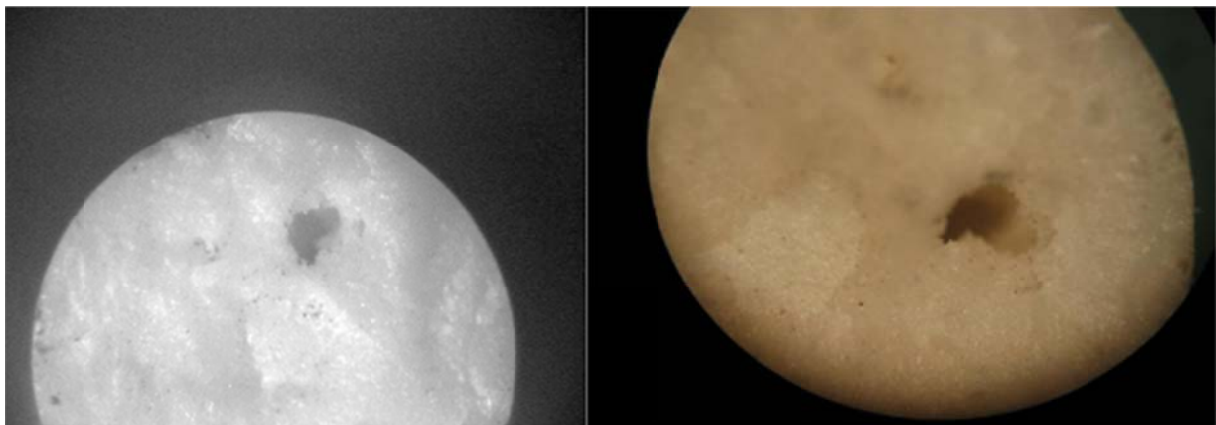


Figure C - 6 Inhomogeneity (hole) in technical ceramic bars

As a possible solution for this lack in homogeneity, the technique of Hot Isostatic Pressing (HIP) was used. The latter technique can be applied:

- as a production process within a sintering production process;
- as a post-densification process.

The latter post-densification process offers the advantages to enable treatment of the identical materials already used in the other tests.

Disadvantage of this treatment is that surface defects are not treated and there exists the possibility for grain growth in materials.

The densification process was applied on ceramic pins purchased at Ceratec, a Dutch supplier. Bodycote is a company specialized in application of the HIP – process on different industrial applications. The pins to examine in value as a potential breaking element in the fracture test were treated at Bodycote. A schematical image of a HIP installation can be seen

in Figure C - 7, the HIP cycle chart displaying the pressure and temperature chart as used on the ceramic pins used in the tests is displayed in Figure C - 8. As might be expected the costs for the technical ceramic bars and the Hipping are very high.

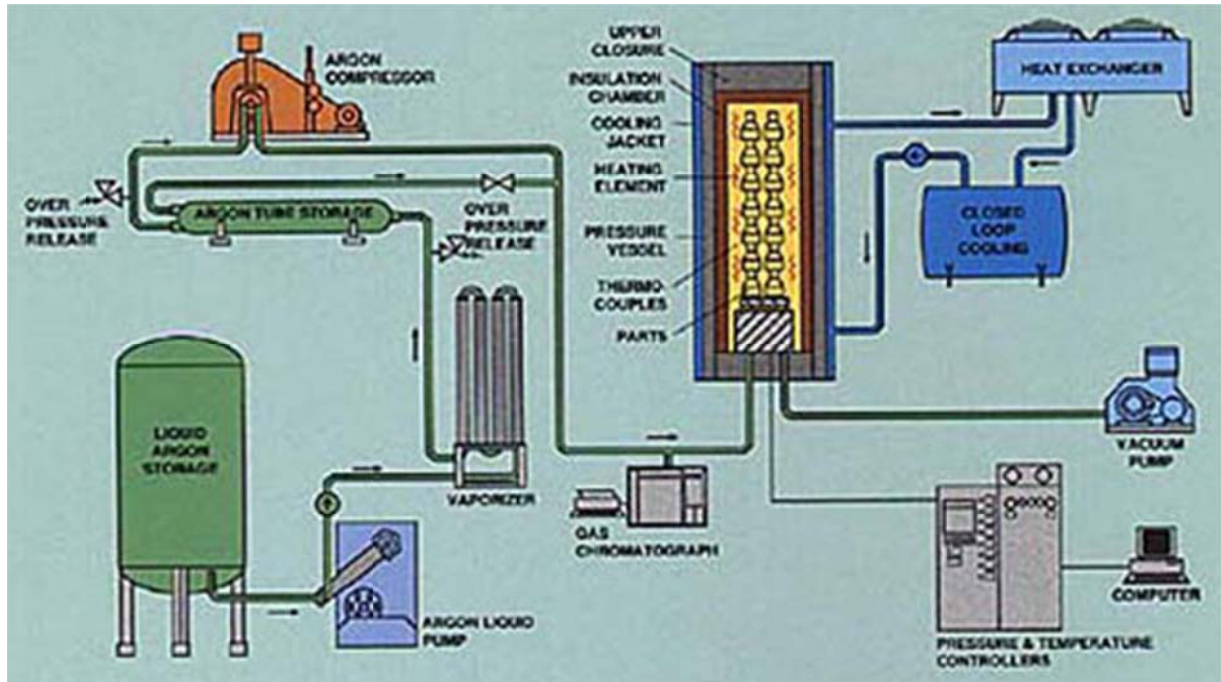


Figure C - 7 Schematical view of a HIP installation

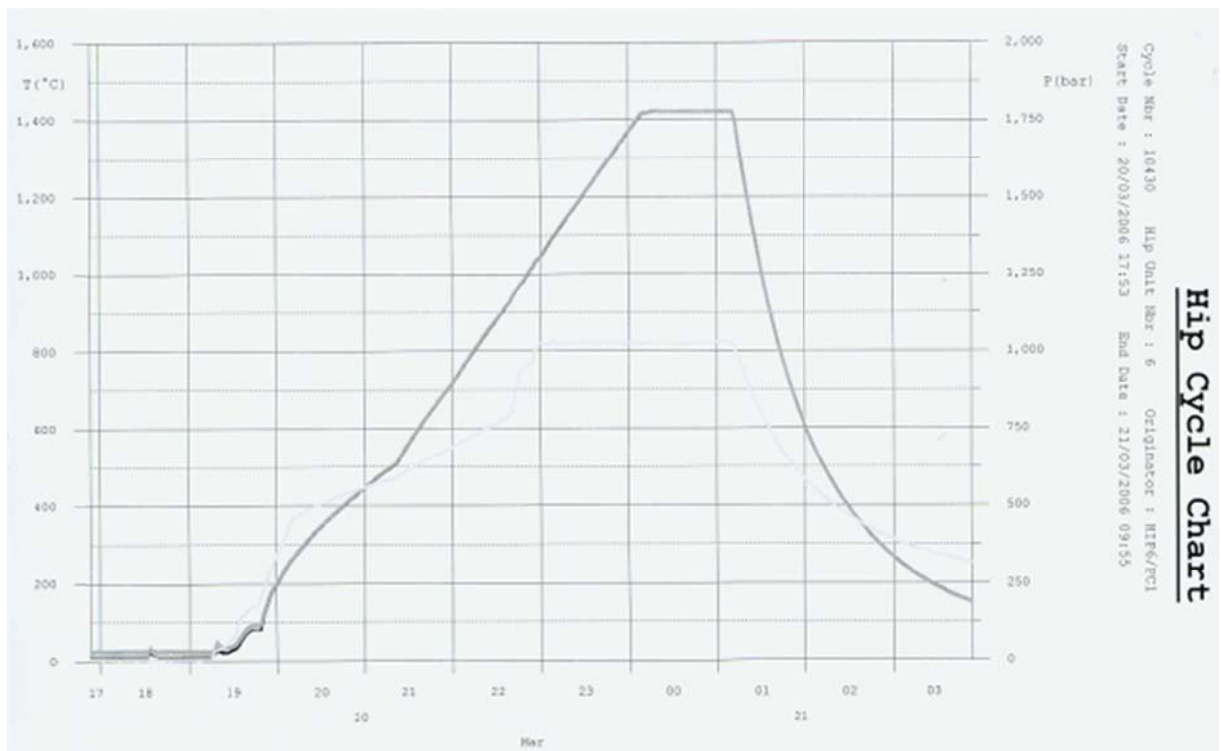


Figure C - 8 Cycle chart from the cycle applied on the pins tested

Evaluation was made after Hipping treatment to determine the properties in comparison with the untreated ceramic material. Bending tests were carried out on an Instron test bench. Pin diameters tested were 3, 4, 5 and 6mm.

Results of Hipped technical ceramics

Diameter 3 mm

Post HIP, the pins meet the demands of low scatter ($\leq 10\%$) and brittle fracture.

Diameters 4, 5 and 6 mm

The length of the HIP – cycle seems to be too short to treat these diameters to their center. Many internal discontinuities remain, leading to large scatter (20 to 45%) on the results of the fracture force making them unusable as fracture element for the breaking test. On the other hand, longer application of the HIP treatment would increase the operational cost of the test way beyond what we can afford.

The HIP treatment certainly has proven to improve the quality of the technical ceramic bars. However the financial added value to the already very high prices of the untreated technical material make use of this approach unfeasible.

Appendix D - Processing procedure Fracture/Explosion test

A processing procedure was developed for determination of the relevant machine parameters lumped mass 'm' [kg] of the actuated moving welding head and damping factor 'b' [kg/s].

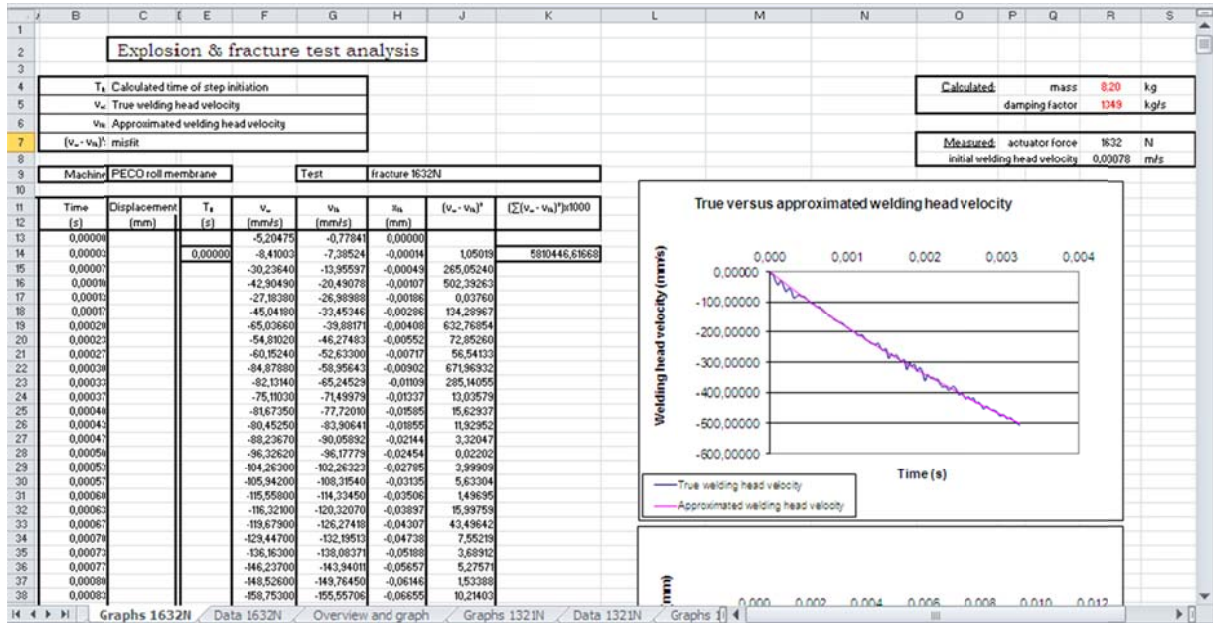


Figure D - 1 Screenshot of spreadsheet for processing fracture and explosion tests

Columns are commented below in the same order as they appear in the spreadsheet

- Column B

Points of time where displacement or velocity measurements are recorded, starting at 0s.

- Column C

Recorded displacement signal of moving welding head.

- Column E

Imaginary time to correct welding head velocity not being zero at moment of fracture.

$$t_0 = -\frac{m}{b} \cdot \ln\left(-\frac{v_0 \cdot b}{F_{fracture}} + 1\right) \quad [\text{s}]$$

- Column F

Recorded velocity signal of moving welding head. (or calculated from displacement signal)

$$\frac{x_n - x_{n-1}}{t_n - t_{n-1}} \quad [\text{m/s}]$$

- Column G

Approximated welding head velocity.

$$v_{th}(t) = -\left[\left(-\frac{F_{fracture}}{b} \cdot \left(e^{-\frac{b}{m}t} - 1\right)\right) - \left(v_0 e^{-\frac{b}{m}t}\right)\right] \quad [\text{m/s}]$$

- Column H
Approximated welding head displacement.

$$x_{th}(t) = -\frac{F_{fracture} \cdot m}{b^2} \cdot \left(e^{-\frac{b}{m} \cdot (t+t_0)} + \frac{b}{m} \cdot (t+t_0) - 1 \right) \quad [\text{mm}]$$

- Column I
Shift in displacement

$$x_n - x_1 \quad [\text{mm}]$$

- Column J
Square of the difference between true and approximated welding head velocities, (misfit).

$$(v_w - v_{th})^2$$

- Column K
Summation of the squares of differences between true and approximated welding head velocities.

$$\sum (v_w - v_{th})^2$$

Supplementary, the measured value of the force at which fracture took place must be inserted in cell L7 and the true measured initial velocity in cell L8.

Graphs

Two graphs are produced:

1. Comparison of velocities
True measured velocity is compared with approximated velocity.
2. Comparison of displacements
True measured displacement is compared with approximated displacement.

Processing procedure

1. Set up fracture of explosion test on machine to test.
2. Using a data acquisition system, measure welding head velocity (or displacement) during response on fracture or explosion. Record force. Record current.
3. In the data acquisition program, determine the exact moment of fracture or start of displacement in the total recorded signals. Starting from the point of time of the fracture or the initiation of movement, cut the signals and export them for instance to MS excel.
4. Import the velocity signal (or the displacement signal) in function of time into columns B and F or C.
5. Input the measured initial welding head velocity in cell R8.

Appendix E - Design procedure Spring Follow Up system.

E1 Based on Belleville washers (not intended for conducting current)

If it shows from the results of the fracture tests that the total lumped mass of the moving welding head is too large, a spring follow-up system might bring a solution. On the other hand, when we calculate the drop in force on a collapsing weld and the latter appears to be too high, the same spring follow-up system can avoid expulsion problems and resulting inferior welding quality. Indeed, when mass [m] and damping factor [b] of a tested machine are defined by means of a fracture- or an explosion test and when the highest acceleration peak and the corresponding welding head velocity occurring at this point in time are measured during a projection weld in practice on this specific machine, the actuator force needed to achieve this kinematical condition can be calculated. The latter portion of the actuator force is at that point in time no longer available to compress the workpieces to maintain the weld in compressed condition and definitely will lead to expulsions. These problems will nearly never occur on applications where actuator force levels can be set at high values in relation to the moving welding head mass. But nearly all projection welding applications are vulnerable for this specific problematic since one cannot apply high mechanical loads on the workpieces to avoid excessive deformations. In practice, a large lumped mass of the welding head with its according large inertia indeed will lead to a slow follow-up behaviour as a result. The use of the spring follow-up system is intended specifically to decrease the mass underneath the springs to be forced into movement when the welds deforms. When the actuator system exerts its load, the spring system and the workpieces are loaded. When deformation is induced when the weld pool is formed, a drop in reaction force results leading to initiating moving of the smaller mass of the welding head underneath the springs, driven by the compressed springs. A spring system can only be designed based on the displacement needed during the weld and on the weld pressure that is needed. In projection welding, this displacement is part of the height of the projection embossments. As a rule of thumb we can state that the allowed drop in force of the spring system can only be 5% of the welding force with a total displacement of the projection height.

Choice of springs with low hysteresis is advantageous as are high damping effects since this will more quickly dampen out vibrations caused by the follow-up system. Of course, the spring system needs to be designed as low as possible in the moving welding head actuator system in order to achieve a lumped mass below the springs as low as possible.

Example calculation on a Dalex pedestal projection welder:

Demands towards the spring package:

Welding force of 2000daN, meaning the springs will be loaded with this force.

Weld application: projections of 1mm height.

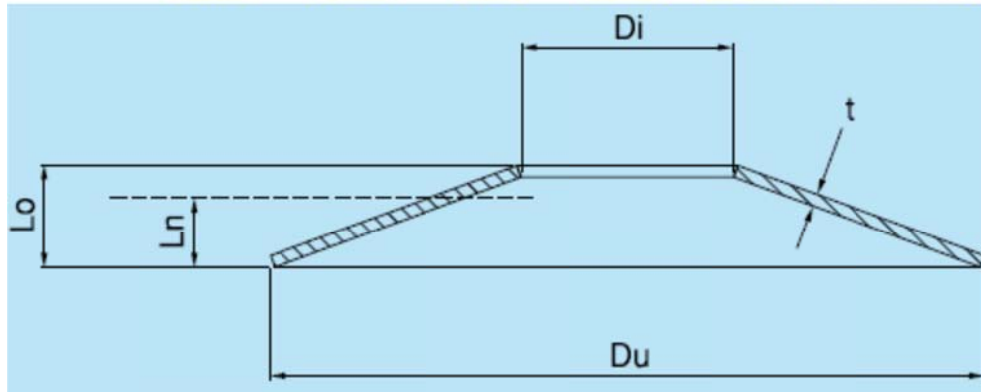
The spring system thus needs to be able to follow a displacement of 1mm and only lead to a drop in force of maximum 5%.

Calculation:

Belleville disc springs from eg. Amatec

Springs marked with R are made from stainless steel.

Du	Di	t	Lo	Ln	Fn Newton	Nummer
76,20	25,40	3,43	5,13	4,17	7655	S84190*
	38,10	2,36	4,80	3,63	4937	S84200*



Art. Nr.: S84200

$$\begin{aligned}
 D_i &= 38.10\text{mm} \\
 D_u &= 76.20\text{mm} & D_u/D_i &= 2 \\
 t &= 2.36\text{mm} \\
 L_o &= 4.80\text{mm} & L_o/t &= 2.03 \\
 L_n &= 3.63\text{mm} \\
 P_1 &= 4444 - 5431\text{N (working range)} \\
 P &= 7251\text{N (max. force to flat)} \\
 h &= L_o - t = 4.80 - 2.36 = 2.44\text{mm} \\
 &= \text{unloaded height of truncated cone of free spring}
 \end{aligned}$$

$$h/t = 2.44 / 2.36 \cong 1$$

When 4 discs in parallel ==> 1778 – 2172daN
 ⇨ Spring displacement $s = L_o - L_n = 1.17\text{mm}$

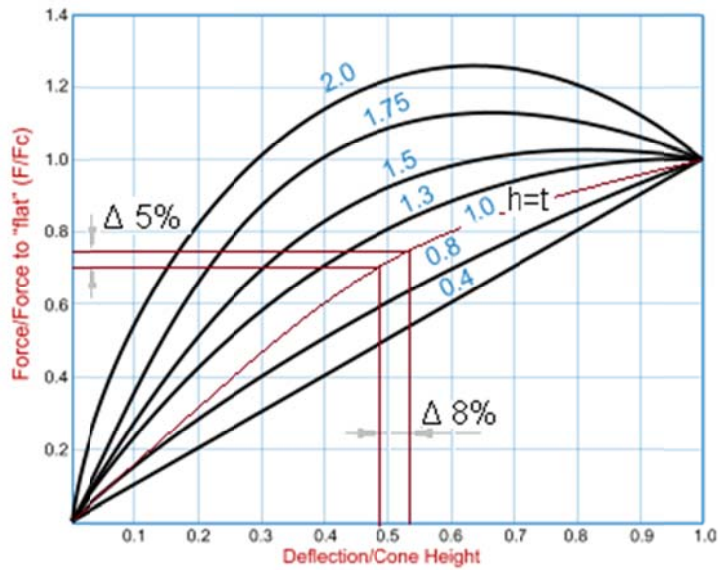


Figure E - 1 Belleville spring characteristic

If we limit the force loss to 5% → from Figure E - 1, we read: $0.08 * 2.44\text{mm} = 0.1952\text{mm}$ spring displacement allowed.

If we want to have follow-up movement by means of the Belleville springs of 1mm with force loss limited to the preset 5% → $1 / 0.1952 = 5$ series stacks of 4 parallel discs each.

Sizing:

1778 – 2172daN,	single = 4.80mm, 4 parallel = 11.88mm, 4 parallel in 5 series stack = 59.4mm (unloaded) Single = 3.63mm, 4 parallel = 8.63mm, 4 parallel in 5 series stack = 43.15mm (loaded)
1334 – 1629daN,	single = 4.8mm, 3 parallel = 9.52mm, 3 parallel in 5 series stack = 47.6mm (unloaded) Single = 3.63mm, 3 parallel = 8.35mm, 3 parallel in 5 series stack = 41.75 mm (loaded)
889 – 1086daN,	single = 4.80mm, 2 parallel = 7.16mm, 2 parallel in 5 series stack = 35.8mm (unloaded) single = 3.63mm, 2 parallel = 5.99mm, 2 parallel in 5 series stack = 29.95mm (loaded)
445 – 543daN	single = 4.80mm, in 5 series stack = 24mm (unloaded) single = 3.63mm, in 5 series stack = 18.15mm (loaded)

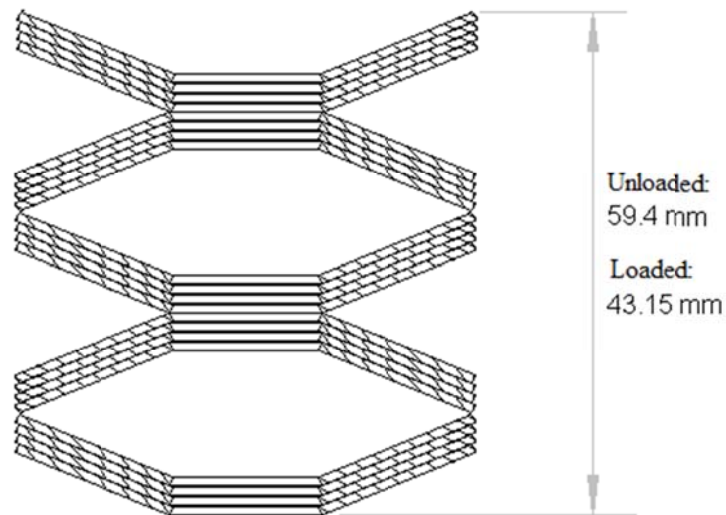


Figure E - 2 Stack of 4 parallel Belleville springs in 5 times series

Four discs stacked in parallel cause friction and hysteresis. This can be solved by stacking the discs next to one another instead of in each other.

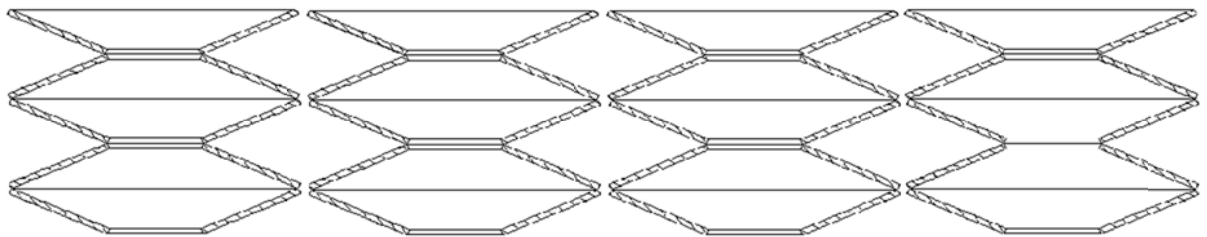


Figure E - 3 Belleville spring stack split separate in 4 parallel

E2 Based on Copper leaf springs (intended for conducting current)

As can be seen in Figure E - 4 below, on the left side a photograph of a spring mounted on a test machine, on the right side a schematical representation, the copper follow-up leaf spring can be separated in four separate leaf springs (see arrows in the image). These separate springs are mounted per two in series and subsequently in parallel. As a result of the latter, in calculating the spring constant of one single spring also gives us the spring constant of the total spring package.

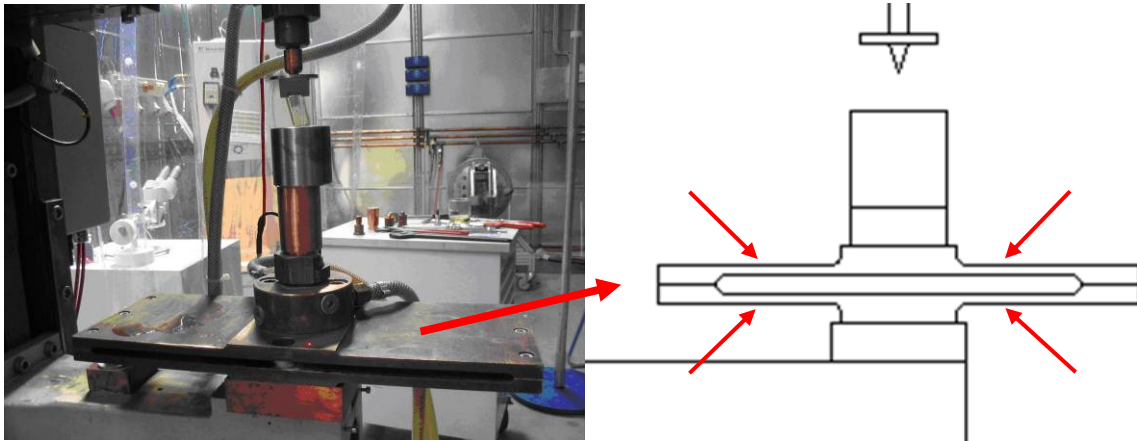


Figure E - 4 Copper follow-up spring mounted on lower welding head

When we restrict the loss in force (at projection collapse) to 5 % (cell C6) at a given actuator force (cell C5), this leads to a deflection following this actuator force that must be 20 times the height of the projection. So assuming the projection height is 0,3mm, the deflection needs to be 6 mm, following formula $\delta = \frac{0,3}{5} \cdot \frac{\text{Projection height}}{\frac{\text{Allowed drop in force}}{100}}$ (cel C16). The spring has a linear characteristic. In this way we know the deflection required to be made by the spring at a given actuator force. This has to be within the mechanical properties of the material used to build the spring.

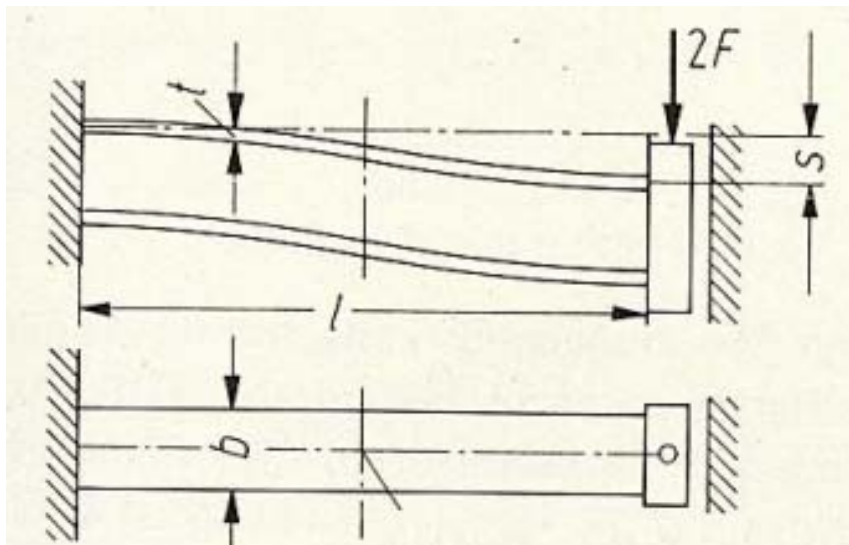


Figure E - 5 Leaf spring deflection

The spring constant “c” is written as $\frac{F}{\delta}$ ($\frac{\text{Actuator force}}{\text{deflection}}$).

From $c = \frac{b \cdot h^3 \cdot E}{L^3}$ follows that:

$$L = \sqrt[3]{\frac{b \cdot h^3 \cdot E \cdot \delta}{F}} \text{ [mm]}$$

In this formula, “b” is the width (cell C9) of the leaf spring, “h” its thickness (eg. cell G5, all cells in red, “E” is the E-modulus of the material used (cell c7) and “F” the actuator force. In this formula, “F and δ ” are given values by the boundary conditions we request. After input of “b and h”, the springs length “L” results. After varying the values of “b and/or h” we find a series of lengths that possibly can be used for this spring. There is however another restriction, namely the mechanical strength of the leaf spring that has not been taken into account. The material we aim to use in the application of a conductive leaf follow-up spring will be presumably a Copper alloy offering a good combination of electrical and mechanical properties. For instance the choice can be made to use CCZ (Copper Chromium Zirconium alloy) having a maximum tensile strength of 410 N/mm² (cel c10). We apply a safety coefficient (cel c11). Cell c12 gives us the “allowed stress”. Subsequently, the allowed bending stress value “ σ ” is calculated: $\sigma = \frac{3 \cdot F \cdot L}{b \cdot h^2} \left[\frac{N}{mm} \right]$. This value may never exceed the maximum tensile strength of the material used, even considering a safety coefficient. All combinations not meeting these demands will be considered as “not applicable”. These cells are marked “yellow” with an “if-function”. The cells marked in blue give the length of the complete follow-up spring. The latter is twice the length of the single spring calculated above added with twice the length of the connecting pieces at the springs ends (where the three bolts are visible in the image) (cell c13) and finally the central stiffer area with increased thickness to allow mounting of the spring to the lower welding head and mounting of the lower electrode holder respectively (cel c14).

Example calculation:

Assume: F = 3000 N

Allowed force loss: 5%

E-modulus: 125000 N/mm²

Projection height: 0,25 mm

Spring width: 100 mm

Tensile strength: 410 N/mm²

Safety coefficient: 1,2

Length connecting pieces at ends: 30 mm

Length central elevated part: 100 mm

Calculation:

If these values are entered in the spreadsheet, the most compact spring is the one with a thickness of 7.3 mm.

Entered in the formula:

$$L = \sqrt[3]{\frac{b \cdot h^3 \cdot E \cdot \delta}{F}} \text{ [mm]}$$

It gives us: $\sqrt[3]{\frac{100 \cdot 7.3^3 \cdot 125000.5}{3000}} = 200.86 \text{ mm}$ (cell K20)

Subsequently we need to check if the allowable stress value is not exceeded:

$$\sigma = \frac{3 \cdot F \cdot L}{b \cdot h^2} \left[\frac{N}{mm} \right]$$

This gives,

$$\sigma = \frac{3 \cdot 3000 \cdot 200.89}{100 \cdot 7.3^2} = 339.27 \text{ N/mm}^2$$

This is just below $\frac{410 \text{ N/mm}^2}{1.2} = 341.66 \text{ N/mm}^2$

Finally the full length of the spring:

$$\text{Total length} = (2 \cdot 200.89) + (2 \cdot 30) + 100 = 561.8 \text{ mm}$$
 (cell L20)

Appendix F - Procedure and manual for processing the Voltage – Current U-I-Characteristics of a Resistance Welding Power Source.

F.1. Introduction

See 4.3.1. in Measuring Procedures

F.2. Measuring procedure and manual for measuring and processing data

This section discusses in detail how current and voltage are measured in Dewesoft and how the recorded data are processed in Flexpro to U-I-characteristics.

The settings of the different measuring channels on the Data-acquisition are programmed in a setup-file “U-I-weerstandlas.iDS”. Since we can only measure discrete points on a resistance welding power source, we only can define a single point on the characteristic with each measurement. We then have the choice to work with a single point in each measuring file or we measure multiple points in one single measuring file, by inserting pauses between the different measurements.

It is convenient to conduct the measurements in practice by measuring a single point of the characteristic (eg. at short circuit), repeating this measurement each time with a different power setting on the machine, and collecting these data in a single measuring file. Subsequently a second point on the characteristic is measured for the different power settings on the machine and this procedure is repeated for several loads.

This programmed setup-file also allows for the primary characteristic to be measured. In total 4 input channels were configured.

SLOT	ON/OFF	NAME	AMPLIFIER	PHYSICAL VALUES	ZERO	SET
0	ON	INPUT 1	DAQP-V 10 V .. 10 kHz	SECONDARY CURRENT [A] -1,002E5 1,002E5	ZERO	INPUT 0
1	ON	INPUT 2	DAQP-V 50 V .. 100 Hz	SECONDARY VOLTAGE [V] -50,01 50	ZERO	INPUT 1
2	ON	INPUT 3	DAQP-V 5 V .. 10 kHz	PRIMARY CURRENT [A] -3922 4281	ZERO	INPUT 2
3	OFF	INPUT 4	DAQP-V 0.01 V .. 50 kHz	U [V] -0,0099996 0,0099998	ZERO	INPUT 3
4	ON	INPUT 5	DAQP-DMM 1000 V .. 1 kHz	PRIMARY VOLTAGE [V] -999,2 999,7	ZERO	INPUT 4

If accessibility to the primary side of the machine is limited, it is possible to disable input channels 2 and 4 if wanted.

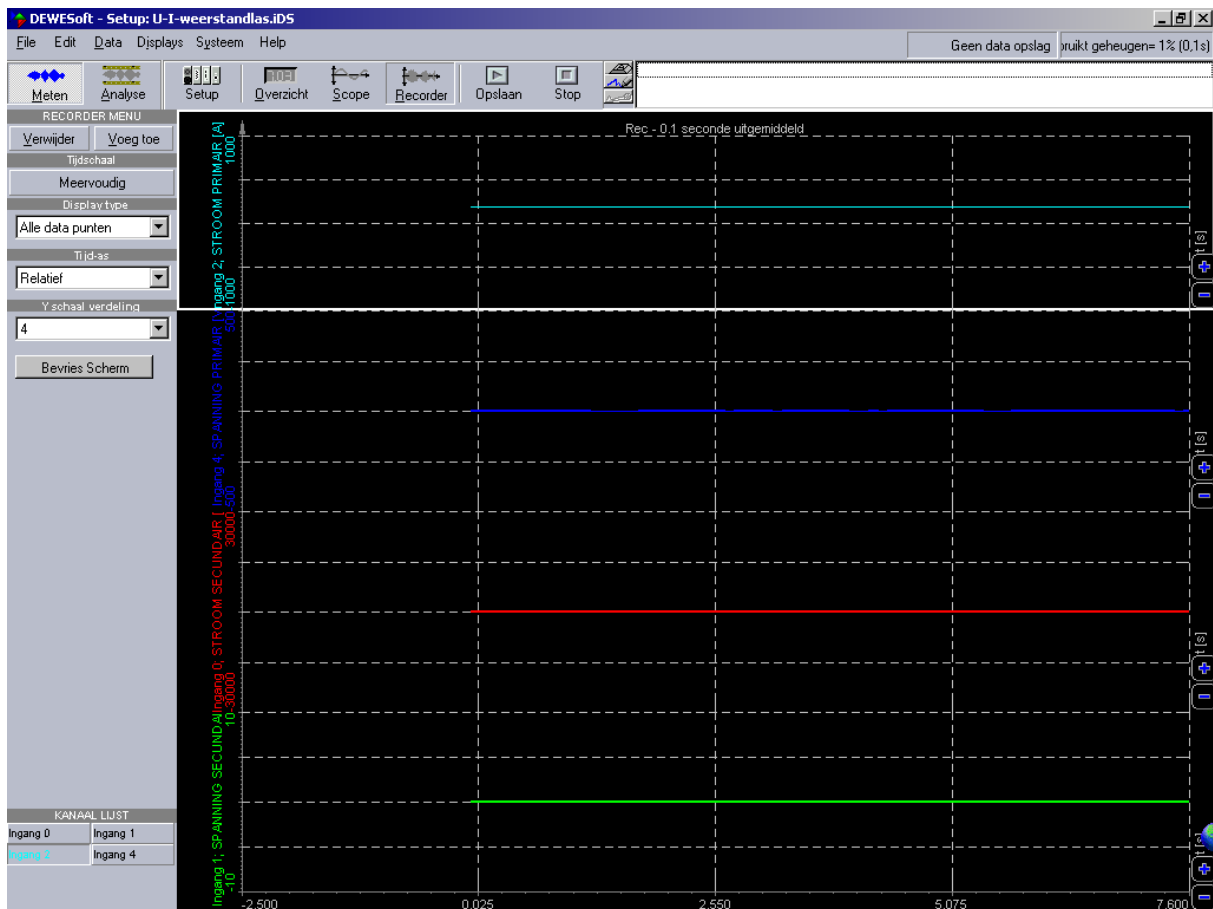
The Rogowski-coils used are positioned both around primary and secondary current leads and switched on. Two pairs of voltage clamps are needed to measure primary and secondary voltage.

At this stage, the first point of the characteristic to be measured needs to be chosen. Processing in Flexpro is programmed to start with the short circuit point meaning welding without a workpiece between the electrodes. It is important to reduce the welding time set to a

minimum in order not to create a thermal overload on the electrodes that could potentially damage them.

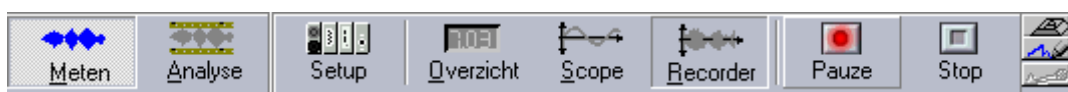
Also the amount of different current or heat settings on the machines' control box that we want to supply to every single load setting on the measuring resistance needs to be chosen here (≤ 10). On most machine control boxes, current can be preset as a 'percentage' [%] or in 'per mille' [‰] of the maximum available power the machine can deliver. For ease of processing it is best to work in steps of 10% or multitudes of 10, for instance in steps of 10 (10,20,30,40,50,60,70,80,90,99) or in steps of 20 (20,40,50,60,70,80,99) etc....

Then all is set to start the measurement, through the menu bar we open the recorder screen where all activated measuring channels are visual and operational.

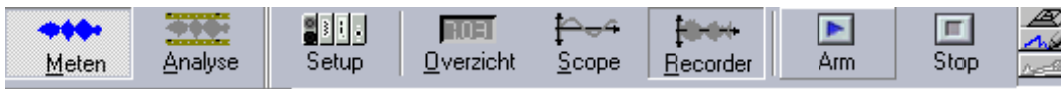


When we hit the 'record' button, a communication field opens where comments regarding that specific measurement can be added. To maintain an overview over the different measurements made, this field can better be commented.

When we hit the "OK"-button, the measurement starts. We set the machine to the lowest heat setting (10%) and after measuring the first flow of current we pause the measurement.

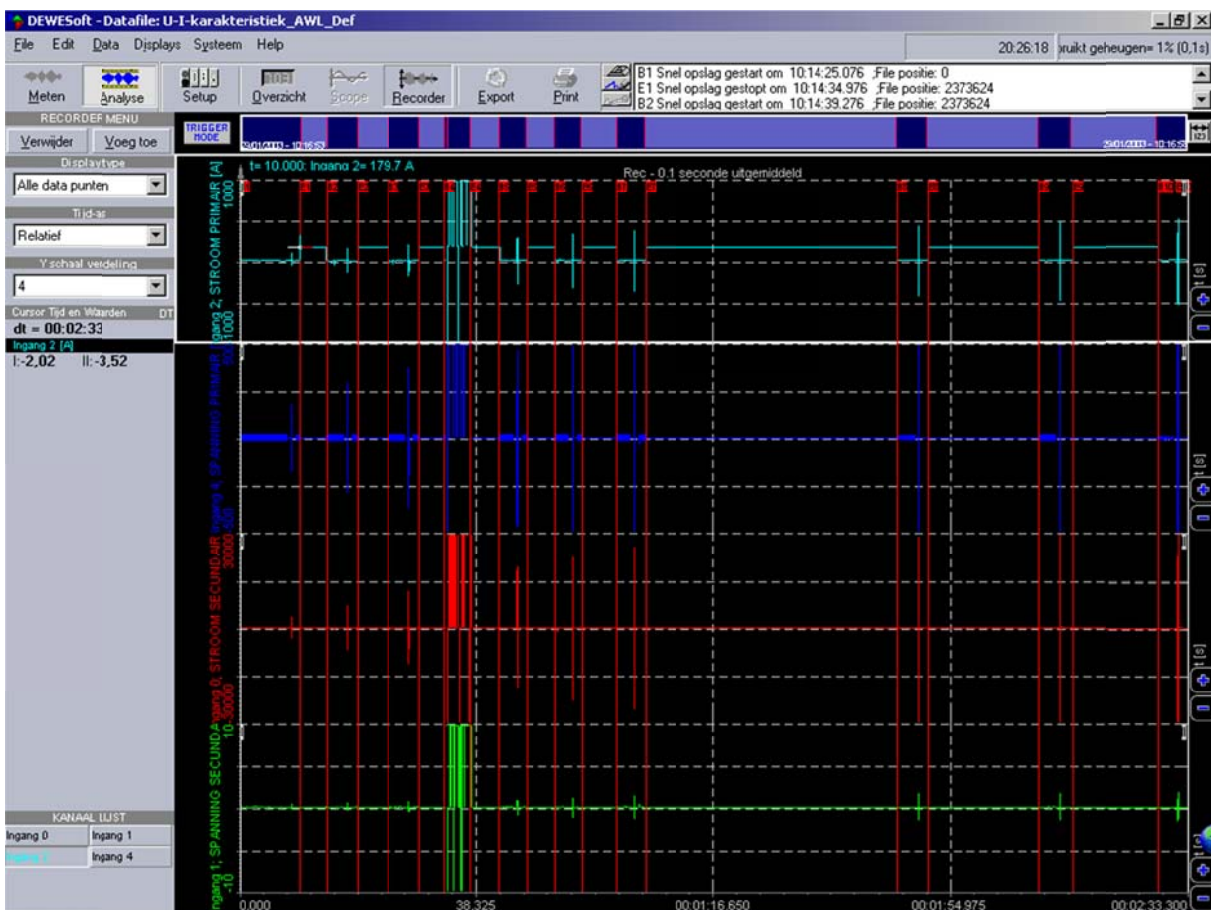


Thus the measuring file is not closed, only no incoming signals are recorded. The latter gives us the time to switch the machines' control box to the next heat setting (20%). When this is done, we restart recording by pressing the “Arm” –button.



Once this flow of current (at 20% heat setting) is measured, we pause the measurement again, raise the heat setting again and restart recording. This procedure is repeated until all heat settings in our scope are measured at this one specific load. After the last measurement, the measuring file is closed (“Stop”). In this way we obtain the short circuit point of the characteristic at all heat settings.

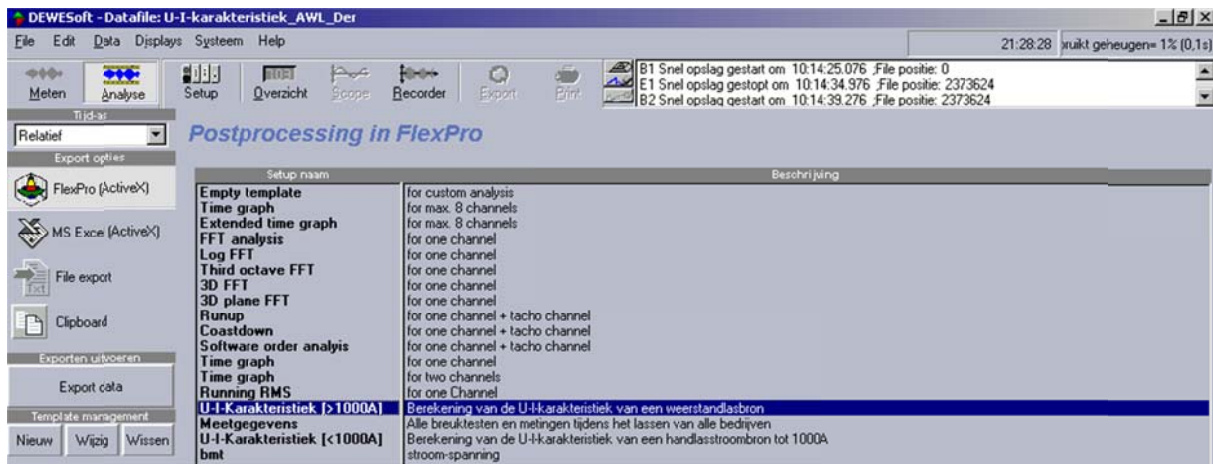
It is good practice to have a quick look at the measured file after each series of measurements. This is done by hitting the ‘Analyse’ –button after the stopping of the measurement.



The entire procedure can subsequently be repeated for all other loading points of the characteristic.

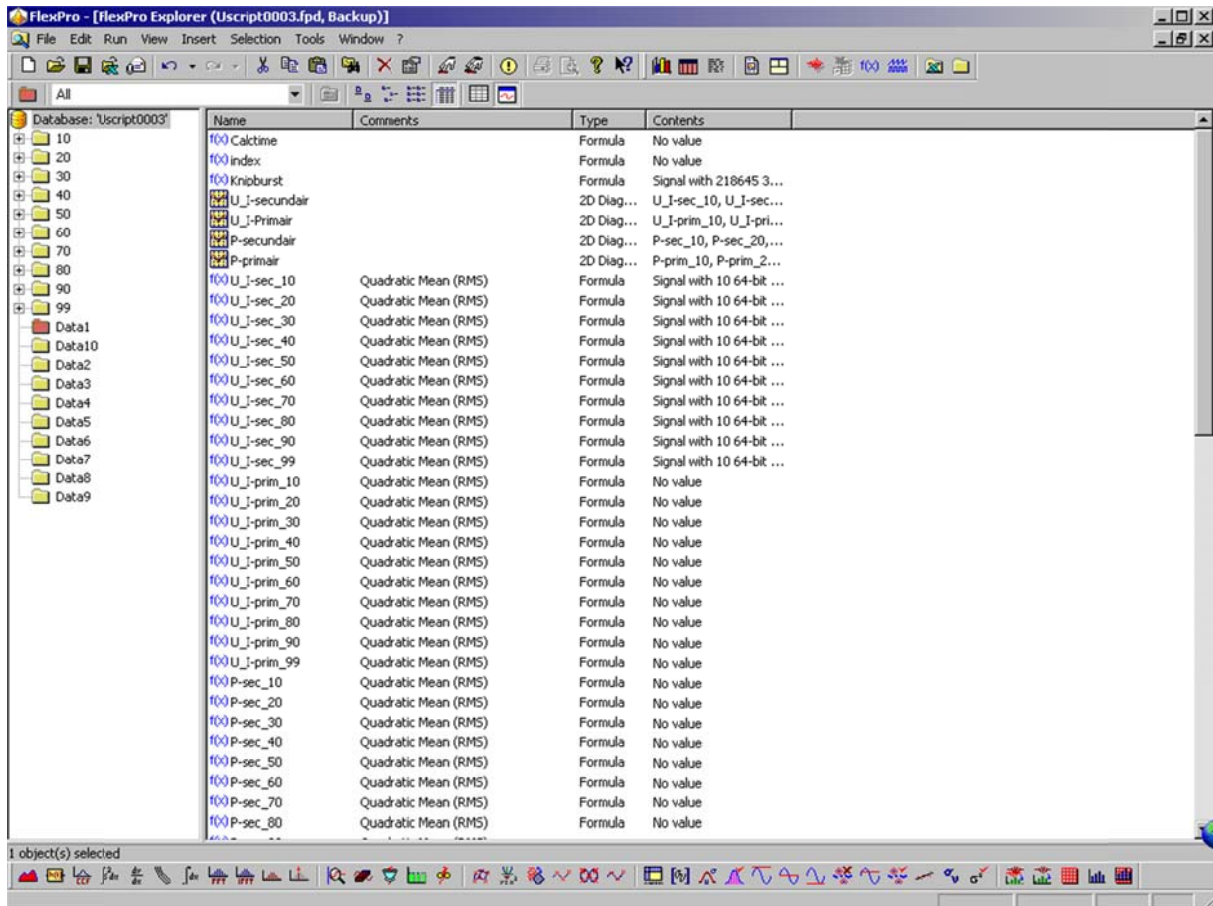
Afterwards, all measured files can be exported to Flexpro one by one.

By hitting the ‘Analyse’-button once (or twice), an overview of all measured files is displayed. The first one we open is the one of the short-circuit point. We subsequently hit the ‘Export’-button followed by choosing the script “U-I-characteristic [>1000A] under “setup-name”.



The measurement is exported by hitting the “Export data”-button. Flexpro opens automatically.

The different measurements within the measured file are automatically placed in a number of folders (Data1,Data2,Data3,...), equal to the total number of current levels measured. Each folder contains 4 signals, Signal0, Signal1, Signal2 en Signal3 matching with secondary current, secondary voltage, primary current and primary voltage respectively.



Also the folders of all possible current characteristics are already present in the script (10,20,30,40,...,99). The intention is that for instance folder “10” should contain all points of the U-I-characteristic at a preset heat-setting of 10%.

In a next stage, each Datafolder is dragged under the matching “current-folder”.

Suppose we measured the current in steps of 10%. Then Data1 is dragged to folder “10”, Data2 to folder “20”, etc, and finally Data10 is dragged to folder “99”. If however we work in steps of 20, than Data1 is dragged to “20”, Data2 to folder “40”, etc....

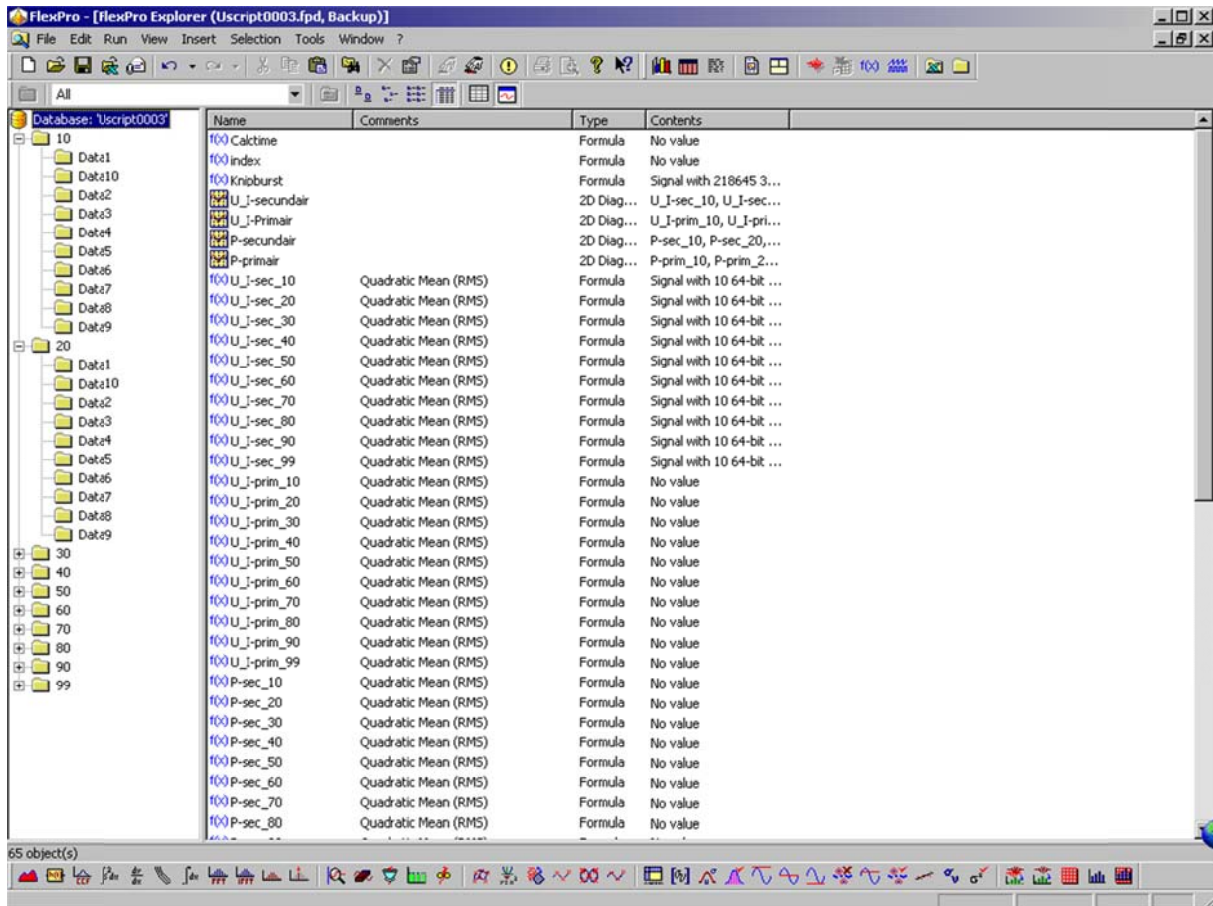
If we did NOT work in steps of 10%, the unused folders may NOT be removed. Example: Suppose we measured in steps of 20%, folders “10”, “30”, “50”, “70”, “90” CAN NOT be removed.

When there are one or more erroneous measurements (it can happen that an operation on the machine goes wrong), than these are not dragged to the matching folders but removed.

If a measurement is missed, this can be stored in a separate measuring file and need to be exported one by one and placed under the correct “current folder”.

This procedure is repeated until all measured points of the U-I-characteristic are placed in the matching current folders.

As an example, the image below shows how all points of the “U-I-characteristic” (from short circuit to no-load at 10% and 20% heat setting are organized.



In processing, there is the choice between a number of graphs, e.g. the secondary “U-I-characteristics”, the primary “U-I-characteristics”, the secondary power characteristics and the primary power characteristics. By depressing the matching icon of each representation, calculation is started and the results are displayed graphically.



F.2.1. Calculation method of primary and secondary U-I-characteristics

The calculation method is explained based on one single heat setting, 10%. For all other heat settings, calculation is likewise.

The essence of the calculation is in calculating an RMS-value of every measured signal, be it primary or secondary current or voltage.

The image below shows as an example the secondary current in the short circuit point at a heat setting of 10%. The RMS-value of this signal needs to be calculated.

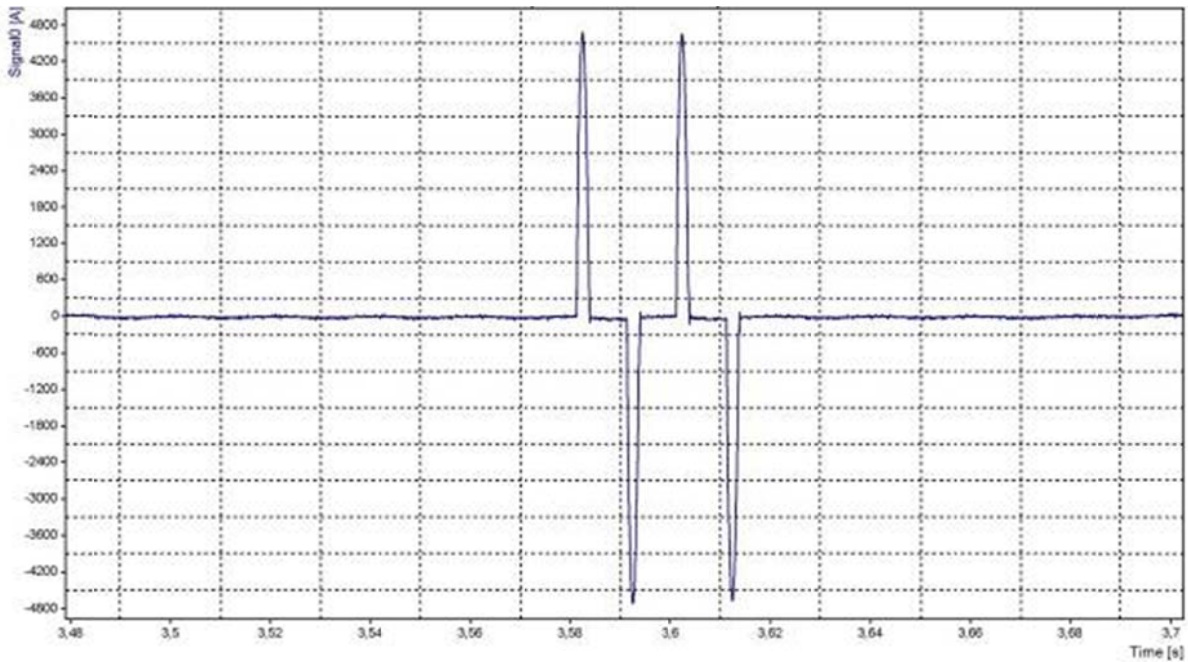


Figure F - 1 Short circuit point: secondary current at 10%

To obtain a correct RMS-value, the current pulses need to be isolated from the complete measured signal (there is measured over more time than the actual time the current flow lasted). A function “index” was created for this purpose that searches the start and the end of the actual current flow. The “index” function searches the indexes of these start and end points (the position of the points in the signal) and sends them back. The Flexpro script of this function is given below as an illustration.

Arguments Data

Data = Knipburst(Data, 0.05)

Data1 = smooth(Absolute(Data), 10)

_Max = Maximum(Data1)

if Datastructure(_Max) >= STRUCT_DATASERIES then

_Max = Maximum(_Max)

End

*Data1 = LevelCrossings(Data1, 0.400000000000000 * _Max, 0.010000000000000 * _Max, EVENT_BOTH, EVENT_INDEX)*

NSamples = numberofelements(Data1)

i = Data1[0]

j = Data1[NSamples-1]

If Data[i] > 0 then

Do

i = i - 1

While Data[i] > 0 and Data[i] <= Data[i+2]

else

Do

i = i - 1

While Data[i] < 0 and Data[i] >= Data[i+2]

end

```

If Data[j] > 0 then
  Do
    j=j+1
  While Data[j] > 0 and Data[j] <= Data[j-2]
else
  Do
    j=j+1
  While Data[j] < 0 and Data[j] >= Data[j-2]
end

Return {i,j}

```

Once the indexes of the actual weld time are found, the RMS-value can be calculated. This is done with the following function.

$$I[9] = \text{Mean}(I1[\text{index}[0], \text{index}[1]], \text{MEAN_SQUARE})$$

These calculations are made both for primary and secondary currents.

In the normal representation of a static characteristic (U-I-characteristic), the first point is the point at NO-load. The first point measured at each heat setting is the point at short-circuit. The latter meaning that to obtain a correct representation of the U-I-characteristic, we should reverse our measured points. In the calculation this issue is dealt with.

As an example, in the image below, the calculated primary and secondary U-I-characteristics of our laboratory AWL resistance welding machine are shown.

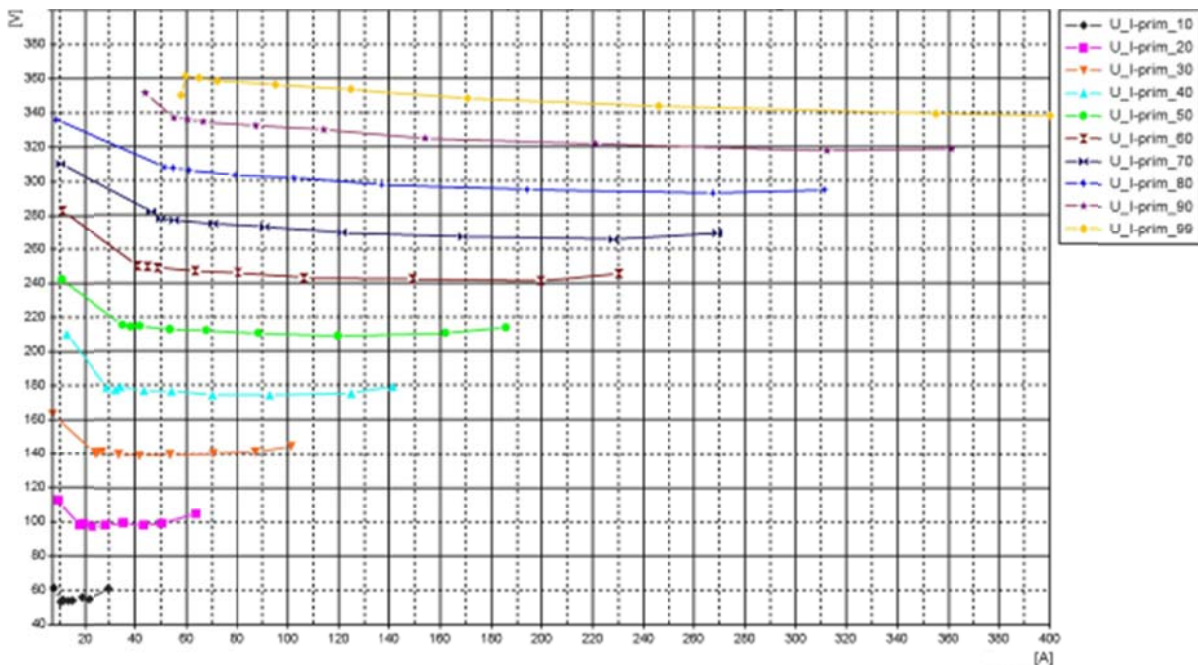


Figure F - 2 Primary U-I characteristics at different current-levels

When we load the machine secondary with a current of 27 kA, we draw a current on the primary side of 400A and this results in a voltage drop on the primary side of 20V.

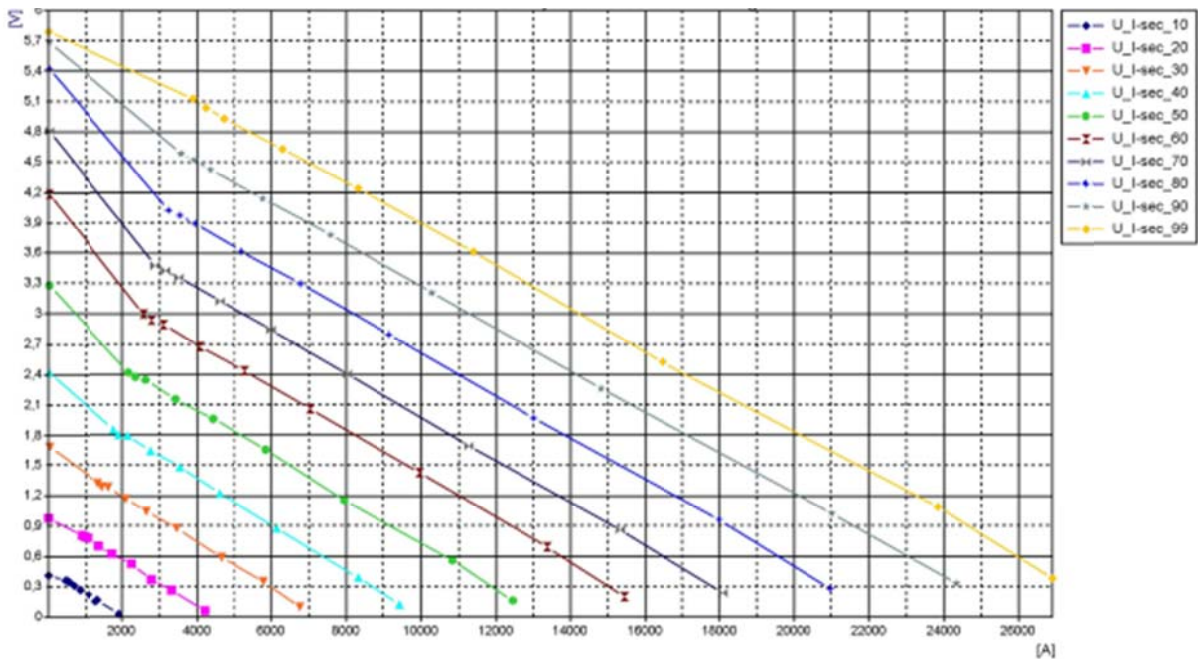


Figure F - 3 Secondary U-I characteristics at different current-levels

F.2.2. Calculation of primary and secondary power in time

Calculation of primary and secondary power in time is simple and based on the U-I-characteristics already available. The U-component is multiplied with the I-component. At first we need to check if the U-I-characteristic in question effectively exists. If we worked with steps other than 10%, not all U-I-graphs exist and it is then useless to calculate the power of these. The Flexpro script for calculating the power is given below.

Arguments Data

i=0

If Data[0] <> ? then

P = Data

Nsamples = Numberofelements(Data)

For i=0 to Nsamples-1 do

*P.Y[i] = Data.X[i] * Data.Y[i]*

end

Return P

else Return {??}

end

The following images show the primary and secondary power curve of our AWL machine.

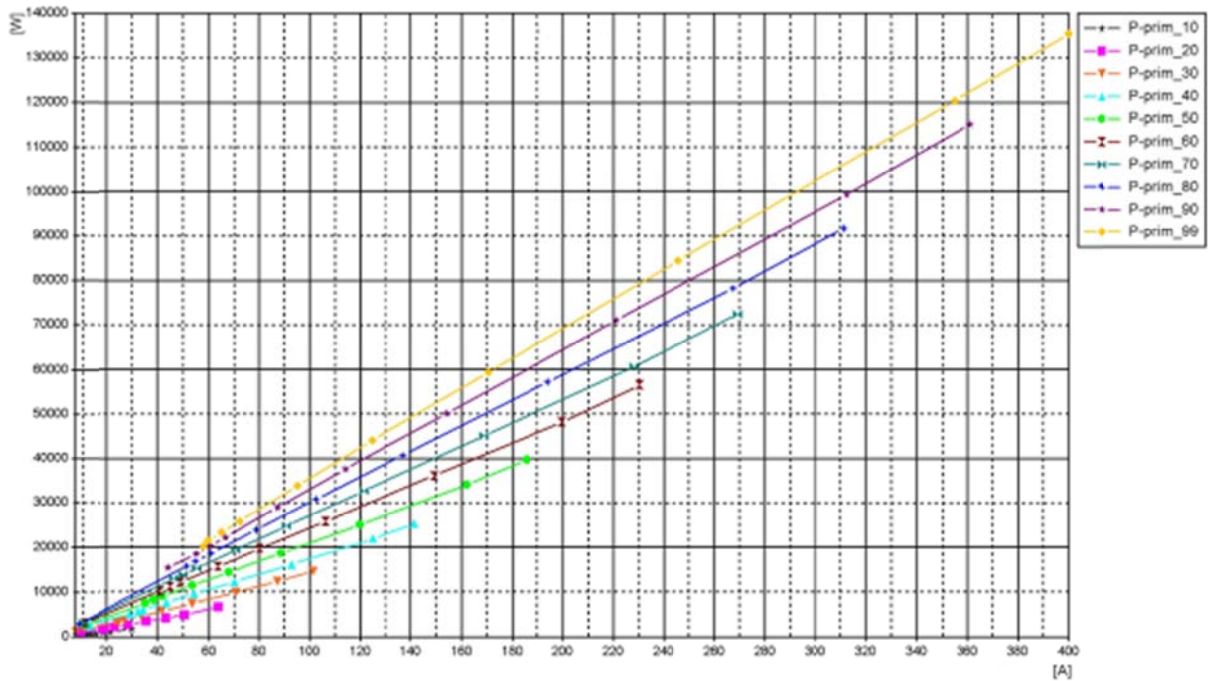


Figure F - 4 Primary Power Curve

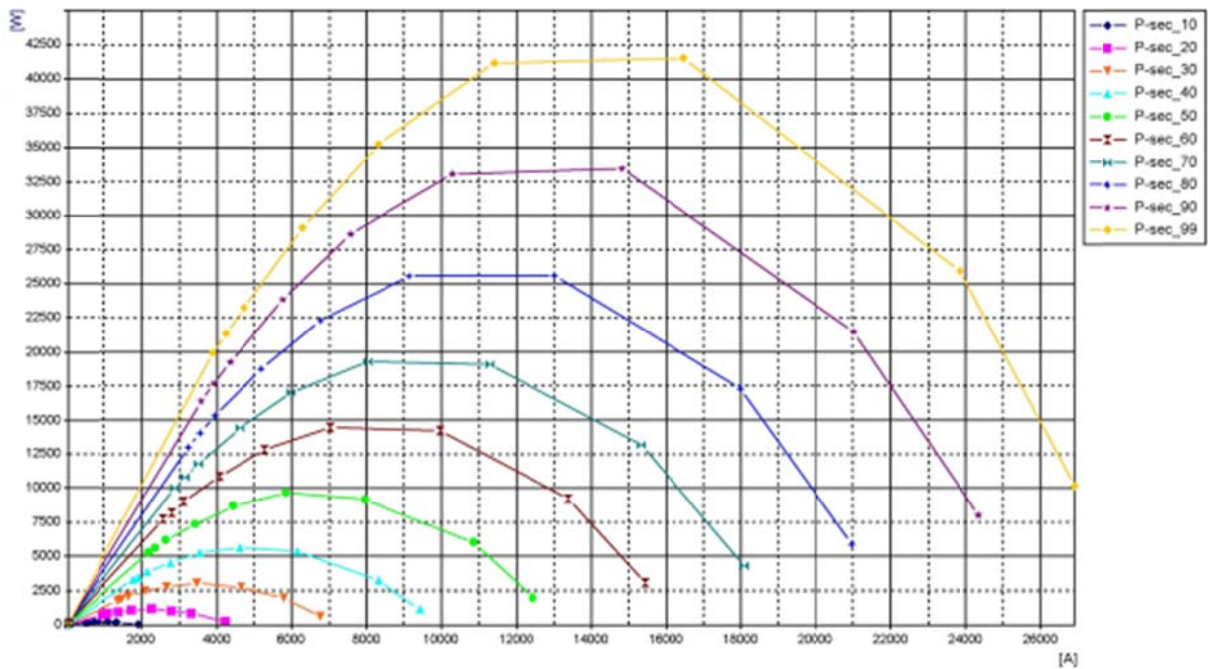


Figure F - 5 Secondary Power Curve

F.3. Conclusion

Measuring and processing one or more U-I-characteristics of a resistance welding machine is somewhat more complex in comparison with an arc welding power source. Measurement on a power source of for instance an arc welding machine is possible with a continuously changing load resistance where all points of one characteristic can be captured in one single measurement. This cannot be done on a resistance welding machine where a number of discrete load resistance values can be offered to its power source. Because currents delivered by resistance welding machines are relatively high in magnitude and can only be delivered during short times, the use of a liquid resistance that offers the possibility to change its

resistance continuously is not possible. For this reason, the portable discrete variable resistance system was developed by the author to enable in situ measurement of both U-I characteristics as power characteristics on any resistance welding machine. Semi-automated processing was developed that requires a minimum in handling to calculate the measured characteristics and display them graphically. However, this processing procedure limits the number of measured points per characteristic and the number of characteristic per machine.